eman ta zabal zazu
Universidad del País Vasco
Euskal Herriko Unibertsitatea

Mesenchymal stromal cells-based sustainable strategies for wound management: from valorized cell delivery systems to cell-free therapies

Kevin Las Heras Zapata

Vitoria-Gasteiz, 2023

Universidad del País Vasco Euskal Herriko Unibertsitatea

NAZIOARTEKO BIKAINTASUN CAMPUSA
CAMPUS DE EXCELENCIA INTERNACIONAL

Mesenchymal stromal cells-based sustainable strategies for wound management: from valorized cell delivery systems to cell-free therapies

Kevin Las Heras Zapata

Vitoria-Gasteiz, 2022

NanoBioCel research group

Laboratory of Pharmaceutics, School of Pharmacy

University of the Basque Country (UPV/EHU)

Acknowledgments for the financial support

This doctoral thesis has been funded by the Spanish Ministry of Economy and Competitiveness through the "RETOS" Program (NANGROW project, RTC-2017-6696-1) the AF2017-82292-R grant, the CI/AEI/FEDER, UE (RTI2018-097100-B-C22), through the ICTS "Nanbiosis" (Drug Formulation Unit, U10) and through the Basque Government (Grupos Consolidados, IT907-16). Kevin Las Heras gratefully acknowledges the predoctoral grant provided by the Basque Government (PRE_2018_1_041).

Acknowledgments to the editorials

Authors thank the editorials for granting permission to reuse the published articles in this thesis. The published versions can be accessed at the following links:

Las Heras, K. *et al*. Green chemistry, *2020, 22*(10): 3445-3460 (Appendix 1) DOI: 10.1039/D0GC00089B

Jimenez-Martin, J. and Las Heras, K. *et al*. Materials Today Bio, *2022*, 15: 100273 (Appendix 2) DOI: 10.1016/j.mtbio.2022.100273

The third work derived from this doctoral thesis (Appendix 3) has been sent to Bioactive Materials international journal.

Las Heras, K. *et al.* Stem Cell Research & Therapy, 2022, 13(1):1-18 (Appendix 4) DOI: 10.1186/s13287-022-02824-0

Las Heras, K. *et al*. Journal Of Controlled Release, *2020*, 328: 532-550 (Appendix 5) DOI: 10.1016/j.jconrel.2020.09.039

Las Heras, K. *et al*. Biomaterials Advances, 2022, 135: 212738 (Appendix 6) DOI: 10.1016/j.bioadv.2022.212738.

Agradecimientos

Con los renglones que, en este manuscrito dejo, termina una de las etapas más bonitas de mi vida personal y profesional. Estos más de 4 años de tesis doctoral han sido, de lejos, los de mayor crecimiento mental y emocional que he tenido en mi (no tan corta) vida. Pero este camino, por suerte, no lo he recorrido solo. A continuación, detallaré las personas que de una manera u otra han contribuido a que el viaje haya sido un poco más fácil y a los cuales llevaré con estima en mis recuerdos.

En primer lugar, quiero mencionar a mis directores, Rosa y Edorta, quienes me dieron la oportunidad de hacer la tesis y me acompañaron en todas las etapas de esta. Rosa, gracias por confiar en un estudiante de 4º año de farmacia con cara de niño bueno y una nota media regulera que un día apreció por el despacho. Por darme confianza, alas para experimentar y salirme del papel y por no decirme nunca no a ideas que, a veces, parecían más delirios. A Edorta por haber estado ahí en todo momento y por hablar mí mismo idioma, el de la pasión y la motivación. Por retroalimentar nuestras ideas, ofrecerme conocimientos y consejos personales y profesionales durante todos estos años, que tanto me han hecho crecer y crecerme.

En segundo lugar, quiero mencionar a mis compañeras de laboratorio por el aprendizaje y los momentos que hemos compartido. Gracias Saioa por haberme llevado en brazos en mis comienzos y haberme inculcado la rigurosidad, marca "control de calidad", en el trabajo. Gracias Itxaso por, primeramente, haberme aguantado estos 4 años (que sé que a veces no es fácil), y segundo, por la siempre buena predisposición que has tenido para enseñarme, ayudarme, regañarme y acompañarme en esto. A Lorena por todos los momentos juntos, las cremas de oliva, Salamanca, Valencia, los quebraderos de cabeza del citómetro… seguro que me dejo alguno más… A Ainhoa y Sara por toda la ayuda que me habéis brindado siempre con una sonrisa y por todos los consejos personales, laborales y de "politiqueo" que me habéis dado. A Jon por haber compartido conmigo una pequeña fracción de la tesis, nuestra pasión musical y haber sabido elegir lo mejor para estar bien con uno mismo. Al resto de NanoBiocel, los que quedan y los que se fueron… gracias por vuestra calidad humana. Finalmente, Elena, quiero agradecerte el haber entrado en mi vida. Compartir un camino así, con una

persona como tú, con tus valores, tu cariño, tu personalidad, tu sapiencia y tu energía, hace que todas las cosas de este sean algo único y genuino. *Ab imo pectore*.

Por otro lado, quiero agradecer al Dr. Pedro Guerrero, a la Dra. Koro de la Caba y a todo el grupo de investigación de Biomat por toda la ayuda y el trabajo juntos para poder sacar adelante los trabajos de esta tesis doctoral. También quiero agradecer al grupo de "Exosomas" del CIC BioGUNE y en especial al Dr. Juan Manuel Falcón-Perez por haberme dado la oportunidad de formarme en su laboratorio. Gracias al resto de personas del equipo, Félix, María, Jone etc. por la predisposición, la amabilidad y todos los conocimientos que allí me prestaron. Gracias también al Dr. Jose Javier Aguirre por todo el trabajo y ayuda que me ha brindado en cada artículo e investigación en la que hemos colaborado juntos, siempre predispuesto.

In addition, thanks to Dr. Jae Won Shin from the University of Illinois at Chicago (UIC) for allowing me the opportunity to learn from his laboratory and team. Also, I want to share some words to my Chicago family. Thanks to my Indians for the heartwarming environment and memories that we created. Thank you Koushik for being like a brother, teaching me so many things (chemist things) inside and outside the lab, for the "writing nights", for the Zara moments and many more that I will remember forever. Thank you Prerak and Sai for being the greatest and nicest people in the world, for the trips, Pete´s, Devon St. and for all the moments that we collected in the lab and in the Indian's house. Another mention to my Korean, Ik Sung, thank you for being always open to help, for all the laughs, the football matches and the "BBQs" from the rooftop. Thanks to my Mexican, Ambar, for all the moments, the food, the Spanish-Mexican jokes and the Chicago knowledge you shared with me. Also, thanks Dr. Sing Wan for all the support, help and all the tips that you gave me during our short period together. Finally, thank you Basma for helping me with everything (including science) in Chicago since the month before arriving there. I will always be hungry for another Chilango.

Finalmente quiero dejar unas palabras a las personas de fuera del ámbito profesional que han estado ahí durante todo este tiempo. A mi grupo de música, Oslo Ovnies y a cada uno de sus miembros, Javi, Isra, Guille y Aitor, gracias por estos más de 6 años juntos, por la familia que hemos creado, por recorrernos la península tocando y componer 2 álbumes, más de 20 canciones, que han sido la mayor vía de escape en los momentos más difíciles. Hacer una tesis es "pan comido" comparado con mantener la

salud mental de un grupo de 5 tarados llenos de “red flags”, crear nuevos géneros musicales, hacer crecer un grupo de rock y tocar con las bandas que un día idolatramos. Gracias también a mis amigos, a Sergines por las charlas sobre “datos y matemáticas”, música, los bolos y féstis, las burguers, las pizzas… a Ángela por nuestra amistad, por estar siempre ahí preocupándote y ayudándome hasta con los artículos de esta tesis. A Mario por haber aportado su grano de arena en esto con la famosa portada para *Green Chemistry* y por todos los momentos y proyectos audiovisuales que hemos hecho juntos durante esta vida. A todos los que me dejo y se han cruzado en mi camino durante este tiempo; amigos, cuadrilla, monitores, compañeros de piso, sanitarios etc. gracias.

Y por último gracias de corazón a mis padres por haberme brindado una vida tan fácil. Por haberme inculcado unos principios y unos valores en un entorno de cariño, apoyo y bondad que me han hecho ser la persona que soy hoy. Gracias por acompañarme, aconsejarme y estar ahí siempre en todas mis decisiones y momentos vitales. Gracias a mi hermana Marta, por ser una rebelde sin causa y por apoyarme en mis proyectos, cuales quiera fueran, como si de ella formasen parte también. Gracias también a mis tíos Manolo y Mari Carmen por ser una extensión más de mis padres y apoyarme en este camino. A mis primos Carla y Gonzalo, que a pesar de la distancia (a veces la mayor que puede existir en este globo terráqueo) siempre están ahí. A mi abuela Carmen, que nos dejó cuando estaba en Chicago, por toda la familia que creaste, cuidaste, educaste y que siempre te recordará. A mi abuela Angelita, mis abuelos Enrique y José allá donde estén, primos, tíos, tías, Chus, Nines y demás familia que me ha acompañado en este tiempo. Gracias a todos de corazón.

Y no quiero terminar estos párrafos sin agradecer esta tesis al sistema público de enseñanza de este país, sin el cual estos renglones que hoy escribo jamás se hubieran producido. En estos tiempos donde la oscuridad oligárquica atenta una vez más contra la libertad de la sociedad de a pie y sus derechos, defender lo más preciado de un país, sus servicios públicos, es la única garantía de crecimiento, desarrollo y libertad.

Esta tesis, va por vosotros

"*Siempre nos hemos definido por la capacidad de superar lo imposible. Y contamos estos momentos. Estos momentos cuando nos atrevemos a apuntar más alto, a romper barreras, a alcanzar las estrellas, a dar a conocer lo desconocido. Contamos estos momentos como nuestros logros más orgullosos, pero perdimos todo eso. O, ¿tal vez nos hemos olvidado de que todavía somos pioneros y apenas hemos comenzado? Nuestros mayores logros no pueden quedar atrás, nuestro destino está por encima de nosotros*"

Cooper, Interstellar (Cristopher Nolan, 2014)

Glossary

ATR-FTIR: Attenuated total reflectance Fourier-transform infrared

AT-SLS: AT-MSCs loaded into the SLS

BCI: Blood clotting index

cBM-MSCs: Circulating bone marrow derived mesenchymal stromal cells

CH: β-Chitin

DAMPs: Damage-associated molecular patterns

DMEM: Dulbecco's modified Eagle's medium

ECM: Extracellular matrix

EMA: European medicines agency

EMEM: Eagle´s minimum essential medium

EVs: Extracellular vesicles

FBR: Foreign body response

GF: Growth factors

GZ: Gauze

HDFs: Human dermal fibroblasts

HF-MSCs: Hair follicle derived mesenchymal stromal cells

HF-SLS: HF-MSCs loaded into the SLS

LDH: Lactate dehydrogenase

LPS: Lipopolysaccharide

MC: Merocel

mlEVs: Medium-large EVs

MMPs: Matrix metalloproteinases

MSCs: Mesenchymal stromal cells

MSC-Ds: Mesenchymal stem cell-based dressings

NTA: Nano tracking analysis

PAMPs: Pathogen-associated molecular patterns

PRP: Platelet rich plasma

sEVs: Small EVs

SLS: Sponge-like scaffolds

SOD: Superoxide dismutase

SPI: Soy protein isolate

TIMPs: Tissue inhibitor of matrix metalloproteinases

TNFα: Tumor necrosis factor alpha

WB: Western Blot

XPS: X-ray photoelectron spectroscopy

Index

Chapter 1

Introduction

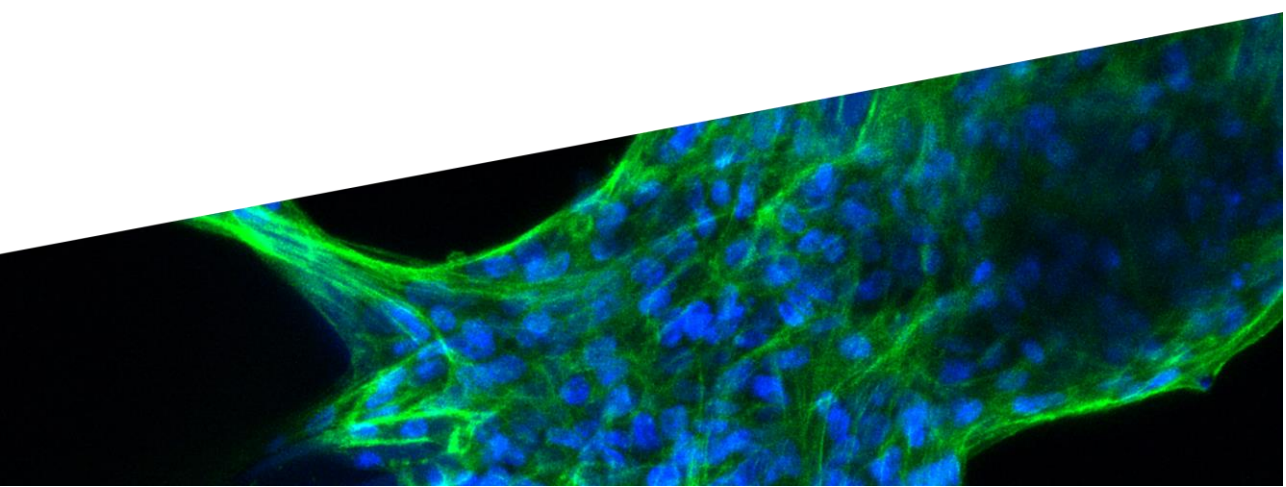

1. State of The Art

Tissue injury is as old as human being is. Since childhood, when we sustain numerous scrapes and cuts, to elderly, when illness, surgery or trauma may result in greater tissue injuries, we recurrently experience the life cycle of tissue damage and repair. Generally, wounds heal within days or weeks after an uneventful and unimpeded course. However, shortcomings on the wound healing process do occur leading an impeded skin barrier. Presently, wounds are widely divided into acute and chronic with specific subtypes in both categories [1]. When tissue injury is given, all wounds can be considered acute, regardless of their nature. However, when these injuries take more than three months to heal, they can be considered "chronic" [2]. Among the physiological and pathological states that can cause a delayed healing; aging, diabetes, infections, vascular problems and cancer are the main causes [3].

The wound healing process after tissue injury involves a complex interplay of multiple cell types — immune cells, skin cells, mesenchymal stromal cells (MSCs) etc. —, molecular mediators and their surrounding extracellular matrix (ECM) in a very precise and well-orchestrated cascade. Thus, understanding the spatio-temporal molecular and cellular events that can lead to an impaired tissue repair is essential for development of more effective and precise therapies. In healthy individuals, the wound healing process comprises four stages: hemostasis, inflammation, proliferation and remodeling [4] (**Fig. 1**).

Hemostasis occurs after a tissue injury to recover the barrier function of skin. It triggers a peroxide gradient and vasoconstriction processes to finally attract platelets to close the injury forming a clot and impeding the loss of blood. Furthermore, this blood clot will serve as "scaffold-like" structure for the migration of skin and immune cells [5]. Platelets within the clot release a wide variety of cytokines and growth factors that will eventually induce the activation and migration of immune cells, fibroblasts, endothelial cells, smooth muscle cells, and circulating bone marrow derived MSCs (cBM-MSCs) to the wound niche [6-8] (**Fig. 1**).

The inflammation phase initiates a few hours after the wound is given and is fueled by the presence of damage-associated molecular patterns (DAMPs) and pathogen-associated molecular patterns (PAMPs). Neutrophils first and monocyte and

macrophages secondly, infiltrate the wound niche killing pathogens removing debris and damaged extracellular matrix. In this phase, monocytes transform predominately into M1 macrophages (pro-inflammatory) in order to magnify the inflammatory scenario and attract more cells [9].

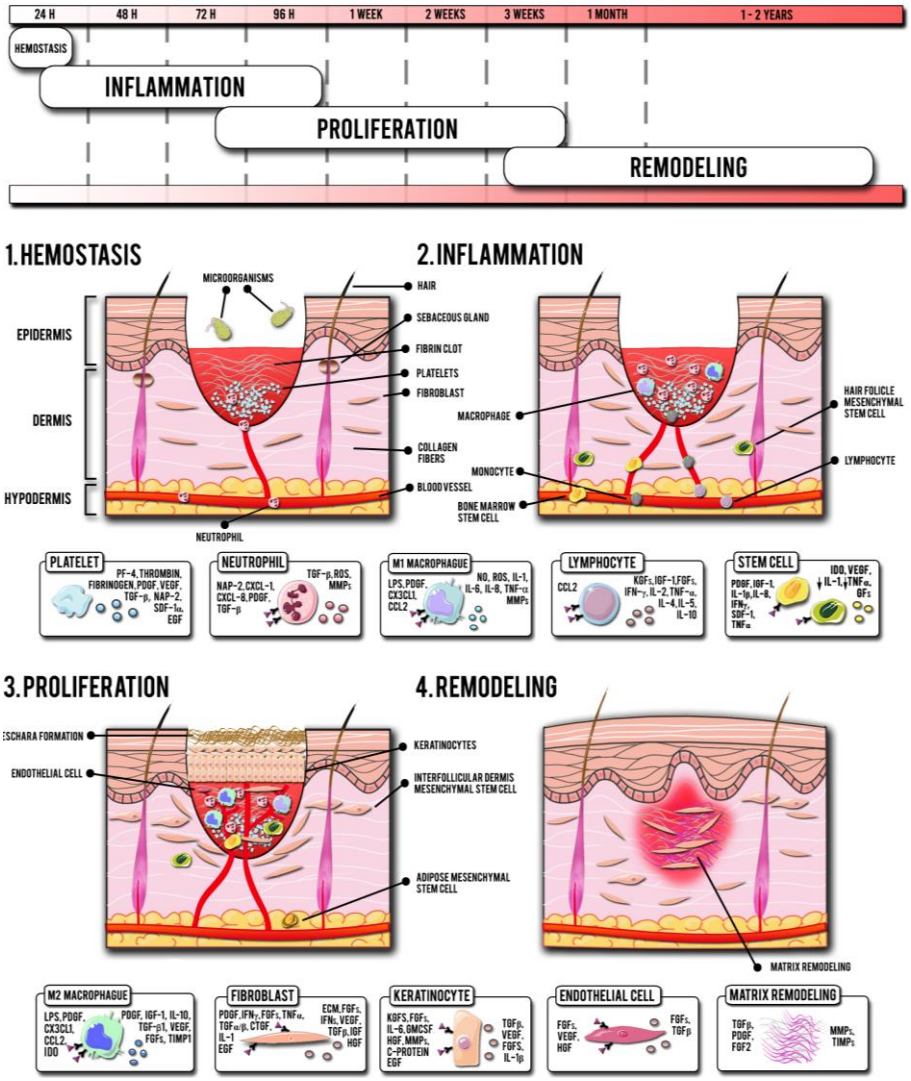

Fig. 1. Wound healing phases: Hemostasis, inflammation, proliferation and remodeling. Cell boxes: the left-handed cytokines and growth factors (GFs) stimulate cells and the right-handed ones are secreted by these cells (Appendix 5) [10].

Lymphocytes — γδ + T cells and αβ + T cells — are the latest cell types that arrive to the wound niche exhibiting important roles in the defense against pathogens and the survival and growth of immune cells, fibroblasts and keratinocytes [10,11]. In the later stage of the inflammation phase, monocytes and M1 macrophages start to polarize into M2 Macrophages (anti-inflammatory) in order to increase cell migration, proliferation and ECM formation. The switching to the M2 profile enable macrophages to release different mediators that will assist in a normal transition to the proliferation phase [12]. The role of MSCs in this stage is crucial exhibiting immunomodulatory, anti-inflammatory and pro-regenerative effects. Both BM-MSCs and hair follicle derived MSCs (HF-MSCs) play an important part on modulating the response of αβ + T cells, monocytes, macrophages, granulocytes and dendritic cells [13-15]. Finally, MSCs are able to produce and remodel ECM, orchestrate angiogenesis and eventually differentiate into different skin cell types [16] (Fig. 1).

After the first days post tissue injury, with the resolution of inflammation, the proliferation phase begins. In this stage of the wound healing the immature tissue will give to the formation of a mature granulation tissue, restoring the vasculature network and covering the denuded wound surface [17]. Fibroblasts have an important task here depositing and remodeling large amounts of ECM to close tissue gaps. On the other hand, this re-epithelialization process requires the migration and proliferation of keratinocytes that will eventually achieve wound coverage, followed by stratification and differentiation to rebuild the skin epidermal barrier [4,10,18]. Here, the neovascularization process reaches a high importance through both angiogenesis and vasculogenesis [19]. In this stage, both BM-MSCs and adipose tissue derived MSCs (AT-MSCs) are directly implicated in the formation of granulation tissue and re-epithelialization. In this sense, MSCs are able to, on the on hand; differentiate into different skin cell types such as keratinocytes and fibroblasts and, on the other hand, release multiple mediators that influence the activation, migration and proliferation of these cell types (Fig. 1) [14,20,21].

Finally, the remodeling phase extends for months or years and is characterized by a decrease in cellular presence and vasculature. Here, fibroblasts, the key players in this phase, act increasing the amount of type I collagen and breaking down disorganized collagen that previously served as a template, manly of type III. Finally, the production of

matrix metalloproteinases (MMPs) and tissue inhibitor of MMPs (TIMPs) will modulate the formation and fate of the final mature tissue (Fig. 1) [22,23].

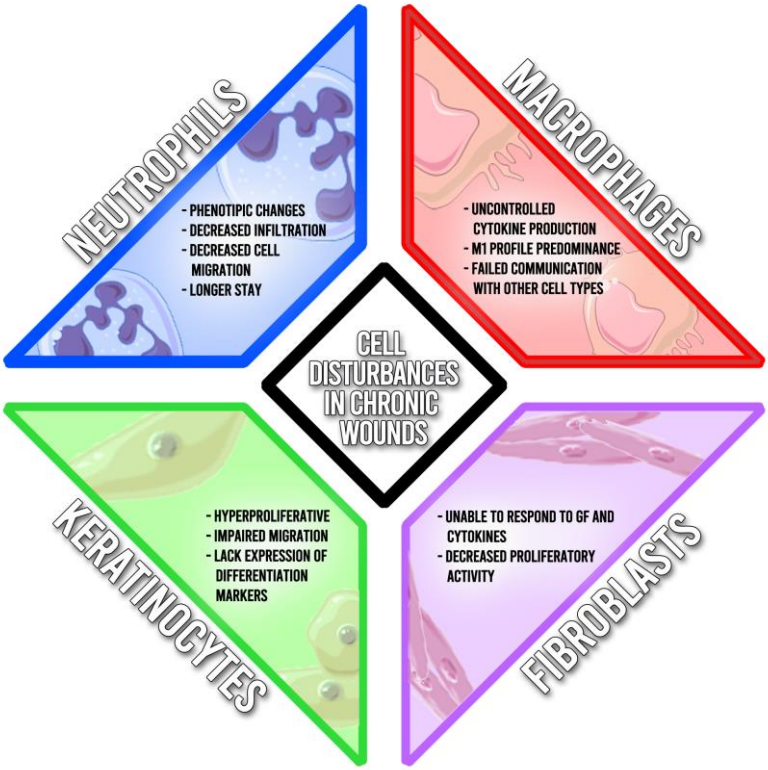

Fig. 2. Cellular disturbances in chronic wounds. (Appendix 6) [24].

Despite a precise and well-orchestrated process of healing and due to different disorders, tissue repair can result insufficient leading to persistent skin damage [2,10]. This is the case of some acute wounds that become stagnant in the hemostasis phase of the normal healing process, usually because of nasal surgeries, deep nasal injuries or as side effects of coagulopathies, metabolic problems, some cancers or genetic disorders [10,25]. For example, in pathologies like severe epistaxis — generally posterior epistaxis —, these wounds can appear repeatedly causing important problems to patients' quality of life and needing a continuous medical monitoring and care [25]. Nowadays, the non-surgical treatment of choice for these acute hemorrhagic wounds comprises the employment of pressure and biomaterial-based strategies for wound

covering and blood absorption — gauze, dressings etc. — [26,27]. However, there is still a lack of treatments that can avoid cauterization or surgery and that reduce blood loss and healing time while increasing patient's quality of life — e.g. discomfort on epistaxis patients when extracting/introducing the gauze or nasal packs —.

On the other hand, some skin injuries can become stagnant in the second phase of the normal wound healing process, the inflammatory phase, causing long-term non-healing wounds or chronic wounds. These wounds are characterized by a constant inflammatory status, impaired angiogenesis, re-epithelialization, and a dysregulated cytokine and growth factor intercommunication due to an elevated protease activity. Inflammatory mediators such as IL-1, IL-6, tumor necrosis factor alpha (TNFα) and MMPs are persistently upregulated whereas the expression of TIMPs appears downregulated [1,10,18]. Due to the impaired intercommunication, different disturbances occur also at a cellular level (Fig. 2). Neutrophils and macrophages show predominately pro-inflammatory phenotypes with an increased stay in the wound niche and inflammatory cytokine secretion [28-30]. On the other hand, fibroblasts and keratinocytes are unable to migrate accordingly to help form the granulation tissue and achieve re-epithelialization [31-34]. All these cellular and molecular disturbances impede a correct deposition of ECM and a proper formation of granulation tissue. Despite the fact that there is currently a wide variety of available treatments for these wounds in the market, there is still a need for more precise and effective therapies that tackle the multiple factors involved in the wound healing process. In this sense, biomaterial-based strategies, in the form of dressings, have been the leading options for the treatment of chronic wounds [24]. However, these biomaterials should provide not only adequate physicochemical and moisture retentive properties, but should also support the healing process, orchestrating the cellular and molecular behavior and modulating the microenvironment of the wound.

Whether the process of healing fails in the first phase (acute hemorrhagic wounds), or in the second phase (chronic wounds), the biomaterial-based approach is the first choice for the treatment of both injuries. Thus, in the last decades numerous biomaterial-based therapies have been developed with multiple functionalities; antibacterial [35], antioxidant [36], pro-coagulant [37], immunomodulatory [38], angiogenic [39] and ECM remodeling properties [40]. However, the treatment of chronic wounds requires a more complex approach that can eventually act at different levels of the healing process. Consequently,

in the current century, the combination of cells with biomaterials has emerged in order to better mimic the native ECM and properly recapitulate the native skin functionality. In this regard, these dressings provide a scaffold with his own bioactive properties that support cell retention while, on the other hand, cells are able to continuously secrete mediators that interact with the wound microenvironment helping to achieve a faster and functional healing [24]. The first of its kind was approved in 1998 by the FDA under the name of Apligraf®. This cell-based dressing was composed of neonatal fibroblasts in a bovine type I collagen scaffold and tried to mimic the dermis of the skin (Skin equivalent) [41]. In the next years, after Apligraf® commercialization, other skin equivalents were approved not only mimicking the dermis, but also the epidermis — employing also keratinocytes — [42]. However, despite this approach was very promising, issues with dressing-rejections and inferior effectiveness, in clinical trials against decellularized ECM-based dressings, impeded their widespread implementation in clinic [43-45].

On the other hand, the development of dressings combining biomaterials with MSCs was growing rapidly due to the demonstrated efficacy of these cells for treating different pathologies with a persistent inflammatory component such as diabetes mellitus, graft vs host disease and Chron´s disease [46]. In this sense, MSCs demonstrated to exhibit unique immunomodulatory and pro-regenerative properties (**Fig. 3**) making them key players for the repair of chronic and inflamed injured tissues. Thus, the combination of MSCs with biomaterials to form MSC-based dressings (MSC-Ds) can not only provide external wound protection, moisture retention and a scaffold for delivery of cell mediators etc., but MSC-Ds can also be considered as niches for MSCs differentiation or stemness preservation [24]. Thus, these MSC-Ds orchestrate the wound closure through the paracrine release of different mediators such as GFs, cytokines and extracellular vesicles (EVs) with a lower risk of rejection than the skin equivalents [47,48]. Recently, different works have demonstrated a great safety and efficacy in the use of MSC-Ds for chronic wound management, however, there is a harsh regulatory pathway and elevated production cost for these cell-based therapies [49]. Thus, despite being a great therapeutic option with promising chronic wound management, these shortcomings could reduce companies' investment in developing such therapies, slowing down their implementation in clinic.

Fig. 3. Effects of MSCs in wound healing (Appendix 6).

Nevertheless, with the growing concern of reducing the carbon footprint and being environmentally respectful in the contemporaneous society, a great number of companies are starting to re-think products sources and processes [50,51]. In this regard, "circular economy" is gaining popularity among a wide number of industries — food, chemistry, construction etc. — as a manner of reduce costs, waste and obtain cheaper raw materials with multiple applicability [52-54]. Thus, by using valorized waste, companies could reduce expenses making the development of new therapies, such as MSC-Ds, cheaper and cost-effective. One of the most interesting industries for waste revalorization to develop health-related therapies is food industry. By-products of the food industry are often discarded while they can be a great source of cheap, scalable and sustainable source of biomaterials [55]. Consequently, ensuring a great network of interconnected health-related industries and research entities with others, such as food industry, can promote the development of cheaper treatments, with a more sustainable approach, helping also to reduce companies' carbon footprint.

Despite the use of a "circular economy" thinking will help to reduce production costs and commercialization times, there will be still a complicated regulatory pathway until production approval. Research with MSCs started more than 30 years ago however, nowadays, only two MSCs-based therapies have received the marketing approval by the European medicines agency (EMA), Holoclar and Darvadstrocel [56]. Consequently, in the past years, a growing number of works have investigated the paracrine signaling of MSCs — that has been stated as the main responsible for their therapeutic potential — to develop cell-free MSC-based therapies [57-59]. Among the bioactive mediators that exhibit pro-regenerative effects, EVs have gained the overall attention. In the form of membrane-surrounded cargoes, EVs carry information in DNAs, RNAs, proteins and lipids in order to mediate intercellular communication [60]. These mediators have demonstrated, as well as their parental MSCs, to have efficacy in tissue repair and in inflammatory related scenarios, among other pathologies [61-63]. EVs are more easily handled, characterized, controlled and stored than MSCs. Nowadays, some clinical trials are being conducted with EV-related products. However, none of the EV-based therapy has received marketing approval yet. Nevertheless, a wide variety of marketed and "under-use" products and therapies present EVs on its composition, under a regulatory blind point, such as platelet rich plasma (PRP) and its derivatives [64] or some ECM-based bioscaffolds [65]. These examples may predict a great therapeutic impact of EVs in the near future of health, with the first marketed EV-based products.

To sum up, biomaterial-based therapies have been stablished as the "gold standard" for the treatment of some acute and chronic wounds. Development of new biomaterials with improved potential under a cheaper and more sustainable way, using valorized by-products, could open the gap for next-generation therapies. However, the complexity of chronic wound healing, in comparison to acute wound healing, requires a step-forward approach by combining MSC-based or derived therapies with biomaterials to fully tackle the different cellular and molecular dysregulations.

2. Methodology

2.1 Materials

The soy protein isolate (SPI) was supplied by ADM Protein Specialties Division (PROFAM 974) and the β-chitin (CH) was extracted from fresh squid pens (Loligo sp.), kindly supplied by a local fish market. The SPI sulphur content and aminoacidic composition were measured by using a Euro EA elemental analyzer and a Biochrom 30+ amino acid analyzer respectively. For extracting the CH, the squid pens were washed with water, and then threated with NaOH (1 M) at a ratio of 1:20 (w/v) under stirring at room temperature for 24 h, in order to avoid the deacetylation of the native CH. After, samples were filter and the solid fraction (CH) was washed with water until neutral pH and finally freeze dryed. As determined by an elemental analysis in a previous study, the amount of C and N present in CH was, respectively, 42.1% and 6.2%. Besides, the average degree of acetylation was 95.9%. As for glycerol (99.01% purity), it was provided by Panreac (Spain) and employed as a plasticizer.

Cell culture conditions

L929 fibroblasts (ATCC, Manassas, USA) were cultured on Eagle's minimum essential medium (EMEM) (ATCC® 30-2003™) supplemented with 10% (v/v) horse serum and 1% (v/v) penicillin–streptomycin. HF-MSCs were isolated and characterized from hair follicles (HFs) as previously described [66] and further cultured in Dulbecco's modified Eagle's medium (DMEM 49166-029, Gibco) supplemented with 10% of fetal bovine serum (FBS, Gibco) and 1% (v/v) penicillin/streptomycin (P/S, Gibco). AT-MSCs (ATCC® PCS-500-011TM) were also cultured under the same conditions. Adult Human Dermal Fibroblasts (HDFs, ATCC® PCS-201-012™) were cultured in fibroblasts basal medium (ATCC PCS-201-030TM) adding the fibroblasts growth kit-low serum (ATCC® PCS-201-041™) and 1% (v/v) penicillin/streptomycin (P/S, Gibco). Human umbilical vein endothelial cells (HUVECs, Lonza® C2517A) were cultured in the EGMTM-2 Endothelial Cell Growth Medium-2 BulletKitTM (Lonza® CC-3162) with 1% (v/v) penicillin/streptomycin (P/S, Gibco). HF-MSCs and AT-MSCs were used at passages from 5 to 9 for EVs isolation. HDFs were used at passages 3 to 7. HUVECs were used at passages 3 to 7. Cells were incubated in a humidified incubator at 37 °C under a 5% CO2 atmosphere. Phosphate buffered saline (PBS) pH 7.4 (Gibco, 11593377) was used for cell culture.

Blood obtention

Blood was acquired from healthy volunteers according to the protocols approved by the Ethics Committee for Researching Involving Biological Agents & GMOs (Procedure number: M30/2021/257) and the Ethics Committee for Research Involving Human Beings of the University of the Basque Country (Procedure number: M10/2021/256).

2.2 Preparation of the SLS

Firstly, we mixed 5 g of SPI with 30 wt % CH (based on SPI dry basis) and 125 mL of distilled water were added. Then, we adjusted the pH to 10 with NaOH (1 M) before heating the solution at 80 ^{o}C for 30 min under magnetic stirring. Afterwards, we added 30 wt % glycerol (based on SPI dry basis) to the solution. It was heated for another 30 min at the same conditions to obtain a homogenous blend. Finally, the blend was poured into molds, kept in a freezer at −22 ^{o}C for 48 h and, eventually, freeze-dried for 72 h to obtain the SLS. Next, according to further assays, we cut the SLS with a hollow punch into discs with different diameters. To study the effect of a previous conditioning step of the SLS on the different parameters, we divided samples in 3 groups: lyophilized SLS, that did not undergo any previous conditioning step; hydrated SLS, which were immersed into PBS for 5 min; dialyzed SLS, which were immersed into 1.6 L of Milli-Q water under constant stirring and refreshed twice. Both the hydrated and the dialyzed samples underwent a final freeze-drying process in order to be used in a dried state.

The SLS were compared with a standard gauze (Medicomp® 5 x 5 cm, Hartmann bv, Nijmegen, The Netherlands) and with Merocel® (MC) (Medtronic Xomed, Jacksonville, Fla.).

2.3 Morphology, XPS and ATR-FTIR analysis

We studied the morphology of the SLS, gauze and MC surface by using a Hitachi S-4800 field emission scanning electron microscope (FE-SEM) (Hitachi High-Technologies Corporation, Tokyo, Japan) at a beam accelerated voltage of 5 kV. SLS, gauze and MC were cut into discs of 8 mm diameter, mounted on a metal stub with an adhesive tape and coated with gold under vacuum (JFC-1100) in an argon atmosphere prior to testing.

Furthermore, we studied the SLS by atomic force microscopy (AFM) under ambient conditions. We obtained AFM images using a scanning probe microscope (Nanoscope IIIa Multimode™, Bruker). We also employed Tapping mode in air using an integrated tip/cantilever at 200–400 kHz resonance frequency, 0.6–1.0 Hz scan rate and 20–80 N/m force constant.

X-ray photoelectron spectroscopy (XPS) was performed in a SPECS spectrometer using a monochromatic radiation equipped with Al Kα (1486.6 eV). The binding energy was calibrated by Ag 3d5/2 peak at 368.28 eV. All spectra were recorded at 90° take-off angle. Survey spectra were recorded with 1.0 eV step and 40.0 eV analyzer pass energy and the high-resolution regions with 0.1 eV step and 20 eV pass energy. Moreover, all core level spectra were referred to the C 1s peak at 284.6 eV. We analyzed spectra using the CasaXPS 2.3.19 software, and peak areas were quantified with a Gaussian–Lorentzian fitting procedure.

We also used attenuated total reflectance Fourier-transform infrared (ATR-FTIR) spectroscopy to identify the characteristic functional groups of the SLS. Measurements were performed with a Nicolet Nexus FTIR spectrometer, equipped with a MKII Golden Gate accessory, Specac, with a diamond crystal as ATR element at a nominal incidence angle of 45° with a ZnSe lens. We recorded measurements in the 4000-750 cm-1 region, using 32 scans at a resolution of 4 cm-1.

2.4 Degradation studies

In order to determine the weight loss due to hydrolytic and enzymatic effect, lyophilized SLS of 8 mm diameter were weighed and subsequently immersed in different solutions. We used 2 mL of PBS (completely filled) for the hydrolytic degradation and a collagenase P solution (Sigma-Aldrich, Spain), at a concentration of 0.5 mg/mL in culture medium, for the enzymatic degradation. Finally, we incubated all SLS at 37 °C. At different time points, samples were removed, lyophilized and weighed again to determine the remaining weight (%).

2.5 Pore analysis, porosity and swelling capacity

Pore sizes were determined from SEM micrographs using Image J software. We approximately measured up to 100 pores, randomly selected from different samples. To

determine the porosity of the scaffolds, we performed a liquid displacement method using ethanol 98% as the liquid medium, because of its ability to permeate through scaffolds without inducing matrix swelling or shrinkage. 24 SLS were immersed into a known volume (*V1*) of ethanol and degassed for 5 min with a vacuum pump. The total volume of ethanol and ethanol-impregnated SLS was recorded as *V2*. Finally, we removed the ethanol-impregnated SLS, and the residual volume of ethanol was recorded as *V3*. The porosity (ε) of the SLS was calculated with the following equation:

$$\varepsilon\,(\%) = \frac{V_1 - V_3}{V_2 - V_3} \times 100$$

In order to calculate the swelling curve, different pre-weighed SLS of 8 mm diameter were immersed into 5 mL of PBS at room temperature and also weighed again at various time points (2 s, 0.5, 1.5, 5, 10, 20, and 30 min).

2.6 Cytotoxicity assays

We performed this assay following the ISO 10993-5:2009 guidelines for biological evaluation of medical devices. Cytotoxicity assay was performed either by direct contact of the SLS with the cells (direct cytotoxicity) or by exposing the cells to a lixiviate fluid of these SLS (indirect cytotoxicity).

In the direct cytotoxicity assay, we used SLS of 8 mm diameter and measured the L-929 fibroblasts viability employing CCK-8 reagent (Sigma-Aldrich, Spain). Briefly, we seeded 35,000 cells/well in 500 μL/well of EMEM complete medium in a 24 well plate. Subsequently, we incubated the cells for 24 h at 37 ^{o}C. Then, we aspirated the medium and added 300 μL of fresh medium, placing the SLS in direct contact with the bottom of the well. After 48 h of incubation, we removed the SLS, and the medium was replaced by 370 μL/well of CCK-8 solution in medium (1:11) and incubated for 4 h. Afterwards, we read the absorbance with a plate reader (Infinite® 200 PRO series, Tecan Trading AG, Männedorf, Switzerland) at 450 nm, using 650 nm as the reference wavelength. We used cells without SLS exposure as a control group (100% of viability).

In the indirect cytotoxicity assay, we exposed L-929 fibroblast to a lixiviate fluid of SLS (incubating at 37 ^{o}C for 24 h in culture medium at constant stirring following the ISO 10993-5:2009). We utilized a Benchtop OrionTM 2-star pH meter (Fisher Scientific SL,

Madrid, Spain) and an Osmomat 030 (Genotec, Berlin, Germany) to respectively measure both the pH and the osmolarity of the lixiviate fluid, using culture medium without SLS as control and fresh medium without the incubation process as "fresh". Firstly, we seeded 5,000 cells/well in a 96 well plate with 100 μL/well of medium and incubated them for 24 h at 37 ^{o}C. Then, we replaced the medium by 100 μL/well of the collected lixiviate fluid, and the plate was subsequently incubated at 37 ^{o}C for 24 h. Finally, the lixiviate fluid was removed, and 110 μL/well of CCK-8 solution in medium (1:11) was added. After 4 h of incubation, we read the absorbance as already described for the direct cytotoxicity. Cells with lixiviate fluid without SLS (culture medium incubating at 37 ^{o}C for 24 h under stirring equal as the other lixiviates) were used as control group (100% of viability).

2.7 In vivo biocompatibility of the SLS

In order to understand the biological reaction to the implanted biomaterials, we divided SLS of 6 mm diameter in 4 different groups: lyophilized, hydrated, dialyzed and lipopolysaccharide (LPS) soaked SLS as a negative control group. We immersed all the SLS in PBS for 5 min before being implanted, except the LPS SLS that were contrastingly immersed in a 100 ng/mL LPS in PBS solution. We conducted all the experiments following the protocols approved by the Institutional Ethical Committee for Animal Experimentation of the University of the Basque Country (Procedure number: M20_2018_004). We subcutaneously implanted the SLS from the aforementioned four groups in male 8-week-old C57BL/6 mice for 14 days (one SLS per mouse, 3 mice per group). A two-week's time point was selected in the present study because it has been well established as suitable time to resolve both immune and fibrotic responses to implanted materials, in C57BL/6 mice [67,68].

In the procedure, we anesthetized mice with isoflurane (Isoflo®, Esteve, Spain) and used a scalpel to make a small incision (< 1 cm) in the central dorsal surface. We employed blunt forceps to create a pocket for the SLS in the subcutaneous space. After implantation, we closed the wounds with two sutures. Next, we monitored and housed mice for 14 days. Moreover, we did not observe signs of discomfort after surgery throughout the study.

Histological analysis

After 14 days, we euthanized mice by CO2 asphyxiation. We made different incisions, excising the SLS (and surrounding tissue) and fixed in 3.7% paraformaldehyde overnight. Then, the biopsies were bisected, embedded in paraffin and sectioned in layers of a thickness of 5 μm. We stained the slices by hematoxylin-eosin (H&E) and Masson's trichrome (MT), using standard procedures. Images were analyzed by a blinded histopathologist, utilizing the QuPath analysis software (Centre for Cancer Research & Cell Biology at Queen's University, UK) to evaluate the foreign body reaction (FBR) to the subcutaneous implant. All the results have been normalized by a blinded histopathologist vs the weight of each scaffold. The cellular response was determined following a scale in which every cellular FBR received a value within a range from 0 to 4: 0, absence of macrophages (MC) or polimorphonuclear neutrophils (PMNN); 1, very low presence of MC or PMNN; 2, low presence of MC or PMNN; 3, abundant presence of MC or PMNN; and 4, very abundant presence of MC/PMNN.

2.8 Mechanical characterization

The mechanical properties of the dry SLS, gauze and MC were tested by compression test and cyclic compression test. An Instron 5969 mechanical tester — equipped with a 50 N load cell — was used at a compressive rate of 0.5 mm s^{-1} up to 70% strain. As MC is commercialized in lyophilized form, it was expanded before the test, by wetting and completely drying it off. Several parameters were calculated in order to compare the mechanical properties of the materials:

The maximum stress of each cycle relative to the maximum stress of the first cycle was calculated as follows:

$$Relative\ stress\ (\%) = \frac{Stress\ (cycle\ x)}{Stress\ (cycle\ 1)} x100$$

Young's modulus was calculated for all the strains of the first cycle of each biomaterial, using the following equation:

$$Young's\ modulus\ (kPa) = \frac{Stress\ (kPa)}{\left[Strain \frac{\%}{100}\right]}$$

Damping coefficient was calculated by means of the stress-strain curves of the materials, both for cycle 1 and for cycle 10. The following equation was used:

$$Damping\ coefficient = \frac{D}{U}$$

where *D* is the dissipated energy (area between the loading and unloading curves) and *U* is the total input energy (area under the loading curve). All the areas under the curve where calculated using the software GraphPad Prism 8.0.1.

Besides, an expansion force test was performed, hydrating samples of dry materials and recording the upwards stress displayed by the expansion of the material during water absorption.

2.9 Blood studies

Whole blood clotting *in vitro*

Hemoglobin content of the samples was quantified using a Hemoglobin Assay Kit (Sigma-Aldrich, USA), by measuring absorbance of the samples (*Is*) with a plate reader (Infinite® 200 PRO series, Tecan Trading AG, Männedorf, Switzerland) at 400 nm.

For the whole blood clotting test, citrated whole blood — 9:1 whole blood to 3.8% sodium citrate — was obtained from a healthy human donor. First, 0.2 mL of the citrated whole blood was added to preheated (30 min at 37 °C) samples of the materials disposed in a 24 well plate. After this, 20 µL of $CaCl_2$ (0.2 M) were added to start coagulation. The plate with the materials was incubated under 30 rpm agitation for 10 min at 37 °C. Afterwards, 2 mL of deionized water were added in each well to hemolyze the erythrocytes that were not within the clot formed in the material. The deionized water containing the non-adhered and hemolyzed erythrocytes was collected and its hemoglobin content was quantified. 5 µL of $CaCl_2$ (0.2 M) and 50 µL of citrated whole blood were added to 750 µL of deionized water, and the absorbance of this solution was used as the reference value (*Ir*). The absorbance of an empty well was also measured (*Io*). Blood Clotting Index (*BCI*) of each sample was calculated using the following equation:

$$BCI\ (\%) = \frac{(Is - Io)}{(Ir - Io)} x\ 100$$

With the purpose of visually evaluating the clotting capacity of each material, 150 mg of each material were disposed in Eppendorf tubes, subsequently adding 500 µL of

citrated whole blood and 500 μL of $CaCl_2$ (10 mM). After incubating the Eppendorf tubes for 1 min at 37 °C, they were turned upside down and gently shaken to observe the formed clots

Hemolysis assay *in vitro*

For the assessment of hemocompatibility in vitro, citrated whole blood — 9:1 whole blood to 3.8% sodium citrate — from a healthy donor was obtained and diluted 1:5 in normal saline. Samples of each material were disposed in a 24-well plate. Diluted whole blood was added to each sample in an amount of the 80% of each material's swelling capacity. The plate was incubated for 1 h at 37 °C. Samples were moved to conical centrifuge tubes and centrifuged for 10 min at 3,000 rpm. The supernatant of each sample was collected and its hemoglobin content was quantified as described before. 150 μL of whole blood was added to deionized water and to normal saline, in order to use these solutions as positive (*Ir*) and negative (*Io*) controls, respectively. Hemolysis rate was calculated using the following equation:

$$Hemolysis\ (\%) = \frac{(Is - Io)}{(Ir - Io)} x\ 100$$

Erythrocyte adhesion *in vitro*

To evaluate erythrocytes adhesion to the material, citrated whole blood — 9:1 whole blood to 3.8% sodium citrate — was collected from a healthy donor. Samples of each material were cut and each sample was placed in a Petri dish. Citrated whole blood was added to each sample in an amount of the 80% of each material's swelling capacity, and they were incubated for 5 min at 37 °C. Next, 5-10 mL of deionized water were gently added by the edge of the dish until the water touched the sample and blood started to flow. More deionized water was added until a total volume of 50 mL for each sample. Each material was carefully moved to a clean Petri dish, and the liquid in each old Petri dish, — containing the erythrocytes that could not adhere to the sample —, was collected. The hemoglobin content of this solution was quantified as described before. This measurement accounts for hemoglobin outside the material, that is, the erythrocytes that could not adhere to the material.

Afterwards, hemoglobin within the materials was measured, which accounts for the amount of erythrocytes adhered to each sample. 10 mL of deionized water were added straightly on the material — so that the previously adhered erythrocytes would be released — and the hemoglobin content in the resultant solution was quantified as described before.

For both the hemoglobin outside and within the material, a positive control was prepared by mixing 200 μL of blood and 50 mL of deionized water. Hemoglobin concentration (mg dL^{-1}) of each sample was calculated using the following equation provided by the Hemoglobin Assay Kit, and results of each sample were normalized against the blood volume added to the control group:

$$[Hemoglobin] = \frac{(Is - Io)}{(Ir - Io)} x\ 100 \frac{mg}{dL} x\ df$$

where *Is* is the absorbance of the tested solution; *Io* is the absorbance of the blank (water); *Ir* is the absorbance of the calibrator provided in the Hemoglobin Assay Kit; 100 mg/dL is the concentration of the diluted calibrator; *df* is the dilution factor, which was calculated for each sample depending on the volume of blood and deionized water added.

Citrated whole blood was also added to samples of each material and the adhesion of erythrocytes was visually evaluated using SEM micrographs.

2.10 Platelet adhesion *in vitro*

Adhesion of platelets to the materials was studied through a Lactate Dehydrogenase (LDH) Assay Kit (Sigma-Aldrich, USA), which allows to quantify platelet adhesion by measuring the LDH released by platelets when they are lysed, according to a reported method [69]. Briefly, citrated whole blood — 9:1 whole blood to 3.8% sodium citrate — was obtained from a healthy donor. After centrifuging it at 480 g for 10 min at 4 °C with 4 a/d, PRP was obtained. The serum above the buffy coat was collected from the centrifuged blood samples and kept in citrated tubes. Samples of each material were disposed in a 24-well plate and PRP was added to each sample in an amount of the 80% of each material's swelling capacity, and they were incubated for 30 min at 37 °C. Normal saline was gently added to each well until the samples were immersed, so that the non-

adhered platelets could be removed from the material, and all samples were moved to a new 24-well plate. 1 mL of Triton X-100 1%-PBS was added straightly on the material, in order to lyse the platelets that had adhered to the material. After incubation for 1 h at 37 °C, each solution of Triton and lysed platelets was collected and LDH content was measured according to the protocol provided by the manufacturer (Sigma-Aldrich, USA) of the LDH Kit. To prepare the negative (Io) and positive (Ir) controls, 200 µL of PRP were added to 1 mL of PBS and Triton X-100 1%, respectively. Absorbance of the lysed platelets of each samples (Is) were measured with a plate reader (Infinite® 200 PRO series, Tecan Trading AG, Männedorf, Switzerland) at 400 nm, and normalized against the PRP volume added to the controls. LDH release (%) relative to the positive control was calculated using the following equation:

$$LDH\ release\ (\%) = \frac{(Is - Io)}{(Ir - Io)} x\ 100$$

PRP was also added to samples of each material and the platelet adhesion was visually evaluated using SEM micrographs.

2.11 *In vivo* hemostatic efficacy

To evaluate the hemostatic efficacy in vivo, a rat-tail amputation model was used. This experiment was conducted following the protocols approved by the Institutional Ethical Committee for Animal Experimentation of the University of the Basque Country (Procedure number: M20/2021/362). Wistar rats — with weights between 250 - 300 g (Janvier Labs, Le Genest-Saint-Isle, France) — were anesthetized with isoflurane (Isoflo®, Esteve, Spain), and 2.5 cm from the end of their tail was cut using a scalpel. The tail was immediately placed in air for 10 s to guarantee normal blood loss, after which the wound was brought into direct contact with the corresponding pre-weighed material, holding it with a pre-weighed gauze. The wound was uncovered every minute to check if bleeding persisted. For this reason, bleeding time (min) was assessed by assigning a score to each period at which bleeding ceased, as follows: 0 - 3 min: 1; 3 - 6 min: 2; 6 - 9 min: 3; >9 min: 4. Therefore, a lower bleeding time score represents a faster hemostatic effect. The blood-impregnated samples were weighed again to calculate total blood loss (g).

2.12 MSC-SLS formulation, analysis and viability measurement

To prepare the MSC-SLS, MSCs — both AT-MSCs (AT-SLS) and HF-MSCs (HF-SLS) —were seeded in 8 mm diameter SLS in a volume equivalent to the 80% of swelling of each SLS. Ratios of MSCs seeding were 25,000 and 50,000 cells per mg of SLS with and average weight of 10 mg per unit. After 6 h of incubation, the MSC-SLS were placed in contact with the culture media through the wound-like transwell system as depicted in Fig.1. Following, the MSC-SLS were incubated for 3 and 7 days and the supernatants were taken for secretome analysis. At these time-points, the MSC-SLS were rinsed with PBS and stained with Calcein AM (Thermofisher, Invitrogen C1430) following manufacturer´s protocol. After that, MSC-SLS were visualized in a Nikon epi-fluorescence microscope equipped with a DSD2 confocal modulus (Nikon) to analyze the MSCs behaviour and viability.

Soluble secretome analysis

The cytokine secretion analysis was performed by using a custom Quantibody® ELISA array (TebuBio). Briefly, the supernatants from 7 days MSC-SLS incubation were studied for the secretion of Angiogenin-1, bFGF, EGF, KGF, HGF, IGF-I, VEGF, PDGF-AA, IL-1 ra, IL-6, IL-8, MCP-1, RANTES, SDF-1α and TGF-β1. First, the slides were placed at room temperature for 2 h. Then, wells were washed for 30 min with 100 μL of sample diluent. After discarding the diluent, 100 μL of samples and standards were added and slices were incubated for 2 h under stirring. Then, wells were washed five times with wash buffer I under stirring and five more times with wash buffer II. After that, 80 μL of detection antibody were added for 2 h, washed as mentioned and incubated, protected from the light, with 80 μL of Cy3 dye for 1 h. Finally, the slices were washed and sent to the manufacturer for the analysis. A custom standard curve was prepared for each slide following manufacturer's instructions with the standard mixture provided.

2.13 Evaluation of protection against ROS-induced cytotoxicity

To measure the protective effect of the MSC-SLS on HDFs under a highly oxidative environment, 10,000 cells/well were seeded in a 96-well plate for 24h. After that, two approaches were followed. In the first experiment, 30 mM of H_2O_2 were mixed 1:1 with the supernatant of 24 h incubated MSC-SLS for 2 h. Then, 100 μL the mixture were added into the wells and incubated for 30 min. After that, wells were washed twice with PBS and incubated for 6 h with 100 μL of serum free HDFs medium. Finally, wells were washed

twice with PBS and incubated for 4 h with a 1:10 mixture of CCK8 (Merck, 96992) in complete medium. Absorbance was read with a plate reader (Infinite® 200 PRO series, TecanTrading AG) at 450 nm, using 650 nm as the reference wavelength. In the second experiment, cells were pretreated with 100 μL of the supernatant of 24 h incubation MSC-SLS in DMEM for 6 h. After washing twice with PBS, 100 μL of 15 mM of H_2O_2 in serum free media were added for 30 min. Thereafter, wells were washed twice with PBS and incubated for 6 h with 100 μL of serum free HDFs medium. Finally, wells were washed twice with PBS and incubated for 4 h with a 1:10 mixture of CCK8 in complete medium and the absorbance was read at 450 nm, using 650 nm as the reference wavelength. Supernatants of 24 h incubated SLS and complete HDFs medium were used as controls. Cells without H_2O_2 were used as positive controls

2.14 Evaluation of protection against hyperglycaemia-induced cytotoxicity

For the evaluation of the protective effect of MSC-SLS over HDFs hyperglycemia-induced cytotoxicity, 10,000 cells/well were seeded in a 96-well plate for 24 h. Then, cells were washed with PBS twice and incubated with 100 μL treatments for 6 h. Supernatants of 24 h incubated MSC-SLS or SLS were used. HDFs complete medium was used as a positive control and serum free HDFs medium was used as blank group. After the incubation time, cells were washed twice and 100 μL of serum free media with 150 μM of glucose (Merck, 108337) were added. After 24 h, cells were washed twice, incubated for 4 h with a 1:10 mixture of CCK8 in serum free medium and the absorbance was read at 450 nm, using 650 nm as the reference wavelength. This process was repeated at 48 h and at 72 h. Cells without high glucose treatment were used as non-cytotoxic control. Images of cells at 72 h were taken using an optical microscope. Cell viability at 72 h was also observed with calcein AM/Ethidium homodimer and each well was photographed by a Nikon epi-fluorescence microscope equipped with a DSD2 confocal modulus (Nikon, Japan).

2.15 *In vitro* wound healing evaluation

To evaluate whether the MSC-SLS can promote the migration of HDFs and HaCaTs, an in vitro wound healing assay or scratch assay was performed. Briefly, 5×10^5 cells/mL of HDFs and $1{,}5 \times 10^6$ cells/mL of HaCaTs were seeded on each part of the two-well

IBIDI culture inserts® in 6-well plates (IBIDI, 80209) and incubated for 8 h. PBS outside the inserts was added to minimize the evaporation of medium. Secondly, both wells were washed with PBS and serum-free medium was added overnight to minimize the cell proliferation. After that, the inserts were extracted creating the wound and wells were washed with PBS to discard the detached cells. Thereafter, the wound-like transwell system was disposed and the MSC-SLS were placed on each well with 1mL of serum-free medium (HDFs) or 1:6 medium in serum-free medium (HaCaTs) and incubated for 48 h. SLS without MSCs and wells without treatment were used as controls. At pre-defined time-points — 0 h, 4 h, 6 h, 8 h, 12 h, 24 h, 36 h and 48 h — images of the closing area were taken by an optical microscope (Nikon). The migration area between wound edges was calculated by using the ImageJ software and the wound closure was calculated by the following equation where *So* and *Sn* represent the initial wound area and wound area at different time points, respectively:

$$Wound\ closure\ \% = \frac{So - Sn}{So} x100$$

2.16 Tube formation assessment

Firstly, 15 μL of Matrigel® (Corning, 356231) were added into the μ-Plate angiogenesis 96-well plates (IBIDI, 89646) and let polymerize for 30 min at 37 °C. Then, HUVECs were seeded over the matrix bed at a density of 4.5×10^5 cells/mL in 70 μL of MSC-SLS supernatants — incubated 24 h, 48 h, 96 h and 168 h using the wound-like transwell system in DMEM medium — and 24 h supernatant of SLS in the matrigel bed. Complete DMEM medium incubated 24 h was used as control and supplemented HUVECs medium was used as positive control. After 24 h of incubation, HUVECs where stained with calcein AM and each well was photographed by a Nikon epi-fluorescence microscope. The tube formation was analyzed using Image J Software. The VEGF release by the MSC-SLS at 24 h, 48 h, 96 h and 168 h of incubation was measured using the VEGF Quantikine ELISA (R&D Systems, DVE00) following manufacturer's instructions.

2.17 *In vivo* wound healing assessment

Animals

The *in vivo* studies were performed with 8-week-old male db/db (BKS.Cg-m+/+Leprdb/J) mice (Janvier laboratories). All the experiments followed the procedure number M20/2019/258 approved by the University of the Basque Country ethical committee for animal experimentation. Animals were housed individually with ad libitum access to water and food and a light-dark cycle of 12 h.

Wound healing assay

Firstly, mice were anesthetized with isoflurane (Isoflo®, Esteve) and completely peeled their dorsal hair. After that, two 10 mm diameter silicon rings were sutured on each side of the back using a 3–0 nylon suture in order to avoid wound contraction. Then, two full thickness wounds were made extending through the panniculus carnosus, using an 8 mm diameter scalpel (AcuPunch, Acuderm). Wounds were well-cleaned with saline and treatments were applied over the wounds and covered with one layer of petrolatum gauze (Tegaderm®, 3M) and two adhesive tapes. Mice were then divided into 4 groups: (i) untreated control, (ii) SLS group, (iii) AT-SLS group and (iv) HF-SLS group. At day 7 treatments were removed, wounds cleaned and new treatments were applied. Half of the mice were sacrificed by CO_2 inhalation at day 7 and the remaining ones at day 15.

Evaluation of wound healing

The macroscopic closure of wound was evaluated throught all the experiment. Thus, on days 8 and 15 wounds were photographed using a meter for post analysis scaling. The wound area was measured using Image J software. Finally, the wound closure percentage was calculated using the following equation:

$$Wound\ closure\ \% = \frac{Final\ wound\ area\ (px2)}{Initial\ wound\ area\ (px2)}\ x\ 100$$

Histological analysis of wound healing

On days 8 and 15, mice were sacrificed to obtain the wound necropsies. The wound and surrounded tissue were fixed with 3.7% paraformaldehyde for 24 h and ethanol until processing. After that, the necropsies were bisected, embedded in paraffin and sectioned in 5 μm slices. Finally, tissues were stained by hematoxylin-eosin (H&E) for overall wound analysis and by Masson´s Trichrome for collagen deposition analysis. All measurements were performed by a blinded histopathologist.

The analysis of the re-epithelialization process was performed following Sinha. et al. scale [70]. Briefly, each wound was classified within a scale between 0 to 4 in which: 0, only the wound edges was re-epithelialized; 1, less than half of the wound was re-epithelialized; 2, more than half of the wound was re-epithelialized; 3, the entire was re-epithelialized with irregular thickness; 4, wound completely re-epithelialized with normal thickness.

The wound maturity status and the resolution of inflammation was measured using the scale described by Garcia-Orue et. al [71]. Briefly, wounds were rated from 0 to 4 as followed. 0, no sign of inflammation. 1, acute inflammation in which the formation of fibrin, the pyogenic membrane and the migration of neutrophils and leucocytes was observed. 2, diffuse acute inflammation in which the pyogenic membrane is almost non-existent and there was formation of granulation tissue and angiogenesis. 3, chronic inflammation with an observed fibroblasts proliferation and predominance. 4, resolution and healing, no chronic inflammation observed and occasionally round cells can be found.

Finally, the collagen deposition was measured by using Image J software. Briefly, images were deconvoluted using the Masson´s trichrome option of "colour deconvolution 2" plugin. The blue channel was selected, the treshold was adjusted at 114 and the percentage of collagen was measured with the same parameters for all wounds.

2.18 EVs isolation and characterization

EVs isolation

All relevant data regarding the production, isolation and experimental section have been submitted to the EV-TRACK knowledgebase (EV-TRACK ID: EV210337). EVs were isolated and purified from the supernatant of HF-MSCs and AT-MSCs. At 70-80% of confluency, cells were washed thrice with PBS and the culture medium was replaced with EVs-depleted DMEM. After 72 h of production, the culture medium was collected and new medium was added. After three collections, cells were trypsinized, counted and further re-cultured. The collected medium was first centrifuged at 2,000 × g for 10 min at 4 ^{o}C to discard cell debris and then, freeze at -80 ^{o}C until the isolation and purification was given. All further centrifugation processes were performed at 4 ^{o}C. In brief, thawed

culture supernatants were differentially centrifuged at 10,000 × g for 30 min to obtain medium-large EVs (m-lEVs) — pellet 10K (P10K) — and the resulting supernatants at 100,000 × g for 90 min — pellet 100K (P100K) — to obtain small EVs (sEVs). To reduce contaminating proteins, all pellets (P10K and P100K) were re-suspended in ice-cold PBS and ultracentrifuged again. Finally, both pellets were immediately re-suspended in 120 μL of ice-cold PBS and freeze at -80 ºC until use.

Nanoparticle tracking analysis

Particle concentration and size distribution within EV preparations was analyzed using the nanoparticle-tracking analysis (NTA), by measuring the rate of Brownian motion in a NanoSight LM10 system (Malvern Panalytical, Malvern, UK). The system was equipped with a fast video-capture and particle-tracking software. NTA post-acquisition settings were the same for all measurements. Each video was analyzed to give the mean, mode, and median vesicle size, as well as an estimate of the concentration. For measurement, original EVs suspension were diluted 1:100 with PBS and a volume of 500 μL were loaded on the camera, and 3 consecutive video recording of 40 seconds each were taken for every sample quantified.

Western blotting

PBS-resuspended EVs or cell lysates were mixed with 4×NuPAGE LDS Sample Buffer (Thermo Fisher Scientific, Waltham, MA, USA). The samples were incubated for 5 min at 37 °C, 65 °C, and 95 °C, and separated on 4–12% precast gels (from Thermo Fisher Scientific, Waltham, MA, USA), at a concentration of 5 μg/lane (Bradford determination). The proteins were transferred into PVDF membranes with the iBLOT2 system (Thermo Fisher Scientific, Waltham, MA, USA). Antibodies employed were: mouse monoclonal antibody against CD9 #209302 (R&D), Grp78 #40 (BD, East Rutherford, NJ, USA), CD13 #3D8 (Santa Cruz Biotechnology, Dallas, Tx, USA), EEA1 #14 (BD, East Rutherford, NJ, USA), CD63 #H5C6 (DSHB, Iowa City, IA, USA), LAMP1 #H4A3 (DSHB, Iowa City, IA, USA), alpha tubulin 1 #DM1A (Santa Cruz Biotechnology, Dallas, Tx, USA), CD81 #JS81 (BD, East Rutherford, NJ, USA), rabbit antibody against COX IV #4850 (Cell Signaling Technologies, Danvers, Ma, USA). All the primary antibodies were diluted 1:1000. Horseradish peroxidase (HRP)-conjugated secondary antibodies anti-mouse, rabbit and

goat, were purchased from Jackson ImmunoResearch Lab, (West grove, PA, USA) to ensure minimal cross-reactivity across species.

Bead-based multiplex flow cytometry assay

All isolated EVs were subjected to a surface-marker characterization by using a flow cytometry bead-based multiplex analysis (MACSPlex Exosome Kit, human, Miltenyi Biotec. 130-108-813). Samples were processed according to manufacturer's protocol. Briefly, 2 μg of EVs were mixed with 120 μL of manufacturer's buffer and then, 15 μL of the MACSPlex Exosome Capture Beads were added. Then, 15 μL of the detection antibody cocktail — 5 μL of each MACSPlex exosome detection reagent CD9, CD63, CD81 — were added. After that, samples were incubated 1 h at room temperature, protected from the light, on rotation — 450 rpm —. Next, 500 μL of MACSPlex buffer were added and samples were centrifuged at 3000 $\times$ g for 5 min. Subsequently, 500 μL of supernatant were discarded and another 500 μL of buffer were added. Samples were incubated for 15 min at room temperature on rotation, protected from the light and then centrifuged 5 min at 3000 $\times$ g. Finally, 500 μL of supernatants were discarded and approximately 150 μL of samples were re-suspended and used for the analysis. The flow cytometry analysis was performed using the MACSQuant® Analyzer 10 (Miltenyi Biotec) and results were processed with the MACSQuant Analyzer 10 software (Miltenyi Biotec). The 39 single bead populations were gated to determine the APC signal intensity on each bead population and the median fluorescence intensity (MFI) for each capture bead was measured. For each population, background was corrected by subtracting the respective MFI values from non-EVs controls that were treated exactly like the EVs-samples. Furthermore, values of the corresponding isotype control were also subtracted. Only positive markers are shown in the graphics.

Cryo electron microscopy (Cryo-EM)

EVs (3-5 μL) were spotted on glow-discharged lacey grids and cryo-fixed by plunge freezing at -180 ^{o}C in liquid ethane with a Vibrobot (FEI, The Netherlands). Grids were observed with a JEM-2200FS/CR TEM (JEOL, Japan), operating at 200 kV. Image measurements were performed with Image J software and between 80-120 single EVs were measured on each group for size and protein-decoration analysis.

2.19 *In vitro* wound healing evaluation of EVs

To evaluate whether the EVs can promote the migration of HDFs an in vitro wound healing assay or scratch assay was performed. For that, HDFs were seeded — 70 μL at a density of $5x10^5$ cells/mL — in each side of the 2 well IBIDI culture inserts® in 24-well plates and subsequently were incubated for 8 h. Secondly, the culture medium was aspired and serum-free medium was added in order to minimize the cell proliferation. After an overnight incubation, culture inserts were extracted and the scratch was performed. Then, HDFs were washed with PBS, EVs were administered — $2.5x10^9$ EVs/mL of P10K and $1x10^{10}$ EVs/mL of P100K — in 300 μL of serum-free medium and cells were incubated for 48 h. At pre-defined time-points — 0 h, 6 h, 12 h, 24 h, 36 h and 48 h — images of the closing area were taken by an optical microscope.

2.20 Evaluation of EVs protection against ROS-induced cytotoxicity

For EVs ROS protection measurement, HDFs —$1x10^5$ cells/well — were seeded in a 96-well plate and allowed to adhere. After 24 h, cells were washed with PBS and the EVs pre-treatment — $1x10^{11}$ EVs/mL of P10K and $3x10^{11}$ EVs/mL of P100K — was added for 2 h and 6 h respectively. After that, cells were washed and then incubated for 30 min under a ROS environment — 100 μL of serum free medium with 15 mM of H_2O_2 —. Then, cells were washed with PBS and incubated overnight in serum free medium to minimize the proliferation of the surviving cells. Finally, cells were washed with PBS and 100 μL of CCK8, 1:10 diluted in serum free culture medium, were added. After 4 h of incubation, the absorbance was read at 450 nm, using 650 nm as the reference wavelength. An alternative co-culture ROS assay was performed as follows. HDFs — $1x10^5$ cells/well — were seeded in a 96-well plate and allowed to adhere. After 24 h, cells were washed with PBS and then EVs were added in 100 μL of serum free medium with 625 μM of H_2O_2 for 4 h. After that, cells were washed with PBS and 100 μL of CCK8, 1:10 diluted in serum free culture medium, were added. After 4 h of incubation, absorbance was read. For all assays, medium with non-EVs control batches processed equally to the EVs batches was used as control and complete medium was used as positive control.

2.21 Evaluation of EVs protection against hyperglycaemia-induced cytotoxicity

For the evaluation of the protective effect of EVs under hyperglycemia, 10,000 HDFs were cultured in 96 well plates for 24 h. After that, HDFs were pre-treated with EVs —

$1x10^{11}$ EVs/mL of P10K and $3x10^{11}$ EVs/mL of P100K — for 6 h, rinsed with PBS and exposed to hyperglycaemic conditions of 150 mM glucose in HDFs serum-free culture medium. Cells pre-treated with non-EVs control batches processed equally to the EVs batches were used as control. Cells pre-treated with complete medium were used as a positive control. Results were normalized against cells grown under non-hyperglycaemic conditions. The metabolic activity was observed at 24 h, 48 h and 72 h by CCK8 assay as described earlier. Cell viability at 72 h was also observed with calcein AM/Ethidium homodimer and each well was photographed by a Nikon epi-fluorescence microscope equipped with a DSD2 confocal modulus (Nikon, Japan).

2.22 EVs tube formation assessment

Briefly, 15 μL of Matrigel® matrix were added into the μ-Plate angiogenesis 96 well plates and let polymerize for 30 min at 37 °C. HUVECs were seeded at a density of 4,5 $x10^5$ cells/mL in 30 μL of complete medium, 15 μL of PBS and 25 μL of EVs — $2x10^{11}$ EVs/mL of P10K and $3,5x10^{11}$ EVs/mL of P100K — in the matrigel bed. Medium with non-EVs control batches processed equally to the EVs batches was used as control. Complete medium was used as positive control. Following an incubation of 24 h, each well was photographed by an optical microscope. After that, cells where stained with calcein AM and each well was photographed

2.23 Statistical analysis

Results are expressed as the mean ± standard deviation. When normally distributed, results were analyzed through Student's two-tailed t-test, to compare between two independent groups, or through a one-way ANOVA test for multiple comparisons. Based on the Levene test for the homogeneity of variances, Bonferroni or Tamhane post-hoc analyses were applied. In contrast, Mann-Whitney's non-parametric analysis was applied for non-normally distributed data. All the statistical computations were performed using SPSS 25.0 (SPSS®, Inc., Chicago, IL, USA).

3. Hypothesis and Objectives

The development of novel biomaterials suitable for wound healing purposes should meet very precise criteria: adequate biocompatibility and mechanical properties, great fluid absorption ability — blood, exudates etc. — and the capacity to adhere cells into their microarchitecture. In the case of acute hemorrhagic wounds, additional key properties should be considered such as great blood absorption and hemostatic capacity. However, not all these properties are enough for treating a very complex dysregulation such as the one exhibited by chronic wounds. For this scenario, it is essential to tackle the multiple factors involved, at the same time, and modulate the response within the progression of healing. In previous studies we developed biomaterial-based therapies with different characteristics, forms and bioactives on their composition — films [72], nanofiber meshes [71,73] and hydrogels [74] —.

In this doctoral thesis, we aimed to develop a more complete biomaterial, following a circular economy thinking, which can tackle multiple stages of the wound healing process. In this sense, designing SLS with hemostatic properties, which can be combined with MSCs, could be an interesting advance for treating multiple wounds that are stuck in different healing phases. Thanks to their anti-inflammatory, immunomodulatory and proregenerative properties, the MSCs have demonstrated to be very effective for treating multiple pathologies. However, despite the use of MSCs combined with biomaterials holds a promising potential, in this work we aimed to explore also the EVs fraction of the MSCs secretome. Thus, this cell-free alternative presents the advantages of being; more easily handled, characterized, standardized, stored and potentially safer than MSCs while exhibiting also therapeutic properties.

To accomplish this purpose, four specific objectives are considered:

1. To develop and characterize the SLS in terms of morphological, physicochemical and mechanical properties, eventually analyzing their biocompatibility (Appendix 1).

2. To study the physicochemical behavior in presence of blood and hemostatic properties of the SLS, comparing them to marketed options (Appendix 2).

3. To analyze the wound healing capacity of the SLS when are loaded with MSCs both *in vitro* and *in vivo* (Appendix 3).

4. To characterize and compare the different MSCs-EVs populations and MSCs sources and test their potency for wound healing applications (Appendix 4).

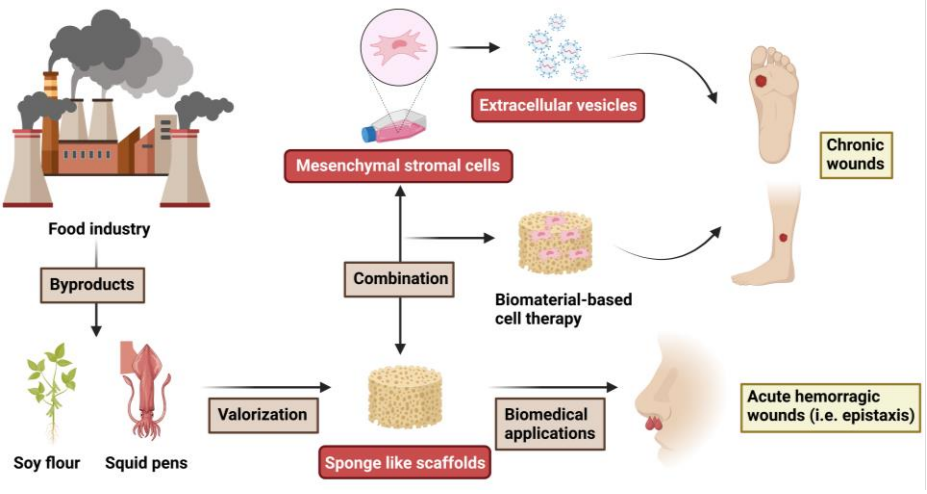

Graphical abstract. Schematic representation of the objectives of the present doctoral thesis.

4. Results and discussion

In the beginning of this thesis, we formulated the SLS and performed different experiments to obtain a complete characterization by employing multiple techniques (Study I). We wanted to add an additional point of view using for their composition valorized by-products from the food industry. For this, we employed SPI and CH as forming biopolymers. We selected these two components due to their broad valorization potential, non-toxicity, biocompatibility, biodegradability, abundance and availability at relatively low-cost, promising characteristics for the development of novel therapies for health-related applications.

As depicted in **Fig. 4A, B** we obtained highly porous SLS with an elevated specific surface that provide interesting features for high fluid absorption and cell attachment, communication and migration. The surface orography was analyzed by AFM in 3 x 3 μm scanning areas (**Fig. 4C**). As can be seen, the SLS showed a homogeneous and dense morphology with low roughness, confirming an adequate compatibility between the SPI and CH. We further analyze the interactions of the SPI with the CH by FTIR analysis (**Fig. 4D**). The samples exhibited three characteristic bands common to all proteins: the amide I band at 1630 cm^{-1}, associated with C=O stretching, the amide II band at 1530 cm^{-1}, corresponding to N–H bending, and the amide III band at 1230 cm^{-1}, related to C–N stretching and N–H bending. We also observed, between 1180 and 953 cm^{-1}, the characteristic bands of polysaccharides [75]. XPS studies were also performed to analyze the functional groups located on the surface of SLS (**Fig. 4E**). The oxygen represented the 23.6% of the surface composition (O–C=O/O=C–N), the nitrogen represented the 8.03% (C=N/C–N) and the carbon represented the 66,91% for C–H/C–C (284.8 eV), and the 2.00% for O–C=O (290.1 eV). These results confirmed that the interactions between the SPI and CH were mainly physical; hydrogen bonding between the hydroxyl groups of CH and the polar groups (hydroxyl, carboxyl, and amino) in SPI amino acids.

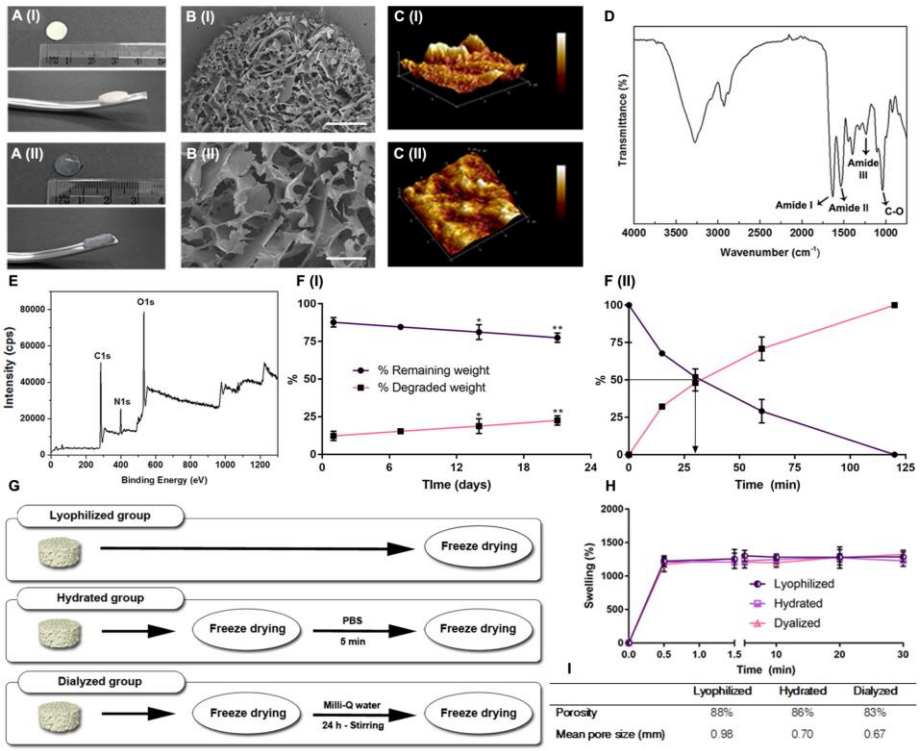

Fig. 4. SLS Characterization. A (I). SLS of 8 × 1.5 mm in a dry state. A (II). SLS of 8 × 1.5 mm in a wet state. B (I). SEM micrograph of SLS. Scale bar is 1 mm. B (II). SEM micrograph zoomed. Scale bar is 0.25 mm. C (I) and C (II). AFM images of the surface topography for a scan area of 3.0 μm × 3.0 μm. D. ATR-FTIR spectrum. E. XPS survey spectra of the SLS. C 1s (284.6 eV), N 1s (399.3 eV) and O 1s (532.0 eV). F (I). Hydrolytic degradation. F (II). Enzymatic degradation. G. Scheme of the different processed SLS groups. H. Swelling curve. I. Table of porosity and mean pore size of SLS.

After that, we measured a very important property for chronic wound and hemorrhagic scenarios, the degradation profile of SLS when exposed to biological fluids. For that, we analyzed the degradation kinetics of SLS in aqueous medium (**Fig. 4F (I)**) for 21 days and in a medium with collagenase (**Fig. 4F (II)**) for 2h. As can be observed, the degradation in aqueous medium during 21 days was only of about 25% and was related to the release of glycerol. The reinforcement of the SPI with the CH conferred the SLS more stability due to the intra-sheet hydrogen bonds on the CH structure [76]. In contrast, in the presence of collagenase, the SLS were completely degraded in only 2 h. This is of high interest since collagenases — mainly MMP-1, MMP-8 and MMP13 — are present in chronic

wounds and could help to degrade the SLS *in vivo* helping to replace these with the ECM secreted by the MSCs [77].

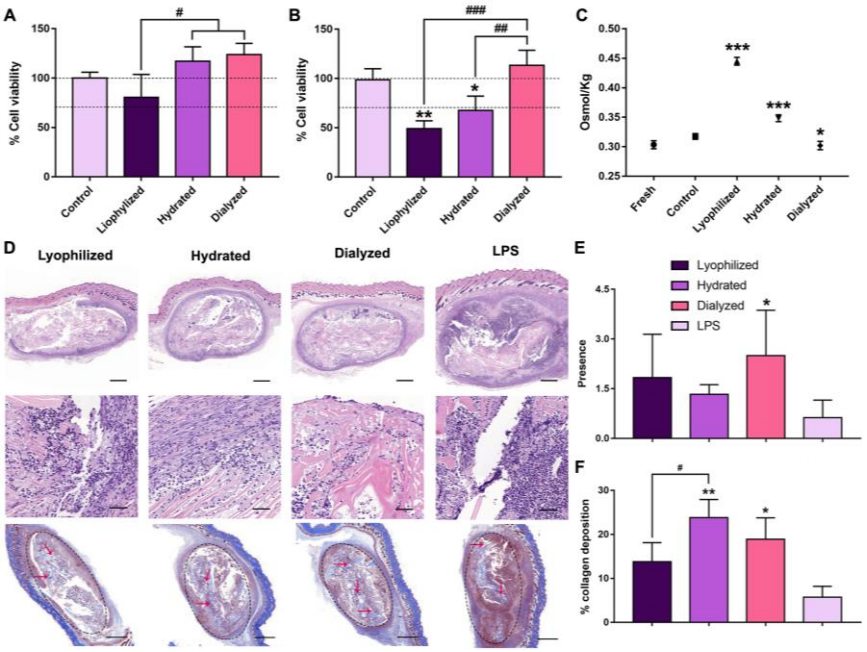

Fig. 5. SLS Biocompatibility analysis. A. Direct cytotoxicity. B. Indirect cytotoxicity. Lines mark the 100% and 70% cell viability. C. Lixiviates osmolarity for indirect cytotoxicity. * indicates $p < 0.05$; ** indicates $p < 0.01$; *** p indicates <0.001 in comparison with the control group. $^{\#}$ indicates $p < 0.05$; $^{\#\#}$ indicates $p < 0.01$; $^{\#\#\#}$ indicates $p < 0.001$ between groups. D. Histology of the implanted SLS. The first two rows are H&E stainings of all groups of SLS at different magnifications. Scale bars are 500 μm and 50 μm respectively. The third row represents the Masson´s trichrome staining. Scale bars are 800 μm. E. Ratio between macrophages and neutrophils in H&E staining. * indicates $p < 0.05$ in comparison with the LPS group. F. Collagen deposition into the SLS in Masson´s trichrome staining. * indicates $p < 0.05$; ** indicates $p < 0.01$ in comparison with the LPS group. # indicates $p < 0.01$ between different groups.

After an initial general physicochemical evaluation, we decided to process the SLS in order to potentially increase their biocompatibility (**Fig. 4G**). It is well known that previous hydration or dialysis steps can decrease the cytotoxicity of biomaterials; however, these steps can alter their microstructure, porosity and mechanical properties. For that, we analyzed the SLS water absorption capacity, pore profile and porosity after the pre-

conditioning steps. The maximum swelling was about 1200% and was achieved in less than 30 seconds for all groups (Fig. 4H). The porosity values were in the range of those adequate for both nutrient and oxygen transport, as well as for the removal of wastes for all groups [78,79]. In the case of the pore size, we obtained a significant decrease with the pre-conditioning steps related with the second freeze-drying process (Fig. 4I). Nevertheless, values were above 0.3 mm that is stated essential for vascularization of constructs and the correct oxygenation and nutritional contribution to the hosted cells [80,81].

Another important requirement that any biomaterial should met, is to exhibit an adequate biocompatibility. Hence, we performed a cytotoxicty analysis in a direct and indirect manner following the ISO 10993-5:2009 guidelines for biological evaluation of biomedical devices (Fig. 5A, B). As observed, only the dialyzed group showed viabilities above 70% in both experiments. The reason behind the cytotoxicity in the lyophilized and hydrated group was an increased osmolarity, which could be related to the release of glycerol, to values that could alter L929 replication (Fig. 5C) [82]. Finally, we tested all groups in an immunocompetent C57BL/6 mice model to confirm that the *in vitro* values could be correlated *in vivo*. The immune response of these animals is known to have a very aggressive innate immunity and mimic, in a relevant way, the foreign body response (FBR) of humans [83]. We used lipopolysaccharide (LPS)-soaked SLS as positive controls for inflammation. As observed in Fig. 5D the presence of polimorphonuclear neutrophils was higher in the LPS group than in the rest of the groups, as expected. The ratio of macrophages/neutrophils was depicted in Fig. 5E and the only significant difference that we observed against the LPS group was in the dialyzed group. Finally, in the collagen deposition both the hydrated and dialyzed groups showed differences against the LPS group (Fig. 5F).

In summary, the developed SLS presented a highly porous and interconnected microstructure with high hydrophilicity and fluid absorption capacity. Furthermore, a previous conditioning step — hydration or dialysis — demonstrated to be essential to ensure biocompatibility, minimize the inflammatory response and maximize the integration of SLS within the host tissue. As a result, we decided to employ dialyzed SLS for the rest of the studies.

After the initial characterization, we further analyzed functionality for these SLS (Study II). Thus, one of the most interesting properties that we discovered was found in the SPI fraction. It was described that the SPI could exhibit pro-coagulant effects due to it is a source of vitamin K1 [84-86]. Numerous blood coagulation factors of the clotting cascade — including prothrombin and factors VII, IX, X —, require of this vitamin for its activation [87]. Furthermore, the RGD motifs presented on the SPI are of great interest for cell attachment, including platelets, potentially boosting their aggregation [88,89]. With these precedents, we planned a study to test the hemostatic properties of the SLS and compared them to the ones exhibited by two of the most utilized commercial nasal packs in the clinic, Merocel® (MC) and gauze (GZ).

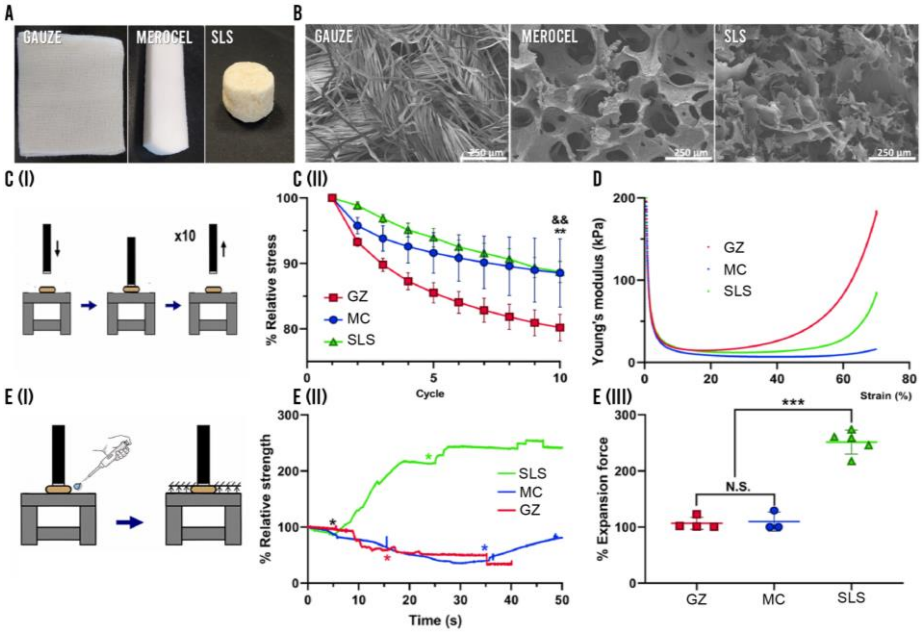

Fig. 6. SLS, MC and GZ morphology and mechanical characterization. A. Macroscopic images of GZ, MC and SLS. B. SEM micrographs. Scale bars are 250 μm. C (I). Scheme of the cyclic compression test. C (II). Relative percentage stress of biomaterials for 10 cyclic compressions. $^{\&\&}$ indicates $p < 0.01$ GZ in comparison to MC. ** indicates $p < 0.01$ GZ in comparison to SLS. D. Young's modulus at increasing strains. E (I). Scheme of the expansion force test. E (II). Relative expansion strength curves of biomaterials. * indicates the moment in which water was added to each group. Relative expansion force. *** indicates $p < 0.001$ SLS in comparison to the other groups. N.S. non-significance.

First, we compared the morphological and mechanical properties of these three biomaterials. As can be seen both visually and throught the SEM micrographs, MC and the SLS presented similar microporous sponge-like matrices while the gauze presented a fibrillar structure (Fig 6A, B). Despite the gauze shows thousands of interconnected fibers forming a mesh, the space between the fibers does not present well-defined pores. In contrast, MC and SLS demonstrated to exhibit a well-defined and interconnected pore microarchitecture.

The morphology and microstructure of biomaterials is closely related to the mechanical properties that they exhibit. In this vein, hemostatic biomaterials for epistaxis should present adequate elasticity, resistance to deformation, capacity to make pressure on the nostril walls without damaging them, shape memory and a smooth surface that helps to alleviate patient's discomfort during the treatment [90]. Consequently, we started carrying out a cyclic compression strain-stress mechanical test along 10 cycles (Fig. 6C (I)). As observed in Fig. 6C (II) the relative stress needed to deform the tested biomaterials decreased substantially cycle after cycle, reducing their ability to resist deformation. This effect, known as cyclic softening, is caused by irreversible deformations of the internal microstructure of the biomaterials caused by the continuous deformation [91,92]. Interestingly, we observed that both MC and SLS demonstrated similar values of maximum stress at the end of the 10 cycles, while the gauze showed a higher descent (Fig. 6C (II)). Secondly, we measured the Young's modulus for all the strains of the first cycle for each group. The Young's modulus defines the ability of a material to resist changes in length when is subjected to a compressive exercise. Consequently, this measurement is known to be directly correlated to the stiffness of a material [93,94]. As depicted, the modulus, at low strains, is similar for all groups; however, at higher strains, all groups started to differentiate of each other (Fig. 6D). In summary, while the GZ group becomes rigid at lower strains, both MC and SLS remain flexible until strain values are higher than 50%. Finally, we evaluated the upwards force displacement of these biomaterials by and expansion force test when absorbing fluids (Fig. 6E (I)). This test would represent the force that these biomaterials could display against a nasal cavity's wall when absorbing fluids and therefore this property seems very interesting for the development of hemostatic biomaterials for epistaxis. As observed in Fig. 6E (II) under the same conditions, MC and GZ groups did not showed an expansion force when they absorbed water. In contrast, the SLS group relative expansion kinetic demonstrates that

it displays an upwards expansion when the water is added (Fig. 6E (III)). The fact that the SLS increase the expansion force up to 2.5 times the initial value, suggest that these would probably be able to exert a higher pressure than the MC and GZ groups to the bleeding zone when absorbing blood.

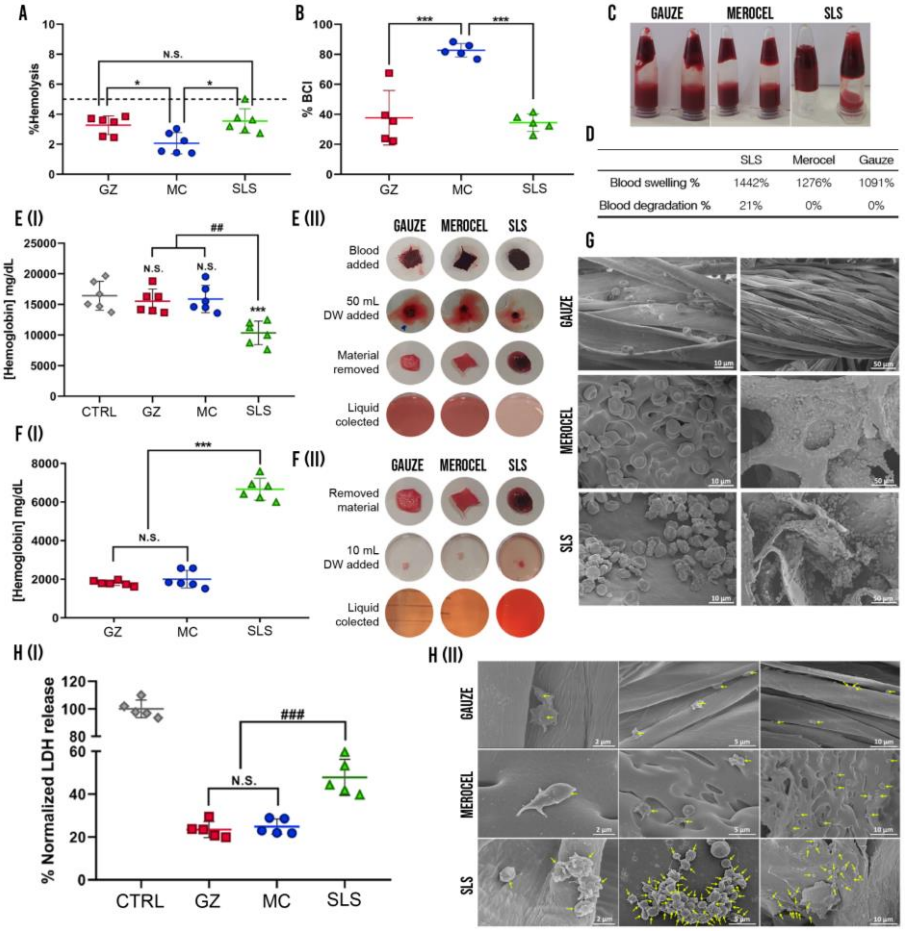

Fig. 7. *In vitro* blood studies. A. Hemolysis assay. Line represents 5% hemolysis. * indicates $p < 0.05$ between groups. N.S. non-significance. B. Blood Clotting Index. *** indicates $p < 0.001$ between groups. C. Image of the tube inversion assay. D. Table for percentage of blood swelling and degradation. E (I). Hemoglobin released by materials after water rinsing. *** indicates $p < 0.001$ in comparison to the control group; ## indicates $p < 0.01$ SLS in comparison to all groups; N.S. non-significance. E (II) Photographs of the appearance of the materials at different stages of the assay. F (I). Hemoglobin within the biomaterials. *** indicates $p < 0.001$ SLS in comparison to the other

groups. N.S. non-significance. F (II) Photographs of the released hemoglobin within the biomaterials. G. SEM micrographs of erythrocytes adhered to the surface of the biomaterials. Scale bars are 10 μm (left images) and 50 μm (right images). H (I). Normalized percentage of LDH release from biomaterials. $^{###}$ indicates $p < 0.001$ SLS in comparison to the other groups. N.S. non-significance. H (II). SEM micrographs of platelets adhered to the surface of the biomaterials (yellow arrows).

Regarding the physicochemical hemostatic properties of SLS, we performed different studies to compare them against the ones exhibited by MC and GZ. For that, we first studied the hemocompatibility of these biomaterials through a hemolysis assay (**Fig. 7A**). All groups were disposed in contact with blood to analyze whether the shear stress or changes in the osmotic pressure could destroy erythrocytes [95]. As observed, none of the groups showed hemolysis values above 5% that is stated as the maxim permitted for biomaterials [96]. Once the hemocompatibility of all tested biomaterials was demonstrated, we analyzed their blood-clotting capacity. For that, we employed the BCI as an indicative of clotting velocity, being the lower BCI the faster blood-clotting rate. As observed in **Fig. 7B**, the MC group obtained a significantly higher value that the one exhibited by the GZ and SLS groups respectively. These findings suggested that the GZ and SLS groups were able to coagulate the blood faster than the MC group. To reinforce these results, we performed the tube inversion assay (**Fig. 7C**). As depicted, in the SLS group the blood remained in the upper part forming a clot while in the GZ and MC groups the blood felt down to the bottom of the Eppendorf confirming a lower clotting capacity on these biomaterials.

Further to these studies, we analyzed the capacity of all biomaterials to swell and degrade in presence of blood (**Fig. 7D**). As depicted in the table, the swelling capacity of SLS was the highest among the three groups. This is of great interest since higher volumes of absorbed blood would result in a stronger tamponade effect eventually reducing bleeding. On the other hand, the more blood absorbed the higher the amount of erythrocytes and platelets that will concentrate into the biomaterial helping to promote hemostasis and clot formation. We also tested the erythrocyte and platelet adhesion to the surface of biomaterials as an indicator of the clotting potential. For erythrocytes, we employed the measurement of hemoglobin to extrapolate cell adhesion. As shown, after loading the materials with blood and rinse those with milli-Q water, the amount of hemoglobin released by the SLS was significantly lower in comparison to the rest of the groups (**Fig. 7E (I-II)**). Then, after releasing the retained blood and measure the

hemoglobin content that remained inside the materials, the SLS demonstrated a significantly higher amount of entrapped hemoglobin (**Fig. 7F (I-II)**). These results, together with a visual confirmation throught SEM micrographs (**Fig. 7G**), suggest that the SLS hold greater erythrocyte adhesion and increased clotting potential than GZ and MC groups. The increased erythrocyte adhesion is of great interest since these cells can accelerate the formation of blood clots [97] and increase blood viscosity thus enhancing the resistance to blood flow [98,99].

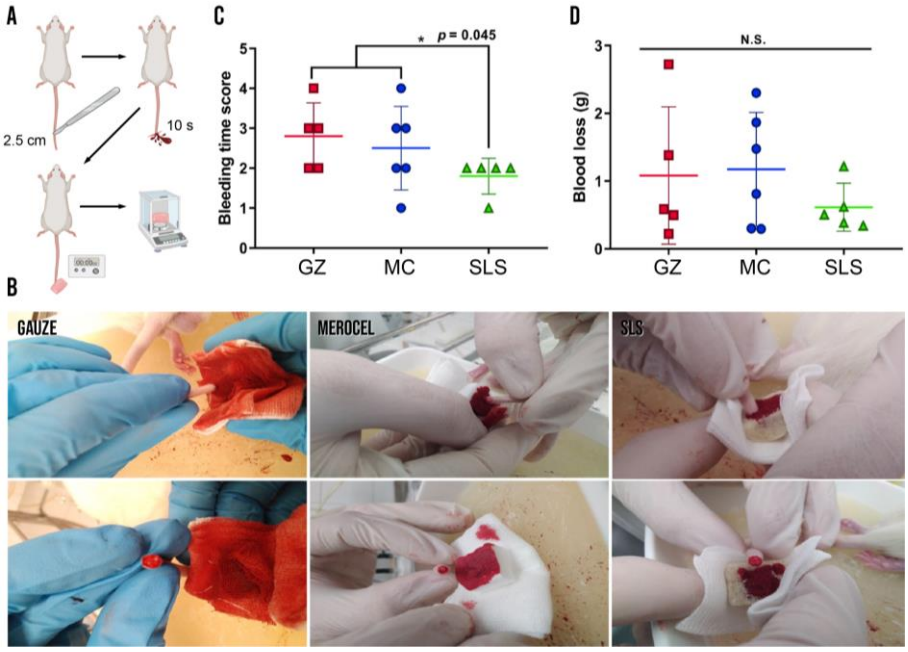

Fig. 8. *In vivo* rat-tail amputation analysis. A. Scheme of the procedure. B. Photographs of the three groups during the *in vivo* experiment. C. Bleeding time score. * indicates $p < 0.05$ SLS in comparison to the other groups. D. Blood loss. N.S. non-significance.

On the other hand, for the analysis of platelet adhesion, we employed the measurement of lactate dehydrogenase (LDH). As shown, the amount of adhered platelets — and then an elevated LDH released from the biomaterials — was significantly higher in the SLS group than in the rest of the groups (**Fig. 7H (I-II)**). This phenomena could be explained by the capacity of the αIIbβ3 integrin receptor of the platelets to bind to the RGD motifs of the SLS, that are absent in the GZ and MC groups [100,101]. The fact that SLS demonstrated an increased platelet adhesion implies that they can promote,

as shown, platelet aggregation and thus boost their hemostatic effect by decreasing the clotting time.

Finally, we employed the rat-tail amputation model to confirm the hemostatic capacity of these materials in an *in vivo* scenario (Fig. 8A, B). We measured the bleeding time and the blood loss (Fig. 8C, D). As observed, the SLS demonstrated to decrease significantly the bleeding time; however, we did not observe significant differences in the quantity of blood lost. Taking all these results together, we could confirm that the SLS exhibited greater hemostatic properties that the gold standards in clinic, making them potential candidates for the treatment of epistaxis scenarios.

In summary, in this study we have demonstrated that the SLS present better mechanical properties and degradation profile that the "gold standards" in clinic for their use in epistaxis scenarios. Furthermore, we have shown that the SLS present high hemostatic capacity in terms of erythrocyte and platelet adhesion and clotting time decrease.

After studying the hemostatic capacity of these SLS, we decided to explore further and test their suitability as cell-hosting systems for chronic wound scenarios (Study III). For that, we decided to combine the SLS with MSCs (MSC-SLS) derived either from adipose tissue (AT-SLS) or from hair follicles (HF-SLS) due to their immunomodulatory and pro-regenerative capacity, as mentioned in the "state-of-the-art" section. First, we seeded the cells and explored their viability over a week by using a transwell-like system in order to mimic, as much as possible, an *in vivo* scenario. We employed two different seeding doses — 25,000 cells (25K) and 50,000 cells (50K) per mg of SLS — and observed their viability at day 3 and 7. As depicted, both cell doses at 3 and 7 days exhibited a great cell spreading and colonization throught the SLS microarchitecture without any sign of cell death (Fig. 9A). As a result, we decided to choose 50,000 cells/mg as the standard dosage for SLS MSC-loading throught the rest of the work. Second, we studied the secreted soluble secretome. For that, we analyzed the accumulated release of mediators at day 7 to compare both MSCs profiles. As depicted in Fig. 9B both MSCs released a great amount of angiogenic, pro-regenerative and anti-inflammatory mediators. The secretion was similar in certain cytokines and growth factors, however some of them such as Ang-1, bFGF, EGF, HGF or IL1-Ra were more secreted by AT-MSCs while HF-MSCs secreted more SDF-1α and TGF-β1. We did not compare the SLS secretion — 3D

environment — against a secretion on a plate — 2D environment — since the unique composition, the mechanical properties and microarchitecture of the SLS influence the MSCs secretory machinery [102].

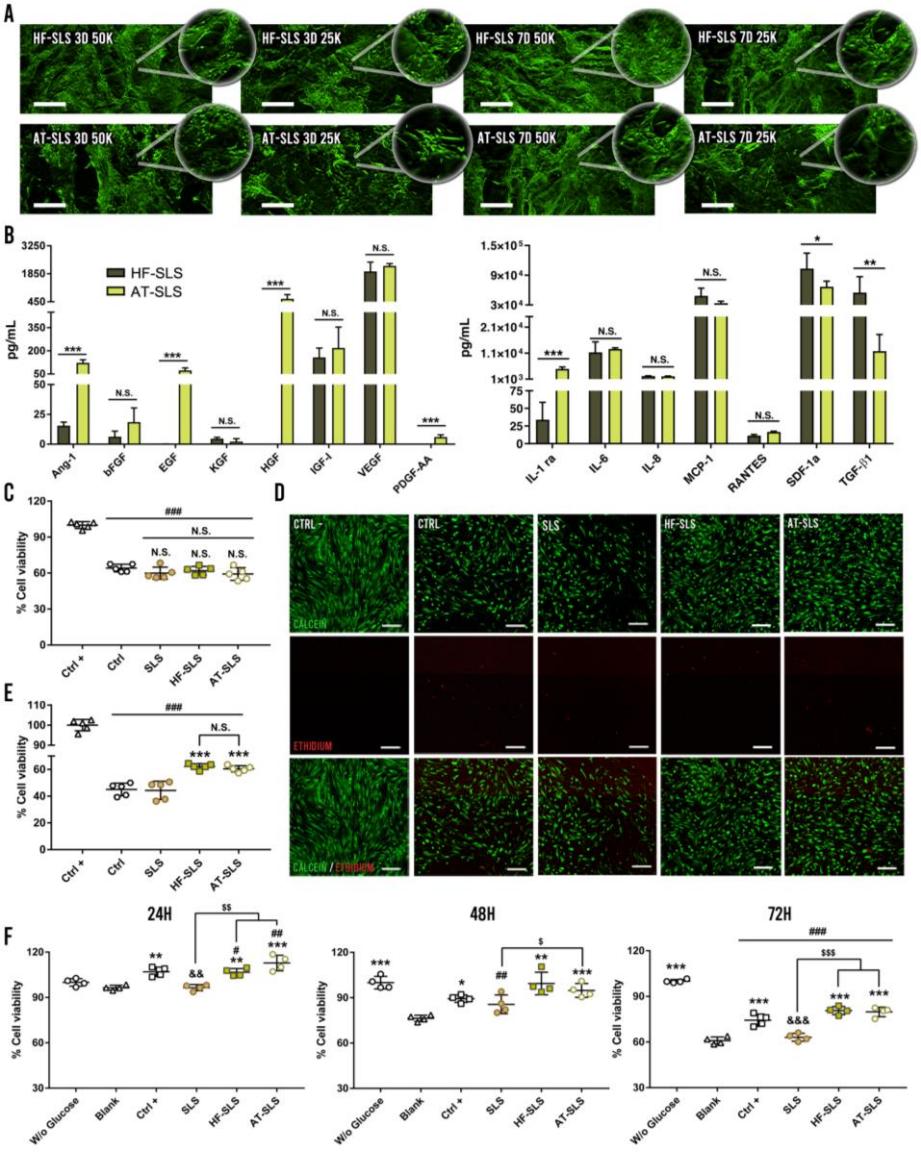

Fig. 9. MSC-SLS monitoring, secretome analysis and cytotoxicity-induced protection. A. MSC-SLS imagining at different cell doses — 25,000 cells/mg SLS (25K) and 50,000 cells/mg SLS (50K) —

and incubation days — 3 days (3D) and 7 days (7D) —. Scale bars are 500 μm. B. Secretome analysis of cytokines and growth factors. * indicates $p < 0.05$, ** indicates $p < 0.005$ and *** indicates $p < 0.001$ between groups. N.S. non-significance. C. Percentage of cell viability when the MSC-SLS secretome and controls were mixed with H_2O_2 and then incubated with HDFs. $^{###}$ indicates $p < 0.001$ in comparison to the positive control. D. Images of calcein/ethidium stained HDFs pretreated, after 24h of exposure to ROS. Scale bars are 200 μm. E. Percentage of cell viability when HDFs were pretreated with the treatments. *** indicates $p < 0.001$ in comparison to the control and SLS groups. $^{###}$ indicates $p < 0.001$ in comparison to the positive control. N.S. non-significance. F. Cell viability under hyperglycemia-induced cytotoxicty. * indicates $p < 0.05$, ** indicates $p < 0.005$, *** indicates $p < 0.001$ in comparison to the blank group. $^{#}$ indicates $p < 0.05$, $^{##}$ indicates $p < 0.005$, $^{###}$ indicates $p < 0,001$ in comparison to the group without glucose. $^{&&}$ indicates $p < 0.005$, $^{&&&}$ indicates $p < 0.001$ in comparison to the positive control group. $^{\$}$ indicates $p < 0.05$, $^{\$\$}$ indicates $p < 0.005$, $^{\$\$\$}$ indicates $p < 0.001$ between groups.

Usually, in chronic wound scenarios, the amount of ROS is very high, generating inflammation and hindering, in that way, the cell-to-cell communication and integrity [103]. Therefore, reducing the amount of ROS or protecting cells against the ROS-induced cytotoxicty and death has been an interesting move in the development of new therapies. It has been described that MSCs release certain types of superoxide dismutase (SOD) that can act as ROS scavengers [104]. However, as observed in **Fig. 9C** when we mixed the secretome of MSC-SLS, SLS or control with the ROS-fueled media and placed it in HDFs, we did not observed protection. In contrast, when we pretreated HDFs with the secretome of MSC-SLS and then exposed to the ROS, we observed a significant protective effect for both AT-SLS and HF-SLS groups (**Fig. 9D, E**). It has been described that some soluble mediators secreted by these MSCs could have a role in this protective effect: IL-1ra, PGE-2 or bFGF that has shown to reduce ROS induced oxidative stress [105-107].

In addition to the ROS-induced cytotoxicty, we also investigated the hyperglycemic-induced cytotoxicity of MSC-SLS on HDFs during 3 days (**Fig. 9F**). We observed the protective effect of MSC-SLS pre-treatment at 24h and it was maintained until 72h. The differences observed at 24h were greater at 48h and 72h where AT-SLS and HF-SLS showed a higher percentage of cell survival than the blank and SLS groups and similar to the positive control. As described, elevated levels of glucose can increase ROS levels as well as the concentration of other enzymes — i.e. xanthine oxidase — that can be involved in cytotoxicity and eventually apoptosis [108]. We hypothesize that, as well as in

the previous experiment, some mediators released by the MSCs that may reduce direct ROS cytotoxicity could also be acting in this scenario, helping HDFs to reduce hyperglycaemia-associated cytotoxicity.

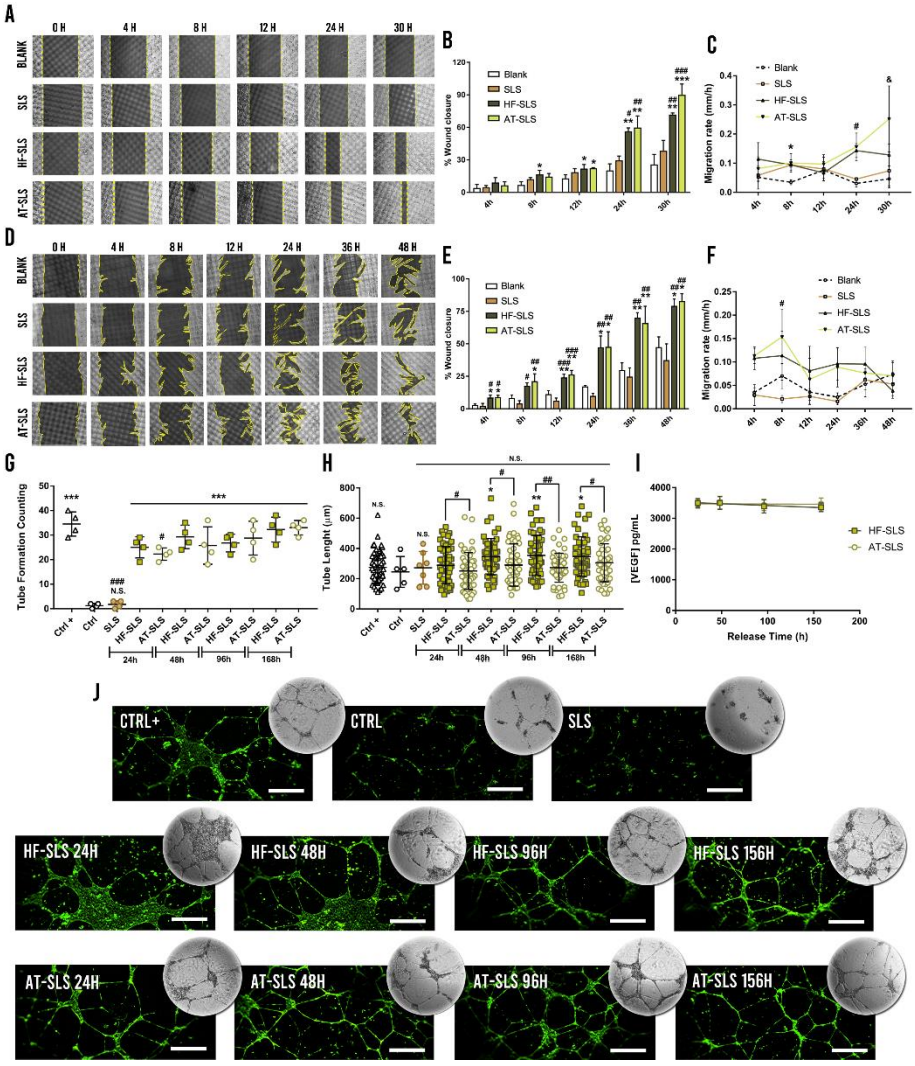

Fig.10. *In vitro* wound healing and tube formation assays. A. Images of the HaCaTs cells at different time-points of the scratch assay. B. Percentages of HaCaTs wound closure. * indicates $p < 0.05$, ** indicates $p < 0.005$ and *** indicates $p < 0.001$ in comparison to the blank group. # indicates $p < 0.05$, ## indicates $p < 0.005$ and ### indicates $p < 0.001$ in comparison to the SLS group. C.

Migration rate of HaCaTs at different time points. * indicates $p < 0.05$ all groups in comparison to the blank group. # indicates $p < 0.05$ AT-SLS and HF-SLS in comparison to the SLS and blanks groups. & indicates $p < 0.05$ AT-SLS in comparison to the blank group. D. Images of the HDFs cells at different time-points of the scratch assay. E. Percentages of HDFs wound closure. * indicates $p < 0.05$, ** indicates $p < 0.005$ and *** indicates $p < 0.001$ in comparison to the blank group. # indicates $p < 0.05$, ## indicates $p < 0.005$ and ### indicates $p < 0.001$ in comparison to the SLS group. F. Migration rate of HDFs at different time points. # indicates $p < 0.05$ AT-SLS and HF-SLS against SLS and blanks groups. G. Number of formed tubes per well. *** indicates $p < 0.001$ in comparison to the control group. # indicates $p < 0.05$, and ### indicates $p < 0.001$ in comparison to the positive control group. N.S. non-significance in comparison to the control group. H. Tube length. * indicates $p < 0.05$, ** indicates $p < 0.005$ and N.S. non-significance in comparison to the control group. # indicates $p < 0.05$, and ## indicates $p < 0.005$ between groups. I. VEGF amount in MSC-SLS secretome administered at different time-points. J. Calcein stained and optical microscope images of the formed tubes. Scale bars are 400 μm.

Numerous works have stated that in the chronic wound niche, the migration of numerous cell types results impaired due to a harsh environment that impede a correct cell-to-cell communication [109-111]. In that way, helping these cells to increase their motility and migratory capacity would eventually benefit the formation of granulation tissue and the correct closure of wounds. As depicted in **Fig. 10A, B** both MSC-SLS demonstrated to increase the migration and wound closure on HaCaTs in comparison to the SLS without cells and the non-treated blank group. Interestingly, we did not observe the effect before 4h but we did at 8 h and it was maintained throught all the experiment (**Fig. 10C**). As well as with HaCaTs, we also observed the pro-migratory effect in HDFs (**Fig. 10D, E**). Similarly, we detected the effect at 8h and it was maintained until the end of the experiment (**Fig. 10F**). We did not found significant differences between AT-SLS and HF-SLS for both experimental cells, HDFs and HaCaTs. The release of a high amount of mediators such as IL-6, TGF-β1 or bFGF, that has been described to have an impact on HaCaTs and HDFs migration, could explain the great results observed in the *in vitro* wound healing assay [111,112].

Finally, after showing pro-migratory efficacy, protective effects against cell death under stressful environments and angiogenic potential, we tested the MSC-SLS in a full thickness splinted wound healing assay in db/db mice (**Fig. 11A-D**). As illustrated in **Fig. 11B**, we observed the greatest wound closure in both MSC-SLS groups at both 7 and 14

days. As compared to the control, at days 7 and 14, the wound closure of SLS, AT-SLS and HF-SLS groups was significantly higher. Furthermore, the AT-SLS and HF-SLS groups demonstrated a higher percentage of wound closure than the SLS group at both 7 and 14 days. Finally, as depicted in the healing rate data, only the MSC-SLS groups showed a significantly higher wound closure against the control at 14 days (Fig. 11C). Furthermore, we did not observe differences between the AT-SLS and the HF-SLS groups at any of the time-points.

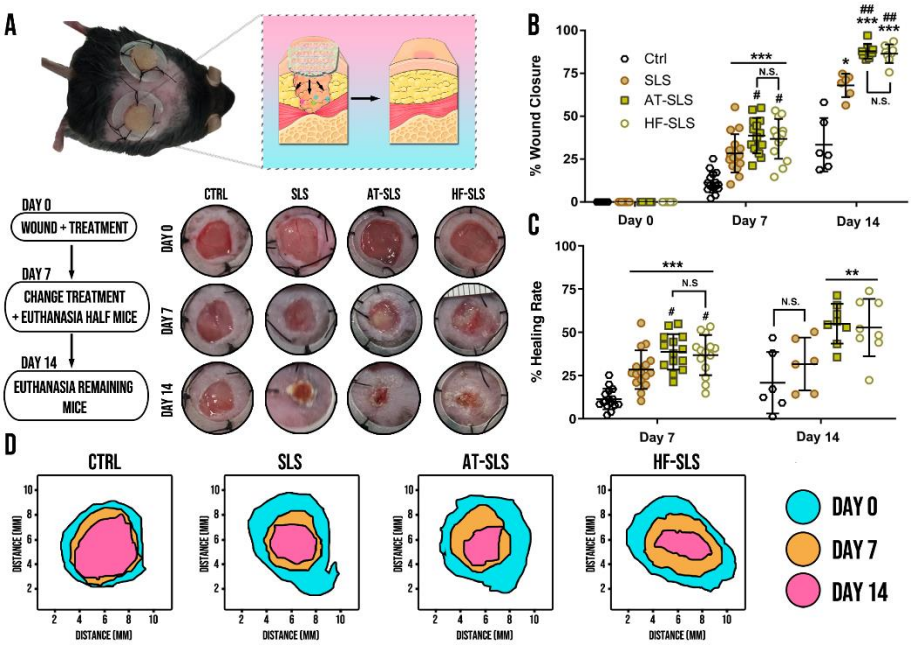

Fig.11. *In vivo* wound healing assessment. A. *In vivo* procedure scheme and wound closure photographs. B. Percentage of wound closure at different time points. * indicates $p < 0.05$, *** indicates $p < 0.001$ in comparison to the control group. # indicates $p < 0.05$, ## indicates $p < 0.005$ in comparison to the SLS group. N.S. Non significance. C. Percentage of healing rate. ** indicates $p < 0.005$, *** indicates $p < 0,001$ in comparison the control group. # indicates $p < 0.05$, in comparison to the SLS group. N.S. Non significance. D. Model of the wound closure at different time points.

We further performed histological analyses of wound necropsies. As shown in Fig. 12A, B we obtained significant differences in the re-epithelialization status of wounds

among the treated groups at 14 days. Both AT-SLS and HF-SLS demonstrated a more mature wound with better re-epithelialization that the control group; however, we did not found significant differences against the SLS group.

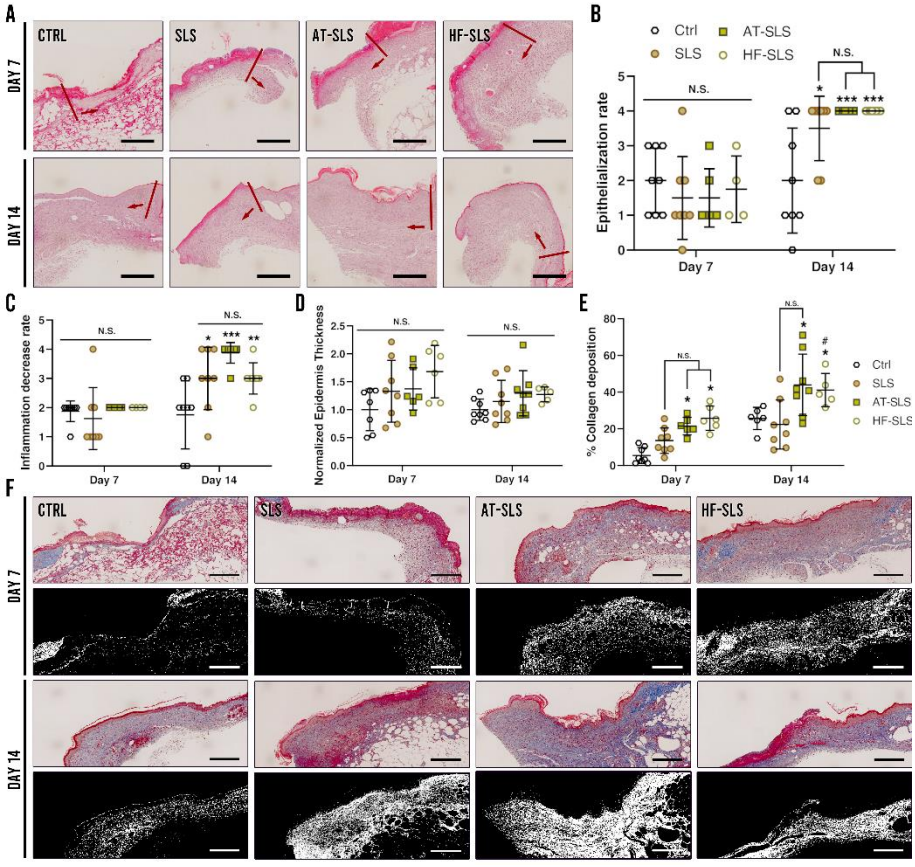

Fig.12. Histological analysis. A. H&E staining. Scale bars are 300 μm. Arrows indicate the wound zone. B. Epithelialization rate. C. Inflammation decrease rate. D. Normalized epidermis thickness analysis. E. Percentage of collagen deposition. * indicates $p < 0.05$, ** indicates $p < 0.005$, *** indicates $p < 0.001$ in comparison to the control group. # indicates $p < 0.05$ against the SLS group. N.S. Non-significance. F. Masson´s trichrome staining. In black: deconvoluted images of collagen.

The re-epithelialization results were supported with the data obtained in the inflammation decrease rate (Fig. 12C). As depicted, at day 14 the three groups with treatment showed significant differences against the control group. However, we did not

observe differences between the MSCs groups and the SLS group. Nevertheless, on these groups, we observed inflammation values above 3 depicting that the main process happening in the wound niche was fibroblast proliferation (proliferative phase). In contrast, in the control group, values below 2 showed that the wounds were still on a diffuse acute inflammatory phase. We did not observe differences between groups when comparing the epidermis thickness of wounds, which can act as an indicator of a more advanced healing (**Fig. 12D**). Finally, we measured the collagen deposition using the Masson´s trichrome staining (**Fig. 12E, F**). As observed, we obtained significant differences at both 7 and 14 days. At these time-points, AT-SLS and HF-SLS demonstrated an increased collagen deposition on the wound niche in comparison to the control and SLS groups. The effect may be attributed to the influence of MSCs since the SLS groups did not exhibit differences against the control. These results are in agreement with the ones observed by other authors using different MSCs delivery systems *in vivo* [113,114].

In summary, in this study we have shown that the SLS are adequate matrices for MSCs hosting. Furthermore, the wide variety of mediators released by these MSC-SLS have demonstrated to protect HDFs against ROS and hyperglycemia induced cytotoxicity, increase HDFs and keratinocytes migration and promote HUVECs angiogenesis. Eventually, the MSC-SLS have demonstrated to decrease the wound healing time *in vivo*, increasing re-epithelialization, collagen deposition and decreasing inflammation.

Finally, after exploring the efficacy of the MSC-SLS and, as a cell-therapy alternative, we decided to investigate the EVs fraction of the MSCs secretome. It has been widely described that EVs secreted by MSCs exhibit therapeutic effects in tissue repair and wound regeneration — proliferative, pro-angiogenic, immunomodulatory, antiapoptotic, etc. — [115-117]. Despite AT-EVs have been widely studied, this was the first work describing the EVs produced by HF-MSCs. In this regard, we started this study isolating and characterizing the EVs released from both AT-MSCs and HF-MSCs. We employed differential centrifugation to isolate two populations: m-lEVs — 10,000 x g (P10K) — and sEVs — 100,000 x g (P100K) — (**Fig. 13A**). As depicted, the size of each population ranged from 100 nm to nearly 400 nm for the P100K EVs — with a mean and mode size of 200 and 165 nm respectively — and from 100 to 800 nm for the P10K EVs — with a

mean and mode size of 270 and 200 nm respectively — (Fig. 13B-D). Despite showing great similarities in the morphology and size of EVs between both cell types, the number of EVs produced per cultured cell was significantly higher in the AT-MSCs than the HF-MSCs (Fig. 13E).

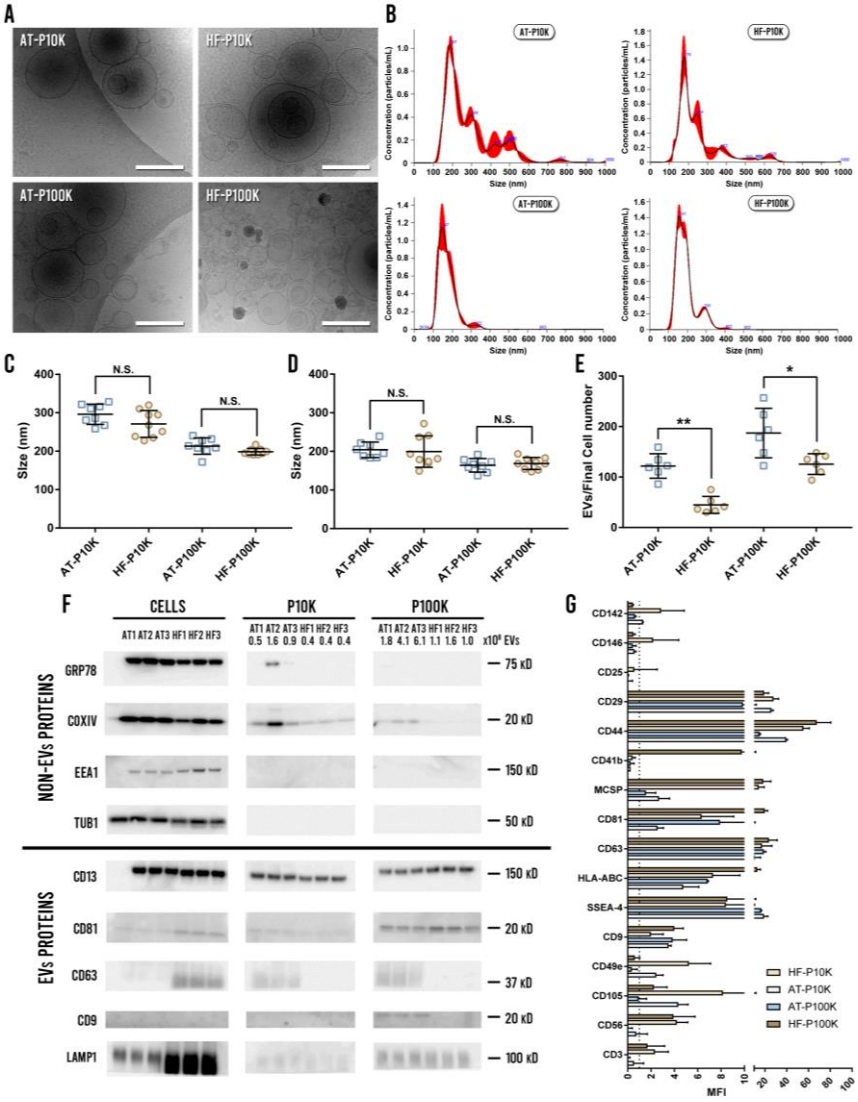

Fig.13. EVs characterization. A. Cryo-EM images of EVs. Scale bars are 200 nm. B. NTA size-profile of the isolated fractions. C. Mean size of different EVs batches. D. Mode size of different EVs

batches. N.S. Non-significance. E. Number of EVs compared to final cell count. * indicates $p < 0.05$, ** indicates $p < 0.005$. F. Western blotting analysis of EVs and non-EVs markers of three different batches. Multiplex bead-based flow cytometry assay for detection of EV surface markers.

We further studied the marker expression on EVs by western blotting (WB) and flow cytometry (**Fig. 13 F, G**). We observed the expression of CD13, CD81 and LAMP1 in P10K and P100K EVs derived from both cell types. In contrast, only AT-EVs showed western blotting bands for the rest of EV markers, with CD63 in both P10K and P100K, and CD9 in P100K. However, we observed the expression of these markers also on HF-EVs in the flow cytometry analysis. The reasons behind these results may lie in technical differences. Due to the different clones used for both the CD9 and CD63 antibodies on each technique, we may have observed these differences in the expression. We further analyzed the presence of non-vesicular markers, including COXIV — mitochondrial — and GRP78 — endoplasmic reticulum — proteins, which appeared mostly in the P10K. Finally, in the flow cytometry analysis we observed the expression of other numerous surface markers: CD3, CD25, CD29, CD41b, CD44, CD49e, CD56, CD105, CD142, CD146, MCSP, HLA-ABC/MHC-I and SSEA-4. The expression of these markers demonstrated that AT and HF-EVs may be involved in a great number of biological processes such as tissue regeneration, stemness maintenance, cell adhesion, immunomodulation etc.

After the initial characterization, we employed the MSC-EVs on a battery of functional assays to test their potency for wound healing applications. First, we studied the efficacy of EVs for increasing HDFs migration. As observed in **Fig. 14A, B** all the studied groups, large and small EVs, of both cell types, demonstrated a significant increase in HDFs migration. As well as with the MSC-SLS, the effect was observed at 8 h and it was maintained until the end of the experiment (**Fig. 14C**). Thus, the efficacy of secretome-based therapies for wound closure should be attributed not only to the soluble fraction, but also to the EVs fraction.

Regarding the angiogenic potential of MSC-EVs, different studies have highlighted the properties exhibited by EVs secreted from BM-MSCs or umbilical cord MSCs (UC-MSCs). These effect has been attributed to the transfer of pro-angiogenic proteins and mi-RNAs including miR-31or miR-125 among others [118,119]. Here, we found that all of our EVs

groups exhibited an increased tube formation in HUVECs with similar values to the ones observed in the positive control group (Fig. 15A). In contrast, the tube length was similar for all groups (Fig. 15B). Finally, as well as with the tube formation, the number of branching points was higher in the EVs than in the control (Fig. 15C, D). In addition, AT-P10K, HF-P10K and HF-P100K showed a significantly higher number of branching points that in the positive control. Once again, we did not observe differences among the EV-groups in the different parameters measured.

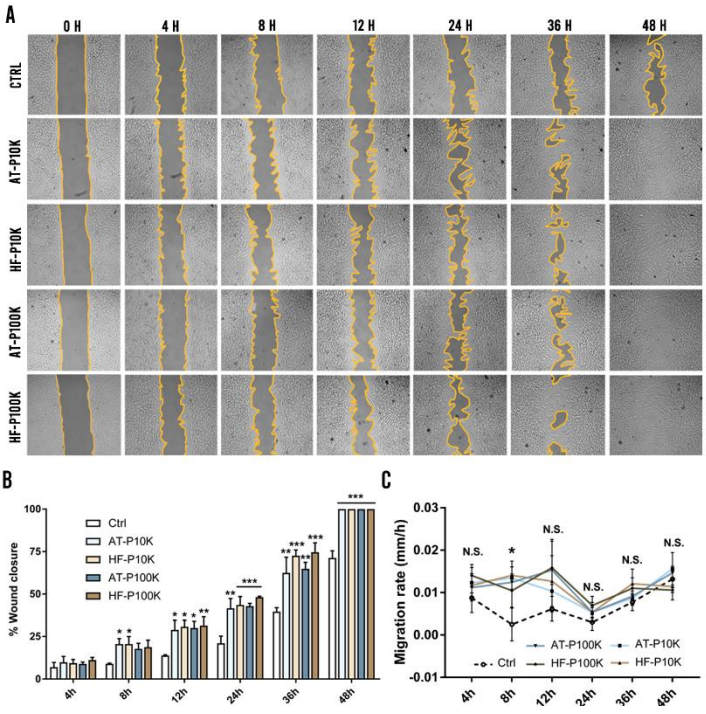

Fig.14. EVs scratch assay. A. Images of the treated and control groups at different time-points. B. Percentage of wound closure. * indicates $p < 0.05$, ** indicates $p < 0.005$, *** indicates $p < 0.001$ in comparison the control group. C. Migration rate of HDFs at different time-points. * indicates $p < 0.05$ of all groups in comparison to the control group. N.S. Non-significant.

In the same way that in the MSC-SLS studies, we also tested the ability of EVs to protect HDFs against ROS induced cytotoxicity (Fig. 15E). Some works have demonstrated that EVs derived from different cell populations can protect diverse cell

types against ROS-induced apoptosis [120-123]. Here, we did not achieve protective effects in any of the studied conditions with any of our EVs-fractions or cell types. Comparing these results, to the ones obtained before in the MSC-SLS study, we hypothesize that the soluble fraction of the secretome, or the combination of both, is the key effector to protect HDFs against ROS induced cytotoxicity. We found one work studying the MSC-EVs protective effects on HDFs; however, they used serum in the experimental media, which could have alter the obtained results [120].

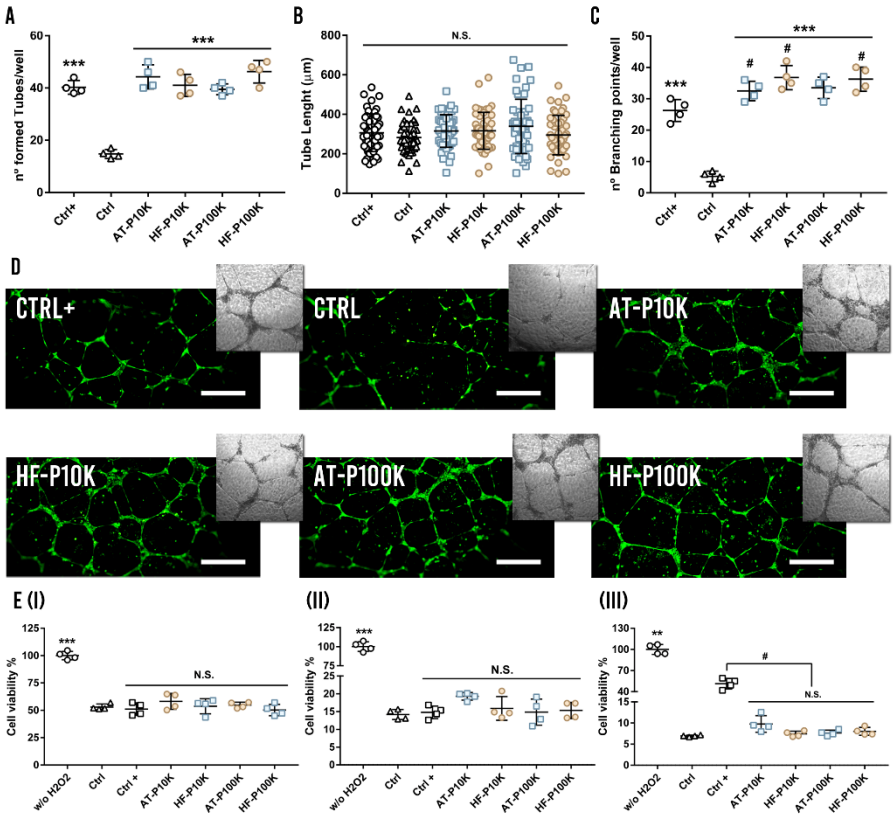

Fig.15. Angiogenesis and antioxidant assays. A. Number of formed tubes per well. B. Diameter length of the formed tubes. C. Number of branching points. *** indicates $p < 0.001$ in comparison the control group, # indicates $p < 0.05$ in comparison to the positive control group, N.S. non-significance. D. Calcein-stained fluorescence and brightfield images of the formed vessels. Scale bars are 500 μm. E. Cell survival under a H_2O_2-mediated ROS. (I) after a 2 h pre-treatment with EVs,

(II) after a 6 h pre-treatment with EVs and (III) under a 4 h co-treatment of cells with EVs and H_2O_2. ** indicates $p < 0.005$, *** indicates $p < 0.001$, N.S. non-significance in comparison to the control group, # indicates $p<0.05$ between groups.

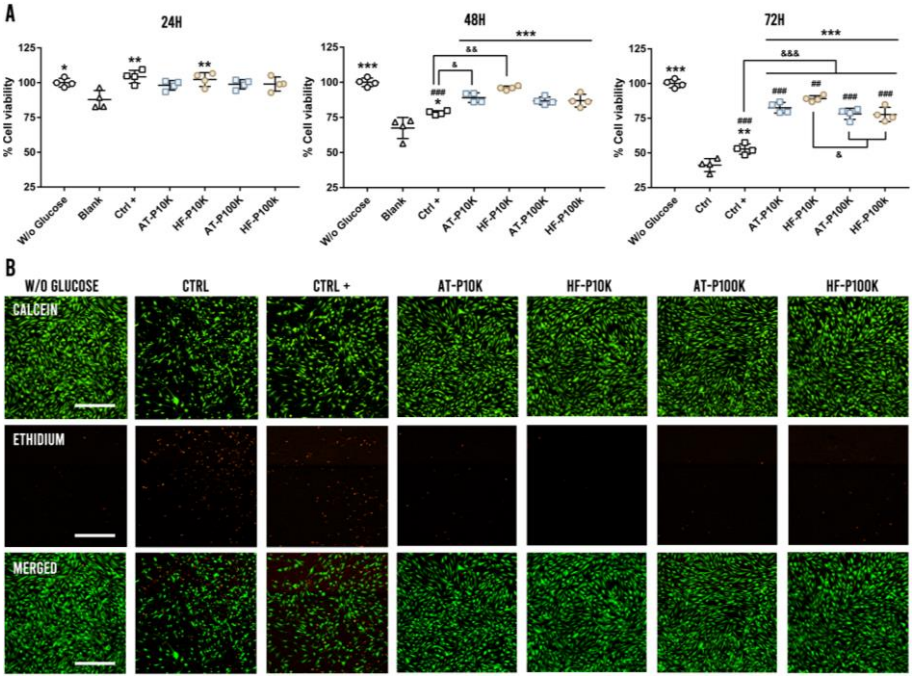

Fig.16. Cell survival under hyperglycemia. A. Percentage of cell viability at 24 h, 48 h and 72 h. * indicates $p < 0.05$, ** $p < 0.005$, *** $p < 0.001$ in comparison to the control group, ## $p < 0.005$, ### $p < 0.001$ in comparison to the w/o glucose group, & $p < 0.05$, && $p < 0.005$, &&& $p < 0.001$ between groups. B. Calcein/ethidium stained images at 72 h of hyperglycemia. Scale bars are 500 μm.

Finally, we explored the protective effects of MSC-EVs when HDFs are exposed to a hyperglycemic environment (**Fig. 16**). Our results depicted that with only a 6 h of pre-treatment, all EVs-fractions were able to protect and increase cell survival of HDFs under a cytotoxic hyperglycemic environment until 72 h of experiment. Interestingly, our results were significantly better than those obtained in the positive control group. Briefly, we found that both P10K and P100K from AT-MSCs and HF-MSCs were able to increase HDFs metabolism and viability under a hyperglycemic condition. These results suggest

that the effect observed with the complete secretome in the study 3 are mediated not only by the soluble secretome but also by the EVs-fraction.

In summary, in this study we found that the MSC-EVs are involved in a wide variety of physiological pathways. Furthermore, we demonstrated that the EVs were able to increase HDFs migration, survival under hyperglycemia and promote HUVECs angiogenesis. These results pointed that the observed effects in our previous study were also mediated by the EVs fraction. Consequently, we confirmed that this therapy could has a promising potential for wound healing purposes.

5. Bibliography

[1] P. Martin, R. Nunan, Cellular and molecular mechanisms of repair in acute and chronic wound healing, Br. J. Dermatol. 173 (2015) 370-378.

[2] A. Stojadinovic, J.W. Carlson, G.S. Schultz, T.A. Davis, E.A. Elster, Topical advances in wound care, Gynecol. Oncol. 111 (2008) S70-S80.

[3] S.A. Eming, P. Martin, M. Tomic-Canic, Wound repair and regeneration: Mechanisms, signaling, and translation, Science Translational Medicine. 6 (2014) 265sr6.

[4] B.K. Sun, Z. Siprashvili, P.A. Khavari, Advances in skin grafting and treatment of cutaneous wounds, Science. 346 (2014) 941-945.

[5] R.G. Reish, E. Eriksson, Scars: A Review of Emerging and Currently Available Therapies, Plast. Reconstr. Surg. 122 (2008).

[6] R.M. Thushara, M. Hemshekhar, Basappa, K. Kemparaju, K.S. Rangappa, K.S. Girish, Biologicals, platelet apoptosis and human diseases: An outlook, Crit. Rev. Oncol. 93 (2015) 149-158.

[7] J. Hardwicke, D. Schmaljohann, D. Boyce, D. Thomas, Epidermal growth factor therapy and wound healing — past, present and future perspectives, The Surgeon. 6 (2008) 172-177.

[8] E.M. Golebiewska, A.W. Poole, Platelet secretion: From haemostasis to wound healing and beyond, Blood Rev. 29 (2015) 153-162.

[9] L.M. Morton, T.J. Phillips, Wound healing and treating wounds: Differential diagnosis and evaluation of chronic wounds, J. Am. Acad. Dermatol. 74 (2016) 589-605.

[10] K. Las Heras, M. Igartua, E. Santos-Vizcaino, R.M. Hernandez, Chronic wounds: Current status, available strategies and emerging therapeutic solutions, J. Control. Release. 328 (2020) 532-550.

[11] W.L. Havran, J.M. Jameson, Epidermal T Cells and Wound Healing, J. Immunol. 184 (2010) 5423.

[12] P. Krzyszczyk, R. Schloss, A. Palmer, F. Berthiaume, The Role of Macrophages in Acute and Chronic Wound Healing and Interventions to Promote Pro-wound Healing Phenotypes, Frontiers in Physiology. 9 (2018).

[13] K.A.U. Gonzales, E. Fuchs, Skin and Its Regenerative Powers: An Alliance between Stem Cells and Their Niche, Developmental Cell. 43 (2017) 387-401.

[14] M.S. Hu, M.R. Borrelli, H.P. Lorenz, M.T. Longaker, D.C. Wan, Mesenchymal Stromal Cells and Cutaneous Wound Healing: A Comprehensive Review of the Background, Role, and Therapeutic Potential, Stem Cells International. 2018 (2018) 6901983.

[15] L. Liu, Y. Yu, Y. Hou, J. Chai, H. Duan, W. Chu, H. Zhang, Q. Hu, J. Du, Human umbilical cord mesenchymal stem cells transplantation promotes cutaneous wound healing of severe burned rats, PLoS One. 9 (2014) e88348.

[16] S. Motegi, O. Ishikawa, Mesenchymal stem cells: The roles and functions in cutaneous wound healing and tumor growth, J. Dermatol. Sci. 86 (2017) 83-89.

[17] I. AUKHIL, Biology of wound healing, Periodontol. 2000. 22 (2000) 44-50.

[18] S. Barrientos, O. Stojadinovic, M.S. Golinko, H. Brem, M. Tomic-Canic, PERSPECTIVE ARTICLE: Growth factors and cytokines in wound healing, Wound Repair and Regeneration. 16 (2008) 585-601.

[19] F. Moccia, S. Negri, M. Shekha, P. Faris, G. Guerra, Endothelial Ca2+ Signaling, Angiogenesis and Vasculogenesis: Just What It Takes to Make a Blood Vessel, International Journal of Molecular Sciences. 20 (2019).

[20] M. Sasaki, R. Abe, Y. Fujita, S. Ando, D. Inokuma, H. Shimizu, Mesenchymal Stem Cells Are Recruited into Wounded Skin and Contribute to Wound Repair by Transdifferentiation into Multiple Skin Cell Type, J. Immunol. 180 (2008) 2581.

[21] K.C. Rustad, V.W. Wong, M. Sorkin, J.P. Glotzbach, M.R. Major, J. Rajadas, M.T. Longaker, G.C. Gurtner, Enhancement of mesenchymal stem cell angiogenic capacity and stemness by a biomimetic hydrogel scaffold, Biomaterials. 33 (2012) 80-90.

[22] J.M. Reinke, H. Sorg, Wound Repair and Regeneration, Eur. Surg. Res. 49 (2012) 35-43.

[23] M. Xue, C.J. Jackson, Extracellular Matrix Reorganization During Wound Healing and Its Impact on Abnormal Scarring, Advances in Wound Care. 4 (2015) 119-136.

[24] K.L. Heras, M. Igartua, E. Santos-Vizcaino, R.M. Hernandez, Cell-based dressings: A journey through chronic wound management, Biomaterials Advances. 135 (2022) 212738.

[25] J. Li, J. Chen, R. Kirsner, Pathophysiology of acute wound healing, Clin. Dermatol. 25 (2007) 9-18.

[26] D.T. Ubbink, F.E. Brölmann, Go, Peter M. N. Y. H., H. Vermeulen, Evidence-Based Care of Acute Wounds: A Perspective, Advances in Wound Care. 4 (2015) 286-294.

[27] R. Beck, M. Sorge, A. Schneider, A. Dietz, Current Approaches to Epistaxis Treatment in Primary and Secondary Care, Dtsch. Arztebl Int. 115 (2018) 12-22.

[28] O. Soehnlein, S. Steffens, A. Hidalgo, C. Weber, Neutrophils as protagonists and targets in chronic inflammation, Nature Reviews Immunology. 17 (2017) 248-261.

[29] O. Soehnlein, S. Steffens, A. Hidalgo, C. Weber, Neutrophils as protagonists and targets in chronic inflammation, Nature Reviews Immunology. 17 (2017) 248-261.

[30] T.A. Wynn, K.M. Vannella, Macrophages in Tissue Repair, Regeneration, and Fibrosis, Immunity. 44 (2016) 450-462.

[31] B. Bucalo, W.H. Eaglstein, V. Falanga, Inhibition of cell proliferation by chronic wound fluid, Wound Repair and Regeneration. 1 (1993) 181-186.

[32] T. Demidova-Rice, M.R. Hamblin, I.M. Herman, Acute and Impaired Wound Healing: Pathophysiology and Current Methods for Drug Delivery, Part 2: Role of Growth Factors in Normal and Pathological Wound Healing: Therapeutic Potential and Methods of Delivery, Adv. Skin Wound Care. 25 (2012).

[33] J. Cha, T. Kwak, J. Butmarc, T. Kim, T. Yufit, P. Carson, S. Kim, V. Falanga, Fibroblasts from non-healing human chronic wounds show decreased expression of βig-h3, a TGF-β inducible protein, J. Dermatol. Sci. 50 (2008) 15-23.

[34] M.L. Usui, J.N. Mansbridge, W.G. Carter, M. Fujita, J.E. Olerud, Keratinocyte Migration, Proliferation, and Differentiation in Chronic Ulcers From Patients With Diabetes and Normal Wounds, J. Histochem. Cytochem. 56 (2008) 687-696.

[35] P.A. Shiekh, A. Singh, A. Kumar, Exosome laden oxygen releasing antioxidant and antibacterial cryogel wound dressing OxOBand alleviate diabetic and infectious wound healing, Biomaterials. 249 (2020) 120020.

[36] L. Hu, L. Zou, Q. Liu, Y. Geng, G. Xu, L. Chen, P. Pan, J. Chen, Construction of chitosan-based asymmetric antioxidant and anti-inflammatory repair film for acceleration of wound healing, Int. J. Biol. Macromol. 215 (2022) 377-386.

[37] C. Wang, J. Cherng, C. Liu, T. Fang, Z. Hong, S. Chang, G. Fan, S. Hsu, Procoagulant and Antimicrobial Effects of Chitosan in Wound Healing, International Journal of Molecular Sciences. 22 (2021).

[38] A.B. Sousa, A. Águas P., M.A. Barbosa, J.N. Barbosa, Immunomodulatory biomaterial-based wound dressings advance the healing of chronic wounds via regulating macrophage behavior, Regen Biomater. 9 (2022) rbac065.

[39] S. He, T. Walimbe, H. Chen, K. Gao, P. Kumar, Y. Wei, D. Hao, R. Liu, D.L. Farmer, K.S. Lam, J. Zhou, A. Panitch, A. Wang, Bioactive extracellular matrix scaffolds engineered with proangiogenic proteoglycan mimetics and loaded with endothelial progenitor cells promote neovascularization and diabetic wound healing, Bioactive Materials. 10 (2022) 460-473.

[40] H. Capella-Monsonís, A. De Pieri, R. Peixoto, S. Korntner, D.I. Zeugolis, Extracellular matrix-based biomaterials as adipose-derived stem cell delivery vehicles in wound healing: a comparative study between a collagen scaffold and two xenografts, Stem Cell Research & Therapy. 11 (2020) 510.

[41] L. Zaulyanov, R.S. Kirsner, A review of a bi-layered living cell treatment (Apligraf) in the treatment of venous leg ulcers and diabetic foot ulcers, Clin. Interv. Aging. 2 (2007) 93-98.

[42] W. Oualla-Bachiri, A. Fernández-González, M.I. Quiñones-Vico, S. Arias-Santiago, From Grafts to Human Bioengineered Vascularized Skin Substitutes, International Journal of Molecular Sciences. 21 (2020).

[43] C.M. Zelen, T.E. Serena, L. Gould, L. Le, M.J. Carter, J. Keller, W.W. Li, Treatment of chronic diabetic lower extremity ulcers with advanced therapies: a prospective, randomised, controlled, multi-centre comparative study examining clinical efficacy and cost, Int Wound J. 13 (2016) 272-282.

[44] M.A. Towler, E.W. Rush, M.K. Richardson, C.L. Williams, Randomized, Prospective, Blinded-Enrollment, Head-To-Head Venous Leg Ulcer Healing Trial Comparing Living, Bioengineered Skin Graft Substitute (Apligraf) with Living, Cryopreserved, Human Skin Allograft (TheraSkin), Clin. Podiatr. Med. Surg. 35 (2018) 357-365.

[45] M.J. Carter, C. Waycaster, K. Schaum, A.M. Gilligan, Cost-Effectiveness of Three Adjunct Cellular/Tissue-Derived Products Used in the Management of Chronic Venous Leg Ulcers, Value in Health. 17 (2014) 801-813.

[46] M. Otero-Viñas, V. Falanga, Mesenchymal Stem Cells in Chronic Wounds: The Spectrum from Basic to Advanced Therapy, Advances in Wound Care. 5 (2016) 149-163.

[47] J. Guo, H. Hu, J. Gorecka, H. Bai, H. He, R. Assi, T. Isaji, T. Wang, O. Setia, L. Lopes, Y. Gu, A. Dardik, Adipose-derived mesenchymal stem cells accelerate diabetic wound healing in a similar fashion as bone marrow-derived cells, American Journal of Physiology-Cell Physiology. 315 (2018) C885-C896.

[48] L. Xu, L. Ding, L. Wang, Y. Cao, H. Zhu, J. Lu, X. Li, T. Song, Y. Hu, J. Dai, Umbilical cord-derived mesenchymal stem cells on scaffolds facilitate collagen degradation via upregulation of MMP-9 in rat uterine scars, Stem Cell Research & Therapy. 8 (2017) 84.

[49] Y. Han, X. Li, Y. Zhang, Y. Han, F. Chang, J. Ding, Mesenchymal Stem Cells for Regenerative Medicine, Cells. 8 (2019).

[50] I. Tennison, S. Roschnik, B. Ashby, R. Boyd, I. Hamilton, T. Oreszczyn, A. Owen, M. Romanello, P. Ruyssevelt, J.D. Sherman, A.Z.P. Smith, K. Steele, N. Watts, M.J. Eckelman, Health care's response to climate change: a carbon footprint assessment of the NHS in England, The Lancet Planetary Health. 5 (2021) e84-e92.

[51] A.J. McMichael, C.D. Butler, Promoting Global Population Health While Constraining the Environmental Footprint, Annu. Rev. Public Health. 32 (2011) 179-197.

[52] F.G. Santeramo, Circular and green economy: the state-of-the-art, Heliyon. 8 (2022).

[53] C.P. Ginga, J.M.C. Ongpeng, M.K.M. Daly, Circular Economy on Construction and Demolition Waste: A Literature Review on Material Recovery and Production, Materials. 13 (2020).

[54] E.G. Feigal, K. Tsokas, S. Viswanathan, J. Zhang, C. Priest, J. Pearce, N. Mount, Proceedings: International Regulatory Considerations on Development Pathways for Cell Therapies, Stem Cells Transl Med. 3 (2014) 879-887.

[55] T.C. Sarker, Azam, Shah Md Golam Gousul, G. Bonanomi, Recent Advances in Sugarcane Industry Solid By-Products Valorization, Waste and Biomass Valorization. 8 (2017) 241-266.

[56] A. Pinho-Gomes, J. Cairns, Evaluation of Advanced Therapy Medicinal Products by the National Institute for Health and Care Excellence (NICE): An Updated Review, PharmacoEconomics - Open. 6 (2022) 147-167.

[57] P.R. Baraniak, T.C. McDevitt, Stem cell paracrine actions and tissue regeneration, Regenerative Medicine. 5 (2010) 121-143.

[58] A. Nagelkerke, M. Ojansivu, L. van der Koog, T.E. Whittaker, E.M. Cunnane, A.M. Silva, N. Dekker, M.M. Stevens, Extracellular vesicles for tissue repair and regeneration: Evidence, challenges and opportunities, Adv. Drug Deliv. Rev. 175 (2021) 113775.

[59] E. Munoz-Perez, A. Gonzalez-Pujana, M. Igartua, E. Santos-Vizcaino, R.M. Hernandez, Mesenchymal Stromal Cell Secretome for the Treatment of Immune-Mediated Inflammatory Diseases: Latest Trends in Isolation, Content Optimization and Delivery Avenues, Pharmaceutics. 13 (2021).

[60] R. Kalluri, V.S. LeBleu, The biology, function, and biomedical applications of exosomes, Science. 367 (2020) eaau6977.

[61] D. Tsiapalis, L. O'Driscoll, Mesenchymal Stem Cell Derived Extracellular Vesicles for Tissue Engineering and Regenerative Medicine Applications, Cells. 9 (2020).

[62] J. Cabral, A.E. Ryan, M.D. Griffin, T. Ritter, Extracellular vesicles as modulators of wound healing, Adv. Drug Deliv. Rev. 129 (2018) 394-406.

[63] O.P.B. Wiklander, M.Á Brennan, J. Lötvall, X.O. Breakefield, S. EL Andaloussi, Advances in therapeutic applications of extracellular vesicles, Science Translational Medicine. 11 (2019) eaav8521.

[64] J. Wu, Y. Piao, Q. Liu, X. Yang, Platelet-rich plasma-derived extracellular vesicles: A superior alternative in regenerative medicine? Cell Prolif. 54 (2021) e13123.

[65] L. Huleihel, G.S. Hussey, J.D. Naranjo, L. Zhang, J.L. Dziki, N.J. Turner, D.B. Stolz, S.F. Badylak, Matrix-bound nanovesicles within ECM bioscaffolds, Science Advances. 2 e1600502.

[66] B. Hernaez-Estrada, A. Gonzalez-Pujana, A. Cuevas, A. Izeta, K.L. Spiller, M. Igartua, E. Santos-Vizcaino, R.M. Hernandez, Human Hair Follicle-Derived Mesenchymal Stromal Cells from the Lower Dermal Sheath as a Competitive Alternative for Immunomodulation, Biomedicines. 10 (2022) 253. doi: 10.3390/biomedicines10020253.

[67] J.C. Doloff, O. Veiseh, A.J. Vegas, H.H. Tam, S. Farah, M. Ma, J. Li, A. Bader, A. Chiu, A. Sadraei, S. Aresta-Dasilva, M. Griffin, S. Jhunjhunwala, M. Webber, S. Siebert, K. Tang, M. Chen, E. Langan, N. Dholokia, R. Thakrar, M. Qi, J. Oberholzer, D.L. Greiner, R. Langer, D.G. Anderson, Colony stimulating factor-1 receptor is a central component of the foreign body response to biomaterial implants in rodents and non-human primates, Nat. Mater. 16 (2017) 671-680.

[68] J. Li, A.D. Celiz, J. Yang, Q. Yang, I. Wamala, W. Whyte, B.R. Seo, N.V. Vasilyev, J.J. Vlassak, Z. Suo, D.J. Mooney, Tough adhesives for diverse wet surfaces, Science. 357 (2017) 378-381.

[69] H.K. No, N. Young Park, S. Ho Lee, S.P. Meyers, Antibacterial activity of chitosans and chitosan oligomers with different molecular weights, Int. J. Food Microbiol. 74 (2002) 65-72.

[70] U.K. Sinha, L.A. Gallagher, Effects of steel scalpel, ultrasonic scalpel, CO2 laser, and monopolar and bipolar electrosurgery on wound healing in guinea pig oral mucosa, Laryngoscope. 113 (2003) 228-236.

[71] I. Garcia-Orue, G. Gainza, F.B. Gutierrez, J.J. Aguirre, C. Evora, J.L. Pedraz, R.M. Hernandez, A. Delgado, M. Igartua, Novel nanofibrous dressings containing rhEGF and Aloe vera for wound healing applications, Int. J. Pharm. 523 (2017) 556-566.

[72] I. Garcia-Orue, E. Santos-Vizcaino, A. Etxabide, J. Uranga, A. Bayat, P. Guerrero, M. Igartua, K. de la Caba, R.M. Hernandez, Development of Bioinspired Gelatin and Gelatin/Chitosan Bilayer Hydrofilms for Wound Healing, Pharmaceutics. 11 (2019).

[73] I. Garcia-Orue, G. Gainza, P. Garcia-Garcia, F.B. Gutierrez, J.J. Aguirre, R.M. Hernandez, A. Delgado, M. Igartua, Composite nanofibrous membranes of PLGA/Aloe vera containing lipid nanoparticles for wound dressing applications, Int. J. Pharm. 556 (2019) 320-329.

[74] I. Garcia-Orue, E. Santos-Vizcaino, P. Sanchez, F.B. Gutierrez, J.J. Aguirre, R.M. Hernandez, M. Igartua, Bioactive and degradable hydrogel based on human platelet-rich plasma fibrin matrix combined with oxidized alginate in a diabetic mice wound healing model, Biomaterials Advances. 135 (2022) 112695.

[75] P. Guerrero, J.P. Kerry, K. de la Caba, FTIR characterization of protein–polysaccharide interactions in extruded blends, Carbohydr. Polym. 111 (2014) 598-605.

[76] T. Garrido, A. Etxabide, K. de la Caba, P. Guerrero, Versatile soy protein films and hydrogels by the incorporation of β-chitin from squid pens (Loligo sp.), Green Chem. 19 (2017) 5923-5931.

[77] U. Eckhard, E. Schönauer, D. Nüss, H. Brandstetter, Structure of collagenase G reveals a chew-and-digest mechanism of bacterial collagenolysis, Nature Structural & Molecular Biology. 18 (2011) 1109-1114.

[78] Q.L. Loh, C. Choong, Three-Dimensional Scaffolds for Tissue Engineering Applications: Role of Porosity and Pore Size, Tissue Engineering Part B: Reviews. 19 (2013) 485-502.

[79] D.W. Hutmacher, Scaffolds in tissue engineering bone and cartilage, Biomaterials. 21 (2000) 2529-2543.

[80] T. Mygind, M. Stiehler, A. Baatrup, H. Li, X. Zou, A. Flyvbjerg, M. Kassem, C. Bünger, Mesenchymal stem cell ingrowth and differentiation on coralline hydroxyapatite scaffolds, Biomaterials. 28 (2007) 1036-1047.

[81] C.M. Murphy, F.J. O'Brien, Understanding the effect of mean pore size on cell activity in collagen-glycosaminoglycan scaffolds, Cell Adhesion & Migration. 4 (2010) 377-381.

[82] C. Libioulle, L. Corbesier, R. Gilles, Changes in major intracellular osmolytes in L-929 cells following rapid and slow application of hyperosmotic media, Comparative Biochemistry and Physiology Part A: Molecular & Integrative Physiology. 130 (2001) 461-470.

[83] J.C. Doloff, O. Veiseh, A.J. Vegas, H.H. Tam, S. Farah, M. Ma, J. Li, A. Bader, A. Chiu, A. Sadraei, S. Aresta-Dasilva, M. Griffin, S. Jhunjhunwala, M. Webber, S. Siebert, K. Tang, M. Chen, E. Langan, N. Dholokia, R. Thakrar, M. Qi, J. Oberholzer, D.L. Greiner, R. Langer, D.G. Anderson, Colony stimulating factor-1 receptor is a central component of the foreign body response to biomaterial implants in rodents and non-human primates, Nat. Mater. 16 (2017) 671-680.

[84] K. Nagai, K. Inouye, Insights into the reaction mechanism of the coagulation of soy protein isolates induced by subtilisin carlsberg, J. Agric. Food Chem. 52 (2004) 4921-4927.

[85] S. Li Tay, H. Yao Tan, C. Perera, The Coagulating Effects of Cations and Anions on Soy Protein, Int. J. Food Prop. 9 (2006) 317-323.

[86] T.E. Williams, L. Arango, M.H. Donaldson, F.M. Shepard, Vitamin K Requirement of Normal Infants on Soy Protein Formula: Does 27 Micrograms of Vitamin K per Liter Meet the Minimum Daily Requirement? Clin. Pediatr. 9 (1970) 79-82.

[87] G. Ferland, The Discovery of Vitamin K and Its Clinical Applications, Ann. Nutr. Metab. 61 (2012) 213-218.

[88] O. Kononova, R.I. Litvinov, D.S. Blokhin, V.V. Klochkov, J.W. Weisel, J.S. Bennett, V. Barsegov, Mechanistic Basis for the Binding of RGD- and AGDV-Peptides to the Platelet Integrin αIIbβ3, Biochemistry (N. Y.). 56 (2017) 1932-1942.

[89] M. Alipour, M. Baneshi, S. Hosseinkhani, R. Mahmoudi, A. Jabari Arabzadeh, M. Akrami, J. Mehrzad, H. Bardania, Recent progress in biomedical applications of RGD-based ligand: From precise cancer theranostics to biomaterial engineering: A systematic review, J. Biomed. Mater. Res. 108 (2020) 839-850.

[90] X. Song, C. Zhu, D. Fan, Y. Mi, X. Li, R.Z. Fu, Z. Duan, Y. Wang, R.R. Feng, A Novel Human-Like Collagen Hydrogel Scaffold with Porous Structure and Sponge-Like Properties, Polymers. 9 (2017).

[91] L. Zhu, J. Qiu, E. Sakai, A high modulus hydrogel obtained from hydrogen bond reconstruction and its application in vibration damper, RSC Adv. 7 (2017) 43755-43763.

[92] M. Jürgens, J. Olbricht, B. Fedelich, B. Skrotzki, Low Cycle Fatigue and Relaxation Performance of Ferritic–Martensitic Grade P92 Steel, Metals. 9 (2019).

[93] L. Zhu, J. Qiu, E. Sakai, A high modulus hydrogel obtained from hydrogen bond reconstruction and its application in vibration damper, RSC Adv. 7 (2017) 43755-43763.

[94] L. Wang, P.H.P. D'Alpino, L.G. Lopes, J.C. Pereira, Mechanical properties of dental restorative materials: relative contribution of laboratory tests, J. Appl. Oral Sci. 11 (2003) 162-167.

[95] M. Weber, H. Steinle, S. Golombek, L. Hann, C. Schlensak, H.P. Wendel, M. Avci-Adali, Blood-Contacting Biomaterials: In Vitro Evaluation of the Hemocompatibility, Frontiers in Bioengineering and Biotechnology. 6 (2018).

[96] J. Zhu, H. Han, F. Li, X. Wang, J. Yu, X. Qin, D. Wu, Peptide-Functionalized Amino Acid-Derived Pseudoprotein-Based Hydrogel with Hemorrhage Control and Antibacterial Activity for Wound Healing, Chem. Mater. 31 (2019) 4436-4450.

[97] A.H. Gillespie, A. Doctor, Red Blood Cell Contribution to Hemostasis, Frontiers in Pediatrics. 9 (2021).

[98] G. Barshtein, R. Ben-Ami, S. Yedgar, Role of red blood cell flow behavior in hemodynamics and hemostasis, Expert Review of Cardiovascular Therapy. 5 (2007) 743-752.

[99] J.W. Weisel, R.I. Litvinov, Red blood cells: the forgotten player in hemostasis and thrombosis, J Thromb Haemost. 17 (2019) 271-282.

[100] M. Alipour, M. Baneshi, S. Hosseinkhani, R. Mahmoudi, A. Jabari Arabzadeh, M. Akrami, J. Mehrzad, H. Bardania, Recent progress in biomedical applications of RGD-based ligand: From precise cancer theranostics to biomaterial engineering: A systematic review, J. Biomed. Mater. Res. 108 (2020) 839-850.

[101] J. Sánchez-Cortés, M. Mrksich, The Platelet Integrin αIIbβ3 Binds to the RGD and AGD Motifs in Fibrinogen, Chem. Biol. 16 (2009) 990-1000.

[102] W.J. King, P.H. Krebsbach, Growth factor delivery: How surface interactions modulate release in vitro and in vivo, Adv. Drug Deliv. Rev. 64 (2012) 1239-1256.

[103] C. Dunnill, T. Patton, J. Brennan, J. Barrett, M. Dryden, J. Cooke, D. Leaper, N.T. Georgopoulos, Reactive oxygen species (ROS) and wound healing: the functional role of ROS and emerging ROS-modulating technologies for augmentation of the healing process, Int Wound J. 14 (2017) 89-96.

[104] Y. Wang, R. Branicky, A. Noë, S. Hekimi, Superoxide dismutases: Dual roles in controlling ROS damage and regulating ROS signaling, J. Cell Biol. 217 (2018) 1915-1928.

[105] D. Nawrocka, K. Kornicka, J. Szydlarska, K. Marycz, Basic Fibroblast Growth Factor Inhibits Apoptosis and Promotes Proliferation of Adipose-Derived Mesenchymal Stromal Cells Isolated from Patients with Type 2 Diabetes by Reducing Cellular Oxidative Stress, Oxid Med. Cell. Longev. 2017 (2017) 3027109.

[106] C. Bouffi, C. Bony, G. Courties, C. Jorgensen, D. Noël, IL-6-dependent PGE2 secretion by mesenchymal stem cells inhibits local inflammation in experimental arthritis, PLoS One. 5 (2010) e14247.

[107] C. Hu, L. Zhao, C. Peng, L. Li, Regulation of the mitochondrial reactive oxygen species: Strategies to control mesenchymal stem cell fates ex vivo and in vivo, J. Cell. Mol. Med. 22 (2018) 5196-5207.

[108] Z. Zhang, J. Li, L. Yang, R. Chen, R. Yang, H. Zhang, D. Cai, H. Chen, The cytotoxic role of intermittent high glucose on apoptosis and cell viability in pancreatic beta cells, J. Diabetes Res. 2014 (2014) 712781.

[109] I.B. Wall, R. Moseley, D.M. Baird, D. Kipling, P. Giles, I. Laffafian, P.E. Price, D.W. Thomas, P. Stephens, Fibroblast dysfunction is a key factor in the non-healing of chronic venous leg ulcers, J. Invest. Dermatol. 128 (2008) 2526-2540.

[110] M. Zou, Y. Teng, J. Wu, S. Liu, X. Tang, Y. Jia, Z. Chen, K. Zhang, Z. Sun, X. Li, J. Ye, R. Xu, F. Yuan, Fibroblasts: Heterogeneous Cells With Potential in Regenerative Therapy for Scarless Wound Healing, Front. Cell. Dev. Biol. 9 (2021) 713605.

[111] M. Piipponen, D. Li, N.X. Landén, The Immune Functions of Keratinocytes in Skin Wound Healing, Int. J. Mol. Sci. 21 (2020) 8790. doi: 10.3390/ijms21228790.

[112] T. Schreier, E. Degen, W. Baschong, Fibroblast migration and proliferation during in vitro wound healing. A quantitative comparison between various growth factors and a low molecular weight blood dialysate used in the clinic to normalize impaired wound healing, Res. Exp. Med. (Berl). 193 (1993) 195-205.

[113] R. Geesala, N. Bar, N.R. Dhoke, P. Basak, A. Das, Porous polymer scaffold for on-site delivery of stem cells – Protects from oxidative stress and potentiates wound tissue repair, Biomaterials. 77 (2016) 1-13.

[114] A. Shafiee, A.S. Cavalcanti, N.T. Saidy, D. Schneidereit, O. Friedrich, A. Ravichandran, E. De-Juan-Pardo M., D.W. Hutmacher, Convergence of 3D printed biomimetic wound dressings and adult stem cell therapy, Biomaterials. 268 (2021) 120558.

[115] O.P.B. Wiklander, M.Á Brennan, J. Lötvall, X.O. Breakefield, S. El Andaloussi, Advances in therapeutic applications of extracellular vesicles, Sci. Transl. Med. 11 (2019) eaav8521. doi: 10.1126/scitranslmed.aav8521.

[116] J. Cabral, A.E. Ryan, M.D. Griffin, T. Ritter, Extracellular vesicles as modulators of wound healing, Adv. Drug Deliv. Rev. 129 (2018) 394-406.

[117] D. Tsiapalis, L. O'Driscoll, Mesenchymal Stem Cell Derived Extracellular Vesicles for Tissue Engineering and Regenerative Medicine Applications, Cells. 9 (2020) 991. doi: 10.3390/cells9040991.

[118] D. Todorova, S. Simoncini, R. Lacroix, F. Sabatier, F. Dignat-George, Extracellular Vesicles in Angiogenesis, Circ. Res. 120 (2017) 1658-1673.

[119] S. Keshtkar, N. Azarpira, M.H. Ghahremani, Mesenchymal stem cell-derived extracellular vesicles: novel frontiers in regenerative medicine, Stem Cell Research & Therapy. 9 (2018) 63.

[120] T. Matsuoka, K. Takanashi, K. Dan, K. Yamamoto, K. Tomobe, T. Shinozuka, Effects of mesenchymal stem cell-derived exosomes on oxidative stress responses in skin cells, Mol. Biol. Rep. 48 (2021) 4527-4535.

[121] Z. Liu, Y. Xu, Y. Wan, J. Gao, Y. Chu, J. Li, Exosomes from adipose-derived mesenchymal stem cells prevent cardiomyocyte apoptosis induced by oxidative stress, Cell. Death Discov. 5 (2019) 79-5. eCollection 2019.

[122] G. Zhao, F. Liu, Z. Liu, K. Zuo, B. Wang, Y. Zhang, X. Han, A. Lian, Y. Wang, M. Liu, F. Zou, P. Li, X. Liu, M. Jin, J.Y. Liu, MSC-derived exosomes attenuate cell death through suppressing AIF nucleus translocation and enhance cutaneous wound healing, Stem Cell Research & Therapy. 11 (2020) 174.

[123] B. Shi, Y. Wang, R. Zhao, X. Long, W. Deng, Z. Wang, Bone marrow mesenchymal stem cell-derived exosomal miR-21 protects C-kit+ cardiac stem cells from oxidative injury through the PTEN/PI3K/Akt axis, PLoS One. 13 (2018) e0191616.

[124] S. Fang, C. Xu, Y. Zhang, C. Xue, C. Yang, H. Bi, X. Qian, M. Wu, K. Ji, Y. Zhao, Y. Wang, H. Liu, X. Xing, Umbilical Cord-Derived Mesenchymal Stem Cell-Derived Exosomal MicroRNAs Suppress Myofibroblast Differentiation by Inhibiting the Transforming Growth Factor-beta/SMAD2 Pathway During Wound Healing, Stem Cells Transl. Med. 5 (2016) 1425-1439.

[125] S.C. Tao, S.C. Guo, M. Li, Q.F. Ke, Y.P. Guo, C.Q. Zhang, Chitosan Wound Dressings Incorporating Exosomes Derived from MicroRNA-126-Overexpressing Synovium Mesenchymal Stem Cells Provide Sustained Release of Exosomes and Heal Full-Thickness Skin Defects in a Diabetic Rat Model, Stem Cells Transl. Med. 6 (2017) 736-747.

[126] Q. Shi, Z. Qian, D. Liu, J. Sun, X. Wang, H. Liu, J. Xu, X. Guo, GMSC-Derived Exosomes Combined with a Chitosan/Silk Hydrogel Sponge Accelerates Wound Healing in a Diabetic Rat Skin Defect Model, Front. Physiol. 8 (2017) 904.

[127] G. Fuhrmann, R. Chandrawati, P.A. Parmar, T.J. Keane, S.A. Maynard, S. Bertazzo, M.M. Stevens, Engineering Extracellular Vesicles with the Tools of Enzyme Prodrug Therapy, Adv Mater. 30 (2018) e1706616.

[128] N. Xu, L. Wang, J. Guan, C. Tang, N. He, W. Zhang, S. Fu, Wound healing effects of a Curcuma zedoaria polysaccharide with platelet-rich plasma exosomes assembled on chitosan/silk hydrogel sponge in a diabetic rat model, Int. J. Biol. Macromol. 117 (2018) 102-107.

[129] C. Wang, M. Wang, T. Xu, X. Zhang, C. Lin, W. Gao, H. Xu, B. Lei, C. Mao, Engineering Bioactive Self-Healing Antibacterial Exosomes Hydrogel for Promoting Chronic Diabetic Wound Healing and Complete Skin Regeneration, Theranostics. 9 (2019) 65-76.

[130] H. Henriques-Antunes, R.M.S. Cardoso, A. Zonari, J. Correia, E.C. Leal, A. Jiménez-Balsa, M.M. Lino, A. Barradas, I. Kostic, C. Gomes, J.M. Karp, E. Carvalho, L. Ferreira, The Kinetics of Small Extracellular Vesicle Delivery Impacts Skin Tissue Regeneration, ACS Nano. 13 (2019) 8694-8707.

[131] C. Wang, C. Liang, R. Wang, X. Yao, P. Guo, W. Yuan, Y. Liu, Y. Song, Z. Li, X. Xie, The fabrication of a highly efficient self-healing hydrogel from natural biopolymers loaded with exosomes for the synergistic promotion of severe wound healing, Biomater. Sci. 8 (2019) 313-324.

[132] S. Shafei, M. Khanmohammadi, R. Heidari, H. Ghanbari, V. Taghdiri Nooshabadi, S. Farzamfar, M. Akbariqomi, N.S. Sanikhani, M. Absalan, G. Tavoosidana, Exosome loaded alginate hydrogel promotes tissue regeneration in full-thickness skin wounds: An in vivo study, J. Biomed. Mater. Res. A. 108 (2020) 545-556.

[133] P.A. Shiekh, A. Singh, A. Kumar, Exosome laden oxygen releasing antioxidant and antibacterial cryogel wound dressing OxOBand alleviate diabetic and infectious wound healing, Biomaterials. 249 (2020) 120020.

[134] S. Ichioka, S. Kouraba, N. Sekiya, N. Ohura, T. Nakatsuka, Bone marrow-impregnated collagen matrix for wound healing: experimental evaluation in a microcirculatory model of angiogenesis, and clinical experience, Br. J. Plast. Surg. 58 (2005) 1124-1130.

[135] T. Yoshikawa, H. Mitsuno, I. Nonaka, Y. Sen, K. Kawanishi, Y. Inada, Y. Takakura, K. Okuchi, A. Nonomura, Wound therapy by marrow mesenchymal cell transplantation, Plast. Reconstr. Surg. 121 (2008) 860-877.

[136] H. Ravari, D. Hamidi-Almadari, M. Salimifar, S. Bonakdaran, M.R. Parizadeh, G. Koliakos, Treatment of non-healing wounds with autologous bone marrow cells, platelets, fibrin glue and collagen matrix, Cytotherapy. 13 (2011) 705-711.

[137] K.C. Moon, H.S. Suh, K.B. Kim, S.K. Han, K.W. Young, J.W. Lee, M.H. Kim, Potential of Allogeneic Adipose-Derived Stem Cell-Hydrogel Complex for Treating Diabetic Foot Ulcers, Diabetes. 68 (2019) 837-846.

[138] X. Zeng, Y. Tang, K. Hu, W. Jiao, L. Ying, L. Zhu, J. Liu, J. Xu, Three-week topical treatment with placenta-derived mesenchymal stem cells hydrogel in a patient with diabetic foot ulcer: A case report, Medicine (Baltimore). 96 (2017) e9212.

[139] S. Hashemi, A.A. Mohammadi, K. Moshirabadi, M. Zardosht, Effect of dermal fibroblasts and mesenchymal stem cells seeded on an amniotic membrane scaffold in skin regeneration: A case series, J Cosmet Dermatol. n/a (2021).

Chapter 2

Conclusions

Este capítulo está sujeto a confidencialidad por el autor

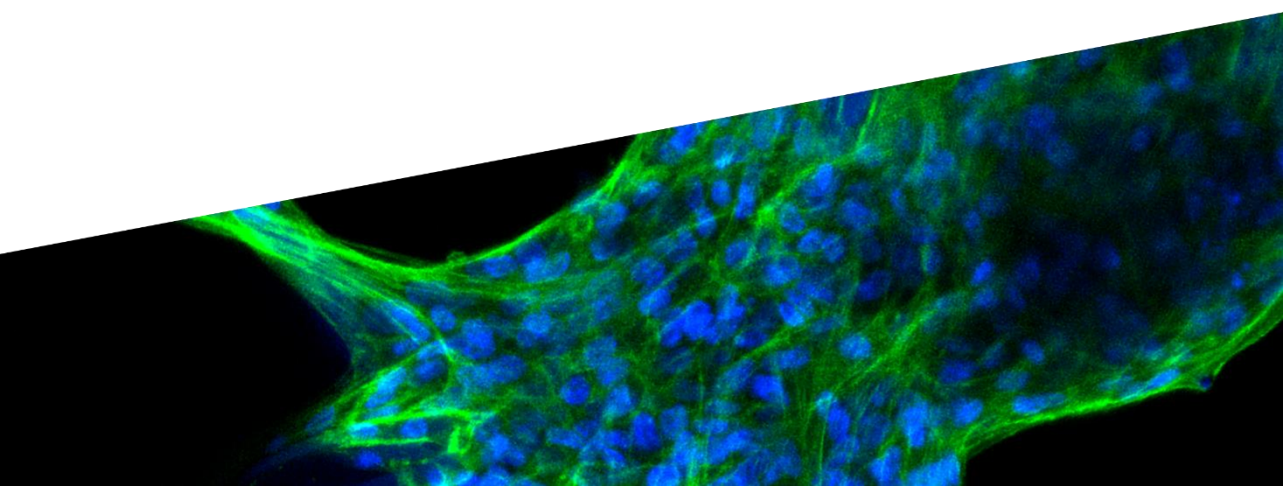

Based on the results obtained in the experimental studies, the main conclusions of this doctoral thesis are the following:

1. The combination of valorized SPI with CH allowed us to obtain highly porous SLS by employing a circular economy strategy, with promising morphological and physicochemical properties, which allows a great fluid absorption capacity. Furthermore, the SLS exhibited an adequate biocompatibility both *in vitro* and *in vivo*, potentiated by a simple pre-conditioning step.

2. The presence of SPI on its composition and the morphological features of the SLS conferred the developed biosystem with hemostatic properties equal or superior to the current gold standards in clinic. Thus, the SLS demonstrated to decrease clotting time and increase erythrocyte and platelet adhesion. Furthermore, the great mechanical properties and degradation behaviour exhibited highlighted the possibility to use these SLS as "next-generation" nasal packs.

3. The SLS demonstrated to be a great niche for MSCs to attach, proliferate and spread into their microarchitecture. Furthermore, the combination of MSCs with SLS exhibited proliferative, pro-angiogenic, antioxidant and protective effects in different skin cell types. Eventually, the MSC-SLS demonstrated to decrease wound closure time, increase re-epithelialization, decrease inflammation and increase collagen deposition *in vivo*.

4. Research on the different subpopulations of EVs secreted by these MSCs allowed us to obtain a "cell-free" therapy suitable for chronic wounds treatment. Thus, both the P10K and the P100K expressed different markers involved in a wide variety of biological processes. Eventually, the EVs showed pro-angiogenic properties on endothelial cells and the ability to increase fibroblasts proliferation, migration and protection against glucose-induced cytotoxicity.

Chapter 3

Appendixes

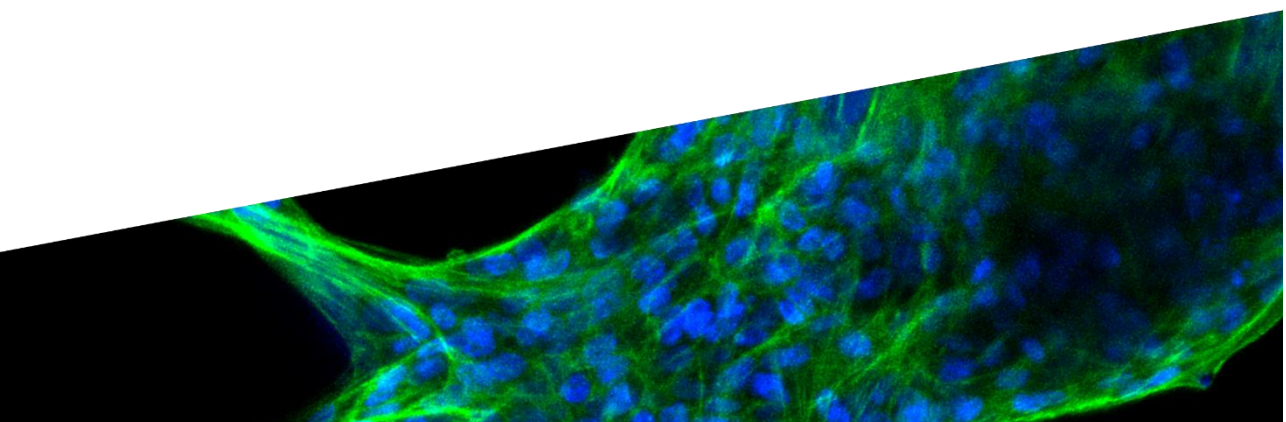

Green Chemistry

ROYAL SOCIETY OF CHEMISTRY

PAPER

View Article Online
View Journal | View Issue

Check for updates

Cite this: Green Chem., 2020, 22, 3445

Soy protein and chitin sponge-like scaffolds: from natural by-products to cell delivery systems for biomedical applications†

K. Las Heras a,1, E. Santos-Vizcaino a,b,1, T. Garrido c, F. Borja Gutierrez d, J. J. Aguirre d,e, K. de la Caba c, P. Guerrero c,*, M. Igartua a,b and R. M. Hernandez a,b,*.

[a] NanoBioCel Group, Laboratory of Pharmaceutics, School of Pharmacy, University of the Basque Country (UPV/EHU), Paseo de la Universidad 7, 01006 Vitoria-Gasteiz, Spain

[b] Biomedical Research Networking Centre in Bioengineering, Biomaterials and Nanomedicine (CIBER-BBN), 01006 Vitoria-Gasteiz, Spain

[c] BIOMAT Research Group, Chemical and Environmental Engineering Department, Engineering College of Gipuzkoa, University of the Basque Country (UPV/EHU), Plaza de Europa 1, 20018 Donostia-San Sebastián, Spain

[d] Hospital Universitario de Álava (HUA) Txagorritxu, Vitoria-Gasteiz 01009, Spain.

[e] Biopraxis Research AIE, Miñano, Vitoria-Gasteiz, Spain

[1] These two authors contributed equally to this work.

* Corresponding authors at: Laboratory of Pharmaceutics, University of the Basque Country, School of Pharmacy (Rosa Maria Hernandez). BIOMAT Research Group, Chemical and Environmental Engineering Department, Engineering College of Gipuzkoa, University of the Basque Country (UPV/EHU) (Pedro Guerrero). Rosa Maria Hernandez and Pedro Guerrero equally share credit for senior authorship.

.....

Published in: ***Green Chemistry***, 2020

Impact Factor 2020: ***10.182*** (Q1, D1)

DOI: 10.1039/d0gc00089b

Cat: Royal Society of Chemistry

Abstract

The increasing necessity of developing new devices for biomedical applications has added a growing social need of being environmentally respectful. In this work, we have shown that natural by-products from the food industry (soy protein and β-chitin) can be an excellent source of biomaterials to produce 3D scaffolds through simpler and cleaner processes. With the mixture of the two polymers, we have developed sponge-like scaffolds (SLS) with great physicochemical properties. Furthermore, a dialysis pre-conditioning step was enough to obtain negligible cytotoxicity in vitro. The predominant M2 macrophage profile, an elevated deposition of collagen fibers and the enhanced neovascularization capacity suggested an excellent biocompatibility also in vivo. Moreover, these SLS were able to promote cell adhesion, proliferation and high load capacity. Finally, h-MSCs 3D-cultured in these SLS released four times higher VEGF than h-MSCs seeded onto 2D plates. The green thinking strategy, properties and biocompatibility of this SLS highlight its potential as a cell delivery system for biomedical applications.

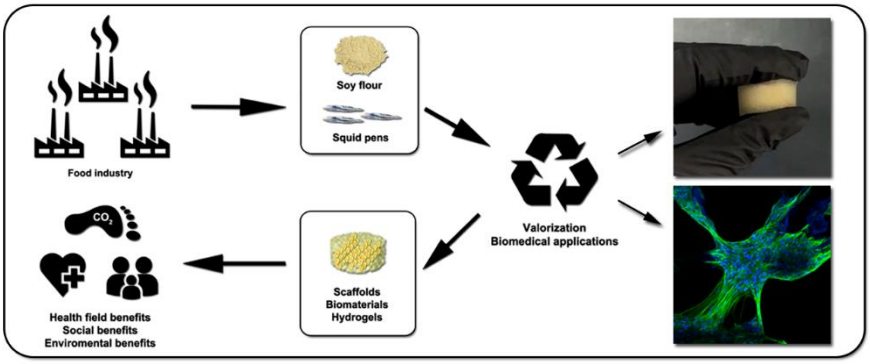

1. Introduction

Nowadays, chronic and degenerative diseases caused by compromised tissues, together with the increase in life´s expectancy, have become one of the

most important healthcare challenges worldwide [1]. Thus, scaffolds have been widely employed due to two main points. On the one hand, the capacity to mimic the extracellular matrix (ECM); on the other hand, the ability to host different cell populations on their porous microarchitecture [2-4]. The retaining of cells, within a 3D environment, enables an optimal tissue repair scenario, protecting the seeded cells from environmental stress and simulating a native-like state for them [5]. However, the search for adequate sources of biomaterials represents one of the challenges to be faced in the field of tissue engineering and regenerative medicine. Simultaneously, food industry produces millions of tons of natural by-products. These by-products are often discarded, instead of being valorized with the aim of reverting to a social benefit. For example, they could become a source of economical, scalable and sustainable biomaterials to develop potentially therapeutic products [6].

Through this study, we followed a green strategy by using biopolymers. These biopolymers were obtained from industrial by-products to develop a brand new sponge-like scaffold (SLS) that does not only serve as a cell delivery system, but also meets the requirements for biomedical applications (Fig. 1). Green chemistry involves the use of safe and clean materials and methods to reduce the toxic and harmful effects of some chemical products and processes. Regarding this context, the use of natural and renewable raw materials to manufacture scaffolds for biomedical applications may become an alternative to synthetic materials. Therefore, the essential purpose of greener materials and technologies is to reduce the adverse effects of pollutants on the environment or humans.

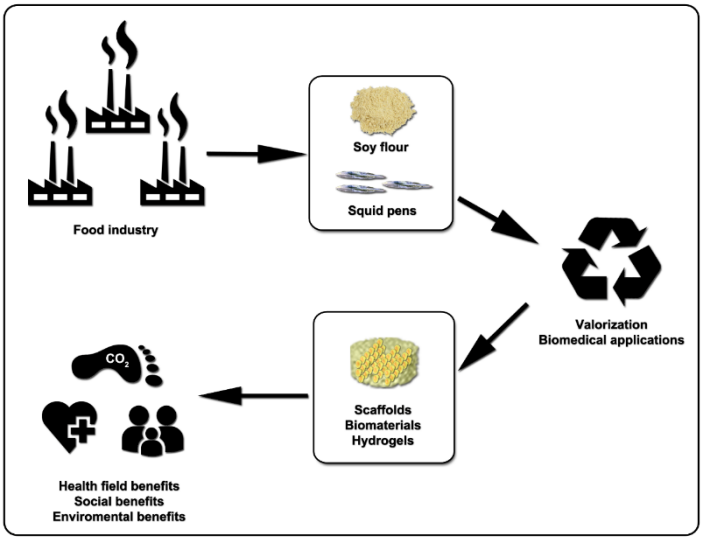

Fig. 1. From natural by-products to biomedical applications. Revalorization of by-products from food industry to develop different devices for biomedical applications.

Given its abundance, biocompatibility, biodegradability and low immunogenicity, soy protein isolate, commonly known as SPI and obtained from soy flour (a by-product of the manufacturing process of soybean industry) [7-9], is emerging as a promising source of biomaterials [10,11]. Additionally, some peptides of the SPI, such as lunasin, own RGD-like sequences [12], required to promote stable cell adhesions on the scaffolds surface [13,14]. Furthermore, SPI also exhibits a variety of peptides that promote both cell migration and proliferation, key factors for tissue regeneration applications [15]. Similarly, the valorization of products from the fishery industry, such as skin or bones, has become a matter of interest within the green strategy [16]. In fact, many works have highlighted the interest in using squid pens as a β-chitin (CH) source, due to their great content in this polysaccharide [17]. Although chitin is more commonly extracted from crab or shrimp shells, the use of squid pens allows to avoid demineralization and decoloration, essential processes in the extraction from seafood shells. The elimination of these processes, as well as all the chemicals and energy involved in them, brings environmental and economic benefits.18 From the biomedical point of view, it is well-described that CH is biodegradable,

biocompatible and that it presents an antibacterial activity and an exempt of toxicity [19,20]. CH is also able to activate polimorphonuclear cells and fibroblasts [21], to increase migration of monocytes/macrophages and to stimulate collagen synthesis [22]. All these characteristics are making this polysaccharide a potential compound for applications in the field of tissue engineering and regenerative medicine [21].

Besides the positive effects of the ecofriendly options, there are still many issues that must be addressed in order to achieve the required properties for specific applications. This work focused on the development of a novel SPI/CH-based SLS and its validation as a cell delivery system for biomedical applications. In this vein, we first studied the surface composition, the morphology, the porosity, the pore profile, the mechanical properties, the degradability and the swelling capacity of the scaffold. Moreover, we evaluated its safety, performing cytotoxicity assays and investigating its biocompatibility in vivo. We also tested its suitability as cell delivery system by assessing cell adhesion and proliferation of 3D-cultured adipose-derived human mesenchymal stem cells (h-MSCs). In addition, we explored the cell-loading capacity of the scaffold and monitored its degradation in function of the initial cell load. Finally, we quantified the vascular endothelial growth factor (VEGF), secreted by 3D-cultured h-MSCs, to discard any possible hindering in the release of bioactive compounds. We hypothesized that this may offer a novel and advanced way of improving the therapeutic resources for regenerative therapies. Hence, this work highlights the potential of using natural and renewable resources, such as plant proteins and marine polysaccharides, as well as simpler and cleaner processes, to manufacture scaffolds with suitable properties for tissue engineering and regenerative medicine, avoiding the use of organic solvents in line with the green chemistry principles and leading to more sustainable products for biomedical applications.

2. Materials and methods

2.1 Materials

SPI, PROFAM 974, was supplied by ADM Protein Specialites Division (Netherlands). Sulphur content in SPI was determined using a Euro EA Elemental Analyzer. Moreover, amino acid composition of the SPI was determined with a Biochrom 30 + amino acid analyzer physiological system.

CH was extracted from fresh squid pens (Loligo sp.), kindly supplied by a local fish market. First, we washed squid pens with water. Then, they were treated with NaOH (1 M) in a relation of 1:20 (w/v) at room temperature and under continuous stirring during 24 h in order to avoid the deacetylation of the native CH. After this process, we filtered the samples and the solid fraction (CH) was washed with distilled water until neutral pH. Finally, CH was freeze-dried and milled to obtain the powder. As determined by an elemental analysis in a previous work [23], the amount of C and N present in CH was, respectively, 42.1% and 6.2%. Besides, the average degree of acetylation was 95.9%. As for Glycerol (99.01% purity), it was provided by Panreac (Spain) and employed as a plasticizer.

The cell lines used in this study were L929 fibroblasts and h-MSCs (ATCC, Manassas, USA). The first one was cultured on Eagle's Minimum Essential Medium (EMEM) (ATCC® 30-2003™) supplemented with 10% (v/v) horse serum and 1% (v/v) penicillin-streptomycin. The h-MSCs (ATCC®, Cat. No: PCS-500-011) were cultured on Mesenchymal Stem Cell Basal Medium (ATCC®, Cat. No: PCS-500-030™) supplemented with the Mesenchymal Stem Cell Growth Kit (ATCC®, Cat. No: PCS-500-040) and 1% (v/v) penicillin-streptomycin. We incubated cell lines in a humidified incubator at 37 °C with a 5% CO2 atmosphere.

2.2 Preparation of the sponge-like scaffolds (SLS)

Firstly, we mixed 5 g of SPI with 30 wt % CH (based on SPI dry basis) and 125 mL of distilled water were added. Then, we adjusted the pH to 10 with NaOH (1 M) before heating at 80 ^{o}C for 30 min under magnetic stirring. Afterwards, we added 30 wt % glycerol (based on SPI dry basis) to the solution, which was heated for other 30 min at the same conditions to obtain a homogenous blend. Finally, the

blend was poured into molds, kept in a freezer at −22 °C for 48 h and then, freeze-dried for 72 h to obtain the SLS. Following, we cut the SLS with a hollow punch into discs, with different diameters, according to the further assays. Finally, in order to study the effect of a previous conditioning step of the SLS on the different parameters, we divided samples in 3 groups. Firstly, lyophilized SLS that did not undergo any previous conditioning step. Secondly, hydrated SLS, which were immersed into PBS for 5 min. Finally, dialyzed SLS, which were immersed into 1.6 L of Milli-Q water under constant stirring and refreshed twice. Both the hydrated and the dialyzed samples underwent a final freeze-drying process in order to be used in a dried state.

2.3 Morphology

We studied the morphology of the SLS surface by using a Hitachi S-4800 field emission scanning electron microscope (FE-SEM) (Hitachi High-Technologies Corporation, Tokyo, Japan) at a beam accelerated voltage of 5 kV. SLS were cut into discs of 8 mm diameter, mounted on a metal stub with an adhesive tape and coated with gold under vacuum (JFC-1100) in an argon atmosphere prior to testing. Furthermore, we studied the SLS by atomic force microscopy (AFM) under ambient conditions. We obtained AFM images using a scanning probe microscope (Nanoscope IIIa Multimode™, Bruker). We also employed Tapping mode in air using an integrated tip/cantilever at 200–400 kHz resonance frequency, 0.6–1.0 Hz scan rate and 20–80 N/m force constant.

2.4 XPS and ATR-FTIR analysis

X-ray photoelectron spectroscopy (XPS) was performed in a SPECS spectrometer using a monochromatic radiation equipped with Al Kα (1486.6 eV). The binding energy was calibrated by Ag 3d5/2 peak at 368.28 eV. All spectra were recorded at 90° take-off angle. Survey spectra were recorded with 1.0 eV step and 40.0 eV analyzer pass energy and the high resolution regions with 0.1 eV step and 20 eV pass energy. All core level spectra were referred to the C 1s peak at 284.6 eV. We analyzed spectra using the CasaXPS 2.3.19 software, and peak areas were quantified with a Gaussian–Lorentzian fitting procedure.

We also used attenuated total reflectance Fourier transform infrared (ATR-FTIR) spectroscopy to identify the characteristic functional groups of the SLS. Measurements were performed with a Nicolet Nexus FTIR spectrometer equipped with a MKII Golden Gate accessory, Specac, with a diamond crystal as ATR element at a nominal incidence angle of 45° with a ZnSe lens. We recorded measurements in the 4000-750 cm-1 region, using 32 scans at a resolution of 4 cm-1.

2.5 Degradation studies

In order to determine the weight loss due to hydrolytic and enzymatic effect, lyophilized SLS (n=5 samples per group) of 8 mm diameter were weighed and subsequently immersed in different solutions. We used 2 mL of PBS (completely filled) for the hydrolytic degradation and a collagenase P solution (Sigma-Aldrich, Spain), at a concentration of 0.5 mg/mL in culture medium, for the enzymatic degradation. Finally, we incubated all SLS at 37 ^{o}C. At different time points, samples were removed, lyophilized and weighed again to determine the remaining weight (%).

2.6 Pore analysis, porosity and swelling capacity

Pore sizes were determined from SEM micrographs using Image J software. We approximately measured up to 100 pores, randomly selected from different samples (n=3 samples per group). In order to observe whether or not the cell seeding changes the pore profile, we also measured approximately up to 50 pores randomly selected from different fluorescent microscopy images of different samples (n=3 samples per group). Furthermore, for the measurements, we chose two different cell concentrations (6h after seeding) and also wet SLS without cells. To determine the porosity of the scaffolds, we performed a liquid displacement method using ethanol 98% as the liquid medium, because of its ability to permeate through scaffolds without inducing matrix swelling or shrinkage [24] SLS were immersed into a known volume (V1) of ethanol and degassed for 5 min with a vacuum pump. The total volume of ethanol and ethanol-impregnated SLS was recorded as V2. Finally, we removed the ethanol-impregnated SLS, and the

residual volume of ethanol was recorded as V3. The porosity (ε) of the SLS was calculated with the following equation:

$$\varepsilon\,(\%) = \frac{V_1 - V_3}{V_2 - V_3} \times 100$$

In order to calculate the swelling curve, different pre-weighed SLS of 8 mm diameter were immersed into 5 mL of PBS at room temperature and also weighed again at various time points (2 s, 0.5, 1.5, 5, 10, 20, and 30 min). The study was performed with the aforementioned three groups of SLS (n=3 samples per group).

2.7 Mechanical evaluation

The compressive properties of the SLS (lyophilized, hydrated and dialyzed) were measured using a mechanical tester (Instron 5969 equipped with a 100 N load cell) at a compressive rate of 1 mm/min up to 80% of strain. This test was performed with dry and wet (5 min in PBS) SLS (n=12 samples per group). We also measured the compressive stress at 10% of strain to compare the compressive strength at that value of strain for the different SLS groups.

2.8 Cytotoxicity assays

We performed this assay following the ISO 10993-5:2009 guidelines for biological evaluation of medical devices. Cytotoxicity assay was performed either by direct contact of the SLS with the cells (direct cytotoxicity) or by exposing the cells to a lixiviate fluid of these SLS (indirect cytotoxicity) (n=4 samples per group).

In the direct cytotoxicity assay, we used SLS of 8 mm diameter and measured the L-929 fibroblasts (ATCC® 30-2003™) viability employing CCK-8 reagent (Sigma-Aldrich, Spain). Briefly, we seeded 35,000 cells/well in 500 μL/well of EMEM complete medium in a 24 well plate. Subsequently, we incubated the cells for 24 h at 37 °C. Then, we aspirated the medium and added 300 μL of fresh medium, placing the SLS in direct contact with the bottom of the well. After 48 h of incubation, we removed the SLS, and the medium was replaced by 370 μL/well of CCK-8 solution in medium (1:11) and incubated for 4 h. Afterwards, we read the absorbance with a plate reader (Infinite® 200 PRO series, Tecan Trading AG,

Männedorf, Switzerland) at 450 nm, using 650 nm as the reference wavelength. We used cells without SLS exposure as a control group (100% of viability).

In the indirect cytotoxicity assay, we exposed L-929 fibroblast to a lixiviate fluid of SLS (incubating at 37 ^{o}C for 24 h in culture medium at constant stirring following the ISO 10993-5:2009). We utilized a Benchtop OrionTM 2-star pH meter (Fisher Scientific SL, Madrid, Spain) and an Osmomat 030 (Genotec, Berlin, Germany) to respectively measure both the pH and the osmolarity of the lixiviate fluid, using culture medium without SLS as control and fresh medium without the incubation process as "fresh". Firstly, we seeded 5000 cells/well in a 96 well plate with 100 μL/well of medium and incubated them for 24 h at 37 ^{o}C. Then, we replaced the medium by 100 μL/well of the collected lixiviate fluid, and the plate was subsequently incubated at 37 ^{o}C for 24 h. Finally, the lixiviate fluid was removed, and 110 μL/well of CCK-8 solution in medium (1:11) was added. After 4 h of incubation, we read the absorbance as already described for the direct cytotoxicity. Cells with lixiviate fluid without SLS (culture medium incubating at 37 ^{o}C for 24 h under stirring equal as the other lixiviates) were used as control group (100% of viability).

2.9 In vivo biocompatibility of the scaffolds

In order to understand the biological reaction to the implanted biomaterials, we divided SLS of 6 mm diameter in 4 different groups (n=3 samples per group): lyophilized, hydrated, dialyzed and lipopolysaccharide (LPS) soaked SLS as a negative control group. We immersed all the SLS in PBS for 5 min before being implanted, except the LPS SLS that were contrastingly immersed in a 100 ng/mL LPS in PBS solution. We conducted all the experiments following the protocols approved by the Institutional Ethical Committee for Animal Experimentation of the University of the Basque Country (Procedure number: M20_2018_004). We subcutaneously implanted the SLS from the aforementioned four groups in male 8-week-old C57BL/6 mice for 14 days (one SLS per mouse, 3 mice per group). A two-week's time point was selected in the present study because it has been well established as suitable time to resolve both immune and fibrotic responses to implanted materials, in C57BL/6 mice [25-28].

In the procedure, we anesthetized mice with isoflurane (Isoflo®, Esteve, Spain) and used a scalpel to make a small incision (< 1 cm) in the central dorsal surface. We employed blunt forceps to create a pocket for the SLS in the subcutaneous space. After implantation, we closed the wounds with two sutures. Next, we monitored and housed mice for 14 days. Moreover, we did not observe signs of discomfort after surgery throughout the study.

2.10 Histological analysis

After 14 days, we euthanized mice by CO2 asphyxiation. We made different incisions, excising the SLS (and surrounding tissue) and fixed in 3.7% paraformaldehyde overnight. Then, the biopsies were bisected, embedded in paraffin and sectioned in layers of a thickness of 5 μm. We stained the slices by hematoxylin-eosin (H&E) and Masson's trichrome (MT), using standard procedures. Images were analyzed by a blinded histopathologist, utilizing the QuPath analysis software (Centre for Cancer Research & Cell Biology at Queen's University, UK) to evaluate the foreign body reaction (FBR) to the subcutaneous implant. All the results have been normalized by a blinded histopathologist vs the weight of each scaffold.

The cellular response was determined following a scale in which every cellular FBR received a value within a range from 0 to 4: 0, absence of macrophages (MC) or polimorphonuclear neutrophils (PMNN); 1, very low presence of MC or PMNN; 2, low presence of MC or PMNN; 3, abundant presence of MC or PMNN; and 4, very abundant presence of MC/PMNN.

We also performed immunohistological studies. In short, tissue slices were deparaffinised and automatically processed according to the U UltraView DAB detection kit (Roche, Switzerland). First, we incubated tissue biopsies with the primary antibodies at 37 °C. The incubation period varied depending on the antibody. On the one hand, 12 min for the anti-CD68 (clone KP-1, Roche, Switzerland); on the other hand, 32 min for the anti-CD163 (MRQ-26 Mouse Monoclonal Antibody, Sigma-Aldrich) and for the anti-ERG (EPR3864 Rabbit Monoclonal Primary Antibody, Roche, Switzerland). Subsequently, biopsies were stained with DAB and hematoxylin as counterstain. Finally, positive cells were

counted using the QuPath analysis software. As abovementioned, the results have been normalized for a blinded histopathologist vs the weight of each scaffold.

2.11 Cell studies in 3D cultures

3D-culturing

For the cell studies in 3D cultures, we used dialyzed SLS in dry state. In this vein, we seeded and rehydrated the SLS with a cell suspension in fresh serum-free medium, in order to avoid the action of the adhesion proteins present in the serum. We also calculated the volume of cell suspension seeded per scaffold as the 80% of the maximum swelling volume of each scaffold, ensuring no overflows at the bottom of the wells. After the optimum time for a stable cell adhesion (37 ^{o}C, 5% CO2) (see section 3.7), we washed the SLS with PBS, and incubated them in culture medium (Supplementary video 1†).

Cell adhesion, load and degradation studies

For cell adhesion, we placed dialyzed SLS of 4 mm diameter (n=5 samples per group) on a 96 well plate. Later, we seeded, as previously mentioned, an average of 60,000 h-MSCs cells per SLS. Thus, at different time-points (0, 2, 4, 6, 8 and 12 h), SLS were shortly rinsed with 100 μL of PBS, and non-adhered cells were counted on a Neubauer chamber. Cells adhered into the SLS were calculated as the subtraction of the total cells seeded minus the cells detached with PBS.

We performed the cell load study repeating the same procedure and considering the optimum cell adhesion time obtained. For that study, we seeded increasing concentrations of cell suspensions (4.0*106, 8.0*106, 1.6*107, 2.0*107, 2.5*107 cells/mL) into dialyzed SLS of 4 mm diameter (n=5 samples per group). After the cell adhesion time, we shortly rinsed the SLS with 100 μL of PBS, and non-adhered cells were counted as it was previously described. We calculated the total number of cells into the SLS, as the subtraction of the total cells seeded minus cells washed with PBS.

For the cell-mediated degradation, we finally incubated the SLS seeded with increasing cell load, for 21 days, in culture medium at 37 ^{o}C. We used the SLS

without cells as a control group. At day 21, we lyophilized and weighed the SLS again to determine the remaining weight.

Cell proliferation

For cell proliferation studies, we seeded 60,000 h-MSCs cells into 4 mm diameter dialyzed SLS (n=5 samples per group) and, after the optimum cell adhesion time, we washed the SLS with 100 μL of PBS and placed in a 24 well plate with 1 mL of fresh complete medium. Then, at pre-determined time-points (6, 24, 48, 96, and 168 h), the SLS were removed, washed with 100 μL of PBS and trypsinized with 100 μL for 5 min. Subsequently, we added 100 μL of neutralizing solution and used the final mix to count the number of cells on a Neubauer chamber. We also used cells seeded onto wells (2D) as control group. Besides, we expressed the results as a ratio of relative viability, using 6 h group as the comparing group.

VEGF in vitro 3D release study

For this assay, we seeded an average of 300,000 cells in both 2D (wells) and 3D (SLS) cultures. After a 7-day incubation, we removed the supernatants of both 2D and 3D cultures, and the accumulative levels of VEGF were quantified by ELISA (Quantikine® ELISA Human VEGF kit, R&D systems), following manufacturer's indications.

2.12 Statistical analysis

We expressed results as the mean ± standard deviation. When normally distributed, we analyzed results through student two-tailed t-test, to compare between two independent groups, or through one-way ANOVA test for multiple comparisons. Based on the Levene test for the homogeneity of variances, we applied Bonferroni or Tamhane post-hoc analysis. In contrast, we applied Mann-Whitney nonparametric analysis for non-normally distributed data. Additionally, we performed all the statistical computations using SPSS 25.0 (SPSS®, INC., Chicago, IL, USA).

3. Results and discussion

3.1 Characterization of SPI

First, we determined the amino acid composition of SPI since this is a factor that influences the physical and structural properties of the developed scaffolds and plays a key role in the functional properties of the resulting biomaterials. As shown in Table 1, we identified a total of 18 amino acids in SPI. The amino acid composition was rich in Glu, Asp, Leu, Ser, Gly, Ala and Pro residues, with Cys and Met as the principal sulphur-containing amino acids. In fact, Cys presents the ability to form both inter-chain and intra-chain disulphide bonds, which play a crucial role in protein-folding pathways and, thus, in protein structure. Furthermore, Trp, Tyr and Met provide the highest antioxidant activity, followed by Cys, His and Phe [29,30]. The amino acid characterization after the SLS preparation is also provided in Table S1† and shows that the amino acid composition did not change after the SLS preparation.

Table 1. Amino acid composition of SPI expressed as number of residues per 100 residues.

SPI amino acid residues																
Asp	Thr	Ser	Glu	Pro	Gly	Ala	Cys	Val	Met	Ile	Leu	Tyr	Phe	His	Lys	Arg	Trp
11.59	3.20	7.06	17.92	6.01	7.93	6.16	0.91	4.05	1.23	3.07	9.14	3.26	5.33	2.21	5.09	4.81	1.03

Regarding the elemental analysis, the sulphur content in SPI was approximately 0.89%. This percentage was related to the disulphide linkages, mainly derived from Cys. Due to this low sulphur content, we incorporated CH into the scaffold formulation to enhance mechanical properties. Thus, CH addition intended to improve those hydrogel functional properties required for biomedical applications, by promoting the interactions between the protein and the polysaccharide [23].

3.2 Preparation of the scaffold and morphology

The scaffold was prepared by freeze-drying (Fig. 2A), obtaining a porous SLS (Supplementary video 2†). Dry and wet SLS are shown in Fig. 2B (I) and Fig. 2B

(II). Furthermore, cross sectional SEM micrographs of lyophilized SLS were taken to analyze the microstructure of these porous SLS (Fig. 2C (I) and Fig. 2C (II)). We observed a highly porous microarchitecture, which provides interesting features for the attachment, the communication and the migration of cell populations seeded inside.

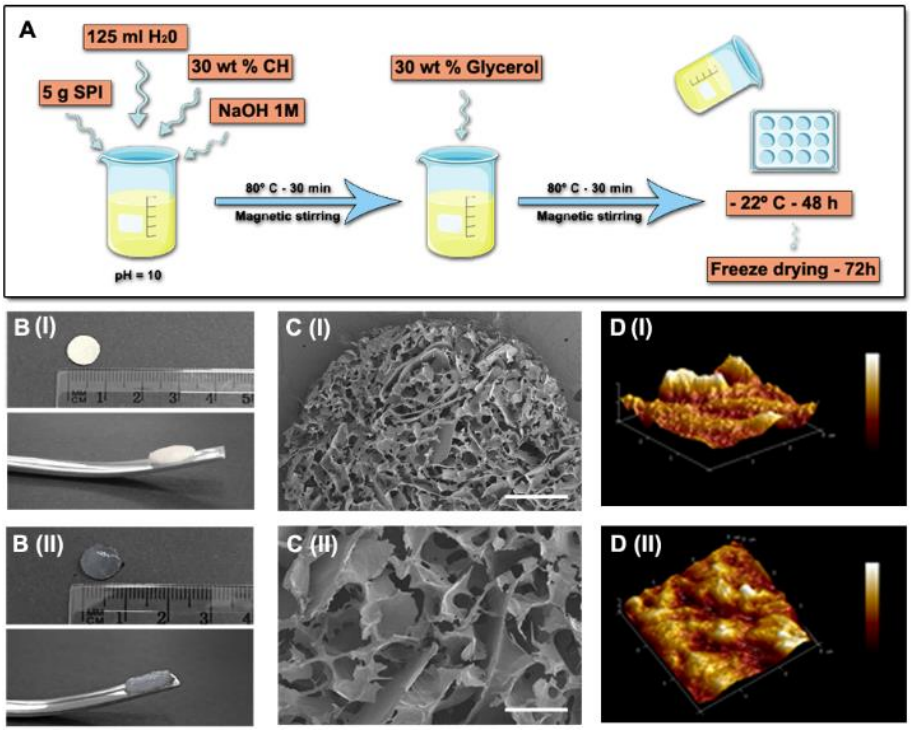

Fig. 2. Preparation of SPI/CH-SLS and morphology characterization. (A) Preparation of the SLS. (B (I)) Lyophilized SLS of 8x1.5 mm in dry state. (B (II)) Lyophilized SLS of 8x1.5 mm in wet state. (C (I)) SEM micrograph of a lyophilized SLS in dry state. Scale bar is 1 mm. (C (II)) SEM micrograph of a lyophilized SLS in dry state. Scale bar is 250 μm. (D (I) and D (II)) AFM images of surface topography for a scan area of 3.0 μm x 3.0 μm.

The surface microstructure was observed by AFM (Fig. 2D (I) and Fig. 2D (II)) in a scanning area of 3 μm x 3 μm. As it can be seen, the SLS showed a homogeneous and dense morphology. The roughness average (Fig. S1†) was 9.15 nm, the root mean square roughness was 11.66 nm, the average height was 21.29 nm, and the

maximum height was 46.65 nm. This homogeneous distribution of heights confirmed an adequate compatibility between SPI and CH.

3.3 XPS, ATR-FTIR and degradation studies

As it was above mentioned, the surface properties of biomaterials are a key aspect in determining the compatibility with the biological environment and, therefore, cellular responses, such as cell attachment and proliferation. Hence, the knowledge of the functional groups located towards the surface is greatly important, since those groups influence the stability in biological media. Consequently, we examined the composition of the scaffold surface by XPS.

The predominant peaks identified were those related to C 1s (284.6 eV), N 1s (399.3 eV) and to O 1s (532.0 eV) (Fig. 3A). In particular, the oxygen that was present on the surface of the SLS as O-C=O/O=C-N (amino acid carboxyl group and amide group in CH) represented the 23.6% of the surface composition. This percentage is considerably important because oxygen influences the stability in biological media [31]. Concerning the nitrogen that was present on the surface as C=N/C-N (amino group in amino acids and amide group in CH), it showed a lower content (8.03%), indicating the low exposure of amino groups towards the surface. As for the C 1s peak, depicted as one peak, it can be decomposed in two peaks corresponding to C-H/C-C (284.8 eV) and O-C=O (290.1 eV), that respectively represent 66.91% and 2.00% of the surface composition. The high content of C-H/C-C bonds indicated the hydrophobic character of the surface and the presence of O-C=O provided functional groups that benefit the bonding capacity of the surface.

Ultimately, we carried out an FTIR analysis (Fig. 3B) in order to confirm the interactions between SPI and CH, as well as their influence in the physicochemical properties of the SLS. The samples exhibited three characteristic bands that were common to all proteins: the amide I band at 1630 cm^{-1}, associated with C=O stretching; the amide II band at 1530 cm^{-1}, corresponding to N-H bending; and the amide III band at 1230 cm^{-1}, related to C-N stretching and N-H bending. It can also be appreciated the characteristic bands of polysaccharides that are located between 1180 and 953 cm^{-1} [32]. Regarding the aforementioned FTIR

spectra and the AFM and XPS results, it can be confirmed that the interactions between SPI and CH were physical interactions by hydrogen bonding between the hydroxyl groups of CH and the polar side groups (hydroxyl, carboxyl, amino) in SPI amino acids. These bonds play a major role in dictating the scaffold structure.

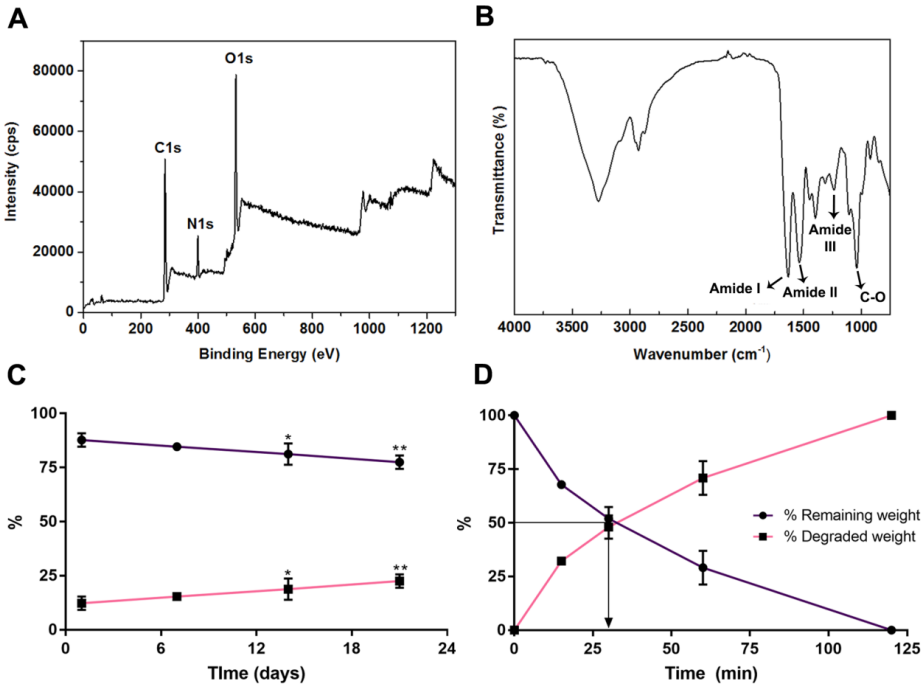

Fig. 3. Molecular characterization and degradation studies. (A) XPS survey spectra of SPI/CH SLS. (B) ATR-FTIR spectrum. (C) Hydrolytic degradation. (D) Enzymatic degradation.

Finally, in the performed hydrolytic and enzymatic degradation studies, we observed the degradation behaviour of the scaffolds when exposed to biological-like conditions. In the hydrolytic exposure (Fig. 3C), only about 25% of its weight was lost within the 21 days of the study. This may be due to the reinforcement of the SPI with CH, a known water-insoluble polysaccharide that possesses intra-sheet hydrogen bonds on its crystal structure, providing more stability to its bonded molecules [23]. In contrast, the enzymatic degradation (Fig. 3D), that will mainly depend on both the number of cleavage sites in the forming polymer and the concentration of available enzymes in the scaffold environment [33], was observed in only 2 hours.

3.4 Porosity, pore analysis and swelling capacity

As it is known, a previous conditioning step of the scaffolds can increase its biocompatibility. On the other hand, repeated hydrate and freeze-drying steps could affect the microstructure, the pore profile and the mechanical properties of the SLS. Therefore, we divided the SLS in 3 groups (Fig. 4A): lyophilized SLS (without any previous conditioning step), hydrated SLS (5 min in PBS) and dialyzed SLS (24 h in Milli-Q water under constant stirring).

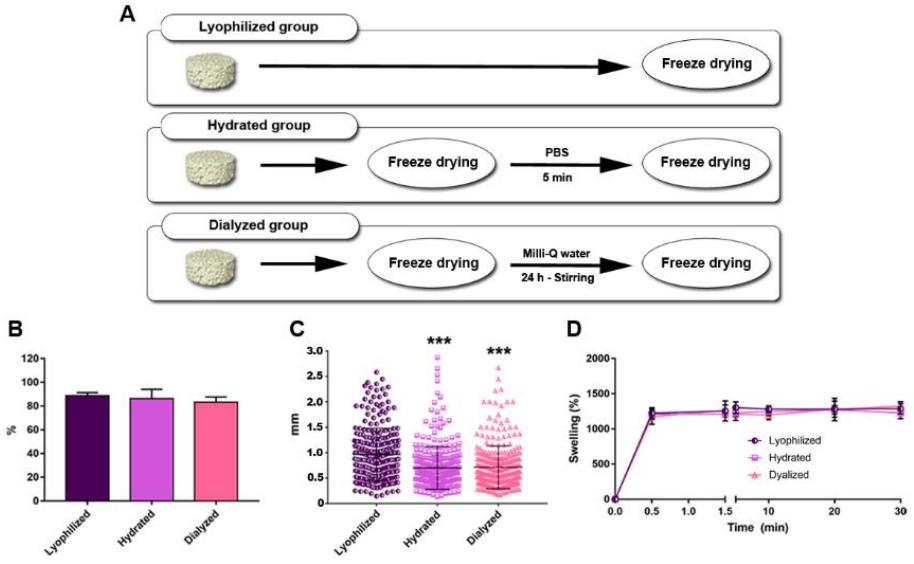

Fig. 4. SLS previous conditioning steps, pore analysis and swelling. (A) Scheme of the different groups of SLS. (B) Porosity of the SLS. (C) Pore size. (D) Swelling curve. *** indicates $p < 0.001$ comparing with lyophilized group.

It is well known that high values of porosity are needed for a great cell proliferation and migration, that may directly affect both nutrient and oxygen transport, as well as removal of wastes [34]. We measured the porosity of the SLS and obtained values between 80-90% (Fig. 4B), typical values for scaffolds that undergo a freeze-drying process [35]. As it was already shown, we did not obtain significant differences between any group, proving that a previous conditioning step of the scaffolds does not cause structural differences at this level.

It has also been widely described that cell behaviour in cell delivery systems is directly affected by the scaffold pore sizes and microarchitecture [34,36]. The measurements that we made showed pore sizes from less than 0.3 mm up to 3 mm for the highest ones, but being 0.3-0.9 mm the most frequent size range for all the groups studied (**Fig. 4C**). Furthermore, we observed significant differences ($p < 0.001$) when comparing the lyophilized group with both the hydrated and the dialyzed groups. These results can be explained due to the additional freeze-drying process undergone by these two groups, since there are no significant differences between the hydrated and the dialyzed group (both groups received different previous conditioning steps but the same number of freeze-drying cycles). It is important to remark that pore sizes greater than 0.3 mm are essential for vascularization of constructs, thereby ensuring the correct oxygenation and nutritional contribution to the seeded cells [37].

Swelling of scaffolds in aqueous media is desirable in SLS used as cell delivery systems, because the pore size would increase initially and will help to accommodate the seeded cells, favoring the cell adhesion. Furthermore, for certain pathologies, such as chronic wounds, a high swelling capacity is interesting due to the absorption of the generated wound exudates. It is also desirable a high swelling grade for bone tissue engineering applications, because it can help fill in and adjust to the bone defect [38]. As it was shown in **Fig. 4D**, these SLS (in all cases) were able to reach almost 1300% of swelling in less than 30 seconds, while maintaining their structure and stability. As detected from FTIR spectra, the high capacity of these SLS for water uptake could be ascribed to the existence of hydrophilic functional groups, such as carboxyl, amino and amide (**Fig. 3B**). Finally, it is interesting to mention that, as it was previously described, the high swelling rates are related to a better biocompatibility of scaffolds in tissue engineering applications [39].

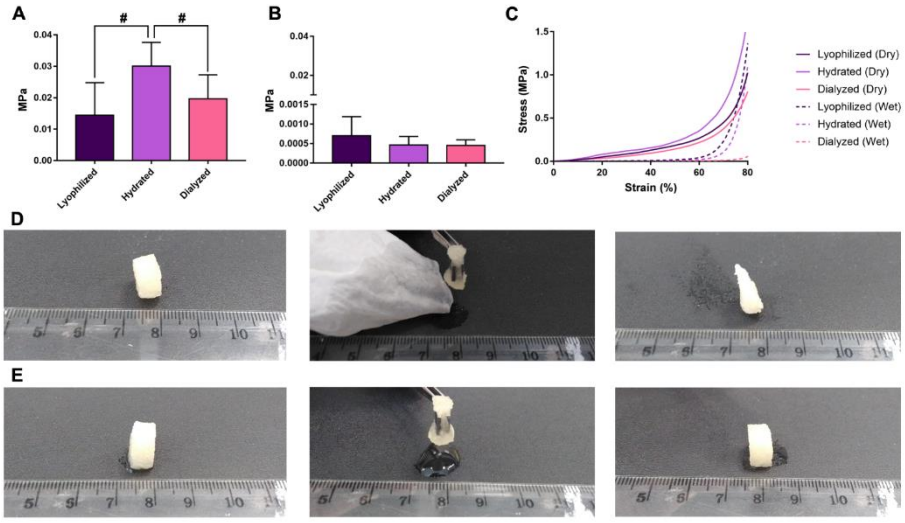

Fig. 5. Mechanical evaluation of SLS. (A) Compressive strength in dry SLS. (B) Compressive strength in wet SLS. (C) Representative compressive stress-strain curves for all groups of SLS either in dry or wet state. # indicates $p < 0.05$ comparing between groups. (D) Photographs demonstrating the incapacity of wet SLS to recover its initial morphology after a full compression. (E) Photographs demonstrating the capacity of wet SLS to recover its initial morphology when reabsorb the lost water after a full compression.

3.5 Mechanical evaluation

The mechanical evaluation of every scaffold is interesting since, for a practical and a long-term clinical use, they must present good properties for a good handling and an adequate resistance to deformation and rupture. For that purpose, we tested the compressive properties up to 80% of strain of both dry and wet SLS. Regarding dry SLS, the hydrated group showed the highest compressive strength properties ($p < 0.05$), compared to the other groups. This result could probably be due to the presence of salts in PBS (**Fig. 5A**). As it is shown in **Fig. S2†**, some amorphous salt crystal formations had been created during the freeze-drying process, increasing the hardness and strength of the hydrated group SLS. As for wet SLS, salt formations are dissolved and, therefore, all groups showed no significance differences ($p > 0.05$) between them in terms of compressive strength (**Fig. 5B**). It is also important to mention that the compressive strength is about 40

times lower in wet SLS than in dry SLS because, under wet conditions, the plasticization effect of water dominates the compressive properties of the SLS, decreasing their mechanical strength [40].

Furthermore, all SLS revealed a typical compressive stress-strain profile of plastic behaviour, exhibiting a lack of initial elastic linear region (Fig. 5C). We observed this plastic behaviour in all the wet SLS, as they were unable to recover their initial shape after applying the deformation forces (Fig. 5D). However, this behaviour is overwhelmed by their high swelling capacity, as they are able to almost recover their initial morphology when reabsorbing the lost water after applying the deformation forces (Fig. 5E and Supplementary video 3†).

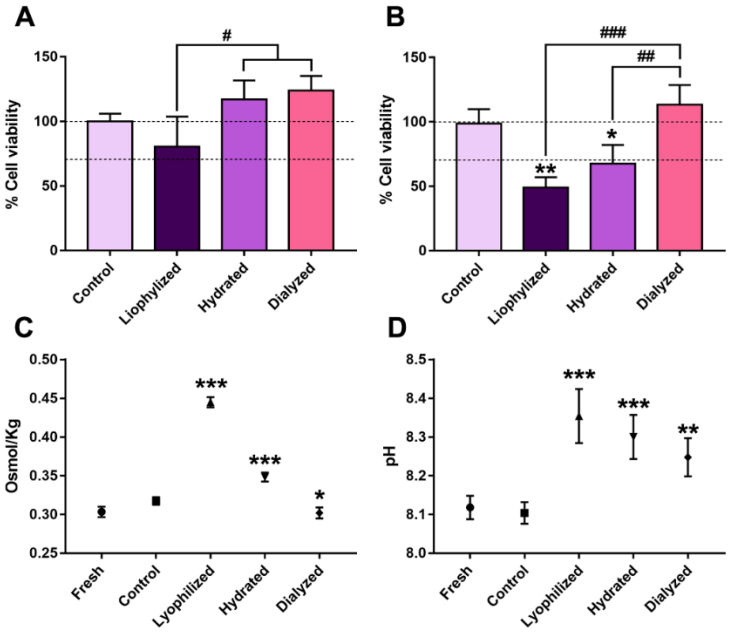

Fig. 6. Cytotoxicity assays. (A) Direct cytotoxicity. (B) Indirect cytotoxicity. Two lines are marking the 100% and the 70% of cell viability. (C) Lixiviates pH of the indirect cytotoxicity. (D) Lixiviates osmolarity of the indirect cytotoxicity. * indicates $p < 0.05$; ** indicates $p < 0.01$; *** p indicates < 0.001 comparing with control group. # indicates $p < 0.05$; ## indicates $p < 0.01$; ### indicates $p < 0.001$ comparing between groups in cytotoxicity assays.

3.6 Cytotoxicity assays

One of the main requirements of any biomaterial is that it must be biocompatible. Hence, we performed both direct and indirect in vitro cytotoxicity assays, following an adapted protocol from the ISO 10993-5:2009 guidelines for biological evaluation of biomedical devices. While in the direct cytotoxicity assay all the SLS were above the 70% of viability (Fig. 6A), only the SLS with a previous dialysis process achieved more than 70% of viability in the indirect cytotoxicity one (Fig. 6B). These values can be explained due to the fact that the extracted lixiviates showed a significant increase not only in the pH but also in the osmolarity (Fig. 6C, Fig. 6D). This was specially evident in both lyophilized and hydrated groups. Thus, the osmotic difference between the hypertonic medium and the cellular cytoplasm can trigger different L-929 cells responses that could give rise their loss of replication [41]. Considering these results, only dialyzed SLS showed a complete absence of toxicity in both assays according to the ISO 10993-5:2009.

3.7 In vivo biocompatibility of the scaffolds

Testing the behavior of these SLS in an immuno-relevant in vivo model is necessary because there are not previous references of their biocompatibility in such organisms. For that reason, we implanted the different groups of SLS in the subcutaneous space of C57BL/6 mice, that have a more aggressive innate immunity and mimic, in a relevant way, the FBR observed in humans [25]. After 14 days, we removed the SLS and processed them histologically to evaluate the FBR. As an additional control, we recreated a “worst case scenario” by also including a group of SLS soaked in LPS, an endotoxin derived from the cell wall of gram-negative bacteria, which are known to elicit strong inflammatory responses.

H&E and Masson´s trichrome stains

We found remarkable quantitative differences in the inflammatory responses to each of the four groups (Fig. 7A, Fig. 7B). All groups showed high cell infiltration inside the SLS but with visual differences between them. The presence of polimorphonuclear neutrophils (PMNN) in LPS group was higher in comparison with the rest of the groups (Fig. 7C, Fig. 7D). Furthermore, we also assessed the

presence of macrophages (MC) in the implant zone and calculated the ratio MC/PMNN. The obtained results showed a significant difference ($p < 0.05$) between the dialyzed and LPS groups (Fig. 7A).

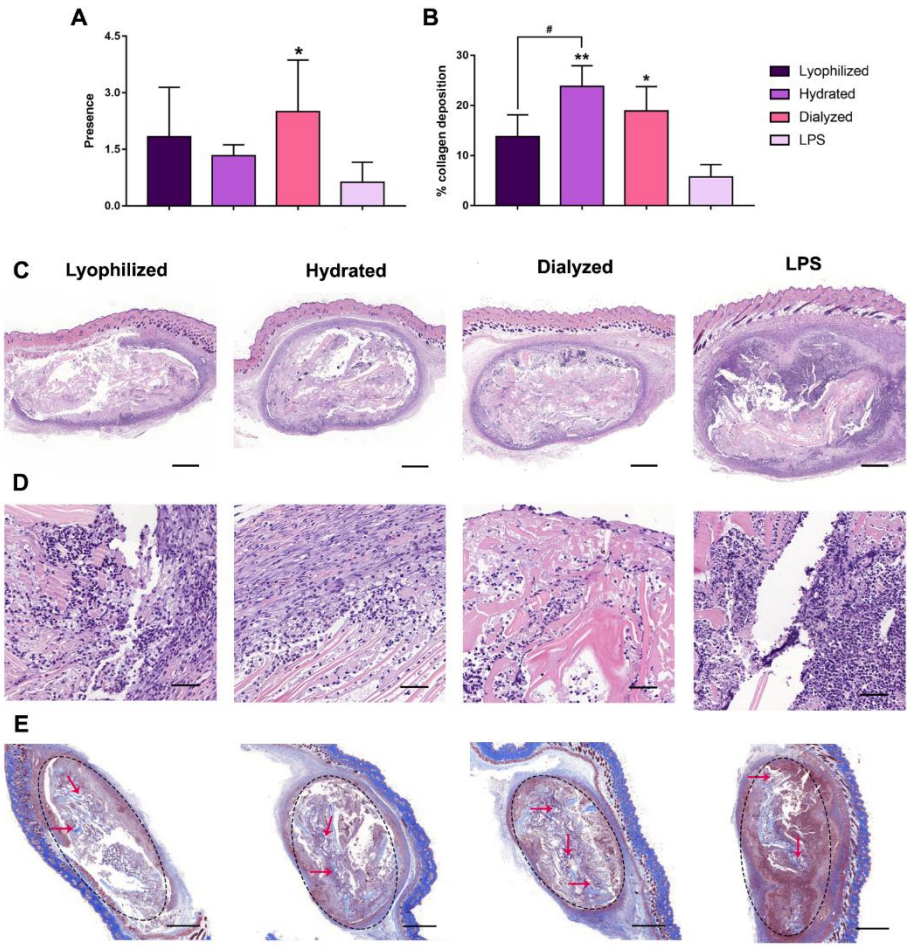

Fig. 7. H&E and Masson´s trichrome stains. (A) Ration between MC and PMNN in the H&E staining. * indicates $p < 0.05$ comparing with LPS group. (B) Collagen deposition into the scaffold. * indicates $p < 0.05$; ** indicates $p < 0.01$ comparing to LPS group. # indicates $p < 0.01$ between different groups. (C, D) H&E staining of all groups of scaffolds at different magnifications. (E) Masson´s trichrome staining. Inside the SLS, red arrows point out blue stained collagen fibers. Scale bars are 500 μm (C), 50 μm (D), 800 μm (E).

When samples were processed with the Masson´s trichrome staining, we observed that the collagen deposition in all the studied groups was principally located inside the SLS rather than in the surroundings of the implants (Fig. 7E), what would be expected in the case of the FBR to low-biocompatible biomaterials [42,43]. Therefore, we may think the SLS were well integrated in the organism, showing an adequate biocompatibility. After the quantitative analysis, the hydrated group particularly showed higher values of collagen deposition with respect to both the LPS group ($p < 0.01$) and the lyophilized group ($p < 0.05$) (Fig. 7B). In addition, the dialyzed group showed also higher values in comparison with the LPS group ($p < 0.01$).

CD68, CD163 and ERG immunostaining

Monocytes/macrophages are considered the most important cells in the initiation, duration and outcome of the host response against implanted biomaterials [44]. Thus, we next examined the phenotype of the infiltrating macrophages by the immunostaining of CD68, as indicator of both classically (M1) and alternatively (M2) activated macrophages, and by the immunostaining of CD163, as marker of M2.

We found that the vast majority of the macrophages presented a M2 anti-inflammatory phenotype, since the CD163/CD68 ratio was near one (Fig. 8A). It is well reported that monocytes/macrophages appear in the implantation niche at the end of the acute inflammatory phase (approximately one week), exhibiting a differing behaviour according to the biocompatibility of the implanted material. If this is low, there is a higher number of M1 pro-inflammatory macrophages with the presence also of forming foreign body giant cells in the implant zone. In contrast, if the biomaterial shows an adequate biocompatibility, the number of M1 macrophages progressively decreases, and M2 macrophages predominate, leading to the ECM remodeling phase [45]. The higher rate of M2 polarized macrophages in all groups may be, in keeping with the findings, reported by other authors in the literature. On the one hand, CH has shown a M2 macrophage profile activation in previous in vivo scenarios [46]. On the other hand, it has been described that some soy peptides inhibited inflammation in LPS-induced macrophage by suppressing NFkB pathway [47]. Strikingly, our scaffold was also

able to inhibit and overcome, up to certain point, the LPS-mediated inflammatory response.

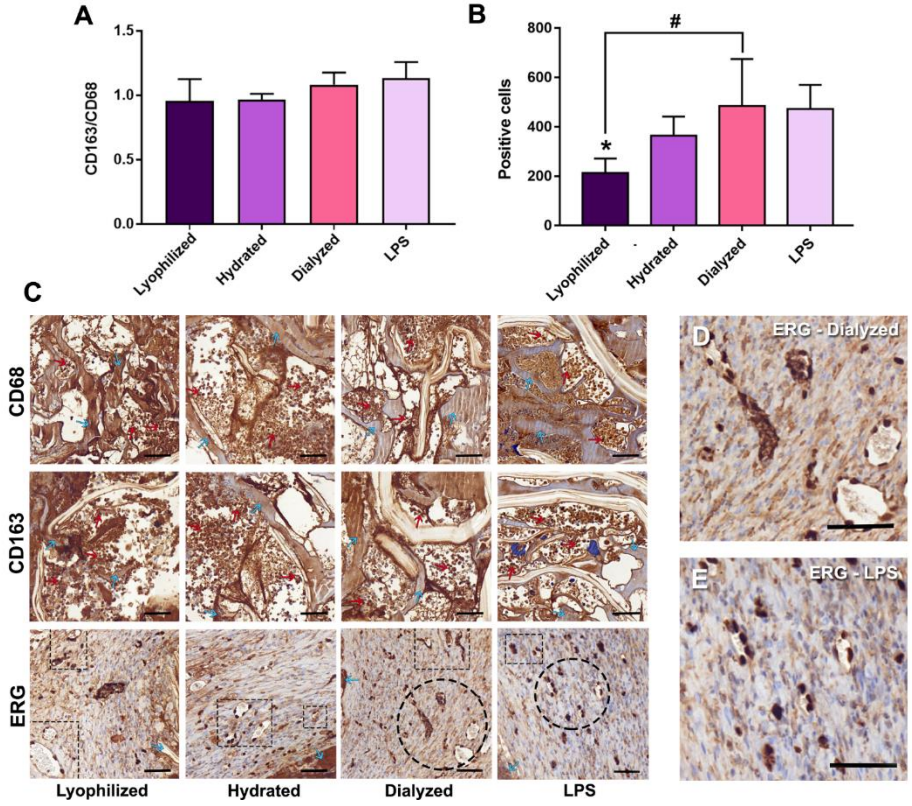

Fig. 8. CD68, CD163 and ERG immunostaining. (A) CD68 – CD163 positively stained cells. (B) ERG staining showing the number of stained endothelial cell nuclei. * indicates $p < 0.05$ comparing to LPS group. # indicates $p < 0.01$ between different groups. (C) Images of the different stainings. The dotted boxes show blood vessels. The difference in the vessel formation of dialyzed and LPS group is showed in two zoomed images from the dotted circles (D, E). Scale bars are 50 μm. Blue arrow shows scaffold fibers and red arrow shows positively marked cells.

Finally, we also measured the number of endothelial cells with an anti-ERG marker. With a previous conditioning step of the SLS, the results revealed that there was an increase in vessel formation, obtaining significant differences between the dialyzed group and the lyophilized group ($p < 0.05$) (Fig. 8B, Fig 8C). Interestingly, we found similar values between the dialyzed and the LPS group. In fact, it has

been widely described that LPS was able to promote angiogenesis [48,49]. However, our results showed qualitative differences between the LPS group and the others, especially with the dialyzed group. As it can be seen in the zoomed images (Fig. 8D and Fig. 8E), the dialyzed group presented larger and more dilated blood vessels with higher number of endothelial cells (Fig. 8C). Furthermore, in the LPS group, smaller vessels with lower number of endothelial cells were formed, in accordance with a less advanced and more primitive angiogenesis process [50,51]

In summary, these results demonstrated that, even if all the groups showed an acceptable biocompatibility, a previous conditioning step (hydration or dialysis) before implantation is highly recommendable to maximize integration with the host's tissue. This is also related to the results obtained in the cytotoxicity studies. In light of these findings, we decided to use the dialyzed scaffolds for the cell studies.

3.8 Cell adhesion, load, and degradation studies with 3D-cultured h-MSCs

We tested the suitability of our SLS as a cell delivery system with h-MSCs. In this sense, for the 3D-culture, as explained before, we seeded and rehydrated the SLS with a cell suspension in fresh serum-free medium (Fig. 9A). In the adhesion assay, we assessed the optimum time required to obtain a stable cell adhesion in the SLS microarchitecture. For such aim, we explored the initial stage of adhesion formation by subjecting seeded cells to a PBS wash at different time points. We calculated the number of h-MSCs that were adhered into the SLS as the total number of cells seeded minus the number of cells released with the PBS wash. We observed that, from 4 hours on, we achieved a plateau around 75.5% ± 3.55% of initially seeded cells (Fig. 9B). Secondly, we evaluated the adhesion reinforcement and the subsequent maturation by exposing cells to trypsinization. Interestingly, a higher number of cells were released at 4h than at the rest of the time points (Fig. 9C). These results may be explained as follows. At early stages of cell adhesion (< 4 h), a greater number of cells were washed-up with the first PBS rinse. Therefore, a smaller number of cells remained to be released afterwards with the trypsin treatment. In contrast, 6 h after seeding, cells exerted stronger unions with

the scaffold as a result of focal adhesion maturation. Thus, even if this implies that more cells abided the first PBS wash, more cells also resisted the subsequent trypsinization and a smaller number of cells were released. Accordingly, we decided that 6 hours was the minimum time required to allow cell adhesion before culturing the SLS in culture medium.

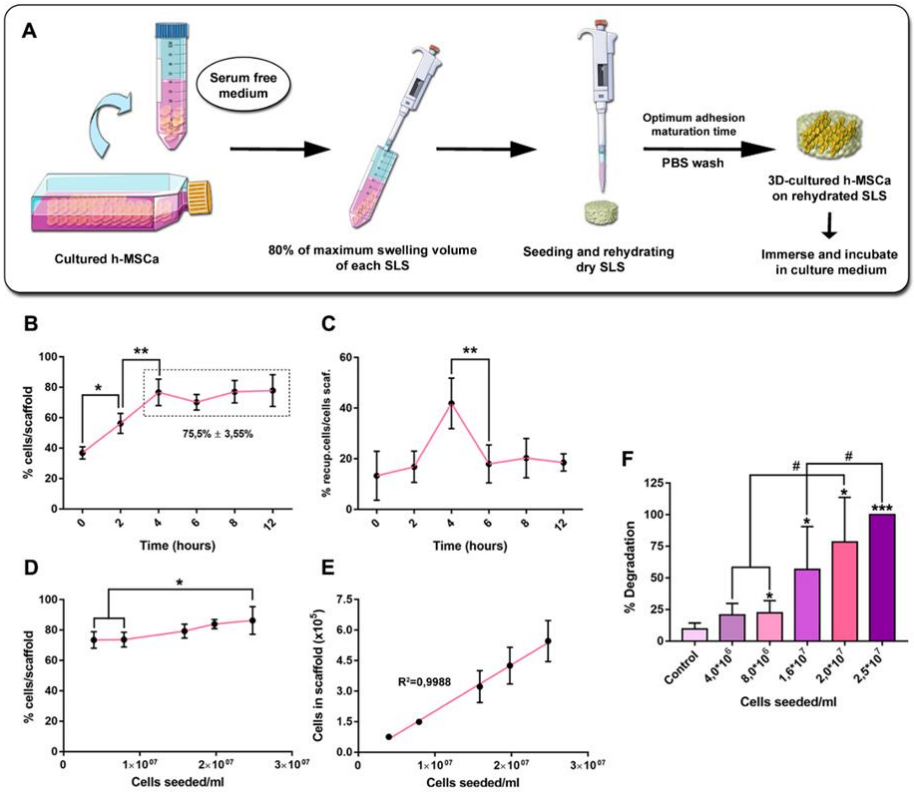

Fig. 9. 3D-cultured h-MSCs studies. (A) Procedure of 3D-culture on SLS. (B, C) Adhesion studies: (B) Early stage; percentage of cells remaining in the scaffold at different time points, (C) Maturation; percentage of cells recuperated with a trypsin treatment in comparison with the total cells of the scaffold. (D, E) Cell load studies: (D) percentage of cells into the scaffold with different cell loads seeded, (E) total number of cells inside the scaffold. * indicates $p < 0.05$; ** indicates $p < 0.01$. (D) Cell mediated degradation. * indicates $p < 0.05$; *** indicates $p < 0.001$ in comparison with the control group; # indicates $p < 0.05$ between groups.

On the other hand, we investigated the maximum cell-load capacity of the SLS by seeding increasing concentration of h-MSCs. The percentage of effectively adhered cells varied between 75-85% (Fig. 9D), obtaining good linearity between the initially seeded cells and the resultant cell-load (R2 = 0.9988). It should be noted that, even with the highest cell-load assayed, we did not reach the saturation of the SLS. These results suggest that, within its microarchitecture, SLS were able to support cell concentrations higher than 500,000 cells in a volume of just 18.85 mm^3 (25,000 cells/mm3) (Fig. 9E).

Finally, we studied cell-mediated degradation in function of the initial cell-load. In fact, the aim of the cell-loaded SLS is to sustain a progressive degradation of the scaffold matrix while the stem cells produce their own extracellular matrix to end up integrating into the host's organism. As expected, the higher the cell concentration we seeded into the SLS, the higher the degradation we observed (Fig. 9F). After 21 days, the initial cell-load will decisively influence the durability of the implanted SPI-CH-SLS. Furthermore, we also measured the pore size; by means of cross-sectional image analysis performed in both SEM and fluorescence micrographs, to observe the influence of cell-seeding on the microarchitecture of the dialyzed SLS. In particular, we assessed the pore size in dry, wet SLS, and in wet SLS seeded with two different cell densities. The results demonstrated no differences between the pore profiles of any assayed group (Fig. S3†).

3.9 Cell proliferation and VEGF release of 3D-cultured h-MSCs

To validate the SLS as a cell delivery system, it was important to understand the behaviour of cells within the SLS in terms of proliferation and release of therapeutic factors. For that purpose, we compared the proliferation rates of cells seeded onto 2D plates (in wells) and 3D-cultured cells (into SLS), obtaining no significant differences between them (Fig. 10A and Fig. 10B). Our findings are in agreement with those authors arguing that microporosities ranging from 10 to 100 μm effectively act as 2D surfaces with curvature [52].

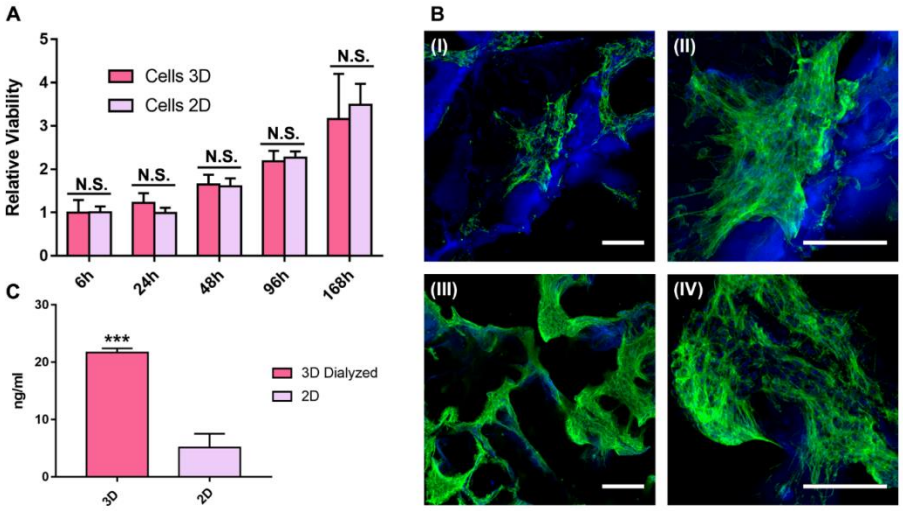

Fig. 10. Proliferation and VEGF production of 3D-cultured h-MSCs. (A) Cell proliferation studies. Cells detached were normalized against 6 h group (B) Confocal fluorescent microscopy images with Phalloidin/DAPI staining of the cells inside the scaffold at 24 h B (I) and B (II), and at 168 h B (III) and B (IV). Scale bars are 150 μm. The scaffold surface shows autoflorescence stained in blue. (C) VEGF in vitro release assay. *** indicates $p < 0.001$.

Next, we quantified and compared the VEGF secreted by both 3D-cultured and 2D plated h-MSCs to rule out any possible hindering in the release of bioactive compounds. We chose VEGF because it is an important mediator involved in angiogenesis, one of the most relevant processes in wound healing, bone regeneration and many other biomedical applications [53,54]. Hence, we found a four-fold increase in VEGF secretion when the same number of cells were 3D-cultured instead of 2D-plated, achieving significant differences ($p < 0.001$) between the groups (Fig. 10C). This increase in the VEGF release is consistent with previous studies published by other authors and may be explained in either chemical or physical terms.

On the one hand, scaffolds with porous matrices have been shown to simulate the ECM in a better way, recreating a biological-like physical condition that, in some cases, leads to stimulate the production of cytokines [34,55]. On the other hand, the composition of the scaffold may also act upregulating the production and release of VEGF. Indeed, it has been described that some soy peptides were

able to increase VEGF production in h-MSCs seeded onto 2D surfaces [56]. Likewise, it has also been described that CH was able to boost the production of VEGF in different cell lines [57]. It has been widely described that, in hypoxic environments, different cell types increase their VEGF production in order to promote neovascularization. In this sense, the higher VEGF production in our 3D-cultured h-MSCs may be attributed to a hypoxic environment inside the SLS. However, this argument is revoked because, with pore sizes mainly from 0.3 mm to 0.9 mm and the elevated porosity presented in these SLS, cell oxygen uptake and viability are ensured [34,37,58].

4. Conclusions

In the present study, we have shown that natural by-products from the food industry can be an excellent source of biomaterials for the development of biomedical devices. The developed SLS showed a highly interconnected porous structure, elevated hydrolytic stability, and excellent swelling and mechanical properties. We also demonstrated that a simple dialysis pre-conditioning was enough to obtain negligible in vitro cytotoxicity, according to the ISO 10993-5:2009. Besides, the predominant M2 macrophage profile, the absence of foreign giant cell formation, the deposition of collagen fibers inside the SLS and the neovascularization capacity suggest that these SLS present an excellent biocompatibility in vivo, especially when subjected to previous conditioning steps (dialysis or hydration). Moreover, the scaffold microarchitecture was able to promote adequate cell adhesion and proliferation, showing the capacity to host a huge amount of h-MSCs in a small volume. Furthermore, h-MSCs 3D-cultured in these SLS were able to release four times higher amount of VEGF than the same number of h-MSCs seeded onto 2D plates. All these findings suggest that the revalorization of natural by-products from different industrial procedures may be of great interest for the development of potentially therapeutically devices. Here, we developed a SLS and validated its use as a cell delivery system with excellent features for biomedical applications. This may offer an alternative and advanced perspective to increase the therapeutic resources for a wide variety of therapies.

Conflict of interest

The authors declare no competing financial interest.

Acknowledgments

NanoBioCel group thanks for the projects SAF2017-82292-R (MINECO/AEI/FEDER, UE), ICTS "NANBIOSIS" (Drug Formulation Unit, U10) and the support from the Basque Country Government (Grupos Consolidados, No ref: IT907-16). K. Las Heras thanks the Basque Government (Department of Education, Universities and Research) for the PhD grant (PRE_2018_1_0412). BIOMAT group thanks the Ministry of Science, Innovation and Universities (RTI2018-097100-B-C22). Authors thank Saioa Santos-Vizcaino for her technical assistance and fruitful discussion. Authors thank Ángela Muro Arpón for help with manuscript revision.

Supplementary information

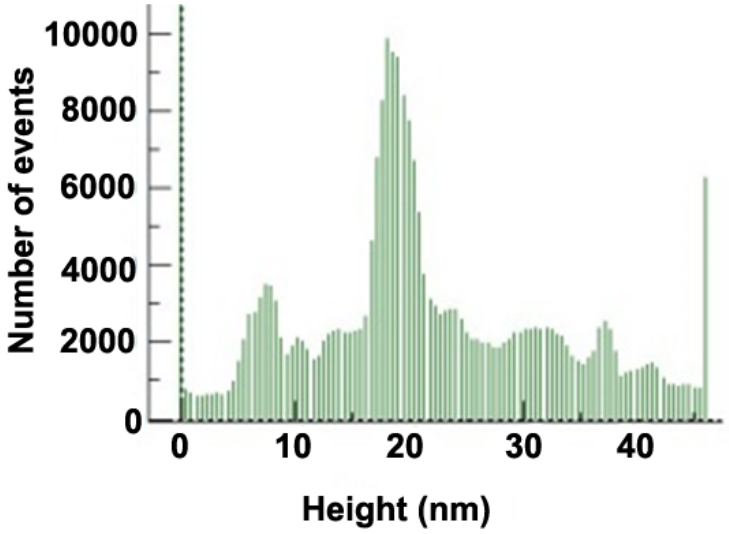

Fig. S1†. AFM distribution of heights

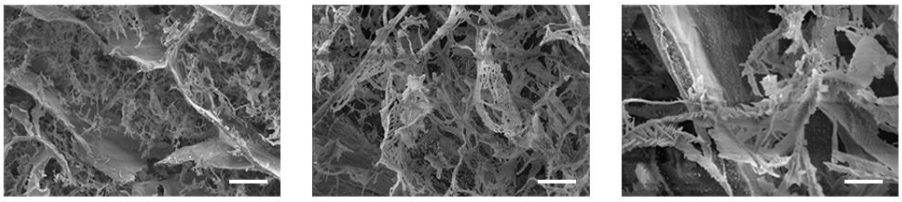

Fig. S2†. SEM micrographs of salt crystals formation in hydrated SLS after the freeze drying process. Scale bars are from left to right: 250 μm, 125 μm and 50 μm.

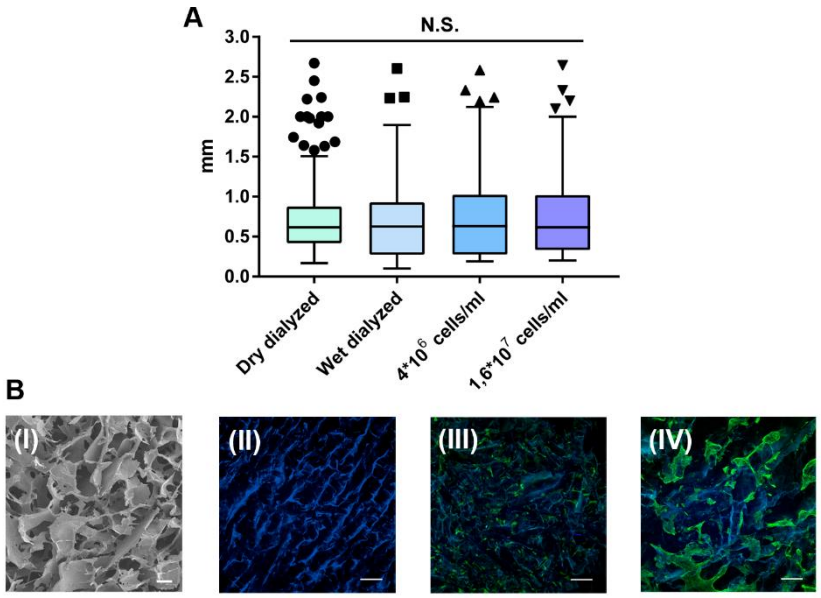

Fig. S3†. Pore size of dialyzed SLS. (A) N.S. indicates Non-significant differences between all groups. (B) SEM and Fluorescent microscopy images of SLS (Phalloidin/DAPI staining). (I) SEM image of a dialyzed SLS (dry). (II) Fluorescence microscopy of a dialyzed SLS (wet). (III) Fluorescence microscopy of a dialyzed SLS with 4*106 cells/ml seeded. (IV) Fluorescence microscopy of a dialyzed SLS with 1,6*107 cells/ml seeded. Scale bars are 300 μm.

Table S1†: Amino acid composition of SPI (scaffold) expressed as number of residues per 100 residues.

SPI amino acid residues (scaffold)																
Asp	**Thr**	**Ser**	**Glu**	**Pro**	**Gly**	**Ala**	**Cys**	**Val**	**Met**	**Ile**	**Leu**	**Tyr**	**Phe**	**His**	**Lys**	**Arg**	**Trp**
11.12	3.22	6.55	17.79	6.68	8.24	6.42	0.89	3.95	1.12	2.97	9.49	3.32	5.12	2.09	4.98	4.96	1.09

References

[1] M. Spector, Biomed. Mater., 2018, 13, 030201.

[2] X. Lv, C. Feng, Y. Liu, X. Peng, S. Chen, D. Xiao, H. Wang, Z. Li, Y. Xu and M. Lu, Theranostics, 2018, 8, 3153-3163.

[3] Q. Huang, Y. Zou, M. C. Arno, S. Chen, T. Wang, J. Gao, A. P. Dove and J. Du, Chem. Soc. Rev., 2017, 46, 6255-6275.

[4] S. Zhang, M. Xing and B. Li, Int. J. Mol. Sci., 2018, 19, 1641.

[5] B. Annabi, A. Tamayol, J. A. Uquillas, M. Akbari, L. E. Bertassoni, C. Cha, G. Camci-Unal, M. R. Dokmeci, N. A. Peppas and A. Khademhosseini, Adv. Mater., 2014, 26, 85-123.

[6] T. C. Sarker, S. M. G. G. Azam and G. Bonanomi, Waste Biomass Valor., 2017, 8, 241.

[7] E. W. Lusas and M. N. Riaz, J. Nutr., 1995, 125, 573-580.

[8] M. Fischer, L. V. Kofod, H. A. Schols, S. R. Piersma, H. Gruppen and A. G. Voragen, J. Agric. Food Chem., 2001, 49, 4463-4469.

[9] A. A. Loman, S. M. Islam, Q. Li and L. K. Ju, Bioprocess Biosyst. Eng., 2016, 39, 1501-1514.

[10] S. Tansaz and A. R. Boccaccini, J. Biomed. Mater. Res. A, 2016, 104, 553-569.

[11] K. B. Chien, E. J. Chung and R. N. Shah, J. Biomater. Appl., 2014, 28, 1085-1096.

[12] C. Chatterjee, S. Gleddie and C. W. Xiao, Nutrients, 2018, 10, 1211.

[13] H. Kurihara and T. Nagamune, J. Biosci. Bioeng., 2005, 100, 82-87.

[14] M. D. Pierschbacher and E. Ruoslahti, Nature, 1984, 309, 30-33.

[15] S. Ahn, C. O. Chantre, A. R. Gannon, J. U. Lind, P. H. Campbell, T. Grevesse, B. B. O'Connor and K. K. Parker, Adv. Healthc. Mater., 2018, 7, 1701175.

[16] I. S. Arvanitoyannis and A. Kassaveti, Int. J. Food Sci. Technol., 2008, 43, 726–74.

[17] H. N. Cuong, N. C. Minh, N. Van Hoa and T. S. Trung, Int. J. Biol. Macromol., 2016, 93, 442-447.

[18] J. Uranga, A. Etxabide, S. Cabezudo, K. de la Caba and P. Guerrero. Sci. Total Environ., 2020, 706, 135747.

[19] R. Singh, K. Shitiz and A. Singh, Int. Wound J., 2017, 14, 276-1289.

[20] S. Deepthi, J. Venkatesan, S. K. Kim, J. D. Bumgardner and R. Jayakumar, Int. J. Biol. Macromol., 2016, 93, 1338-1353.

[21] A. Anitha, S. Sowmya, P. T. S. Kumar, S. Deepthi, K. P. Chennazhi, H. Ehrlich, M. Tsurkanc and R. Jayakumar, Prog. Polym. Sci., 2014, 39, 1644-1667.

[22] R. Jayakumar, K. P. Chennazhi, S. Srinivasan, S. V. Nair, T. Furuike and H. Tamura, Int. J. Mol. Sci., 2011, 12, 1876-1887.

[23] T. Garrido, A. Etxabide, K. de la Caba and P. Guerrero, Green Chem., 2017, 19, 5923-5931.

[24] G. Yang, Z. Xiao, H. Long, K. Ma, J. Zhang, X. Ren and J. Zhang, Sci. Rep., 2018, 8, 1616.

[25] J. C. Doloff, O. Veiseh, A. J. Vegas, H. H. Tam, S. Farah, M. Ma, J. Li, A. Bader, A. Chiu, A. Sadraei, S. Aresta-Dasilva, M. Griffin, S. Jhunjhunwala, M. Webber, S. Siebert, K. Tang, M. Chen, E. Langan, N. Dholokia, R. Thakrar, M. Qi, J. Oberholzer, D. L. Greiner, R. Langer and D. G. Anderson, Nat. Mater., 2017, 16, 671-680

[26] J. Li, A. D. Celiz, J. Yang, Q. Yang, I. Wamala, W. Whyte, B. R. Seo, N. V. Vasilyev, J. J. Vlassak, Z. Suo and D. J. Mooney, Science, 2017, 357, 378-381

[27] A. J. Vegas, O. Veiseh, J. C. Doloff, M. Ma, H. H. Tam, K. Bratlie, J. Li, A. R. Bader, E. Langan, K. Olejnik, P. Fenton, J. W. Kang, J. Hollister-Locke, M. A. Bochenek, A. Chiu, S. Siebert, K. Tang, S. Jhunjhunwala, S. Aresta-Dasilva, N. Dholakia, R. Thakrar, T. Vietti, M. Chen, J. Cohen, K. Siniakowicz, M. Qi, J. McGarrigle, A. C. Graham, S. Lyle, D. M. Harlan, D. L. Greiner, J. Oberholzer, G. C. Weir, R. Langer and D. G. Anderson, Nat. Biotechnol., 2016, 34, 345-352

[28] O. Veiseh, J. C. Doloff, M. Ma, A. J. Vegas, H. H. Tam, A. R. Bader, J. Li, E. Langan, J. Wyckoff, W. S. Loo, S. Jhunjhunwala, A. Chiu, S. Siebert, K. Tang, J. Hollister-Lock, S. Aresta-Dasilva, M. Bochenek, J. Mendoza-Elias, Y. Wang, M. Qi, D. M. Lavin, M. Chen, N. Dholakia, R. Thakrar, I. Lacik, G. C. Weir, J. Oberholzer, D. L. Greiner, R. Langer and D. G. Anderson, Nat. Mater., 2015, 14, 643-651

[29] H. M. Chen, K. Muramoto and F. Yamauchi, J. Agric. Food Chem., 1995, 43, 574-578.

[30] C. Beermann, M. Euler, J. Herzberg and B. Stahl, Eur. Food Res. Technol., 2009, 229, 637-644.

[31] A. Etxabide, C. Vairo, E. Santos-Vizcaino, P. Guerrero, J. L. Pedraz, M. Igartua, K. de la Caba and R. M. Hernandez, Int. J. Pharm., 2017, 530, 455-467.

[32] P. Guerrero, J. P. Kerry and K. de la Caba, Carbohydr. Polym., 2014, 111, 598-605.

[33] J. L. Drury and D. J. Mooney, Biomaterials, 2003, 24, 4337-4351.

[34] Q. L. Loh and C. Choong, Tissue Eng. Part. B Rev., 2013, 19, 485-502.

[35] D. W. Hutmacher, Biomaterials, 2000, 21, 2529-2543.

[36] T. Mygind, M. Stiehler, A. Baatrup, H. Li, X. Zou, A. Flyvbjerg, M. Kassem and C. Bünger, Biomaterials, 2007, 28, 1036-1047.

[37] C. M. Murphy and F. J. O'Brien, Cell Adh. Migr., 2010, 4, 377-381.

[38] Z. Li, H. R. Ramay, K. D. Hauch, D. Xiao and M. Zhang, Biomaterials, 2005, 26, 3919-3928.

[39] A. Hezi-Yamit, C. Sullivan, J. Wong, L. David, M. Chen, P. Cheng, D. Shumaker, J. N. Wilcox and K. Udipi, J. Biomed. Mater. Res. A, 2009, 90, 133-141.

[40] R. M. Felfel, M. J. Gideon-Adeniyi, K. M. Zakir Hossain, G. A. F. Roberts and D. M. Grant, Carbohydr. Polym., 2019, 204, 59-67.

[41] C. Libioulle, L. Corbesier and R. Gilles, Comp. Biochem. Physiol. A Mol. Integr. Physiol., 2001, 130, 461-470.

[42] T. Haase, A. Krost, T. Sauter, K. Kratz, J. Peter, S. Kamann, F. Jung, A. Lendlein, D. Zohlnhöfer and C. Rüder, J. Tissue Eng. Regen. Med., 2017, 11, 1034-1044.

[43] J. Taylor, J. O. Anyango, M. Potgieter, K. Kallmeyer, V. Naidoo, M. S. Pepper and J. R. Taylor, J. Biomed. Mater. Res. A, 2015, 103, 2582-2590.

[44] J. D. Bryers, C. M. Giachelli and B. D. Ratner, Biotechnol. Bioeng., 2012, 109, 1898-1911.

[45] R. Klopfleisch and F. Jung, J. Biomed. Mater. Res. A, 2017, 105, 927-940.

[46] D. Elieh Ali Komi, L. Sharma and C. S. Dela Cruz, Clin. Rev. Allergy Immunol., 2018, 54, 213-223.

[47] B. P. Singh, S. Vij and S. Hati, Peptides, 2014, 54, 171-179.

[48] M. R. Shin, S. K. Kang, Y. S. Kim, S. Y. Lee, S. C. Hong and E. C. Kim, Int. Endod. J., 2015, 48, 705-716.

[49] B. Ma, E. Dohle, M. Li and C. J. Kirkpatrick, J. Tissue. Eng. Regen. Med., 2017, 11, 1779-1791.

[50] P. Carmeliet, F. De Smet, S. Loges and M. Mazzone, Nat. Rev. Clin. Oncol., 2009, 6, 315-326.

[51] L. Diaz-Flores, R. Gutierrez, M. P. Garcia-Suarez, F. J. Saez, E. Gutierrez, F. Valladares, J. L. Carrasco, L. Jr. Díaz-Flores and J. F. Madrid, Histol. Histopathol., 2017, 32, 1239-1279.

[52] E. Santos. R. M. Hernandez, J. L. Pedraz and G. Orive, Trends Biotechnol., 2012, 30, 331-341.

[53] S. Barrientos, H. Brem, O. Stojadinovic and M. Tomic-Canic, Wound Repair. Regen., 2014, 22, 569-578.

[54] K. Hu and B. R. Olsen, Bone, 2016, 91, 30-38.

[55] G. D. Mogosanu and A. M. Grumezescu, Int. J. Pharm., 2014, 463, 127-136.

[56] J. Lee, K. Roh, S. Kim, J. Lee and D. Park, J. Nutr. Biochem., 2012, 23, 1341-1351.

[57] K. M. Lee, H. Shim, G. S. Lee, I. H. Park, O. S. Lee, S. C. Lim and T. J. Kang, Biomol. Ther. (Seoul), 2013, 21, 246-250.

[58] M. Jafari, Z. Paknejad, M. R. Rad, S. R. Motamedian, M. J. Eghbal, N. Nadjmi and A. Khojasteh, J. Biomed. Mater. Res. B Appl. Biomater., 2017, 105, 431-459.

Materials Today Bio 15 (2022) 100273

Contents lists available at ScienceDirect

Materials Today Bio

journal homepage: www.journals.elsevier.com/materials-today-bio

Green hemostatic sponge-like scaffold composed of soy protein and chitin for the treatment of epistaxis

Jon Jimenez-Martin[†a], Kevin Las Heras[†a,c], Alaitz Etxabide[d], Jone Uranga[d], Koro de la Caba[d,e], Pedro Guerrero[d,e,f], Manoli Igartua[a,b,c], Edorta Santos-Vizcaino[*a,b,c], Rosa Maria Hernandez[*a,b,c].

[a] NanoBioCel Research Group, Laboratory of Pharmaceutics, School of Pharmacy, University of the Basque Country (UPV/EHU), Paseo de la Universidad 7, 01006 Vitoria Gasteiz, Spain.

[b] Biomedical Research Networking Centre in Bioengineering, Biomaterials and Nanomedicine (CIBER-BBN), Institute of Health Carlos III, Madrid, Spain.

[c] Bioaraba, NanoBioCel Research Group, Vitoria Gasteiz, Spain.

[d] BIOMAT Research Group, University of the Basque Country (UPV/EHU), Escuela de Ingeniería de Gipuzkoa, Plaza de Europa 1, 20018 Donostia-San Sebastián, Spain.

[e] BCMaterials, Basque Center for Materials, Applications and Nanostructures, UPV/EHU Science Park, 48940, Leioa, Spain.

[f] Proteinmat materials SL, Avenida de Tolosa 72, 20018 Donostia-San Sebastian, Spain.

[†] These authors contributed equally to this work.

*RM Hernandez and E. Santos-Vizcaino equally share credit for senior authorship. E-mail: rosa.hernandez@ehu.eus ; edorta.santos@ehu.eus

.....

Published in: ***Materials Today Bio***, 2022

Impact Factor 2021: ***10.761*** (Q1)

DOI: https://doi.org/10.1016/j.mtbio.2022.100273

Cat: Elsevier

Abstract

The increasing necessity of developing new devices for biomedical applications has added a growing social need of being environmentally respectful. In this work, we have shown that natural by-products from the food industry (soy protein and β-chitin) can be an excellent source of biomaterials to produce 3D scaffolds through simpler and cleaner processes. With the mixture of the two polymers, we have developed sponge-like scaffolds (SLS) with great physicochemical properties. Furthermore, a dialysis pre-conditioning step was enough to obtain negligible cytotoxicity in vitro. The predominant M2 macrophage profile, an elevated deposition of collagen fibers and the enhanced neovascularization capacity suggested an excellent biocompatibility also in vivo. Moreover, these SLS were able to promote cell adhesion, proliferation and high load capacity. Finally, h-MSCs 3D-cultured in these SLS released four times higher VEGF than h-MSCs seeded onto 2D plates. The green thinking strategy, properties and biocompatibility of this SLS highlight its potential as a cell delivery system for biomedical applications.

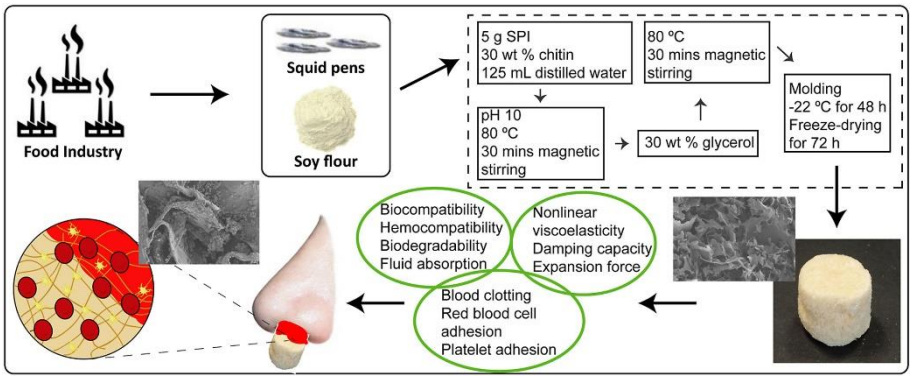

1. Introduction

Nasal hemorrhage, also known as epistaxis or nosebleed, is one of the most common otorhinolaryngology emergencies worldwide. It is estimated that 60% of the world's population will experience an epistaxis episode at least once in their lifetime, although only about 6% to 10% of them would seek medical attention [1]. Despite being usually simple to treat, severe nosebleed might cause serious risks for the patient, especially for those over 70 years, for whom the incidence of these episodes is higher [2]. In addition to this, nasal injury is common after nasal surgery, for which treatment must be started quickly. Several methods are available to treat epistaxis, among which electrocautery, vasoconstrictors, surgical procedures and nasal packing arise as the most popular [3].

Nasal packing, which involves the insertion of a kind of tampon in the nasal cavity, is of special interest for the treatment of epistaxis, offering elevated rates of success [4]. Nevertheless, the choice of the most adequate nasal pack is vital for the outcome of the treatment. The ideal nasal pack should promote hemostasis while being comfortable for the patient, as well as hindering mucosal damage [5]. Therefore, alternatives to currently commercialized nasal packs are needed, since they are commonly nonabsorbable — causing patient's discomfort during removal — and act just by physical pressure tamponade, without any intrinsic hemostatic effect.

Additionally, sustainability is attracting more and more attention in all research areas — including health-related areas — with the aim of reducing the environmental load associated to processes and products. In this sense, environmental analysis is a useful tool to measure emissions throughout the product life. Its principal benefit is that it identifies the environmental impacts within the value chain, which could be redesigned to reduce the environmental burden. Most environmental assessments are studies in which emissions and resource use are classified into categories that can potentially harm the environment, such as global warming potential [6]. Numerous works have been carried out related to the processing of petrochemical-derived materials, but only a few related to those derived from biopolymers [7-10].

In this context, natural polymers are arising as promising compounds for the development of hemostatic materials, being possible to manufacture them as scaffolds that mimic the extracellular matrix (ECM), which permits their reabsorption by the body [11]. These biopolymers are synthesized by living organisms such as plants, animals or microorganisms, and they generally offer good biocompatibility and biodegradability [12]. They might also possess different mechanisms to promote hemostasis..

Following this path, we recently developed and characterized a brand new sponge-like scaffold (SP-CH) based on a green strategy [13], using valorized by-products of the food industry. Even if several biopolymeric sponges has already been developed for the treatment of hemorrhagic wounds [14–16], hardly any of them seems to be directed towards the treatment of epistaxis [17,18], and none of them employs revalorized products for its manufacturing. Our SP-CH was manufactured by the mixture of soy protein isolate (SPI) and β-chitin (CH). The former was obtained from soy flour — a by-product of the manufacturing process of the soy oil industry — while the latter was extracted from fresh squid pens (Loligo sp.). SPI is an abundant biopolymer that shows biocompatibility and low immunogenicity, as well as several peptides with interesting biological functions, such as the RGD-like sequence (Arg-Gly-Asp) containing peptides, providing great cell-adhesive properties [19]. For its part, CH — namely poly (β-(1-4)-N-acetyl-D-glucosamine) — also shows low toxicity due to its natural origin [20], and is biodegradable. Besides, CH is said to activate polimorphonuclear cells and fibroblasts [21], to increase monocyte/macrophage migration and to promote collagen synthesis [22]. While the the SPI provides the sponge with interesting biomedical properties, CH was added in order to enhance the mechanical properties of the material [13]. The initial characterization of our SP-CH revealed its great physicochemical properties, with increased swelling capacity and partial degradability. Besides, the microstructure of the developed scaffolds could promote appropriate cell adhesion and proliferation, while remaining totally biocompatible.

Considering the excellent biomedical properties of the components of our SP-CH, we aimed to analyze its potential as a nasal pack for the treatment of epistaxis,

comparing it with materials widely used as nasal packs during nosebleeds: a basic gauze and Merocel® (MRC), the nasal pack used worldwide as gold standard. We expect our material to present more adequate mechanical properties to be used as a nasal pack, in addition to a greater hemostatic capacity, compared to the aforementioned widely used products. To this end, we first compared their porosity, pore size, degradation, swelling profile and mechanical properties. Additionally, we performed in vitro cytotoxicity studies to confirm the safety of our SP-CH. Then, we investigated their hemostatic potential, including blood clotting capacity and the adhesion of erythrocytes and platelets to the materials. Finally, we evaluated the hemostatic efficacy of each material in vivo. On the other hand, in addition to the physicochemical and biological aspects, the environmental assessment was considered in this work as a key tool to evaluate the impacts of the scaffolds and the processes followed for their manufacture.

2. Materials and methods

2.1 Materials

CH was extracted from fresh squid pens (Loligo sp.), kindly supplied by a local fish market. For the extraction of CH, the squid pens were first washed with water. After that, they were treated with NaOH (1 M) in a ratio of 1 : 20 (w/v) at room temperature and under continuous stirring for 24 h to avoid the deacetylation of the native CH. After filtering the samples, the solid fraction of CH was washed with distilled water until a neutral pH was obtained. The final CH powder was obtained by freeze-drying and milling. SPI, PROFAM 974, was gently supplied by ADM Protein Specialties Division (The Netherlands). Glycerol (99.01% purity), which was employed as a plasticizer, was provided by Panreac (Spain).

The properties of our SP-CH was compared with a standard gauze (Medicomp® 5 x 5 cm, Hartmann bv, Nijmegen, The Netherlands) and with Merocel® (Medtronic Xomed, Jacksonville, Fla.). This commercial nasal pack, which is composed of hydroxylated polyvinyl acetate, and presented as a compressed and dehydrated sponge, is the primary nonabsorbable nasal pack in several emergency departments around the world [23–26].

2.2 Preparation of the sponge-like scaffold (SPI-CH)

In order to prepare the SP-CH, 5 g of SPI were initially mixed with 30 wt % CH (based on the SPI dry basis), followed by the addition of 125 mL of distilled water to the mixture. Next, NaOH (1 M) was employed to adjust the pH to 10, and the solution was heated at 80 °C for 30 min under magnetic stirring. Subsequently, 30 wt % glycerol (based on the SPI dry basis) was added to the blend. So as to achieve a homogeneous blend, it was maintained at 80 °C for other 30 min. The solution was then poured into molds and maintained for 48 h in a freezer at −22 °C. Finally, it was freeze-dried for 72 h in order to complete the preparation of the SP-CH, which was eventually cut into discs using a hollow punch.

2.3 Environmental assessment

Environmental assessment was carried out according to ISO 14040 guidelines and recommendations: goal definition, inventory, impact assessment, and interpretation. The main goal of the study was to assess the environmental impact of the extraction of materials, the manufacturing of scaffolds and biodegradation as the end of life. The software used for this analysis was SimaPro 9.2.0.1 (PRé Consultants, The Netherlands). The materials used in the laboratory, the energy consumption during the extraction process, and the transportation of materials and residues were the resources and processes considered to develop the inventoy phase. The environmental burden related to the production of the scaffolds was determined considering the energy (electricity) and materials (NaOH, glycerol, water) used in the extraction and manufacturing processes. Also transportation of materials, distilled water production and its transportation to the waste treatment plant after use were considered. Data were obtained from Ecoinvent v3 database, which provides data regarding energy production, transport and production of chemicals. The functional unit selected was 1 g. Based on the inventory data, environmental impacts were assessed according to the Hierarchist version of ReCiPe 2016, midpoint (H) v1.05. The impact categories under study were global warming, water consumption, land use, human carcinogenic toxicity, ozone formation (human health), terrestrial ecotoxicity, freshwater ecotoxicity, marine ecotoxicity, human non-carcinogenic toxicity, fine particulate matter formation, terrestrial acidification, freshwater eutrophication, marine eutrophication, mineral

resource scarcity, fossil resource scarcity, ozone formation (terrestrial ecosystems), stratospheric ozone depletion, and ionizing radiation.

2.4 Blood obtention

Blood was acquired from healthy volunteers according to the protocols approved by the Ethics Committee for Researching Involving Biological Agents & GMOs (Procedure number: M30/2021/257) and the Ethics Committee for Research Involving Human Beings of the University of the Basque Country (Procedure number: M10/2021/256).

2.5 Pore size and porosity

A Hitachi S-4800 field emission scanning electron microscope (FE-SEM) (Hitachi High-Technologies Corporation, Tokyo, Japan) was employed to obtain the scanning electron microscopy (SEM) micrographs, using a beam accelerated voltage of 5 kV. All the tested materials were cut into discs of 8 mm diameter, mounted on a metal stub with adhesive tape and coated with gold under vacuum (JFC-1100) under an argon atmosphere before testing.

Image J software was used to measure pore diameters from SEM micrographs, in order to determine pore sizes. Between 75 and 250 randomly selected pores were measured for each material (n = 3 samples per group), and the average pore size for each material was calculated.

To evaluate the porosity of the samples (15 - 20 mg, n = 3 samples per group), a liquid displacement method was performed using 98% ethanol as the liquid medium, since it can diffuse through the samples without causing swelling or shrinkage [27]. V1 was defined as the initial volume of ethanol where the samples were submerged. Degasification was carried out for 5 min using a vacuum pump, so that the samples could be impregnated with the ethanol. V2 was defined as the total volume — ethanol plus soaked sample — after degasification. Last, ethanol-impregnated samples were removed and V3 was defined as the remaining volume of ethanol. The porosity (ε) of each sample was calculated using the equation below:

$$\varepsilon\ (\%) = \frac{V1 - V3}{V2 - V3} x\ 100$$

2.6 Swelling capacity and liquid retention ratio under pressure (LRRP)

Swelling capacity of the materials (15 – 20 mg, n = 4 samples per group) was calculated immersing pre-weighed samples (W0) of each material in 5 mL of PBS. The samples were weighed again (Wt) after 5 s, 15 s, 30 s, 1 min, 5 min and 15 min, to obtain the swelling curves of each material. Swelling at each time point was calculated using the following equation:

$$Swelling\ (\%) = \frac{Wt - W0}{W0} x\ 100$$

Liquid retention ratio under pressure (LRRP) was calculated in order to evaluate the ability of each material to retain the pre-absorbed liquid when a certain pressure is applied. Samples of each material (20 – 25 mg, n = 6 samples per group) were immersed in PBS to absorb as much liquid as possible, and then they were weighed (W_0). Next, known weights — 10 g, 15 g, 30 g and 40 g — were serially placed upon the wet material, carefully collecting the released liquid and weighting the sample again. This procedure was repeated for each weight (W_X). Then, LRRP was obtained using the following equation:

$$LRRP\ (\%) = \frac{Wx}{W0} x\ 100$$

2.7 Hydrolytic degradation

Hydrolytic degradation was studied by immersing pre-weighed (W0) samples (20 – 25 mg, n = 4 samples per group) of each material in 2 mL PBS, and culturing them at 37 °C for different periods of time — 2, 5, 9 and 14 days —. After removing the samples from PBS, they were first lyophilized and then weighed (Wf), in order to calculate the remaining weight (%). Hydrolytic degradation was expressed as the remaining weight of the incubated and lyophilized samples with respect to their initial weight, according to the following equation:

$$Remaining\ weight\ (\%) = \frac{Wf}{W0} x\ 100$$

2.8 Mechanical characterization

The mechanical properties of the dry materials were tested by compression test and cyclic compression test (35 – 45 mg, n = 5 samples per group). An Instron 5969 mechanical tester — equipped with a 50 N load cell — was used at a compressive rate of 0.5 mm s−1 up to 70% strain. As MRC is commercialized in lyophilized form, it was expanded before the test, by wetting and completely drying it off. Several parameters were calculated in order to compare the mechanical properties of the materials:

The maximum stress of each cycle relative to the maximum stress of the first cycle was calculated as follows:

$$Relative\ stress\ (\%) = \frac{Stress\ (cycle\ x)}{Stress\ (cycle\ 1)} x100$$

Young's modulus was calculated for all the strains of the first cycle of each biomaterial, using the following equation:

$$Young's\ modulus\ (kPa) = \frac{Stress\ (kPa)}{\left[Strain \frac{\%}{100}\right]}$$

Damping coefficient was calculated by means of the stress-strain curves of the materials, both for cycle 1 and for cycle 10. The following equation was used:

$$Damping\ coefficient = \frac{D}{U}$$

where D is the dissipated energy (area between the loading and unloading curves) and U is the total input energy (area under the loading curve). All the areas under the curve where calculated using the software GraphPad Prism 8.0.1.

Besides, an expansion force test was performed, hydrating samples of dry materials (35 – 45 mg, n = 5 samples per group) and recording the upwards stress displayed by the expansion of the material during water absorption.

2.9 Cytotoxicity studies

Cytotoxicity of the materials was assessed according to the ISO 10993-5:2009 guidelines for biological evaluation of medical devices. Both direct — direct contact with cells — and indirect — cells exposed to a conditioned medium of each material — cytotoxicity assays were performed. In both cases viability of L-929 fibroblasts (ATCC® 30-2003™) was measured through CCK-8 reagent (Sigma-Aldrich, Spain). After incubating the cells with CCK-8 solution in medium (1:11) for 4 h, the absorbance was read with a plate reader (Infinite® 200 PRO series, Tecan Trading AG, Männedorf, Switzerland) at 450 nm, using 650 nm as the reference wavelength. Cells that were not exposed to the materials — 100% viability — were used as a control group.

In the direct cytotoxicity assay, 35000 cells were seeded per well in a 24-well plate, using 500 μL/well of EMEM complete medium. Next, the cells were incubated for 24 h at 37 °C. After removing the medium, 1 mL of fresh medium was added and each material (10 – 15 mg, n = 4 samples per group) was hydrated and placed in a transwell to bring it into direct contact with the bottom of the well. The materials were removed after 48 h of incubation, replacing the medium with 300 μL/well of CCK-8 reagent.

In the case of the indirect cytotoxicity assay, L-929 fibroblasts were exposed to conditioned medium of each material (n = 5 samples per group), obtained incubating 100 mg of each material with 500 μL of EMEM at 37 °C for 24 h. Firstly, a 96-well plate was used to seed 5000 cells/well in 100 μL/well of medium, and the plates were incubated for 24 h at 37 °C. After, the medium was replaced with 100 μL/well of the corresponding conditioned medium, and the plate was straightaway incubated at 37 °C for 24 h. Eventually, the conditioned medium was removed, and 110 μL/well of CCK-8 reagent was added.

2.10 Blood swelling and degradation in blood

Maximum blood swelling capacity was tested by immersing pre-weighed (W0) samples (15 – 20 mg, n = 5 samples per group) of the materials in 500 μL of blood.

After 2 min, to allow complete blood absorption, samples were weighed again (Wf). The maximum swelling capacity (%) was calculated using the following equation:

$$Swelling\ (\%) = \frac{Wf}{W0} x\ 100$$

To evaluate the degradation of the materials in blood, pre-weighed (W0) samples (15 – 25 mg, n = 4 samples per group) of each material were placed in 24-well plates, using one plate for each time-point tested — 2, 4 and 7 days —. Blood was added to each sample in an amount of a 120% of its maximum blood swelling capacity, and the plates where incubated at 37 °C. At each time-point, samples were washed out with PBS, lyophilized and weighed (Wf). Degradation in blood was expressed as the remaining weight of the incubated and lyophilized samples with respect to their initial weight, according to the following equation:

$$Remaining\ weight\ (\%) = \frac{Wf}{W0} x\ 100$$

2.11 Whole blood clotting *in vitro*

Hemoglobin content of the samples was quantified using a Hemoglobin Assay Kit (Sigma-Aldrich, USA), by measuring absorbance of the samples (Is) with a plate reader (Infinite® 200 PRO series, Tecan Trading AG, Männedorf, Switzerland) at 400 nm.

For the whole blood clotting test, citrated whole blood¬ — 9:1 whole blood to 3.8% sodium citrate — was obtained from a healthy human donor. First, 0.2 mL of the citrated whole blood was added to preheated (30 min at 37 °C) samples of the materials disposed in a 24 well plate (25 – 35 mg, n = 5 samples per group). After this, 20 μL of CaCl2 (0.2 M) were added to start coagulation. The plate with the materials was incubated under 30 rpm agitation for 10 min at 37 °C. Afterwards, 2 mL of deionized water were added in each well to hemolyze the red blood cells (RBCs) that were not within the clot formed in the material. The deionized water containing the non-adhered and hemolyzed RBCs was collected and its hemoglobin content was quantified. 5 μL of CaCl2 (0.2 M) and 50 μL of citrated whole blood were added to 750 μL of deionized water, and the absorbance of this solution was used as the reference value (Ir). The absorbance of an empty well

was also measured (Io). Blood Clotting Index (BCI) of each sample was calculated using the following equation:

$$BCI\ (\%) = \frac{(Is - Io)}{(Ir - Io)} x\ 100$$

With the purpose of visually evaluating the clotting capacity of each material, 150 mg of each material were disposed in Eppendorf tubes, subsequently adding 500 µL of citrated whole blood and 500 µL of CaCl2 (10 mM). After incubating the Eppendorf tubes for 1 min at 37 °C, they were turned upside down and gently shaken to observe the formed clots.

2.12 Hemolysis assay *in vitro*

For the assessment of hemocompatibility in vitro, citrated whole blood — 9:1 whole blood to 3.8% sodium citrate — from a healthy donor was obtained and diluted 1:5 in normal saline. Samples of each material (10 – 15 mg, n = 6 samples per group) were disposed in a 24-well plate. Diluted whole blood was added to each sample in an amount of the 80% of each material's swelling capacity. The plate was incubated for 1 h at 37 °C. Samples were moved to conical centrifuge tubes and centrifuged for 10 min at 3000 rpm. The supernatant of each sample was collected and its hemoglobin content was quantified as described in section 2.8. 150 µL of whole blood was added to deionized water and to normal saline, in order to use these solutions as positive (Ir) and negative (Io) controls, respectively. Hemolysis rate was calculated using the following equation:

$$Hemolysis\ (\%) = \frac{(Is - Io)}{(Ir - Io)} x\ 100$$

2.13 Red blood cell adhesion *in vitro*

To evaluate RBC adhesion to the material, citrated whole blood — 9:1 whole blood to 3.8% sodium citrate — was collected from a healthy donor. Samples of each material were cut (15 – 20 mg, n = 6 samples per group) and each sample was placed in a Petri dish. Citrated whole blood was added to each sample in an amount of the 80% of each material's swelling capacity, and they were incubated for 5 min at 37 °C. Next, 5-10 mL of deionized water were gently added by the edge

of the dish until the water touched the sample and blood started to flow. More deionized water was added until a total volume of 50 mL for each sample. Each material was carefully moved to a clean Petri dish, and the liquid in each old Petri dish, — containing the RBCs that could not adhere to the sample —, was collected. The hemoglobin content of this solution was quantified as described in section 2.8. This measurement accounts for hemoglobin outside the material, that is, the RBCs that could not adhere to the material.

Afterwards, hemoglobin within the materials was measured, which accounts for the amount of RBCs adhered to each sample. 10 mL of deionized water were added straightly on the material — so that the previously adhered RBCs would be released — and the hemoglobin content in the resultant solution was quantified as described in section 2.8.

For both the hemoglobin outside and within the material, a positive control was prepared by mixing 200 µL of blood and 50 mL of deionized water. Hemoglobin concentration (mg dL-1) of each sample was calculated using the following equation provided by the Hemoglobin Assay Kit, and results of each sample were normalized against the blood volume added to the control group:

$$[Hemoglobin] = \frac{(Is - Io)}{(Ir - Io)} x\ 100 \frac{mg}{dL} x\ df$$

where Is is the absorbance of the tested solution; Io is the absorbance of the blank (water); Ir is the absorbance of the calibrator provided in the Hemoglobin Assay Kit; 100 mg/dL is the concentration of the diluted calibrator; df is the dilution factor, which was calculated for each sample depending on the volume of blood and deionized water added.

Citrated whole blood was also added to samples of each material (n = 3 samples per group) and the adhesion of RBCs was visually evaluated using SEM micrographs, obtained as described in section 2.2.

2.14 Platelet adhesion *in vitro*

Adhesion of platelets to the materials was studied through a Lactate Dehydrogenase (LDH) Assay Kit (Sigma-Aldrich, USA), which allows to quantify

platelet adhesion by measuring the LDH released by platelets when they are lysed, according to a reported method [28]. Briefly, citrated whole blood — 9:1 whole blood to 3.8% sodium citrate — was obtained from a healthy donor. After centrifuging it at 480 g for 10 min at 4 °C with 4 a/d, platelet-rich plasma (PRP) was obtained. The serum above the buffy coat was collected from the centrifuged blood samples and kept in citrated tubes. Samples of each material (15 – 20 mg, n = 5 samples per group) were disposed in a 24-well plate and PRP was added to each sample in an amount of the 80% of each material's swelling capacity, and they were incubated for 30 min at 37 °C. Normal saline was gently added to each well until the samples were immersed, so that the non-adhered platelets could be removed from the material, and all samples were moved to a new 24-well plate. 1 mL of Triton X-100 1%-PBS was added straightly on the material, in order to lyse the platelets that had adhered to the material. After incubation for 1 h at 37 °C, each solution of Triton and lysed platelets was collected and LDH content was measured according to the protocol provided by the manufacturer (Sigma-Aldrich, USA) of the LDH Kit. To prepare the negative (Io) and positive (Ir) controls, 200 μL of PRP were added to 1 mL of PBS and Triton X-100 1%, respectively. Absorbances of the lysed platelets of each samples (Is) were measured with a plate reader (Infinite® 200 PRO series, Tecan Trading AG, Männedorf, Switzerland) at 400 nm, and normalized against the PRP volume added to the controls. LDH release (%) relative to the positive control was calculated using the following equation:

$$LDH\ release\ (\%) = \frac{(Is - Io)}{(Ir - Io)} x\ 100$$

PRP was also added to samples of each material (n = 3 samples per group) and the platelet adhesion was visually evaluated using SEM micrographs, obtained as described in section 2.4

2.15 *In vivo* hemostatic efficacy

To evaluate the hemostatic efficacy in vivo, a rat-tail amputation model was used. This experiment was conducted following the protocols approved by the Institutional Ethical Committee for Animal Experimentation of the University of the Basque Country (Procedure number: M20/2021/362). Wistar rats — with weights

between 250 - 300 g (Janvier Labs, Le Genest-Saint-Isle, France) — were anesthetized with isoflurane (Isoflo®, Esteve, Spain), and 2.5 cm from the end of their tail was cut using a scalpel. The tail was immediately placed in air for 10 s to guarantee normal blood loss, after which the wound was brought into direct contact with the corresponding pre-weighed material (250 – 300 mg, n = 6 rats per group), holding it with a pre-weighed gauze (900 – 950 mg). The wound was uncovered every minute to check if bleeding persisted. For this reason, bleeding time (min) was assessed by assigning a score to each period at which bleeding ceased, as follows: 0 - 3 min: 1; 3 - 6 min: 2; 6 - 9 min: 3; >9 min: 4. Therefore, a lower bleeding time score represents a faster hemostatic effect. The blood-impregnated samples were weighed again to calculate total blood loss (g).

2.16 Statistical analysis

Mean ± standard deviation was used to express the results. In the case of normally distributed data, results were analyzed through a one-way ANOVA test. Bonferroni or Tamhane post-hoc analysis was applied based on the Levene test for the homogeneity of variances. In reverse, non-normally distributed data was analyzed by Mann–Whitney's nonparametric analysis. Sample size of each experiment is indicated in the corresponding materials and methods section. $p < 0.05$ was considered statistically significant. Moreover, all the statistical computations were performed using SPSS 25.0 (SPSS®, Inc., Chicago, IL, USA).

3. Materials and methods

3.1 Environmental assessment

The increasing environmental concern has led to assess the suitability of biodegradable polymers extracted from natural and renewable resources. Therefore, biopolymers derived from residual biomass have become an attractive alternative due to their abundance, cost and biodegradability. In this context, CH and soy protein were used in this work. On the one hand, CH can be obtained from shrimp, crabs or squid pens, among others. It should be noted that the CH content varies significantly depending on the source employed for its extraction. When CH is obtained from crustacean shells, CH content is around 20% after a

demineralization process; however, the CH content from squid pens can reach 50%, with a mineral content lower than 3% [29]. On the other hand, soy protein, a by-product from soy oil production, can be purified to obtain SPI. In this process, soy flour is obtained as by-product, which is purified to obtain soy protein powder after centrifugation, acidification and neutralization processes. To determine the environmental load associated with CH and soybean residue valorization, the environmental loads associated with those processes were considered.

All the abovementioned processes were considered to obtain the global environmental results of scaffolds production reported in **Table 1**. The results showed that terrestrial ecotoxicity, global warming and ionizing radiation caused low environmental load in the production of scaffolds, while the other categories contributed minimally to the overall environmental burden. We should note that the environmental burden of terrestrial ecotoxicity is related to soybean production and the generation of energy needed to obtain CH.

Table 1. Impact category values measured in the production of the scaffolds.

Impact Category	Unit	Total
Global warming	kg CO_2 eq	1.7517401
Stratospheric ozone depletion	kg CFC11 eq	8.11E-07
Ionizing radiation	kBq Co-60 eq	0.99109783
Ozone formation, human health	kg NO_x eq	0.00560783
Fine particulate matter formation	kg $PM_{2.5}$ eq	0.00403105
Ozone formation, terrestrial ecosystems	kg NO_x eq	0.005638093
Terrestrial acidification	kg SO_2 eq	0.010339224
Freshwater eutrophication	kg P eq	0.00067464
Marine eutrophication	kg N eq	6.30E-05
Terrestrial ecotoxicity	kg 1,4-DCB	1.4278474
Freshwater ecotoxicity	kg 1,4-DCB	0.023579723
Marine ecotoxicity	kg 1,4-DCB	0.033241366
Human carcinogenic toxicity	kg 1,4-DCB	0.061105474

Impact Category	Unit	Total
Human non-carcinogenic toxicity	kg 1,4-DCB	1.3274998
Land use	m^2a crop eq	0.16276505
Mineral resource scarcity	kg Cu eq	0.001540514
Fossil resource scarcity	kg oil eq	0.48253294
Water consumption	m^3	0.012084432

It is worth noting that the use of squid pens as a source of CH provided environmental benefits. Due to the low amount of inorganic compounds and the lack of pigments in squid pens, demineralization and decolourization processes could be eliminated from the CH extraction process and, thus, the use of chemicals and energy consumption associated with those processes were reduced significantly [30]. In addition, the elimination of those processes entailed economic benefits, since the extraction process implied the employment of smaller amounts of resources (materials, energy, and time) and, at the same time, a higher yield of CH was obtained, compared to that of CH extracted from crustacean shells.

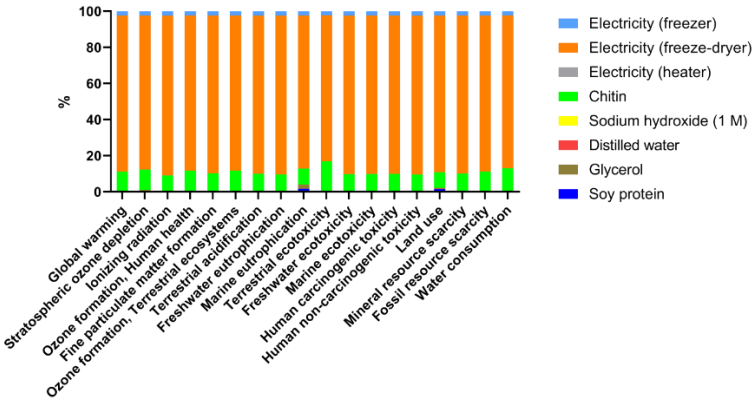

Figure 1. Relative contributions in each impact category for the most relevant processes involved in the entire life cycle of scaffolds. Disaggregating environmental results are displayed in percentage ratios for the most relevant contributing factors..

The relative contributions in each impact category for the most relevant processes involved in the complete life cycle of the scaffolds are shown in **Figure**

1. The environmental results obtained are shown in percentage proportions, where it can be seen that the most relevant contributing factor was electricity consumption in extraction and manufacturing processes. We must remember that the environmental impact calculated in this work was based on the results obtained in the laboratory and gave us an idea of which processes should be optimized to be able to reduce the environmental burden, which could be more easily reduced at an industrial scale.

In addition, Figure 1 shows the environmental results broken down into percentages for each impact category. In this way, the contribution of each stage on the final product could be assessed. In this case, the contributions of the different processes and activities involved throughout the life cycle were calculated as a function of the overall results. As shown in Figure 1, the stages of obtaining CH required energy and this represented more than 80% of the total impact, becoming the factor with the greatest potential for improvement in decision making when scaling-up. In particular, the energy consumed in the scaffold production, specifically the consumption of electricity, played a critical role in the environmental impact, regardless of the impact category considered. Since the scaffolds were produced at laboratory scale, scaling up the processes would lead to reducing the aforementioned environmental impacts.

3.2 Physicochemical characterization

3.2.1 Pore size and porosity

Pore structure of biomaterials that aim to be used as wound healing agents — either to treat hemorrhages or other types of wounds — is of great importance. Differences in the structure of the three materials employed during this study can be appreciated in the macroscopic images (Figure 2A). Even though, differences in the microstructure are of greater importance. The excellent physicochemical properties of our material were already demonstrated in our previous work [13], but we wanted to compare some of these properties between the three materials. In this vein, the gauze was the material with the highest pore size — 479 ± 252 μm —, while MRC and SP-CH showed a very similar pore size distribution, 144 ± 63 and 141 ± 124 μm, respectively (Figure 2B). MRC and SP-CH showed no

significant difference in mean pore size ($p > 0.05$), while both of them showed significant differences with respect to gauze ($p < 0.001$). Pore size can be closely related to the hemostatic capacity of a material [31]. Ideally, a balance should be sought between large pore sizes that allow RBC and platelet internalization and small pores that provide optimal surface area, required for appropriate cell adhesion [32].

Porosity can be related to difficulties in nasal pack removal due to an increase in pack size that would hinder its removal from the nostril. Even though, porosity is required to be high to allow diffusion of nutrients and oxygen [33]. Besides, high porosity is related to elevated surface area, which is of interest for the absorption of wound fluids, either exudates or even blood [34]. As a larger surface area of the material is also related to higher exposition to cells, it can influence cell adhesion and viability as well [35]. In this context, MRC and SP-CH showed similar porosity (**Figure 2C**), 92.97 ± 4.39% and 86.95 ± 1.58%, respectively. Meanwhile, the gauze showed significantly higher porosity than SP-CH, 96.68 ± 0.12%. The difficulties associated with a high porosity might be overcome by the partial degradation of the nasal pack, which would facilitate the painless removal of the pack. In this sense, it is clear that the SP-CH offer advantages in the removal of the pack compared to MRC and the gauze, even if the three of them present high porosities. On the other hand, SEM micrographs (**Figure 2D**) clearly evince that internal structures of the three materials differ. The gauze shows thousands of intertwined fibers forming a mesh, but the space between the fibers does not present well-defined pores, which are required for good liquid retention. For their part, MRC and SP-CH show an internal microstructure of well-defined interconnected pores, which in the case of MRC are more circular and in the case of SP-CH present a more amorphous structure. Together with a similar pore size and porosity, this makes MRC and SP-CH very similar regarding to their internal microarchitecture, which completely differs from that of the gauze.

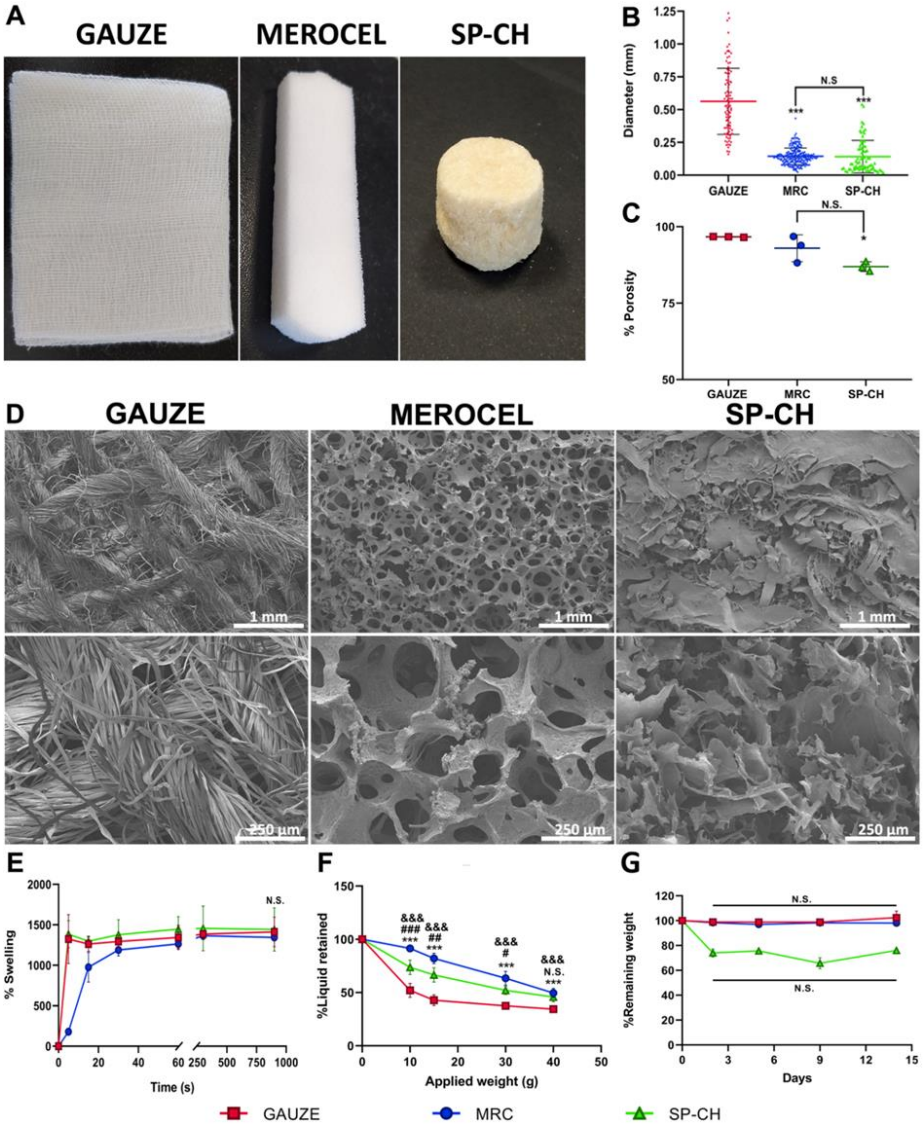

Figure 2. Physicochemical characterization. (A) Macroscopic images of the materials: Gauze, MRC, and SP-CH. (B) Pore size distribution of the materials. (C) Porosity (%) of each material. Error bars, mean ± SD. *$p < 0.05$; ***$p < 0.001$ vs gauze. N.S., nonsignificant ($p > 0.05$). (D) SEM micrographs of dry materials. (E) Swelling profiles. Error bars, mean ± SD. N.S., nonsignificant ($p > 0.05$). (F) Liquid retention ratio under different pressures. Error bars, mean ± SD. &&&$p < 0.001$ gauze vs MRC. #$p < 0.05$; ##$p < 0.01$; ###$p < 0.001$ MRC vs SP-CH. ***$p < 0.001$ gauze vs SP-CH. (G) Hydrolytic degradation. Error bars, mean ± SD. N.S., nonsignificant ($p > 0.05$).

3.2.2 Swelling capacity and Liquid Retention Ration under Pressure (LRRP)

The capacity of biomaterials to absorb fluids is important as it will determine their abilities to absorb the blood present in hemorrhages. We tested the water swelling profiles of the three materials by measuring swelling at different time points (Figure 2E). The three materials showed similar water uptake capacity, with the maximum swelling capacity ranging between 1334 ± 34% (MRC) and 1442 ± 267% (SP-CH) of its initial weight after 15 min. During that period of time, the gauze absorbed 1412 ± 182% of its initial weight. Even if the maximum absorption capacity was similar for the three materials, the swelling profile turned out to be quite different. While SP-CH and gauze achieved a 1383 ± 168% and 1324 ± 302% of their initial weight within only 5 s, respectively, MRC could only swell a 178 ± 21% of its initial weight during the same time. This shows that even if all of them displayed similar maximum absorption capacity, MRC showed delayed swelling, only equaling SP-CH and gauze after 60 s. The water absorption property appears to be especially important in the treatment of epistaxis as the principal way in which nasal packs arrest bleeding is by exerting pressure on the damaged blood vessels of the nasal mucosa to promote hemostasis. After being inserted in the nostril, the nasal pack absorbs wound fluids and expands, maintaining pressure on the wound site. This pressure should be high enough to control the bleeding, but not as high to damage the nasal cavity. Complications associated with excessive pressure include movement of the pack from its initial position [36], obstructed breathing and reduced sense of smell [1], and even necrosis of mucosa and cartilage [24].

Nevertheless, when the pack puts pressure on the nostril's walls, the nostril's walls also put pressure on the pack, thus desorbing part of the previously absorbed fluids. For this reason, we evaluated the capacity of the materials to retain the absorbed liquid under pressure. In this experiment (Figure 2F) both MRC and SP-CH showed significantly greater ($p < 0.001$) water retention capacity compared to gauze, independently of the pressure applied. Besides, MRC displayed significantly better retention at low pressures compared to SP-CH, although both materials turned out to similar ($p > 0.05$) retaining values for pre-absorbed water when the maximum weight — 40 g — was applied, with MRC maintaining 49.58 ± 4.37% and SP-CH 45.83 ± 4.54% of their maximum swelling capacity, while gauze

maintained just 34.44 ± 2.35%. Therefore, even if the three materials showed similar water swelling capacity, gauze is not able to effectively retain the absorbed water when a pressure is applied, and thus loses its ability to exert pressure to the bleeding site, likely due to its internal microstructure, as commented before. Probably one of the major drawbacks of the pressure exerted by the nasal packs is the discomfort caused to the patient, both with the pack in situ and during its removal, with the latter even causing rebleeding, mucosal abrasions, demucozalization and detachment of scars [37]. As pressure is needed to promote hemostasis, these disadvantages always go together with effective nasal packs, as long as they are nonabsorbable.

3.2.3 Hydrolytic degradation

Degradability is a property of increasing popularity among biomaterials for nasal packings, as it reduces both patient discomfort and rebleeding upon removal, among other advantages [38]. In this vein, both gauze and MRC showed no degradation during the 14 days of experiment (Figure 2G), while SP-CH degraded 25.96 ± 3.22% of its initial weight after 48 h. After that measurement, SP-CH showed no more degradation on the following days ($p > 0.05$). These results clearly show that both gauze and MRC are totally nonabsorbable nasal packs, while SP-CH can lose about a 25% of its initial weight after 48 h via hydrolytic degradation, due to the glycerol content (30 wt %) of the SP-CH dissolving in water. This may probably be enough to relieve patient's discomfort and damage associated with pack removal, and to avoid rebleeding episodes, which would suppose a great advantage both for the patient and the clinician [39]. Besides, it is worth mentioning that in our previous work about the SP-CH [13], we demonstrated that it can be enzymatically degraded within 2 hours, using collagenase P.

3.3 Physicochemical characterization

For appropriate handling and clinical use nasal packs must present good mechanical properties and resistance to deformation, thus alleviating patient's concerns about discomfort during the treatment and providing mechanical stability [40].

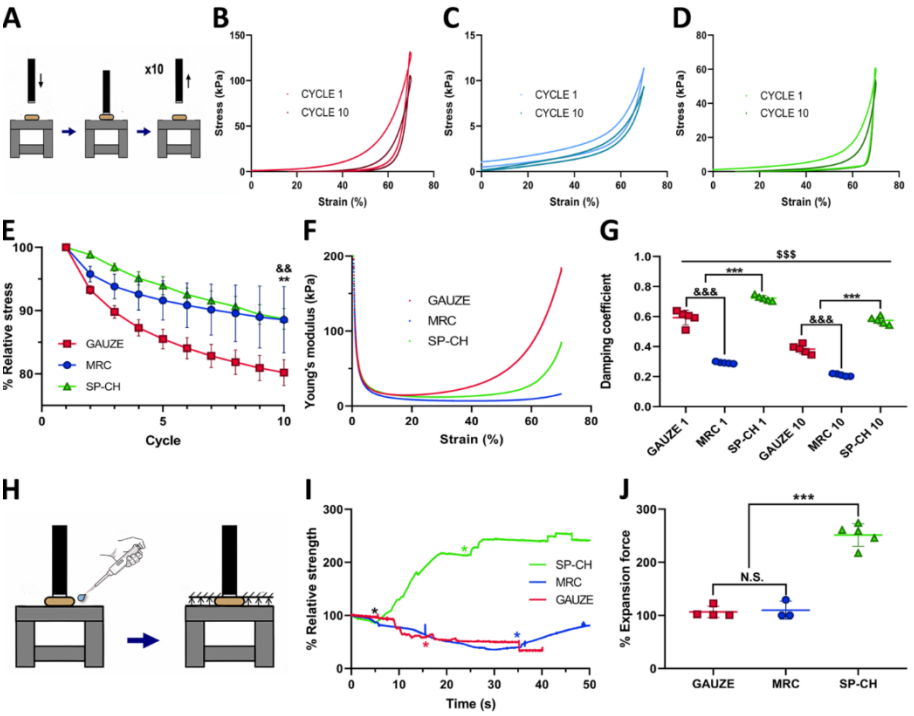

Figure 3. Mechanical characterization. (A) Scheme of the procedure carried out for the cyclic compression test. (B-D) Cyclic compression stress-strain curves of gauze (B), MRC (C) and SP-CH (D). (E) Relative stress (%) of the materials for 10 cyclic compressions. Error bars, mean ± SD. &&p < 0.01 gauze vs MRC. **p < 0.01 by gauze vs SP-CH. (F) Young's modulus of the materials at different strains. (G) Damping coefficients of the material for cycles 1 and 10. Error bars, mean ± SD. &&&p < 0.001 gauze vs MRC. ***p < 0.001 SP-CH vs the other groups. $$$p < 0.001 cycle 1 vs cycle 10 of the same group. (H) Scheme of the procedure carried out for the expansion force test. (I) Relative expansion strength curves of the materials. * indicates the moment at which water was added to each material. (J) Relative expansion force of the materials. Error bars, mean ± SD. ***p < 0.001 SP-CH vs the other groups. N.S., non-significant (p > 0.05).

We carried out a cyclic compression stress-strain test with 10 cycles (**Figure 3A**) to characterize the mechanical properties of the materials (**Figure 3B-D**). These curves show an initial plateau region, followed by a hyperelastic region at higher strains, which is more noteworthy for the gauze and SP-CH than for MRC. For the three materials the relationship between stress and strain is nonlinear, exhibiting nonlinear viscoelasticity, similarly to many body tissues and extracellular matrix

components [41]. This viscoelasticity could be confirmed by the loading and unloading curves of each cycle taking different paths, which occur due to energy dissipation during deformation of the material [42], producing an hysteresis loop between loading and unloading curves. The area under the loading curve represents the total input energy of the cycle and the area under the unloading curve represents the elastic strain energy, while the area between the two curves accounts for the dissipated energy during the compression cycle [43]. In addition to this, gauze showed the highest stress at a strain of 70%, both for cycle 1 and for cycle 10, while MRC showed the lowest, meaning that gauze was the most difficult material to deform up to a strain of 70%, and MRC the easiest one, which could be due to the internal microstructure of each one. SP-CH required an intermediate stress to be deformed up to a 70% of strain.

Nevertheless, the cyclic compression test revealed that the stress needed to deform the materials decreased substantially cycle after cycle (Figure 3E), losing their maximum ability to resist deformation. This phenomenon, which is defined as cyclic softening [44], is probably a consequence of irreversible deformations of the internal microarchitecture caused by the compression [45]. Results of the relative maximum stress (%) (**Figure 3E**) show that the gauze could only maintain a 80.2 ± 2.0% of its maximum stress after 10 cycles, compared to the maximum stress of cycle 1. This is significantly lower ($p < 0.01$) than MRC and SP-CH, that displayed a relative stress of 87.3 ± 5.2% and 88.6 ± 1.6% after 10 cycles, respectively.

Young's modulus defines the ability of a material to withstand changes in length when subjected to compressive loads, and it is useful to measure the stiffness of a material [46]: the higher the Young's modulus, the higher the stiffness of the material. Since the three materials present a nonlinear behavior, Young modulus is not constant but changes depending on the position in the stress-strain curve, and is defined by the slope of the tangent to the curve [47]. Thus, we calculated the Young's modulus for all the strains of the first cycle of each biomaterial (**Figure 3F**). Initially, the three samples presented a high Young's modulus, which rapidly decreased when strain started to increase. As strained became higher, the Young modulus of gauze and SP-CH started to increase again at strains coinciding with the ones in which the hyperelastic region of each material began — around 25%

of strain for the gauze and 50% of strain for SP-CH —. This could indicate that at 25% of strain, all the cotton layers forming the gauze are very compact, and consequently the stiffness of the sample strongly increases. Meanwhile, the internal microstructure of the SP-CH would not get completely compact until a strain of 50%. MRC showed no meaningful increase of its Young's modulus at higher strains, indicating that its stiffness remained low throughout all the compression process. Summing up, while gauze becomes rigid at low strains, both MRC and SP-CH remain flexible until a strain of 50% is achieved.

As commented before, the cyclic loading and unloading produced dissipation of energy within the material, which is usually a result of the viscoelastic behavior of the material or general damage to the structure [48]. Since viscoelastic nature of the three materials could be previously confirmed by the profile of the stress-strain curves and the presence of the hysteresis loop, energy dissipation can be attributed to that viscoelastic behavior. The area of this hysteresis loop — that is, the area between the loading and unloading curves — is directly linked to the damping capacity of the material [49], which is defined by the damping coefficient — or mechanical loss coefficient —, that measures to which extent a material can dissipate vibrational energy [50]. This property depends on factors such as the type of material, internal forces, sizes of geometry and the surface of the material [51], and seems to be of greater importance in biological materials for their protection via damping the impact waves [52]. Damping capacity is commonly high in materials such as foams, elastomers and polymers [50], and therefore they are widely used as damping materials [53]. Since a nasal pack is inevitably subjected to mechanical compression when inserted in the nostril, we evaluated the damping coefficient of the three materials for cycle 1 and 10, calculating it as the ratio of the energy dissipation — area of the hysteresis loop — and the total input energy — area under de loading curve — for the given cycle [51]. For the first cycle, SP-CH presented a damping coefficient of 0.72 ± 0.02, which was significantly higher ($p < 0.001$) than the ones obtained for gauze and MRC, 0.59 ± 0.05 and 0.29 ± 0.01, respectively. Comparing the first cycle's coefficient to the cycle 10's, all the materials significantly ($p < 0.001$) lost damping capacity, probably due to irreversible alterations in their internal microstructure caused by the cyclic compression. Even though, SP-CH presented a damping coefficient of

0.57 ± 0.03 in cycle 10, which is still significantly higher ($p < 0.001$) than the ones calculated for gauze and MRC, 0.38 ± 0.03 and 0.21 ± 0.01, respectively. These results indicate that our material has an increased capacity to dampen the impact waves and mechanical forces that may be produced with the pack placed in the nasal cavity.

To evaluate the upwards force displayed by the materials when they absorb water, we performed an expansion force test, as illustrated in Figure 3H. This force is representative of the force these materials would display against the nasal cavity's walls when absorbing fluids within the nostril, and therefore this property seems to be of special interest for a nasal pack. Figure 3I shows the relative expansion strength curves of the materials throughout time, compared to their initial strength. Both gauze and MRC displayed null expansion force when absorbing water, even decreasing their initial strength after adding water to the sample. In contrast, SP-CH's relative expansion curve evinces that when absorbing water, it displays an increasing upwards force, caused by its expansion. This is numerically represented in Figure 3J, in which the maximum expansion force (%) displayed during the experiment is calculated with respect to the initial expansion force. Results confirmed that gauze and MRC have no capacity to display an upwards force when absorbing water, just increasing the initial expansion force up to a 107 ± 11% and 110 ± 17%, respectively. Conversely, SP-CH presented an expansion force of 250 ± 24% with respect to the start of the experiment, which supposes a significantly higher ($p < 0.001$) expansion force than for gauze and MRC. Even if high expansion forces can be related to delayed mucosal healing, this is not a common concern in biomaterials with high expansion capacities [54,55]. Thus, we truly believe that a sponge-like material with such a modest expansion force will not cause mucosal damage, but it would probably be able to exert a higher pressure to the bleeding site when absorbing wound fluids within the nostril to promote hemostasis.

3.4 Cytotoxicity studies

Direct and indirect cytotoxicity were evaluated in order to confirm the biocompatibility of the materials. A protocol from the ISO 10993 5:2009 guidelines

for biological evaluation of biomedical devices was adapted to carry out these assays. Both in direct (Figure 4A) and indirect (Figure 4B) cytotoxicity assays the three materials showed cell viability above 70%, and thus their biocompatibility could be confirmed. In both assays, no significant differences were found in biocompatibility between MRC and SP-CH ($p > 0.05$), but gauze showed significantly higher biocompatibility in comparison to SP-CH in the direct cytotoxicity assay ($p < 0.05$). In contrast, in the indirect cytotoxicity assay, SP-CH turned out to be significantly more biocompatible than the gauze ($p < 0.05$).

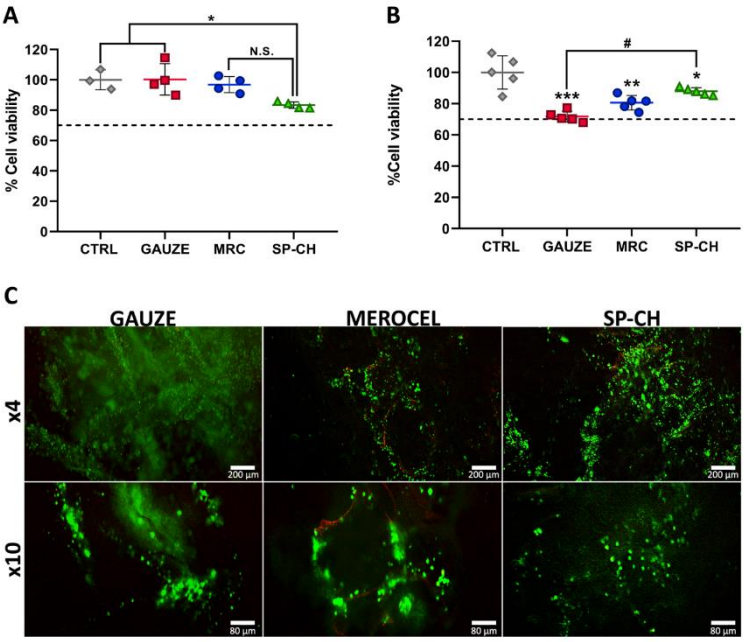

Figure 4. Cytotoxicity studies. (A) Direct cytotoxicity. (B) Indirect cytotoxicity. The line marks the 70% cell viability. Error bars, mean ± SD. N.S., non-significant ($p > 0.05$). *$p < 0.05$; **$p < 0.01$; ***$p < 0.001$ vs control group. #$p < 0.05$ gauze vs SP-CH. (C) Live/Dead micrographs of the cell-cultured materials, with calcein-ethidium staining. Scale bars are 100 and 40 µm in the above and below rows, respectively.

We also performed the Live/Dead staining method to visually prove that these biomaterials allowed viability of L-929 cells cultured upon them (Figure 4C), with practically all cells alive (green colored) in all the samples, and just a few dead

cells — red colored — present in the MRC images. These studies proved that the SP-CH is adequate for biomedical use without causing any cytotoxicity to the cells present in the nasal cavity and surrounding tissues.

3.5 Blood performance

3.5.1 Degradation in blood

To test the degradation profile of the materials in a more biologically relevant fluid, we evaluated their blood degradation profile (Figure 5A). Results showed that SP-CH degrades in contact with blood, while gauze and MRC do not, as confirmed by the images of the materials after incubation with blood (Figure 5B). After 4 days of incubation in blood, the gauze presented a weight of 110 ± 2% with respect to its initial weight, while MRC presented a remaining weight of 103 ± 1%. In contrast, SP-CH maintained a 79 ± 2% of its weight after 4 days of incubation in blood, meaning that it could degrade a 21 ± 2% of its initial weight during that period of time. This would probably facilitate its removal from the patient's nostril once the nasal pack reaches its goal.

Interestingly, the gauze and MRC not only did not degrade but their weight slightly increased after being incubated with blood — although samples were lyophilized before weighing — to eliminate all the fluids present in the samples. This might be due to blood cells and proteins adhering to these materials, which could not be completely eliminated. This indicates that these materials could have degraded to some level, but that the adherence of these blood components would balance out that degradation. Therefore, the degradation profile of SP-CH could also have been underestimated by the adhesion of blood components as in the case of gauze and MRC, which would mean that our material has even better blood degradation properties. The fact that SP-CH degrades a fifth part of its weight after 4 days, confirms that this material can be used as a partly absorbable nasal pack, with the benefits that this entails, thereby alleviating concerns such as pain during removal and wound healing disruption [56], or decreasing the incidence of nasal adhesions [57].

3.5.2 Blood swelling capacity

Blood swelling capacity is essential for biomaterials intended to be used in hemorrhagic wounds, and seems to be of greater importance than the water swelling profile because of the presence of blood in the site of application. For this reason, we evaluated the maximum blood absorption of the three materials (Figure 5C). Gauze showed a blood swelling capacity of 1091 ± 20% with respect to its initial weight. MRC absorbed significantly more blood than the gauze ($p < 0.05$), with a mean blood absorption of 1276 ± 40%. For its part, SP-CH showed significantly higher blood swelling capacity compared to both gauze and MRC ($p < 0.05$), absorbing up to 1442 ± 117% of blood respect to its initial weight. This increased blood swelling capacity of SP-CH is advantageous from different point of views. On the one hand, higher volumes of blood absorbed would result in a stronger tamponade effect to the injury, which is necessary to arrest bleeding. On the other hand, the more blood volume the pack absorbs the higher amount of RBCs and platelets will be concentrated within the biomaterial, promoting hemostasis and thrombus formation.

3.5.3 Hemolysis assay *in vitro*

We conducted a hemolysis assay (Figure 5D) in order to evaluate the hemocompatibility of the materials, as biomaterials in contact with blood are required to induce minimal hemolysis — destruction of RBCs in response to shear stress or changes in osmotic pressure [58] —. In this context, the gauze showed a hemolysis rate of 3.27 ± 0.62%, while MRC showed significantly decreased hemolysis rate in comparison with both gauze and SP-CH ($p < 0.05$), exactly 2.1 ± 0.7%. SP-CH caused a hemolysis rate of 3.5 ± 0.8%, which supposes no significant difference in hemocompatibility with gauze ($p > 0.05$). Since 5% of hemolysis is the maximum permitted for biomaterials [59], the three tested biomaterials were proved to be non-hemolytic, and the hemocompatibility of SP-CH could be confirmed.

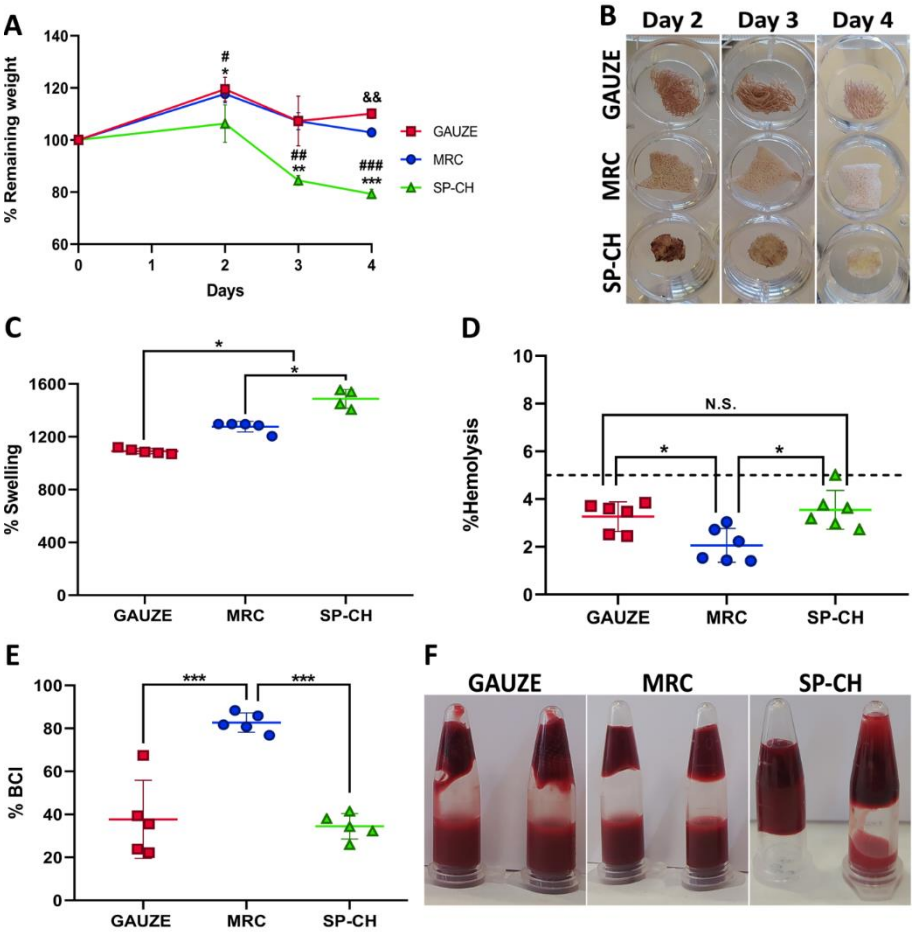

Figure 5. Blood performance. (A) Degradation in blood. Error bars, mean ± SD. &&p < 0.01 gauze vs MRC. #p < 0.05; ##p < 0.01; ###p < 0.001 MRC vs SP-CH groups. *p < 0.05; **p < 0.01; ***p < 0.001 gauze vs SP-CH. (B) Images of the plates corresponding to blood degradation after 2, 3, 4 and 7 days. (C) Maximum blood swelling capacity. Error bars, mean ± SD. *p < 0.05 between groups. (D) Hemolysis assay. The line marks 5% hemolysis. Error bars, mean ± SD. N.S., non-significant (p > 0.05). *p < 0.05 between groups. E) Blood Clotting Index of the materials. Error bars, mean ± SD. *** p<0.001 between groups. (F) Image of the tube inversion method for visually assessing blood coagulation.

3.5.4 Blood clotting *in vitro*

The ability to induce the clotting of blood is of huge importance for biomaterials intended to treat bleeding wounds such as nasal hemorrhages, and thus we assessed blood clotting in vitro for the three materials. For this, we calculated the BCI of the materials (Figure 5E), with a lower BCI indicating a faster blood-clotting rate [60]. MRC showed the highest BCI, and thus the slowest blood-clotting rate, with an index of 82.7 ± 4.5%. The gauze and SP-CH showed significantly lower ($p < 0.001$) BCI compared to MRC, 37.7 ± 18.2% and 34.4 ± 5.9% respectively. With the aim of visually assessing the in vitro blood clotting capacity of the samples, we performed the tube inversion method (Figure 5F). This assay reinforced the results obtained in Figure 5E, confirming the excellent blood clotting capacity of SP-CH, as the blood added to the tubes remained in the upper part forming a strong clot because of the interaction with the SP-CH sponge. For their part, the gauze and MRC were not able to form clots that maintained all the blood in the upper part of the tube, with the majority of the added blood falling to the bottom of the Eppendorf, and thus confirming their decreased hemostatic effect compared to that of SP-CH.

3.6 Red blood cell adhesion *in vitro*

Adhesion of RBCs to the surface of the biomaterial is of great importance to promote hemostasis by the formation of an stable and strong blood plug [61]. The measurement of hemoglobin outside the materials (Figure 6A) represents the amount of RBCs that could not adhere to the material, and thus, a lower hemoglobin concentration outside the material indicates a higher adhesion of RBCs. In this vein, both gauze and MRC showed no significant difference ($p > 0.05$) compared to a control with no RBC adhesion, showing hemoglobin concentrations of 15535 ± 1977 mg/dL and 15882 ± 2231 mg/dL, respectively, while in the control group we measured a hemoglobin concentration of 16245 ± 2365 mg/dL. SP-CH showed significantly decreased ($p < 0.001$) hemoglobin concentration compared to the other groups, concretely 10346 ± 1905 mg/dL, indicating higher RBC adhesion to the surface of the biomaterial. Figure 6B shows the appearance of the materials throughout the experiment, and a higher hemoglobin concentration — and consequently a higher adhesion of RBCs to SP-CH — can be visually confirmed.

In addition to this, we assessed the hemoglobin concentration within the materials (Figure 6C), which can be used as an indicator of the amount of RBCs adhered to the surface of the biomaterials, and thus, in this assay, a higher hemoglobin concentration indicates an increased level of RBC adhesion. Results of this experiment confirmed the outstanding RBC adhesion to SP-CH compared to gauze and MRC. While our biomaterial presented a hemoglobin concentration of 6661 ± 571 mg/dL, these concentrations were 1801 ± 133 mg/dL and 2004 ± 451 mg/dL in the case of the gauze and MRC, respectively. Again, the hemoglobin concentrations — and consequently the RBC adhesion presented graphically — can be visually confirmed in the images of the biomaterials during the experiment (Figure 6D). The SP-CH sample looked darker due to a higher RBC adhesion, and the finally collected and quantified liquid presented a redder color because of an elevated hemoglobin concentration.

Lastly, we evaluated the RBC adhesion through SEM micrographs (Figure 6E) of samples of each biomaterial, which had been previously incubated with blood. Even if MRC shows an acceptable amount of RBCs adhered, the surface of SP-CH shows increased concentration of RBCs, forming big aggregates of cells which are adhered both to each other and to the surface of our biomaterial. Conversely, RBC adhesion to gauze is minimal compared to the other materials. In the SP-CH micrographs some morphologically different RBCs can be observed. These abnormal shaped red blood cells are called echinocytes, and the process through which erythrocytes become echinocytes is named echinocytosis. The reasons for echinocytosis to occur are abundant [62,63], including variations of the electrolyte concentrations, a basic pH, intracellular calcium increase, ATP depletion, or the presence of substances such as lysophosphatidic acid (LPA). These stimuli lead to the exposure of phosphatidylserine (PS) on the outer membrane leaflet of red blood cells [64,65], which is related to the blebbing of the plasma membrane that results in echinocytes formation [66]. Even if the implications of echinocytosis and externalization of PS are not clear yet, these events has been described as a signal for RBC apoptosis [64]. Even though, there are also reasons to believe that the presence of echinocytes can support clot formation, since their formation leads to the formation and release of microvesicles [67,68]. These RBC-derived microvesicles have been said to have a pro-coagulant activity and to promote

thrombin generation [69–71], while hindering anticoagulation processes [70]. This might be due to the exposed PS providing a site for assembly to the prothrombinase and to the tenase enzymes [71], although the real function and mechanisms involving echinocytes are not fully understood yet.

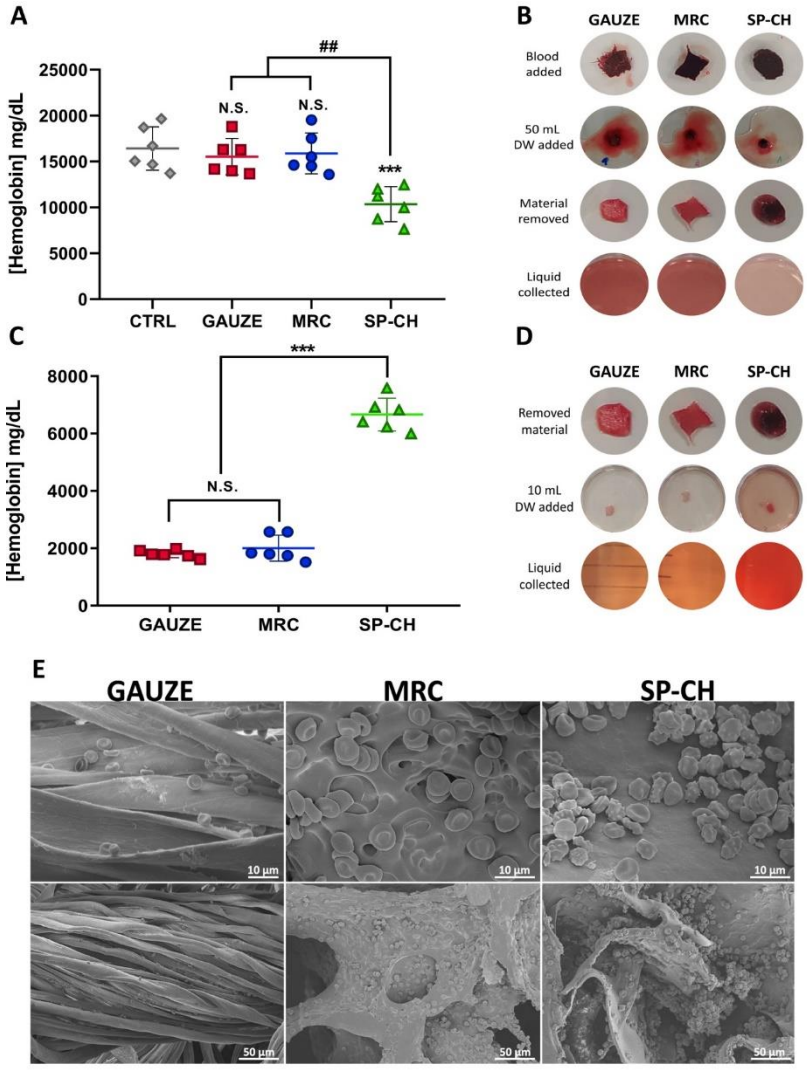

Figure 6. RBC adhesion. (A) Hemoglobin outside the materials. Error bars, mean ± SD. N.S., non-significant ($p > 0.05$). ***$p < 0.001$ vs control group; ##$p < 0.01$ SP-CH vs the other groups. (B) Photographs of the appearance of the materials at different stages of the determination of

hemoglobin outside the materials. (C) Hemoglobin within the materials. Error bars, mean ± SD. N.S., non-significant ($p > 0.05$). ***$p < 0.001$ SP-CH vs the other groups. (D) Photographs of the appearance of the materials at different stages of the determination of hemoglobin within the materials. (E) SEM micrographs of RBCs adhered to the surface of the materials.

These results elucidate the hypothetical hemostatic mechanism of SP-CH, as it has a great capacity to absorb blood and bind the RBCs, concentrating them at its surface. In this sense, the role of RBCs in hemostasis is gaining interest, and recent studies indicate that RBCs migrate to the bleeding site and push platelets toward the endothelium — in a process called margination — in a hematocrit- and shear-dependent manner. They also increase blood viscosity, and thus resistance to blood flow [72], which in turn would further promote RBC aggregation, leading to a vicious cycle that would provoke reduced tissue perfusion [73]. In addition, RBCs can activate platelets and promote their aggregation [74].

3.7 Platelet adhesion *in vitro*

Undoubtedly, platelets are fundamental in the initial stages of hemostasis, being their activation required for the activation of several coagulation factors [75]. When a vessel wall is injured, platelets interact with vascular cells, ECM components and the coagulation system [76]. At this point, platelet adhesion to the damaged endothelium increases, which unleashes a signaling cascade — through tyrosine kinases and G-protein coupled receptors — that will provoke additional recruitment and activation of more platelets. This finally leads to the presentation of a pro-coagulant surface that promotes the creation of a fibrin-rich hemostatic plug at the bleeding site [77]. There, platelets show an activation gradient, from a dense core region of the hemostatic plug where the platelets are highly activated and expose P-selectin, to an outer loosely packed region with decreased platelet activation and absent P-selectin exposure [76]. During platelet recruitment to the injury site, platelets become activated through diverse receptor-specific signaling pathways. Once activated, platelets start to secrete granules — such as δ-granules, which contain ADP, serotonin, polyphosphates, glutamate, histamine and calcium — and undergo shape change, being both vital for the hemostatic process [78].

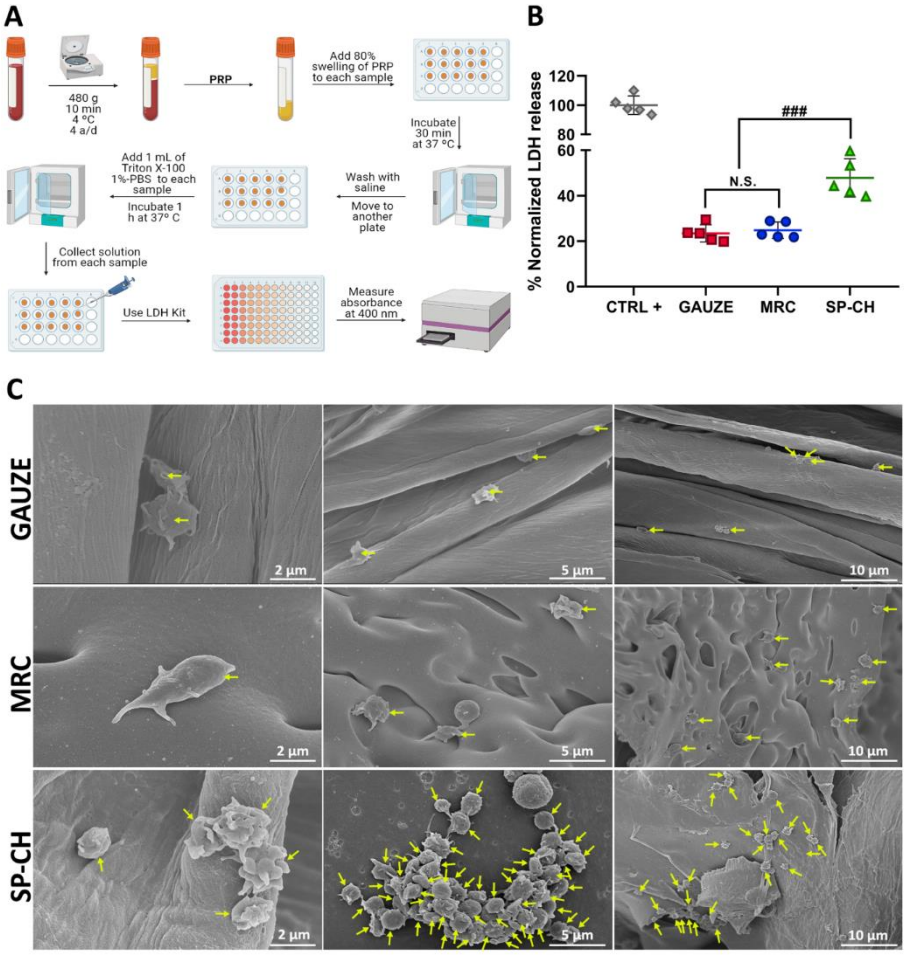

Figure 7. Platelet adhesion. (A) Scheme of the procedure carried out for the determination of platelet adhesion to the materials. (B) Normalized LDH release (%) of the materials. Error bars, mean ± SD. N.S., non-significant ($p > 0.05$). ###$p < 0.001$ SP-CH vs the other groups. n=5 independent samples per group. (C) SEM micrographs of platelets adhered to the surface of the materials. Platelets attached to the materials are marked with yellow arrows.

For this reason, any biomaterial intended to be used with hemostatic purposes should show a good platelet adhesion capacity to its surface to concentrate platelets in the wound site and promote hemostasis. We evaluated the platelet adhesion of the three materials using an indirect method (Figure 7B) that measures the amount of LDH released from a sample, which is directly proportional to the

amount of platelets within it. Both gauze and MRC showed decreased platelet adhesion (Figure 7A), with a LDH release of just a 23.46 ± 3.75% and 24.86 ± 3.61%, respectively, of the one measured for a positive control in which all the added platelets were lysed. For its part, SP-CH presented a LDH release of a 47.8 ± 8.4% of that measured for the positive control, which means a significantly higher ($p < 0.001$) platelet adhesion compared to both the gauze and MRC. SEM micrographs of the materials cultured with PRP (Figure 7C) confirmed the quantitative results obtained in the in vitro platelet adhesion assay, showing that platelet adhesion to gauze and MRC is minimal, while SP-CH shows bigger amounts of platelets adhered to its surface, forming aggregates of platelets, with even some of them activated.

When platelets are forming activated aggregates, they generate a phosphatidylserine-exposing membrane surface, which is essential for the formation of thrombin [76]. In turn, thrombin activates platelets — through hydrolyzation of G-protein- coupled protease-activated receptors (PAR) 1 and 4 [79] — and promotes clot stabilization by converting of fibrinogen to fibrin [80].

We hypothesize that this platelet-thrombin interaction, that boosts the formation of the hemostatic plug, can be influenced somehow by the SP-CH. This is because SPI is a source of phylloquinone — vitamin K1 — [81], which certainly is involved in blood coagulation. Vitamin K serves as a cofactor for the endoplasmic enzyme g-glutamate carboxylase (GGCX), which plays a vital role in the carboxylation of certain protein-bound glutamate residues into g-carboxyglutamate (Gla) [82]. Seven blood coagulation factors — including prothrombin, fVII, fIX, and fX [83] — require this K vitamin-dependent glutamate residue carboxylation in order to bind Ca+2. Therefore, this carboxylation is essential for the formation of ion bridges between the blood-clotting enzymes and phospholipids on platelets' membranes [84], promoting the activation of these coagulation factors.

In addition, it has also been mentioned that the SPI present in the SP-CH has RGD-motif containing peptides [19], which could explain its ability to bind platelets. This is because the RGD sequence is also present in the α-chains of fibrinogen [85], and it is one of the two motifs that bind to the αIIbβ3 integrin receptor of platelets to boost their aggregation [86]. The interaction of these RGD sequences

with platelet integrin αIIbβ3 has been recently described using optical trap-based methods, and the importance of this motif in the hemostatic process has been highlighted [87]. In fact, RGD sequences are recently being used to target platelets with different objectives [88]. Thus, we hypothesize that the increased platelet adhesion capacity of our SP-CH is due to the interaction between the RGD-motifs of the SPI and the αIIbβ3 integrin receptor of the platelets.

3.8 *In vivo* hemostatic efficacy

A rat-tail amputation model (**Figure 8A**) was used to evaluate the in vivo hemostatic properties of the three materials. Photographs of the appearance of the materials (**Figure 8B**) were taken during the experiment. The gauze obtained a mean bleeding time score of 2.8 ± 0.8 (**Figure 8C**), which was similar to MRC's, 2.5 ± 1.0. Meanwhile, SP-CH obtained a significantly lower ($p > 0.05$) bleeding time score, 1.8 ± 0.4, meaning that it could promote hemostasis in vivo faster than both gauze and MRC. Regarding to blood loss (**Figure 8D**), no significant differences were found between groups. The gauze presented a mean blood loss of 1.1 ± 1.0 g, MRC 1.2 ± 0.8 g and SP-CH 0.6 ± 0.3 g. However, it is noteworthy that both gauze and MRC showed an increased deviation among replicates, while blood loss in the SP-CH group remained consistent in all the tested samples, guaranteeing a homogeneous hemostatic efficacy.

We consider that a lack of an epistaxis animal model supposes a limitation in our study. Another in vivo model that reproduces the physiopathology of epistaxis in a more faithful way will be considered for further research. Even though, for the initial evaluation of the general hemostatic properties of our SP-CH, we aimed to choose a model with an adequate relationship between relevance and reduced invasiveness. In this vein, the rat-tail amputation model has been the animal model of choice for many important studies involving the evaluation of hemostatic properties of biomaterials [89–92], and hence it seems to be an appropriate model for this objective. Furthermore, a bigger sample size would probably provide more robust results and reduce biases, making it easier to find significant differences between groups. Nevertheless, the bleeding time results support those obtained

in the in vitro experiments, where SP-CH showed superior hemostatic properties compared to the gauze and MRC.

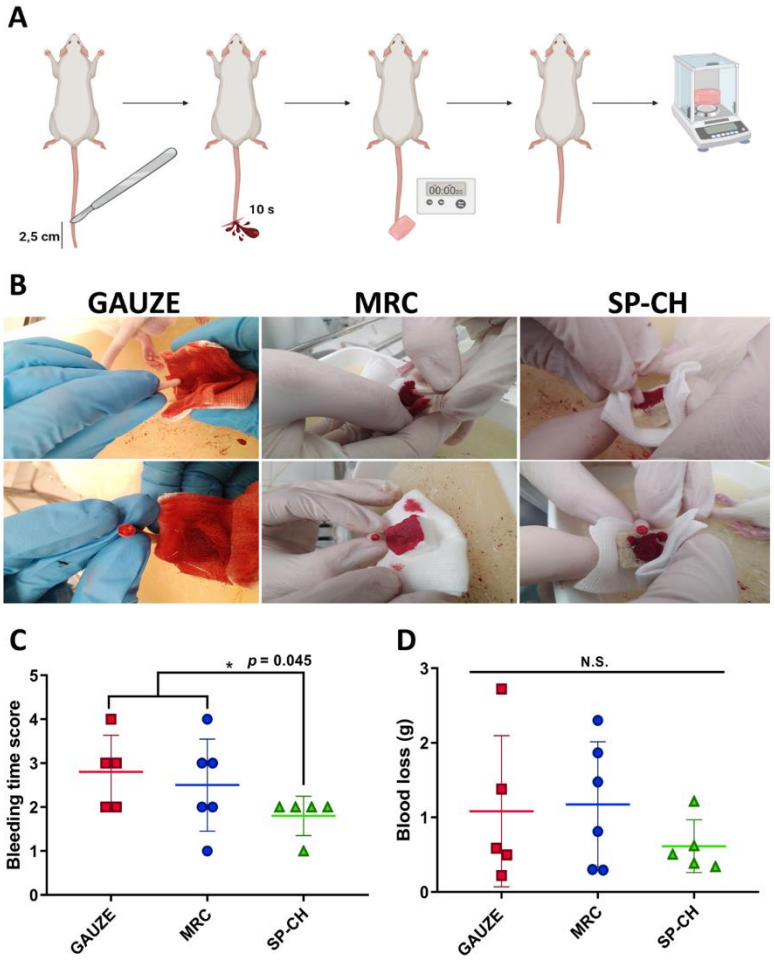

Figure 8. *In vivo* hemostatic efficacy. (A) Scheme of the procedure carried out for the rat-tail amputation model. (B) Photographs of the three materials during the experiment. (C) Bleeding time score of the three materials. Error bars, mean ± SD. *$p < 0.05$ SP-CH vs the other groups. (D) Blood loss (g). Error bars, mean ± SD. N.S., non-significant ($p > 0.05$).

4. Materials and methods

In this study we demonstrated that by-products of the food industry are a valuable and sustainable source of biomaterials that can be employed to

manufacture safe and effective nasal packs with great hemostatic properties. The developed SP-CH presents a greatly interconnected porous microstructure, great water and blood swelling capacity and appropriate retention of the absorbed fluids. Besides, mechanical properties of the biomaterial demonstrated to be adequate for its use as a nasal pack. The biomaterial presented excellent biocompatibility and hemocompatibility in vitro. Interestingly, it was able to degrade partially within a few days, when incubated either in water or in blood, which is becoming more and more important characteristic for nasal packs. Moreover, the hemostatic properties of our SP-CH outperformed those of the two nasal packs used in the clinical routine worldwide: a standard gauze and the commercial synthetic pack Merocel®. Our biomaterial was found to effectively promote blood coagulation in vitro, showing outstanding RBC and platelet binding properties compared to the gauze and MRC, likely due to the intrinsic hemostatic properties of its natural components. Although further research of its hemostatic effect in vivo is needed, SP-CH significantly shortened bleeding time in a rat-tail amputation model. Additionally, the study of the environmental loads associated with the extraction of materials and the manufacturing of scaffolds showed low environmental impacts in all the categories analyzed. All in all, our SP-CH, produced from a renewable and sustainable source of biomaterials (by-products of the food industry) , showed superior mechanical and hemostatic properties compared to MRC and a standard gauze. This way, we have demonstrated that a green and ecofriendly strategy can be followed to develop a biomaterial that outperforms the gold standard in the treatment of epistaxis. This leads us to believe that our SP-CH arises as a potential candidate to be an appropriate nasal pack for the treatment of epistaxis.

5. Acknowledgments

Authors thank Eusko Jaurlaritza (Grupos Consolidados, No ref: IT907-16) and MCI/AEI/FEDER, UE (RTI2018-097100-B-C22).

6. Bibliography

[1] R. Beck, M. Sorge, A. Schneider, A. Dietz, Current Approaches to Epistaxis Treatment in Primary and Secondary Care, Dtsch. Arztebl. Int. 112 (2018) 12–22. https://doi.org/10.3238/arztebl.2018.0012.

[2] D. Passali, V. Damiani, F.M. Passali, M.A. Tosca, G. Motta, G. Ciprandi, E.S. Group, An International Survey on the pragmatic management of epistaxis, Acta Bio-Medica Atenei Parm. 91 (2020) 5–10. https://doi.org/10.23750/abm.v91i1-S.9241.

[3] W.M. Alshehri, M. Wafaa, M.W. Ahmed, A. Albathi, B. Alqahtani, Merocel Surgicel Wrap Technique to Manage Diffuse Epistaxis in Patients with Comorbidities, Int. J. Otolaryngol. 2020 (2020). https://doi.org/https://doi.org/10.1155/2020/8272914.

[4] Y. Abbas, M. Abdelkader, M. Adams, A. Addison, R. Advani, H. , ... Zhang, Nasal Packs for Epistaxis : Predictors of Success, Clin. Otolaryngol. 45 (2020) 659–666. https://doi.org/10.1111/coa.13555.

[5] M. Bresnihan, B. Mehigan, A. Curran, An evaluation of Merocel and Series 5000 nasal packs in patients following nasal surgery : a prospective randomised trial, Clin. Otolaryngol. 32 (2007) 352–355.

[6] M. Curran, L. de Baan, A. De Schryver, R. Van Zelm, S. Hellweg, T. Koellner, G. Sonnemann, M. Huijbregts, Toward meaningful end points of biodiversity, Environ. Sci. Technol. 45 (2011) 70–79.

[7] E. Benetto, C. Jury, G. Kneip, I. Vázquez-Rowe, V. Huck, F. Minette, Life cycle assessment of heat production from grape marc pellets, J. Clean. Prod. 87 (2015) 149–158. https://doi.org/10.1016/j.jclepro.2014.10.028.

[8] Z. Günkaya, M. Banar, An environmental comparison of biocomposite film based on orange peel-derived pectin jelly-corn starch and LDPE film: LCA and biodegradability, Int. J. Life Cycle Assess. 21 (2016) 465–475. https://doi.org/10.1007/s11367-016-1042-8.

[9] I. Leceta, P. Guerrero, S. Cabezudo, K. De La Caba, Environmental assessment of chitosan-based films, J. Clean. Prod. 41 (2013) 312–318. https://doi.org/10.1016/j.jclepro.2012.09.049.

[10] I. Muñoz, C. Rodríguez, D. Gillet, B. M. Moerschbacher, Life cycle assessment of chitosan production in India and Europe, Int. J. Life Cycle Assess. 23 (2018) 1151–1160. https://doi.org/10.1007/s11367-017-1290-2.

[11] R. Valentine, P.J. Wormald, R. Sindwani, Advances in Absorbable Biomaterials and Nasal Packing, Otolaryngol. Clin. North Am. 42 (2009) 813–828. https://doi.org/10.1016/j.otc.2009.07.009.

[12] P. Agrawal, S. Soni, G. Mittal, A. Bhatnagar, Role of polymeric biomaterials as wound healing agents, Int. J. Low. Extrem. Wounds. 13 (2014) 180–190. https://doi.org/10.1177/1534734614544523.

[13] K. Las Heras, E. Santos-Vizcaino, T. Garrido, F.B. Gutierrez, J.J. Aguirre, K. de la Caba, ..., R.M. Hernandez, Soy protein and chitin sponge-like scaffolds: from natural by-products to cell delivery systems for biomedical applications, Green Chem. 22 (2020) 3445–3460. https://doi.org/10.1039/d0gc00089b.

[14] X. Yang, W. Liu, G. Xi, M. Wang, B. Liang, Y. Shi, Y. Feng, X. Ren, C. Shi, Fabricating antimicrobial peptide-immobilized starch sponges for hemorrhage control and antibacterial treatment, Carbohydr. Polym. 222 (2019) 115012. https://doi.org/10.1016/j.carbpol.2019.115012.

[15] H. Cheng, D. Xiao, Y. Tang, B. Wang, X. Feng, M. Lu, G.J. Vancso, X. Sui, Sponges with Janus Character from Nanocellulose : Preparation and Applications in the Treatment of Hemorrhagic Wounds, Adv. Healthc. Mater. 9 (2020) 1901796. https://doi.org/10.1002/adhm.201901796.

[16] C. Liu, X. Liu, C. Liu, N. Wang, H. Chen, W. Yao, G. Sun, Q. Song, W. Qiao, A highly efficient, in situ wet-adhesive dextran derivative sponge for rapid hemostasis, Biomaterials. 205 (2019) 23–37. https://doi.org/10.1016/j.biomaterials.2019.03.016.

[17] R. Hajosch, M. Suckfuell, S. Oesser, M. Ahlers, K. Flechsenhar, A novel gelatin sponge for accelerated hemostasis, J. Biomed. Mater. Res. Part B Appl. Biomater. 94 (2010) 372–379. https://doi.org/10.1002/jbm.b.31663.

[18] Z. Lin, X. Zhang, R. Zeng, Preparation and properties of polyvinyl acetal sponge modified by chitosan, Front. Chem. China. 3 (2008) 172–177. https://doi.org/10.1007/s11458-008-0033-0.

[19] C. Chatterjee, S. Gleddie, C.W. Xiao, Soybean bioactive peptides and their functional properties, Nutrients. 10 (2018). https://doi.org/10.3390/nu10091211.

[20] M. Rinaudo, Chitin and chitosan : Properties and applications, Prog. Polym. Sci. 31 (2006) 603–632. https://doi.org/10.1016/j.progpolymsci.2006.06.001.

[21] A. Anitha, S. Sowmya, P.T.S. Kumar, S. Deepthi, K.P. Chennazhi, H. Ehrlich, M. Tsurkan, R. Jayakumar, Chitin and chitosan in selected biomedical applications, Prog. Polym. Sci. 39 (2014) 1644–1667. https://doi.org/10.1016/j.progpolymsci.2014.02.008.

[22] R. Jayakumar, K.P. Chennazhi, S. Srinivasan, S. V. Nair, T. Furuike, H. Tamura, Chitin scaffolds in tissue engineering, Int. J. Mol. Sci. 12 (2011) 1876–1887. https://doi.org/10.3390/ijms12031876.

[23] S.C. Bagheri, B. Bell, H.A. Khan, Current Therapy In Oral and Maxillofacial Surgery, Elsevier Health Sciences., 2011.

[24] T.L. Viehweg, J.B. Roberson, J.W. Hudson, Epistaxis : Diagnosis and Treatment, J. Oral Maxillofac. Surg. 64 (2006) 511–518. https://doi.org/10.1016/j.joms.2005.11.031.

[25] T. de Aramburu Mera, M. Labella Álvarez, Á. Castellano, M. del Robledo, Alergia, in: Man. CLÍNICO URGENCIAS Del Hosp. Univ. Virgen Del Rocío., 2020: pp. 1–13.

[26] G.D.E. Traslados, I. Grupo, P.D.E. Urgencias, P.D.E. Salud, Protocolos de derivación interhospitalaria urgente de pacientes en la provincia de almería, 2012.

[27] G. Yang, Z. Xiao, H. Long, K. Ma, J. Zhang, X. Ren, J. Zhang, Assessment of the characteristics and biocompatibility of gelatin sponge scaffolds prepared by various crosslinking methods, Sci. Rep. 8 (2018) 1–13. https://doi.org/10.1038/s41598-018-20006-y.

[28] H.K. No, N. Young Park, S. Ho Lee, S.P. Meyers, Antibacterial activity of chitosans and chitosan oligomers with different molecular weights, Int. J. Food Microbiol. 74 (2002) 65–72. https://doi.org/10.1016/S0168-1605(01)00717-6.

[29] E.S. Abdou, K.S.A. Nagy, M.Z. Elsabee, Extraction and characterization of chitin and chitosan from local sources, Bioresour. Technol. 99 (2008) 1359–1367. https://doi.org/10.1016/j.biortech.2007.01.051.

[30] T. Garrido, A. Etxabide, K. De La Caba, P. Guerrero, Versatile soy protein films and hydrogels by the incorporation of β-chitin from squid pens (Loligo sp.), Green Chem. 19 (2017) 5923–5931. https://doi.org/10.1039/c7gc02982a.

[31] C. Zheng, Q. Zeng, S. Pimpi, W. Wu, K. Han, K. Dong, T. Lu, Research status and development potential of composite hemostatic materials, J. Mater. Chem. B. 8 (2020) 5395–5410. https://doi.org/10.1039/d0tb00906g.

[32] C.M. Murphy, F.J. O'Brien, Understanding the effect of mean pore size on cell activity in collagen-glycosaminoglycan scaffolds, Cell Adhes. Migr. 4 (2010) 377–381. https://doi.org/10.4161/cam.4.3.11747.

[33] N. Annabi, J.W. Nichol, X. Zhong, C. Ji, S. Koshy, A. Khademhosseini, F. Dehghani, Controlling the porosity and microarchitecture of hydrogels for tissue engineering, Tissue Eng. - Part B Rev. 16 (2010) 371–383. https://doi.org/10.1089/ten.teb.2009.0639.

[34] Z.M. Huang, Y.Z. Zhang, M. Kotaki, S. Ramakrishna, A review on polymer nanofibers by electrospinning and their applications in nanocomposites, Compos. Sci. Technol. 63 (2003) 2223–2253. https://doi.org/10.1016/S0266-3538(03)00178-7.

[35] F.J. O'Brien, B.A. Harley, I. V. Yannas, L.J. Gibson, The effect of pore size on cell adhesion in collagen-GAG scaffolds, Biomaterials. 26 (2005) 433–441. https://doi.org/10.1016/j.biomaterials.2004.02.052.

[36] F. Javier García Callejo, N. Muñoz Fernández, M. Teresa Achiques Martínez, S.F. Moya-Angeler, M.J. Montoro Elena, J. Marco Algarra, Nasal packing in posterior epistaxis. Comparison of two methods, Acta Otorrinolaringol. (English Ed. 61 (2010) 196–201. https://doi.org/10.1016/s2173-5735(10)70034-x.

[37] D.E. Tunkel, S. Anne, S.C. Payne, S.L. Ishman, R.M. Rosenfeld, P.J. Abramson, J.D. Alikhaani, M.M. Benoit, R.S. Bercovitz, M.D. Brown, B. Chernobilsky, D.A. Feldstein, J.M. Hackell, E.H. Holbrook, S.M. Holdsworth, K.W. Lin, M.M. Lind, D.M. Poetker, C.A. Riley, J.S. Schneider, Clinical Practice Guideline : Nosebleed (Epistaxis), Otolaryngol. Neck Surg. 162 (2020) S1–S38. https://doi.org/10.1177/0194599819890327.

[38] M. Berlucchi, P. Castelnuovo, A. Vincenzi, B. Morra, E. Pasquini, Endoscopic outcomes of resorbable nasal packing after functional endoscopic sinus surgery: A multicenter prospective randomized controlled study, Eur. Arch. Oto-Rhino-Laryngology. 266 (2009) 839–845. https://doi.org/10.1007/s00405-008-0841-3.

[39] P.J. Wormald, R.N. Boustred, T. Le, L. Hawke, R. Sacks, A prospective single-blind randomized controlled study of use of hyaluronic acid nasal packs in patients after endoscopic sinus surgery, Am. J. Rhinol. 20 (2006) 7–10. https://doi.org/10.1177/194589240602000102.

[40] X. Song, C. Zhu, D. Fan, Y. Mi, X. Li, R.Z. Fu, Z. Duan, Y. Wang, R.R. Feng, A novel human-like collagen hydrogel scaffold with porous structure and sponge-like properties, Polymers (Basel). 9 (2017) 1–16. https://doi.org/10.3390/polym9120638.

[41] O. Chaudhuri, J. Cooper-White, P.A. Janmey, D.J. Mooney, V.B. Shenoy, Effects of extracellular matrix viscoelasticity on cellular behaviour, Nature. 584 (2020) 535–546. https://doi.org/10.1038/s41586-020-2612-2.

[42] Z. Wang, M.J. Golob, N.C. Chesler, Viscoelastic Properties of Cardiovascular Tissues, Viscoelastic Viscoplastic Mater. 2 (2016) 64. https://doi.org/10.5772/64169.

[43] D. Yang, J. Hu, X. Ding, Analysis of energy dissipation characteristics in granite under high confining pressure cyclic load, Alexandria Eng. J. 59 (2020) 3587–3597. https://doi.org/10.1016/j.aej.2020.06.004.

[44] M. Jürgens, J. Olbricht, B. Fedelich, B. Skrotzki, Low cycle fatigue and relaxation performance of ferritic–martensitic grade P92 steel, Metals (Basel). 9 (2019) 99. https://doi.org/10.3390/met9010099.

[45] L. Zhu, J. Qiu, E. Sakai, A high modulus hydrogel obtained from hydrogen bond reconstruction and its application in vibration damper, RSC Adv. 7 (2017) 43755–43763. https://doi.org/10.1039/c7ra08272j.

[46] L. Wang, P.H.P. D'Alpino, L.G. Lopes, J.C. Pereira, Mechanical properties of dental restorative materials: relative contribution of laboratory tests, J. Appl. Oral Sci. 11 (2003) 162–167. https://doi.org/10.1590/s1678-77572003000300002.

[47] M. Capurro, F. Barberis, Evaluating the mechanical properties of biomaterials, in: Biomater. Bone Regen. Nov. Tech. Appl., Woodhead Publishing, 2014: pp. 270–323. https://doi.org/10.1533/9780857098104.2.270.

[48] Z. Yousaf, M. Smith, P. Potluri, W. Parnell, Compression properties of polymeric syntactic foam composites under cyclic loading, Compos. Part B Eng. 186 (2020) 107764. https://doi.org/10.1016/j.compositesb.2020.107764.

[49] G. Pilz, P. Guttmann, F. Oesterreicher, G. Pinter, Experimental method for creep characterization of polymeric foam materials in media immersion, Mech. Time-Dependent Mater. 24 (2020) 421–433. https://doi.org/10.1007/s11043-020-09457-x.

[50] M.F. Ahsby, H. Shercliff, D. Cebon, Shake, rattle and roll: cyclic loading, damage and failure, in: H. Shercliff (Ed.), Mater. Eng. Sci. Process. Des., 1st ed., Butterworth-Heinemann, 2007: pp. 186–187.

[51] F. Orban, Damping of materials and members in structures, in: J. Phys. Conf. Ser., IOP Publishing, 2011: p. 012022. https://doi.org/10.1088/1742-6596/268/1/012022.

[52] M. Qwamizadeh, P. Liu, Z. Zhang, K. Zhou, Y.W. Zhang, Hierarchical Structure Enhances and Tunes the Damping Behavior of Load-Bearing Biological Materials, J. Appl. Mech. 83 (2016) 051009. https://doi.org/10.1115/1.4032861.

[53] P. Zhang, M.A. Heyne, A.C. To, Biomimetic staggered composites with highly enhanced energy dissipation: Modeling, 3D printing, and testing, J. Mech. Phys. Solids. 83 (2015) 285–300. https://doi.org/10.1016/j.jmps.2015.06.015.

[54] T.L. Landsman, T. Touchet, S.M. Hasan, C. Smith, B. Russell, J. Rivera, D.J. Maitland, E. Cosgriff-Hernandez, A shape memory foam composite with enhanced fluid uptake and bactericidal properties as a hemostatic agent, Acta Biomater. 47 (2017) 91–99. https://doi.org/10.1016/j.actbio.2016.10.008.

[55] L. Novotny, M. Crha, P. Rauser, A. Hep, J. Misik, A. Necas, D. Vondrys, Novel biodegradable polydioxanone stents in a rabbit airway model, J. Thorac. Cardiovasc. Surg. 143 (2012) 437–444. https://doi.org/10.1016/j.jtcvs.2011.08.002.

[56] J.H. Franklin, E.D. Wright, Randomized, controlled, study of absorbable nasal packing on outcomes of surgical treatment of rhinosinusitis with polyposis, Am. J. Rhinol. 21 (2007) 214–217. https://doi.org/10.2500/ajr.2007.21.3011.

[57] J. Selvarajah, M.F. Mh Busra, A. Bin Saim, R. Bt Hj Idrus, Y. Lokanathan, Development and physicochemical analysis of genipin-crosslinked gelatine sponge as a potential resorbable nasal pack, J. Biomater. Sci. Polym. Ed. 31 (2020) 1722–1740. https://doi.org/10.1080/09205063.2020.1774841.

[58] M. Weber, H. Steinle, S. Golombek, L. Hann, C. Schlensak, H.P. Wendel, M. Avci-Adali, Blood-Contacting Biomaterials: In Vitro Evaluation of the Hemocompatibility, Front. Bioeng. Biotechnol. 6 (2018) 99. https://doi.org/10.3389/fbioe.2018.00099.

[59] J. Zhu, H. Han, F. Li, X. Wang, J. Yu, X. Qin, D. Wu, Peptide-Functionalized Amino Acid-Derived Pseudoprotein-Based Hydrogel with Hemorrhage Control and Antibacterial Activity for Wound Healing, Chem. Mater. 31 (2019) 4436–4450. https://doi.org/10.1021/acs.chemmater.9b00850.

[60] X. Chen, C. Cui, Y. Liu, C. Fan, M. Xiao, D. Zhang, Z. Xu, Y. Li, J. Yang, W. Liu, A robust poly(: N-Acryloyl-2-glycine)-based sponge for rapid hemostasis, Biomater. Sci. 8 (2020) 3760–3771. https://doi.org/10.1039/d0bm00770f.

[61] S.S. Biranje, P. V. Madiwale, K.C. Patankar, R. Chhabra, P. Bangde, P. Dandekar, R. V. Adivarekar, Cytotoxicity and hemostatic activity of chitosan/carrageenan composite wound healing dressing for traumatic hemorrhage, Carbohydr. Polym. 239 (2020) 116106. https://doi.org/10.1016/j.carbpol.2020.116106.

[62] P. Wong, A basis of echinocytosis and stomatocytosis in the disc–sphere transformations of the erythrocyte, J. Theor. Biol. 196 (1999) 343–361. https://doi.org/https://doi.org/10.1006/jtbi.1998.0845.

[63] K.D. Tachev, K.D. Danov, P.A. Kralchevsky, On the mechanism of stomatocyte–echinocyte transformations of red blood cells: experiment and theoretical model, Colloids Surfaces B Biointerfaces. 34 (2004) 123–140. https://doi.org/10.1016/j.colsurfb.2003.12.011.

[64] M.C. Wesseling, L. Wagner-Britz, H. Huppert, B. Hanf, L. Hertz, D.B. Nguyen, I. Bernhardt, Phosphatidylserine exposure in human red blood cells depending on cell age, Cell. Physiol. Biochem. 38 (2016) 1376–1390. https://doi.org/10.1159/000443081.

[65] J. Shin, K. Lim, J. Noh, O. Bae, S. Chung, M. Lee, J. Chung, Lead-induced procoagulant activation of erythrocytes through phosphatidylserine exposure may lead to thrombotic diseases, Chem. Res. Toxicol. 20 (2007) 38–43. https://doi.org/https://doi.org/10.1021/tx060114+.

[66] J.L.N. Wolfs, P. Comfurius, E.M. Bevers, R.F.A. Zwaal, Influence of erythrocyte shape on the rate of Ca2+-induced scrambling of phosphatidylserine, Mol. Membr. Biol. 20 (2003) 83–91. https://doi.org/https://doi.org/10.1080/0968768031000064444.

[67] Y.A. Sheremet, A.N. Popovicheva, G.Y. Levin, Lysophosphatidic acid and human erythrocyte aggregation, Cell Tissue Biol. 8 (2014) 237–243. https://doi.org/10.1134/S1990519X14030110.

[68] D.B. Nguyen, T.B.T. Ly, M.C. Wesseling, M. Hittinger, A. Torge, A. Devitt, Y. Perrie, I. Bernhardt, Characterization of microvesicles released from human red blood cells, Cell. Physiol. Biochem. 38 (2016) 1085–1099. https://doi.org/10.1159/000443059.

[69] J. Tissot, G. Canellini, O. Rubin, A. Angelillo-scherrer, J. Delobel, M. Prudent, N. Lion, Blood microvesicles: from proteomics to physiology, Transl. Proteomics. 1 (2013) 38–52. https://doi.org/10.1016/j.trprot.2013.04.004.

[70] J.K.F. Leal, M.J.W. Adjobo-hermans, G.J.C.G.M. Bosman, Red blood cell homeostasis: mechanisms and effects of microvesicle generation in health and disease, Front. Physiol. 9 (2018) 703. https://doi.org/10.3389/fphys.2018.00703.

[71] S. Chung, O. Bae, K. Lim, J. Noh, M. Lee, Y.S. Jung, C.J. H., Lysophosphatidic acid induces thrombogenic activity through phosphatidylserine exposure and procoagulant

microvesicle generation in human erythrocytes, Arterioscler. Thromb. Vasc. Biol. 27 (2007) 414–421. https://doi.org/10.1161/01.ATV.0000252898.48084.6a.

[72] J.W. Weisel, R.I. Litvinov, Red blood cells: the forgotten player in hemostasis and thrombosis, J. Thromb. Haemost. 17 (2019) 271–282. https://doi.org/10.1111/jth.14360.

[73] G. Barshtein, R. Ben-Ami, S. Yedgar, Role of red blood cell flow behavior in hemodynamics and hemostasis, Expert Rev. Cardiovasc. Ther. 5 (2007) 743–752. https://doi.org/10.1586/14779072.5.4.743.

[74] A.H. Gillespie, A. Doctor, Red Blood Cell Contribution to Hemostasis, Front. Pediatr. 9 (2021) 178. https://doi.org/10.3389/fped.2021.629824.

[75] J.W.M. Heemskerk, E.M. Bevers, T. Lindhout, Platelet activation and blood coagulation, Thromb. Haemost. 88 (2002) 186–193. https://doi.org/10.1055/s-0037-1613209.

[76] H.H. Versteeg, J.W.M. Heemskerk, M. Levi, P.H. Reitsma, New Fundamentals in hemostasis, Physiol. Rev. 93 (2013) 327–358. https://doi.org/10.1152/physrev.00016.2011.

[77] K. Broos, H.B. Feys, S.F. De Meyer, K. Vanhoorelbeke, H. Deckmyn, Platelets at work in primary hemostasis, Blood Rev. 25 (2011) 155–167. https://doi.org/10.1016/j.blre.2011.03.002.

[78] Z. Li, M.K. Delaney, K.A. O'Brien, X. Du, Signaling during platelet adhesion and activation, Arterioscler. Thromb. Vasc. Biol. 30 (2010) 2341–2349. https://doi.org/10.1161/ATVBAHA.110.207522.

[79] S. Nylander, C. Mattsson, Thrombin-induced platelet activation and its inhibition by anticoagulants with different modes of action, Blood Coagul. Fibrinolysis. 14 (2003) 159–167. https://doi.org/10.1097/00001721-200302000-00007.

[80] M. Koupenova, L. Clancy, H.A. Corkrey, J.E. Freedman, Circulating platelets as mediators of immunity, inflammation, and thrombosis, Circ. Res. 122 (2018) 337–351. https://doi.org/10.1161/CIRCRESAHA.117.310795.

[81] D.W. Stafford, The vitamin K cycle, J. Thromb. Haemost. 3 (2005) 1873–1878.

[82] C. Vermeer, Vitamin K, Ref. Modul. Biomed. Sci. (2014). https://doi.org/10.1016/B978-0-12-801238-3.00232-4.

[83] G. Ferland, The Discovery of Vitamin K and Its Clinical Applications, Ann. Nutr. Metab. 61 (2012) 213–218. https://doi.org/10.1159/000343108.

[84] D. Bartusik, D. Aebisher, B. Tomanek, The synthesis and application of vitamins in nanoemulsion delivery systems, in: Emulsions, Academic Press, 2016: pp. 519–555. https://doi.org/10.1016/B978-0-12-804306-6/00015-5.

[85] G. Soslau, R. Class, D.A. Morgan, C. Foster, S.T. Lord, P. Marchese, Z.M. Ruggeri, Unique Pathway of Thrombin-induced Platelet Aggregation Mediated by Glycoprotein Ib, J. Biol. Chem. 276 (2001) 21173–21183. https://doi.org/10.1074/jbc.M008249200.

[86] J. Sánchez-Cortés, M. Mrksich, The Platelet Integrin αIIbβ3 Binds to the RGD and AGD Motifs in Fibrinogen, Chem. Biol. 16 (2009) 990–1000. https://doi.org/10.1016/j.chembiol.2009.08.012.

[87] O. Kononova, R.I. Litvinov, D.S. Blokhin, V. V. Klochkov, J.W. Weisel, J.S. Bennett, V. Barsegov, Mechanistic Basis for the Binding of RGD- and AGDV-Peptides to the Platelet Integrin αIIbβ3, Biochemistry. 56 (2017) 1932–1942. https://doi.org/10.1021/acs.biochem.6b01113.

[88] M. Alipour, M. Baneshi, S. Hosseinkhani, R. Mahmoudi, A. Jabari Arabzadeh, M. Akrami, J. Mehrzad, H. Bardania, Recent progress in biomedical applications of RGD-based ligand: From precise cancer theranostics to biomaterial engineering: A systematic review, J. Biomed. Mater. Res. - Part A. 108 (2020) 839–850. https://doi.org/10.1002/jbm.a.36862.

[89] X. Sun, Z. Tang, M. Pan, Z. Wang, H. Yang, H. Liu, Chitosan/kaolin composite porous microspheres with high hemostatic efficacy, Carbohydr. Polym. 177 (2017) 135–143. https://doi.org/10.1016/j.carbpol.2017.08.131.

[90] C. Feng, J. Li, G.S. Wu, Y.Z. Mu, M. Kong, C.Q. Jiang, X.J. Cheng, Y. Liu, X.G. Chen, Chitosan-Coated Diatom Silica as Hemostatic Agent for Hemorrhage Control, ACS Appl. Mater. Interfaces. 8 (2016) 34234–34243. https://doi.org/10.1021/acsami.6b12317.

[91] X. Cheng, Z. Shao, C. Li, L. Yu, M.A. Raja, C. Liu, Isolation, characterization and evaluation of collagen from jellyfish Rhopilema esculentum Kishinouye for use in hemostatic applications, PLoS One. 12 (2017) e0169731. https://doi.org/10.1371/journal.pone.0169731.

[92] G. Li, K. Quan, C. Xu, B. Deng, X. Wang, Synergy in thrombin-graphene sponge for improved hemostatic efficacy and facile utilization, Colloids Surfaces B Biointerfaces. 161 (2018) 27–34. https://doi.org/10.1016/j.colsurfb.2017.10.021.

Soy protein/β-chitin sponge-like scaffolds immobilizing hair follicle and adipose tissue human mesenchymal stromal cells promote chronic and diabetic wounds healing

LAS HERAS Kevin [1,2], GARCIA-ORUE Itxaso [1,2,3], GARRIDO Tania [4,5], DE LA CABA Koro [4,5], GUERRERO Pedro [4,5,6], IGARTUA Manoli [1,2,3], SANTOS-VIZCAINO Edorta [1,2,3], HERNANDEZ Rosa Maria [1,2,3,*]

[1]NanoBioCel Group, Laboratory of Pharmaceutics, School of Pharmacy (UPV/EHU), 01006 Vitoria-Gasteiz, Spain.
[2]Bioaraba, NanoBioCel Research Group, Vitoria-Gasteiz, Spain.
[3]Biomedical Research Networking Centre in Bioengineering, Biomaterials and Nanomedicine (CIBER-BBN).
[4]BIOMAT Research Group, University of the Basque Country (UPV/EHU), Escuela de Ingeniería de Gipuzkoa, Plaza de Europa 1, 20018 Donostia-San Sebastián, Spain.
[5]BCMaterials, Basque Center for Materials, Applications and Nanostructures, UPV/EHU Science Park, 48940, Leioa, Spain.
[6]Proteinmat Materials SL, Avenida de Tolosa 72, 20018 Donostia-San Sebastián, Spain.
*E-mail addresses rosa.hernandez@ehu.eus

.....

Sent to: Bioactive Materials

Abstract

Chronic wounds are a worldwide problem that affect more than 40 million people every year. The constant inflammatory status accompanied by prolonged bacterial infections reduce patient´s quality of life and life expectancy drastically. One of the most important cell types involved in the wound healing process are mesenchymal stromal cells (MSCs). It has been largely described that MSCs play an important role in the inflammation and proliferation phases of the healing process due to their demonstrated antibacterial, immunomodulatory and pro-regenerative capacity. Thus, in this work we leveraged the therapeutic properties of both adipose tissue MSCs and hair follicle MSCs and combined them with sponge-like scaffolds (MSC-SLS). In this regard, the combination of these cells with biomaterials allowed us to obtain a multifunctional therapy that demonstrated to increase fibroblasts and keratinocytes migration, promote HUVECs angiogenesis and protect fibroblasts from stressful environments. Finally, this MSC-SLS demonstrated to be effective in reducing wound healing time in vivo with also exhibiting a more functional and native-like healed skin.

1. Introduction

Chronic wounds are a complex dysregulation of the normal skin healing process accompanied by constant bacterial infections, vasculature problems that precede hypoxic environments and a prolonged inflammatory status that leads into aberrant ECM deposition and remodeling [1,2]. Despite the enormous paradigm shift in their treatment with the commercialization of the first cell-based (keratinocytes and/or fibroblasts) dressings in the beginning of the XXI century, the general management of chronic wounds has barely changed from the traditional "dressing wound care" [3]. Different studies addressing poor improvements and lower healing rates against numerous decellularized matrices impeded their widespread implementation in clinic [4]. However, the shortcomings of the first generation of cell-based dressings cheered the development of novel combinations that leverage not only the intrinsic therapeutic properties of dressings and cells separately, but also the biochemical, physical and mechanical cues of the forming materials to boost the therapeutic potential of the cells [5,6]. One of the most important cell types involved in the wound healing process are mesenchymal stromal cells (MSCs). It has been largely described that MSCs play an important role in the inflammation and proliferation phases of the healing process due to their demonstrated antibacterial, immunomodulatory and pro-regenerative capacity [1,6,7]. Thus, MSCs orchestrate the healing process acting as switcher buttons for the modulation of different cell types such as macrophages or fibroblasts [8,9].

In a previous study, we demonstrated that an eco-friendly soy-protein combined with β-chitin composed sponge-like scaffolds (SLS) act as effective 3D dressings for MSCs hosting, increasing their secretory potential. Leveraging the RGD motifs present on the soy protein, MSCs demonstrated to attach into the microarchitecture of the SLS, growing, spreading and boosting their intercellular communication machinery [10]. Thus, in this work, we move one-step forward and demonstrate that this combination of MSCs with the SLS (MSC-SLS) is able to increase fibroblasts proliferation, promote neo vascularization and confer protection against reactive oxygen species (ROS) and hyperglycaemia induced cytotoxicity. Throught the literature, Adipose tissue derived MSCs (AT-MSCs) have been use as the gold standard for MSCs-based dressing development [4,11-13].

Here, we have compared the potential of AT-MSCs against one of the most important and easily available MSCs involved in the healing of wounds and skin defects, hair follicle derived MSCs (HF-MSCs) [14,15]. Finally, we have tested the efficacy of these formulations in an in vivo model with impaired healing. However, due to the cost and time of manufacturing, and the "living nature" itself of these MSCs-based dressings, great debate has risen about the placement periods and dressings change times of these formulations. Therefore, in order to integrate into the wound or interact with the microenvironment and respond accordingly, these MSCs-based dressings should be placed in the wound bed longer than the traditional dressings are nowadays. Thus, MSCs could respond accordingly to the changing microenvironment of every step of the wound healing process. In this regard, in this work, we have demonstrated that these MSC-SLS can be placed in wounds for longer periods showing a great efficacy without any sign of bacterial infections nor any other side effects.

2. Materials and methods

Materials

The soy protein isolate (SPI) and the β-chitin were obtained, characterized and combined to form the SLS as previously described [10]. The cells used in this study were AT-MSCs (ATCC, PCS-500-011), adult human dermal fibroblasts (HDFs) (ATCC, PCS-201-012), human umbilical vein endothelial cells (HUVECs) (Lonza, C2519A) and HaCaTs keratinocytes (DKFZ, Germany). HF-MSCs were isolated and characterized from HFs as previously described [15]. Both MSCs were cultured in Dulbecco's modified Eagle medium high glucose (DMEM) (Gibco, 11965) supplemented with 10% (v/v) fetal bovine serum (Gibco, 26140079) and 1% (v/v) penicillin–streptomycin (Gibco, 15140122). HDFs were cultured in fibroblasts basal medium (ATCC, PCS-201-030) supplemented with the fibroblast growth kit-low serum (ATCC, PCS-201-041) and 1% (v/v) penicillin–streptomycin. HUVECs were cultured in the EGM™-2 Endothelial Cell Growth Medium-2 BulletKit™ (Lonza, CC-3162) with 1% (v/v) penicillin–streptomycin. HaCaTs were cultured in DMEM (Gibco, 41965-039) with 10% (v/v) fetal bovine serum and 1% (v/v) penicillin–streptomycin. Phosphate buffered saline (PBS) pH 7.4 (Gibco, 11593377) was

used for cell culture. All cells were incubated in a humidified incubator at 37 °C under a 5% CO2 atmosphere.

MSC-SLS formulation and viability monitorization

To prepare the MSC-SLS, MSCs — both AT-MSCs (AT-SLS) and HF-MSCs (HF-SLS) — were seeded in 8 mm diameter SLS in a volume equivalent to the 80% of swelling of each SLS. Ratios of MSCs seeding were 25,000 and 50,000 cells per mg of SLS with and average weight of 10 mg per unit. After 6 h of incubation, the MSC-SLS were placed in contact with the culture media throught the wound-like transwell system as depicted in Fig.1. Following, the MSC-SLS were incubated for 3 and 7 days and the supernatants were taken for lactate dehydrogenase (LDH) release and cytokine secretion analysis. At these time-points, the MSC-SLS were rinsed with PBS and stained with Calcein AM (Thermofisher, Invitrogen C1430) following manufacturer´s protocol. After that, MSC-SLS were visualized in a Nikon epi-fluorescence microscope equipped with a DSD2 confocal modulus (Nikon) to analyze the MSCs behaviour and viability.

LDH release evaluation

For the LDH release assay the CyQUANT™ LDH Cytotoxicity Assay (Thermofisher, C20300) was performed following the manufacturer´s instructions. Briefly, 50 μL of the 3 and 7 days supernatants were mixed with 50 μL of the reaction mixture and incubated for 30 min protected from the light. After that, 50 μL of stop solution were added and the absorbance was measured within 2 h using a plate reader (Infinite® 200 PRO series, TecanTrading AG) at a wavelength of 490 nm using as a reference 680 nm. Two standard curves of MSCs were prepared, following manufacturer's protocol, to analyze the LDH spontaneous release and the release upon lysis.

Soluble secretome analysis

The cytokine secretion analysis was performed by using a custom Quantibody® ELISA array (TebuBio). Briefly, the supernatants from 7 days MSC-SLS incubation were studied for the secretion of Angiogenin-1, bFGF, EGF, KGF, HGF, IGF-I, VEGF, PDGF-AA, IL-1 ra, IL-6, IL-8, MCP-1, RANTES, SDF-1α and TGF-β1. First,

the slides were placed at room temperature for 2 h. Then, wells were washed for 30 min with 100 μL of sample diluent. After discarding the diluent, 100 μL of samples and standards were added and slices were incubated for 2 h under stirring. Then, wells were washed five times with wash buffer I under stirring and five more times with wash buffer II. After that, 80 μL of detection antibody were added for 2 h, washed as mentioned and incubated, protected from the light, with 80 μL of Cy3 dye for 1 h. Finally, the slices were washed and sent to the manufacturer for the analysis. A custom standard curve was prepared for each slide following manufacturer's instructions with the standard mixture provided by the manufacturer.

In vitro wound healing evaluation

To evaluate whether the MSC-SLS can promote the migration of HDFs and HaCaTs, an in vitro wound healing assay or scratch assay was performed. Briefly, 5×10^5 cells/mL of HDFs and $1{,}5 \times 10^6$ cells/mL of HaCaTs were seeded on each part of the two-well IBIDI culture inserts® in 6-well plates (IBIDI, 80209) and incubated for 8 h. PBS outside the inserts was added to minimize the evaporation of medium. Secondly, both wells were washed with PBS and serum-free medium was added overnight to minimize the cell proliferation. After that, the inserts were extracted creating the wound and wells were washed with PBS to discard the detached cells. Thereafter, the wound-like transwell system was disposed and the MSC-SLS were placed on each well with 1mL of serum-free medium (HDFs) or 1:6 medium in serum-free medium (HaCaTs) and incubated for 48 h. SLS without MSCs and wells without treatment were used as controls. At pre-defined time-points — 0 h, 4 h, 6 h, 8 h, 12 h, 24 h, 36 h and 48 h — images of the closing area were taken by an optical microscope (Nikon). The migration area between wound edges was calculated by using the ImageJ software and the wound closure was calculated by the following equation (**Eq. 1**) where So and Sn represent the initial wound area and wound area at different time points, respectively:

$$(\boldsymbol{Eq.\,1})\ Wound\ closure\ \% = \frac{So - Sn}{So} x100$$

Tube formation assessment

Firstly, 15 μL of Matrigel® (Corning, 356231) were added into the μ-Plate angiogenesis 96-well plates (IBIDI, 89646) and let polymerize for 30 min at 37 °C. Then, HUVECs were seeded over the matrix bed at a density of 4.5×10^5 cells/mL in 70 μL of MSC-SLS supernatants — incubated 24 h, 48 h, 96 h and 168 h using the wound-like transwell system in DMEM medium — and 24h supernatant of SLS in the matrigel bed. Complete DMEM medium incubated 24h was used as control and supplemented HUVECs medium was used as positive control. After 24 h of incubation, HUVECs where stained with calcein AM and each well was photographed by a Nikon epi-fluorescence microscope. The tube formation was analyzed using Image J Software. The VEGF release by the MSC-SLS at 24 h, 48 h, 96 h and 168 h of incubation was measured using the VEGF Quantikine ELISA (R&D Systems, DVE00) following manufacturer's instructions.

Evaluation of protection against ROS induced cytotoxicity

To measure the protective effect of the MSC-SLS on HDFs under a highly oxidative environment, 10,000 cells/well were seeded in a 96-well plate for 24h. After that, two approaches were followed. In the first experiment, 30 mM of H_2O_2 were mixed 1:1 with the supernatant of 24 h incubated MSC-SLS for 2 h. Then, 100 μL the mixture were added into the wells and incubated for 30 min. After that, wells were washed twice with PBS and incubated for 6 h with 100 μL of serum free HDFs medium. Finally, wells were washed twice with PBS and incubated for 4 h with a 1:10 mixture of CCK8 (Merck, 96992) in complete medium. Absorbance was read with a plate reader (Infinite® 200 PRO series, TecanTrading AG) at 450 nm, using 650 nm as the reference wavelength. In the second experiment, cells were pretreated with 100 μL of the supernatant of 24 h incubation MSC-SLS in DMEM for 6 h. After washing twice with PBS, 100 μL of 15 mM of H2O2 in serum free media were added for 30 min. Thereafter, wells were washed twice with PBS and incubated for 6 h with 100 μL of serum free HDFs medium. Finally, wells were washed twice with PBS and incubated for 4 h with a 1:10 mixture of CCK8 in complete medium and the absorbance was read at 450 nm, using 650 nm as the reference wavelength. Supernatants of 24 h incubated SLS and complete HDFs medium were used as controls. Cells without H2O2 were used as positive controls.

Evaluation of protection against hyperglycaemia-induced cytotoxicity

For the evaluation of the protective effect of MSC-SLS over HDFs hyperglycemia-induced cytotoxicity, 10,000 cells/well were seeded in a 96-well plate for 24 h. Then, cells were washed with PBS twice and incubated with 100 μL treatments for 6 h. Supernatants of 24 h incubated MSC-SLS or SLS were used. HDFs complete medium was used as a positive control and serum free HDFs medium was used as blank group. After the incubation time, cells were washed twice and 100 μL of serum free media with 150 μM of glucose (Merck, 108337) were added. After 24 h, cells were washed twice, incubated for 4 h with a 1:10 mixture of CCK8 in serum free medium and the absorbance was read at 450 nm, using 650 nm as the reference wavelength. This process was repeated at 48 h and at 72 h. Cells without high glucose treatment were used as non-cytotoxic control. Images of cells at 72 h were taken using an optical microscope.

In vivo wound healing assessment

Animals

The in vivo studies were performed with 8-week-old male db/db (BKS.Cg-m+/+Leprdb/J) mice (Janvier laboratories). All the experiments followed the procedure number M20/2019/258 approved by the University of the Basque Country ethical committee for animal experimentation. Animals were housed individually with ad libitum access to water and food and a light-dark cycle of 12 h.

Wound healing assay

Firstly, mice were anesthetized with isoflurane (Isoflo®, Esteve) and completely peeled their dorsal hair. After that, two 10 mm diameter silicon rings were sutured on each side of the back using a 3–0 nylon suture in order to avoid wound contraction. Then, two full thickness wounds were made extending through the panniculus carnosus, using an 8 mm diameter scalpel (AcuPunch, Acuderm). Wounds were well-cleaned with saline and treatments were applied over the wounds and covered with one layer of petrolatum gauze (Tegaderm®, 3M) and

two adhesive tapes. Mice were then divided into 4 groups (n = 8): (i) untreated control, (ii) SLS group, (iii) AT-SLS group and (iv) HF-SLS group. At day 7 treatments were removed, wounds cleaned and new treatments were applied. Half of the mice were sacrificed by CO2 inhalation at day 7 and the remaining ones at day 15.

Evaluation of wound healing

The macroscopic closure of wound was evaluated throught all the experiment. Thus, on days 8 and 15 wounds were photographed using a meter for post analysis scaling. The wound area was measured using Image J software. Finally, the wound closure percentage was calculated using the following equation (Eq. 2):

$$(\boldsymbol{Eq.2})\ Wound\ closure\ \% = \frac{Final\ wound\ area\ (px2)}{Initial\ wound\ area\ (px2)}\ x\ 100$$

Histological analysis of wound healing

On days 8 and 15, mice were sacrificed to obtain the wound necropsies. The wound and surrounded tissue were fixed with 3.7% paraformaldehyde for 24h and ethanol until processing. After that, the necropsies were bisected, embedded in paraffin and sectioned in 5 μm slices. Finally, tissues were stained by hematoxylin-eosin (H&E) for overall wound analysis and by Masson´s Trichrome for collagen deposition analysis. All measurements were performed by a blinded histopathologist.

The analysis of the re-epithelialization process was performed following Sinha. et al. scale [16]. Briefly, each wound was classified within a scale between 0 to 4 in which: 0, only the wound edges was re-epithelialized; 1, less than half of the wound was re-epithelialized; 2, more than half of the wound was re-epithelialized; 3, the entire was re-epithelialized with irregular thickness; 4, wound completely re-epithelialized with normal thickness.

The wound maturity status and the resolution of inflammation was measured using the scale described by Garcia-Orue et. al [17]. Briefly, wounds were rated from 0 to 4 as followed. 0, no sign of inflammation. 1, acute inflammation in which the formation of fibrin, the pyogenic membrane and the migration of neutrophils

and leucocytes was observed. 2, diffuse acute inflammation in which the pyogenic membrane is almost non-existent and there was formation of granulation tissue and angiogenesis. 3, chronic inflammation with an observed fibroblasts proliferation and predominance. 4, resolution and healing, no chronic inflammation observed and occasionally round cells can be found.

Finally, the collagen deposition was measured by using Image J software. Briefly, images were deconvoluted using the Masson´s trichrome option of "colour deconvolution 2" plugin. The blue channel was selected, the treshold was adjusted at 114 and the percentage of collagen was measured with the same parameters for all wounds.

Statistical analysis

Results are expressed as mean ± standard deviation. When normally distributed, to compare between two independent groups, results were analyzed through Student's T test or through a one-way ANOVA test for multiple comparisons. Using Levene test for the homogeneity of variances, Bonferroni or Tamhane post-hoc analyses were applied. Finally, for non-normally distributed data Mann–Whitney's non-parametric analysis was applied. All the statistical analysis were performed using SPSS 25.0.

3. Results and discussion

MSC–SLS viability monitorization and soluble secretome analysis

In order to explore the behaviour of the AT-MSCs and HF-MSCs hosted on the SLS, both MSC-SLS were incubated using a wound-like transwell system — where only the surface of the SLS was in contact with the culture medium simulating, as close as possible, the in vivo administration scenario — for 3 and 7 days (Fig.1A)

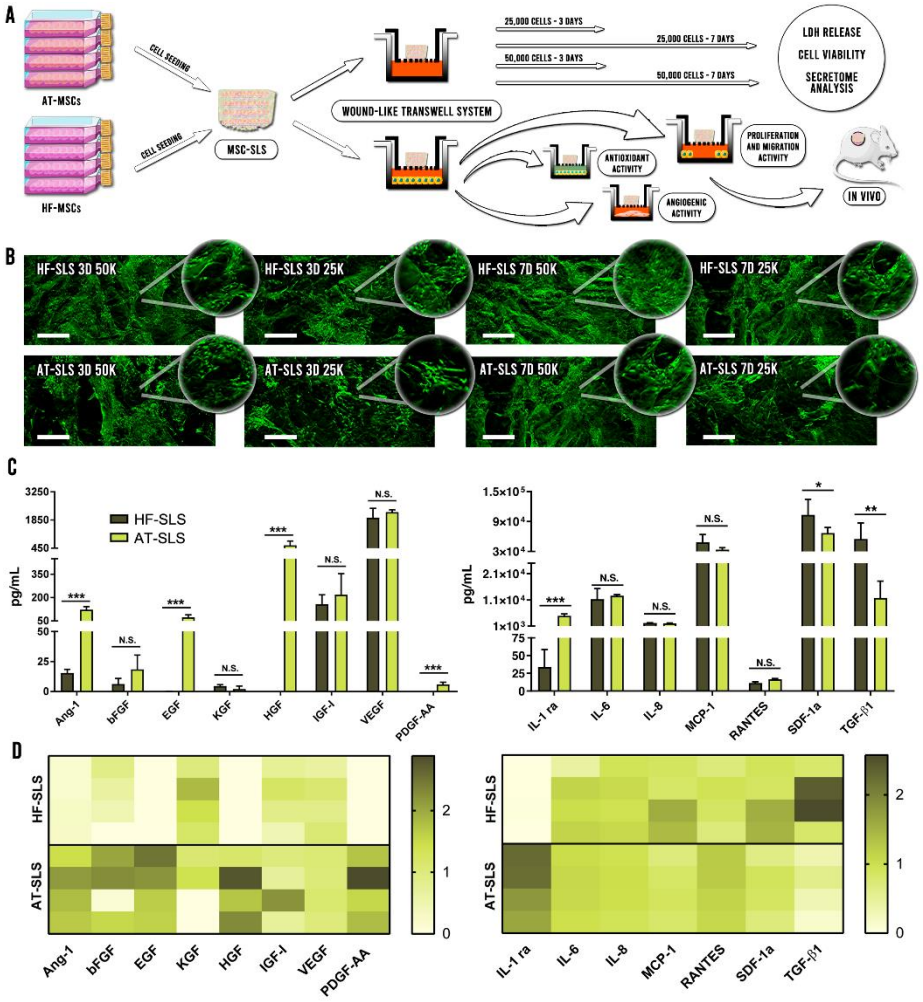

Fig. 1. Experimental scheme, MSC-SLS monitoring and secretome analysis. A. Scheme of MSC-SLS preparation, the transwell-like system disposition and the experimental setup. B. MSC-SLS imagining at different cell hosting doses — 25,000 cells/mg SLS (25K) and 50,000 cells/mg SLS (50K) — and incubation days — 3 days (3D) and 7 days (7D) —. Scale bars are 500 μm. C. Secretome analysis of cytokines and growth factors (n = 3). * $p<0.05$, ** $p<0.005$ and *** $p<0.001$ between groups. N.S. non-significance. D. Heat-map of the cytokine and growth factors release.

As illustrated in **Fig.1B** both AT-SLS and HF-SLS demonstrated that the two cell dosages — 25,000 cells/mg (25K) and 50,000 cells/mg (50K) — were able to let cells grow, spread and colonize the entire microarchitecture of the SLS. To further

confirm the visually great viability and quantify the cell death, a LDH release assay was performed (**Fig. S1**). Despite an observed increase on LDH release of approximately 20% between both doses on HF-SLS and 40% on AT-SLS at both days 3 and 7, the percentage of equivalent lysed cells was below 1% for all groups and time-points. These results confirmed in vitro that placing these treatments for a longer period than normally does — 2-3 days — [17,18], did not result in cell viability decrease nor LDH increase in the "wound niche". As a result, we decided to choose 50,000 cells/mg as the standard dosage for SLS cell loading throught the rest of the work.

In the soluble secretome analysis, the accumulated release of mediators at day 7 was studied to compare the profile of both cell types. As depicted in Fig.1C, D both MSCs released a great amount of pro-regenerative and anti-inflammatory mediators. Among the pro-angiogenic cytokines and growth factors, AT-MSCs released more Ang-1, HGF and PDGF-AA. In contrast, SDF-1α was more secreted by HF-SLS. However, no differences in the secretion of b-FGF, VEGF and IL-8 were found. These results reflect that under the SLS microenvironment — which can affect the secretion of pro-angiogenic factors [10,19,20] — both cells would have a great impact on angiogenesis and vasculogenesis processes. Nevertheless, upon the face-to-face comparison, we speculate that the slight increase in SDF-1α secretion in HF-MSCs and the higher secretion of Ang-1, HFG and PDGF-AA in AT-MSCs could reflect a more important role of HF-MSCs in the vasculogenesis process upon a more important role of AT-MSCs in angiogenesis [21]. The angiogenic potency of AT-MSCs secretome has been widely investigated however, the main role of HF-MSCs in irrigation for hair formation and growth could explain their observed great angiogenic-related secretome profile [22-24]. Throught the pro-regenerative/remodelative mediators involved in the wound healing process, the only differences found between both cell types were; the secretion of EGF and HGF, which was non-detected in HF-MSCs and the secretion of a pro-fibrotic mediator, TGF-β1, which was significantly higher in HF-MSCs. In contrast, the secretion of IGF-1 and KGF was similar for both cell types, being the second, poorly secreted. We could not find precedents in the literature about the secretion of these factors in HF-MSCs nevertheless, we speculate that the composition and microarchitecture of the SLS could be involved in the absence of some factors

production and/or release [25]. Finally, the anti-inflammatory chemokine IL-1ra secretion was significantly higher in the AT-MSCs group. In addition, the secretion of the pro-inflammatory/immunomodulatory chemokines was higher in HF-MSCs for SDF-1α and similar for the rest of mediators analyzed; IL-6, IL-8, MCP-1 and RANTES. Grouping all these results, both MSC-SLS would exert a great therapeutic potential involving angiogenic, pro-regenerative and immunomodulatory roles.

In vitro wound healing evaluation

In the in vitro wound healing evaluation or scratch assay, the pro-migratory effect of MSC-SLS was tested. It has been widely described that in the chronic wound niche, the migration of numerous cell types results impaired due to a harsh environment that impede a correct cell-to-cell communication [26-28]. In that way, helping these cells to increase their motility and migratory capacity would eventually benefit the formation of granulation tissue and the correct closure of wounds. As depicted in Fig. 2A, B both MSC-SLS demonstrated to increase the migration and wound closure of HaCaTs in comparison to the SLS without cells and the non-treated blank group. Interestingly, the effect was not observed bellow 4 h but it was at 8 h and maintained throught all the experiment (Fig. 2C).

As well as with HaCaTs, the pro-migratory effect was also observed in HDFs (Fig. 2D, E). Similarly, the effect was detected at 8 h and maintained until the end of the experiment (Fig. 2F). As depicted, no differences between AT-SLS and HF-SLS were found for both experimental cells, HDFs and HaCaTs. The release of a great amount of numerous mediators such as IL-6, TGF-β1 or bFGF, that has been described to have an impact on HaCaTs and HDFs migration, could explain the great results observed in the in vitro wound healing assay [28,29]. While the pro-migratory capacity of AT-MSCs has been largely described throught the literature, we could not find previous studies addressing the effects of HF-MSCs in this regard, setting here then, a precedent.

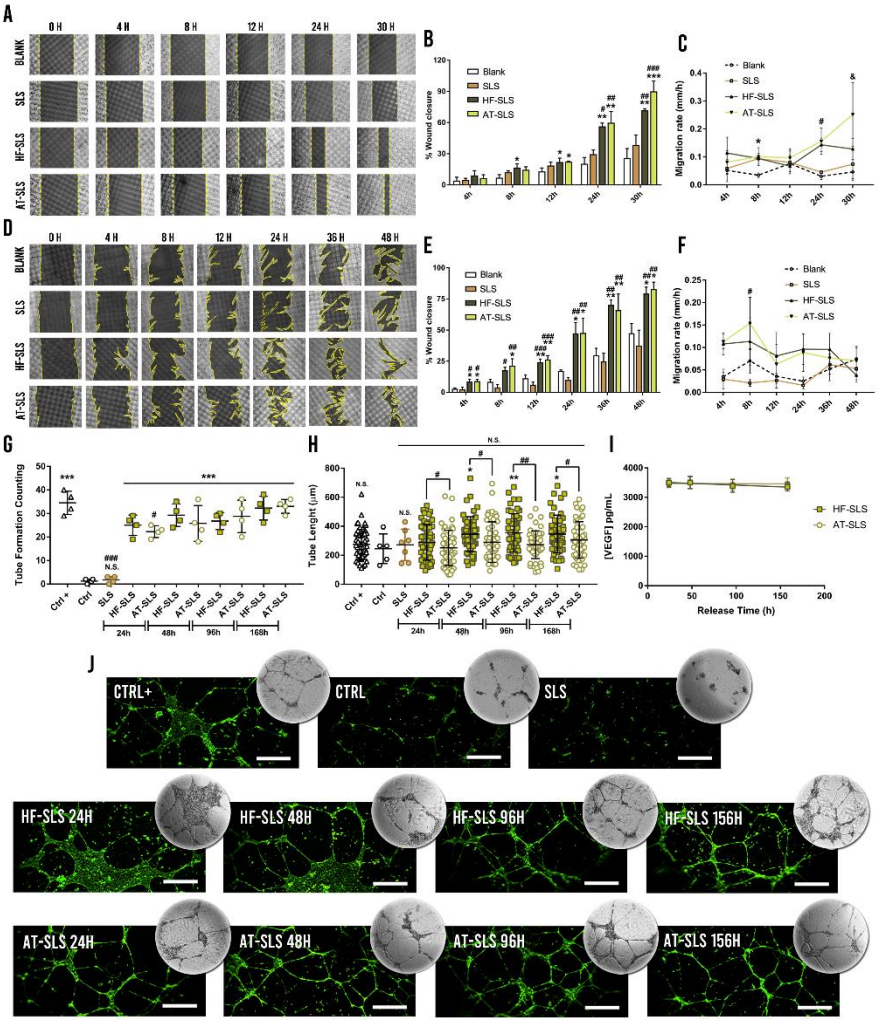

Fig. 2. In vitro wound healing and tube formation assays. A. Images of the HaCaTs cells at different time-points of the scratch assay (n = 3). B. Percentages of HaCaTs wound closure. * $p<0.05$, ** $p<0.005$ and *** $p<0.001$ against blank group. # $p<0.05$, ## $p<0.005$ and ### $p<0.001$ against SLS group. C. Migration rate of HaCaTs at different time points. * $p<0.05$ all groups against the blank group. # $p<0.05$ AT-SLS and HF-SLS against SLS and blanks groups. & $p<0.05$ AT-SLS against blank group. D. Images of the HDFs cells at different time-points of the scratch assay (n = 3). E. Percentages of HDFs wound closure. * $p<0.05$, ** $p<0.005$ and *** $p<0.001$ against blank group. # $p<0.05$, ## $p<0.005$ and ### $p<0.001$ against SLS group. F. Migration rate of HDFs at different time points. # $p<0.05$ AT-SLS and HF-SLS against SLS and blanks groups. G. Number of formed tubes per well (n = 4). *** $p<0.001$ against control group. # $p<0.05$, and ### $p<0.001$

against positive control group. N.S. non-significance against control group. H. Tube length. * $p<0.05$, ** $p<0.005$ and N.S. non-significance against control group. # $p<0.05$, and ## $p<0.005$ between groups. I. VEGF amount in MSC-SLS secretome administered at different time-points. J. Calcein stained and optical microscope images of the formed tubes. Scale bars are 400 μm.

Tube formation assessment

Numerous wounds fail in healing and became chronic due to an impaired blood flow that leads into a poorly oxygenated and nutrient supply lacked wound niche. Therefore, increase the formation of new vessels and thus increase the oxygen and nutrient supply in chronic wounds results an important strategy to be developed. As observed in Fig. 2G-J both MSC-SLS groups demonstrated to exert a great effect on tube formation in HUVECs. Results depicted that MSC-SLS had an angiogenic potency almost similar to that in the positive control and significantly greater than the control and SLS groups. No differences were found between AT-SLS and HF-SLS in terms of tube count. However, in terms of tube length, we observed that HF-SLS produced slightly larger tubes (in diameter) that AT-SLS and positive control groups (Fig. 2H). This could be explained by the observed slightly increase in SDF-1α production of HF-SLS since some works have demonstrated that higher concentrations of this mediator can increase tube length in angiogenesis [30]. Due to the maintenance of the angiogenic effect observed throught 7 days, we tested the supernatants for VEGF release. As depicted in Fig. 2I the amount of VEGF produced by MSC-SLS was similar for both cell types and linear throught the week. This could explain that both MSC-SLS were able to increase tube formation even at 7 days of MSC-SLS incubation confirming, as observed before, the great viability and efficacy of cells after 7 days (Fig. 2G, J).

Evaluation of protection against ROS and hyperglycaemia induced cytotoxicity

Usually, in chronic wound scenarios, the amount of ROS is very high, generating inflammation and hindering, in that way, the cell-to-cell communication and integrity [31]. Therefore, reducing the amount of ROS or protecting cells against the ROS-induced cytotoxicty and death has been an interesting move in the development of new therapies. It has been described that MSCs release certain

types of superoxide dismutase (SOD) that can act as ROS scavengers [32]. However, as observed in Fig. 3A when the secretome of MSC-SLS, SLS or control was mixed with the experimental ROS-fueled media and placed in HDFs, non-effect or protection was observed. These results showed that the secretome released by the MSC-SLS is not able to counteract or act as "scavenger" when is incubated together with H2O2. In contrast, when HDFs were pre-treated with the secretome of MSC-SLS and then exposed to the ROS environment, a statistically significant protective effect was observed for both AT-SLS and HF-SLS (Fig. 3B, C).

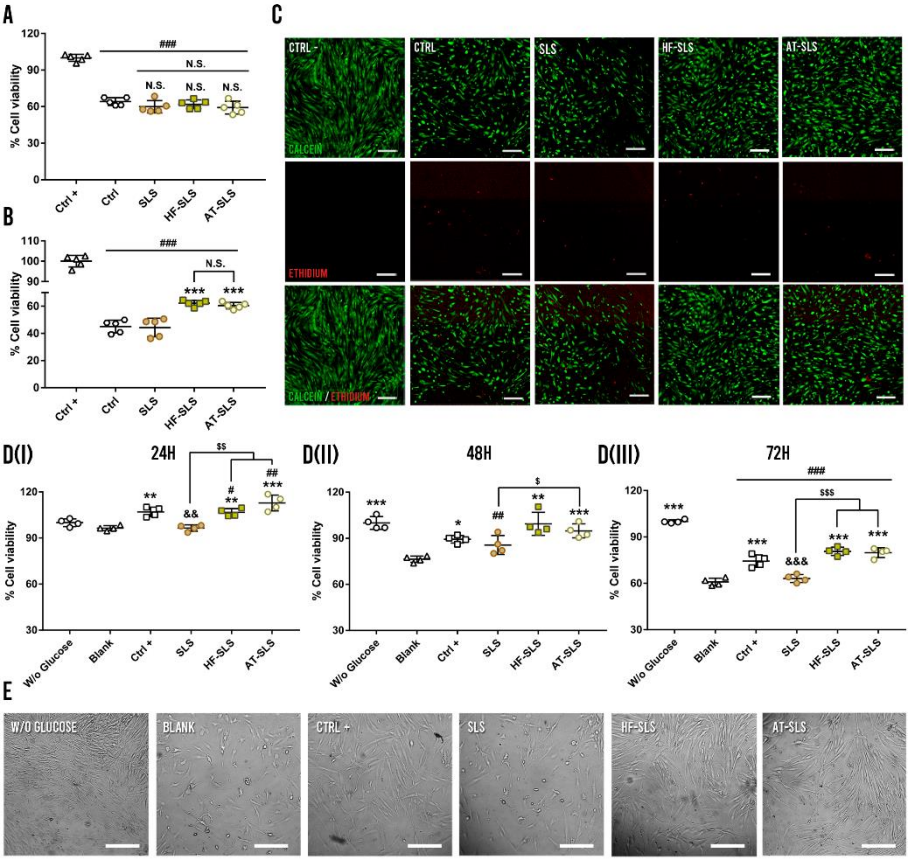

Fig. 3. Cell survival under ROS and hyperglycemia-induced cytotoxicity. A. Percentage of cell viability when the MSC-SLS secretome and controls are mixed with H2O2 and then incubated with HDFs. ### $p<0.001$ against the positive control. B. Percentage of cell viability when HDFs are pretreated with the treatments. *** $p<0.001$ against the control and SLS groups. ### $p<0.001$ against the

positive control. N.S. non-significance. C. Images of calcein/ethidium stained HDFs pretreated, after 24h of exposure to ROS. Scale bars are 200 μm. D. Cell viability under hyperglycemia-induced cytotoxicty. (I) Percentage of cell viability after 24h. (II) Percentage of cell viability after 48h. (III) Percentage of cell viability after 72h. * $p<0.05$, ** $p<0.005$, *** $p<0.001$ against the blank group. # $p<0.05$, ## $p<0.005$, ### $p<0,001$ against the group without glucose. && $p<0.005$, &&& $p<0.001$ against the positive control group. $ $p<0.05$, $$ $p<0.005$, $$$ $p<0.001$ between groups. E. Images of HDFs after 72h of hyperglycemia treatment. Scale bars are 400 uM.

These observations suggest that in the secretome of MSC-SLS some mediators are able to protect HDFs against ROS-induced cytotoxicty and death. In a previous study, we observed that the EVs of both AT-MSCs and HF-MSCs were not able to protect HDFs in similar conditions [33]. In this regard, this effect could be related to some soluble mediators such as IL-1ra — that antagonizes IL-1α, IL-1β and TNF-α —, bFGF that has demonstrated to reduce ROS induced oxidative stress or PGE2 that increases the levels of IL-10 [34-36]. Nevertheless, an important point should be taken into account. Despite SLS without cells have not demonstrated any effect, some studies have shown that the effect of the matrix in which cells are hosted is related to an increased expression of antioxidant enzymes that help to maintain low levels of ROS under excessive H2O2 environment [36]. Whether these results are associated to a matrix-related effect or simply to the secretory machinery of MSCs alone, should be thoroughly investigated in the future.

Diabetic ulcers — a certain type of chronic wounds — are characterized by a constant inflammatory status that lacks of correct oxygenation and nutrient supply due to elevated glucose levels. Thus, this hypoxic status creates an environment with elevated oxidative stress that eventually lead fibroblasts, among other cell types, to die [37,38]. To analyze if MSC-SLS have protective effects under a hyperglycemia-induced cytotoxicity, HDFs were pretreated with the secretome of MSC-SLS and then exposed to a hyperglycemic environment for 3 days. As observed in **Fig. 3D**, the protective effect of MSC-SLS pre-treatment was observed at 24h and maintained until 72h (**Fig 3DI**). Both AT-SLS and HF-SLS demonstrated statistically significant better results than the blank, SLS and positive control groups. The differences observed at 24h were greater at 48h and 72h where AT-SLS and HF-SLS showed a higher percentage of cell survival than the blank and SLS groups and similar to the positive control (**Fig. 3DII-III, E**). These results are in concordance with those obtained by our previous study where EVs from AT-MSCs and

HF-MSCs were also able to protect HDFs from hyperglycemia-induced cytotoxicity [33]. However, the soluble fraction of secretome could also affect the survival of HDFs. It has been described that hyperglycemia destabilizes HIF-1α impairing its function at higher concentrations of 30 mM [38]. The impaired function of HIF-1α leads to a decreased production of VEGF or SDF-1α that are key factors for angiogenesis and eventually for oxygenation and cell survival [39,40]. Thus, treating the wound niche with MSC-SLS secretome would assist different cell types with VEGF and SDF-1α, apart from the EVs fraction, eventually showing a protective effect against hyperglycemia-induced cell death.

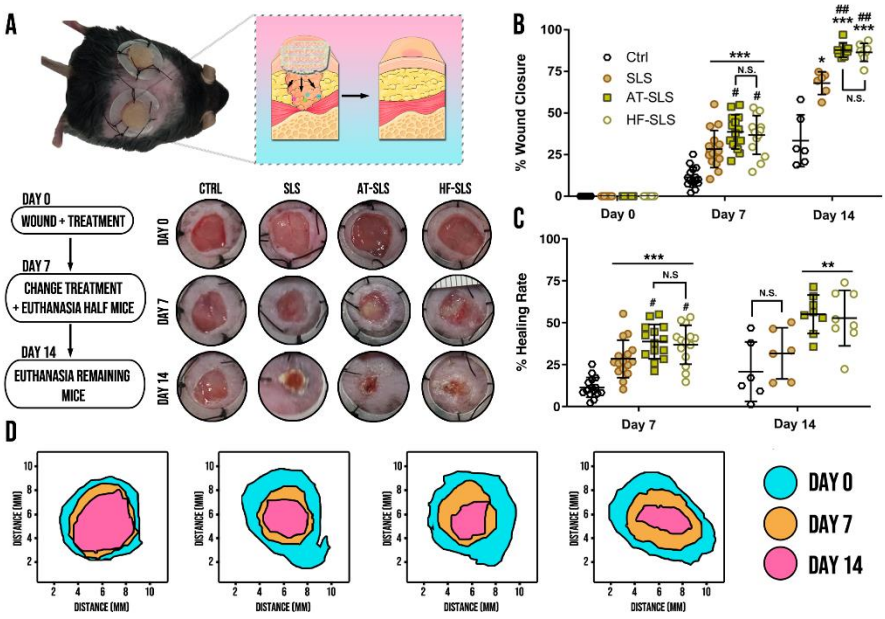

Fig. 4. In vivo wound healing assessment. A. In vivo procedure scheme and wound closure photographs. B. Percentage of wound closure at different time points. * $p<0.05$,*** $p<0.001$ against the control group. # $p<0.05$, ## $p<0.005$ against the SLS group. N.S. Non significance. C. Percentage of healing rate. ** $p<0.005$,*** $p<0,001$ against the control group. # $p<0.05$, against the SLS group. N.S. Non significance. D. Modell of the wound closure at different time points.

In vivo wound healing assessment

After showing great potential in different in vitro assays, the MSC-SLS were finally tested in a full thickness splinted wound healing assay in db/db mice (Fig.

4A-D). As observed in Fig. 4B the greatest wound closure was observed in both MSC-SLS groups at 7 and 14 days. As compared to the control, at day 7, the wound closure of AT-SLS and HF-SLS was significantly higher; in contrast, the SLS group did not show significant differences. However, at day 14 all groups showed significant higher closure against the control group and AT-SLS. Furthermore, the HF-SLS group showed higher percentage of wound closure than the SLS group. Finally, as observed in the healing rate, both MSC-SLS administrations showed wound closure effects against the control (Fig. 4C).

Histological analyses of wound necropsies were also performed. As shown in Fig. 5A, B we observed significant differences in the re-epithelialization status of wounds among the treated groups at 14 days. Both AT-SLS and HF-SLS demonstrated a more mature wound with better re-epithelialization that the control group; however, significant differences against the SLS group were not found. The re-epithelialization results were supported with the data obtained in the inflammation decrease rate (Fig. 5C). As depicted, at day 14 the three groups with treatment showed significant differences against the control group. However, we did not observe differences between the MSCs groups and the SLS group. Nevertheless, on these groups, inflammation values were above 3 depicting that the main process happening in the wound niche was fibroblast proliferation (proliferative phase). In contrast, in the control group, values below 2 showed that the wounds were still on a diffuse acute inflammatory phase. We did not observe differences between groups when comparing the epidermis thickness of wounds, which can act as an indicator of a more advanced healing (Fig. 5D). Finally, we measured the collagen deposition using the Masson´s trichrome staining (Fig. 5E, F). As observed, we obtained significant differences at both 7 and 14 days. At these time-points, AT-SLS and HF-SLS demonstrated an increased collagen deposition on the wound niche in comparison to the control and SLS groups. The effect may be attributed to the influence of MSCs since the SLS groups did not exhibit differences against the control. These results are in agreement with the ones observed by other authors using different MSCs delivery systems in vivo [41,42].

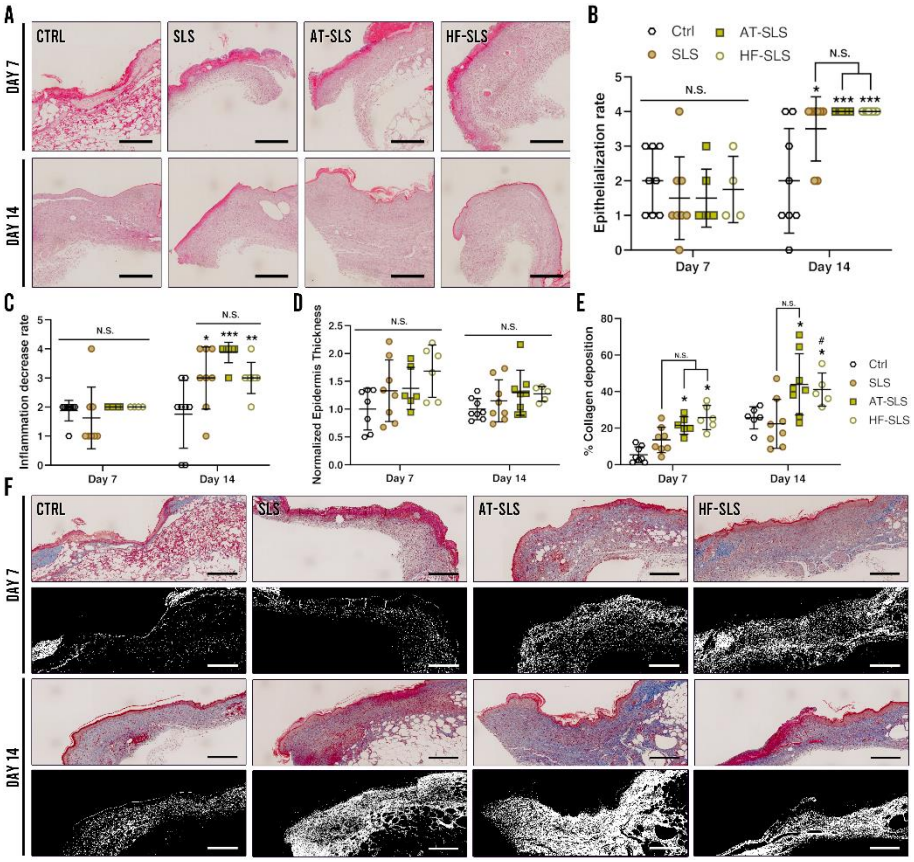

Fig. 5. Histological evaluation of wounds. A. Histological images of wounds on days 7 and 14 processed with H&E. B. Epithelialization rate. C. Inflammation decrease rate. D. Normalized epidermis thickness. E. Collagen deposition in the Masson´s trichrome staining. * $p<0.05$, ** $p<0.005$, *** $p<0,001$ against the control group. # $p<0.05$, against the SLS group. N.S. Non-significance. F. Histological images of wounds on days 7 and 14 stained with Masson´s Trichrome and deconvoluted images of the collagen using the Image J software.

4. Conclusions

In conclusion, in this study we have shown that the developed soy protein combined with β-chitin SLS are adequate matrices for MSCs hosting and spreading. Furthermore, the wide variety of mediators released by these MSC-SLS have demonstrated to protect HDFs against ROS and hyperglycemia induced cytotoxicity, increase HDFs and keratinocytes migration and promote

angiogenesis on HUVECs. Eventually, the MSC-SLS have demonstrated to decrease the wound healing time in vivo, increasing re-epithelialization, collagen deposition and decreasing inflammation.

ETHICS APPROVAL AND CONSENT TO PARTICIPATE

Hair follicles were obtained from occipital scalps of routine hair transplant procedures with the application of FUE technique (Clínica Dermatológica Ercilla, Spain). All patients signed an informed consent under an approved protocol (M10_2019_053, M30_2019_054) by the research ethics committee of the Basque Country.

DATA AVAILABILITY STATEMENT

Raw data is available from the corresponding author upon reasonable request.

COMPETING INTERESTS

The authors declare that no competing interest exists.

AKCNOWLDEGMENTS

This research was funded by the Basque Government (Consolidated Groups, IT907-16 and PRE_2018_1_0412).

SUPPLEMENTARY INFORMATION

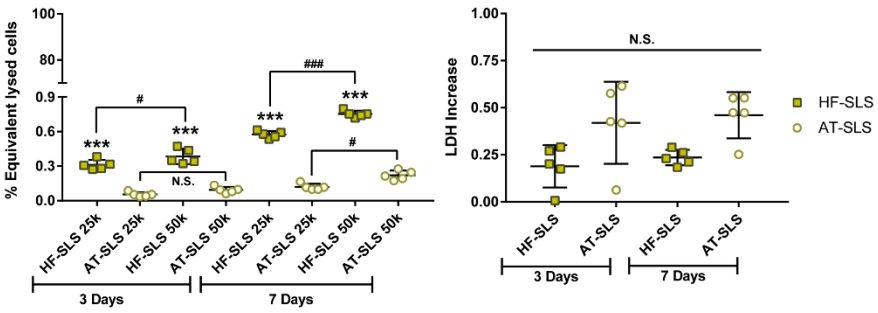

Fig. S1. LDH release of MSC-SLS. The percentage of equivalent lysed cells was calculated comparing the LDH release by the MSC-SLS with the standard curve of lysed MSCs LDH release.

The LDH increase represents the ratio of LDH increase with the higher dose of MSCs 50,000 cells/mg (50K) over the lower dose 25,000 cells/mg (25K). *** $p<0.001$ vs AT-SLS, # $p<0.05$ between groups, ### $p<0.005$ between groups, N.S. non-significance.

REFERENCES

[1] K. Las Heras, M. Igartua, E. Santos-Vizcaino, R.M. Hernandez, Chronic wounds: Current status, available strategies and emerging therapeutic solutions, J. Controlled Release. 328 (2020) 532-550.

[2] M.A. Fonder, G.S. Lazarus, D.A. Cowan, B. Aronson-Cook, A.R. Kohli, A.J. Mamelak, Treating the chronic wound: A practical approach to the care of nonhealing wounds and wound care dressings, J. Am. Acad. Dermatol. 58 (2008) 185-206.

[3] K. Skórkowska-Telichowska, M. Czemplik, A. Kulma, J. Szopa, The local treatment and available dressings designed for chronic wounds, J. Am. Acad. Dermatol. 68 (2013) e117-e126.

[4] K.L. Heras, M. Igartua, E. Santos-Vizcaino, R.M. Hernandez, Cell-based dressings: A journey through chronic wound management, Biomaterials Advances. 135 (2022) 212738.

[5] N. Mitrousis, A. Fokina, M.S. Shoichet, Biomaterials for cell transplantation, Nature Reviews Materials. 3 (2018) 441-456.

[6] M.Á Brennan, P. Layrolle, D.J. Mooney, Biomaterials Functionalized with MSC Secreted Extracellular Vesicles and Soluble Factors for Tissue Regeneration, Adv. Funct. Mater. 30 (2020) 1909125.

[7] R. Guillamat-Prats, The Role of MSC in Wound Healing, Scarring and Regeneration, Cells. 10 (2021).

[8] D.E. Rodríguez-Fuentes, L.E. Fernández-Garza, J. Samia-Meza, S. Barrera-Barrera, A.I. Caplan, H.A. Barrera-Saldaña, Mesenchymal Stem Cells Current Clinical Applications: A Systematic Review, Arch. Med. Res. 52 (2021) 93-101.

[9] E. Munoz-Perez, A. Gonzalez-Pujana, M. Igartua, E. Santos-Vizcaino, R.M. Hernandez, Mesenchymal Stromal Cell Secretome for the Treatment of Immune-Mediated Inflammatory Diseases: Latest Trends in Isolation, Content Optimization and Delivery Avenues, Pharmaceutics. 13 (2021).

[10] K. Las Heras, E. Santos-Vizcaino, T. Garrido, F. Borja Gutierrez, J.J. Aguirre, K. de la Caba, P. Guerrero, M. Igartua, R.M. Hernandez, Soy protein and chitin sponge-like

scaffolds: from natural by-products to cell delivery systems for biomedical applications, Green Chem. 22 (2020) 3445-3460.

[11] P.L. Kang, H.H. Huang, T. Chen, K.C. Ju, S.M. Kuo, Angiogenesis-promoting effect of LIPUS on hADSCs and HUVECs cultured on collagen/hyaluronan scaffolds, Materials Science and Engineering: C. 102 (2019) 22-33.

[12] W. Pu, J. Ren, Y. Chen, J. Shu, L. Cui, Y. Han, J. Xi, X. Pei, W. Yue, Y. Han, Injectable human decellularized adipose tissue hydrogel containing stem cells enhances wound healing in mouse, Colloids Surf. Physicochem. Eng. Aspects. 604 (2020) 125268.

[13] M. Lotfi, H. Naderi-Meshkin, E. Mahdipour, A. Mafinezhad, R. Bagherzadeh, H.R. Sadeghnia, H. Esmaily, M. Maleki, H. Hasssanzadeh, M. Ghayaour-Mobarhan, H.R. Bidkhori, A.R. Bahrami, Adipose tissue-derived mesenchymal stem cells and keratinocytes co-culture on gelatin/chitosan/β-glycerol phosphate nanoscaffold in skin regeneration, Cell Biol. Int. 43 (2019) 1365-1378.

[14] K. Ou, Y. Kuo, C. Wu, B. Huang, F. Pai, H. Chou, T. Saito, T. Ueno, Y. Cho, M. Huang, The Potential of a Hair Follicle Mesenchymal Stem Cell-Conditioned Medium for Wound Healing and Hair Follicle Regeneration, Applied Sciences. 10 (2020).

[15] B. Hernaez-Estrada, A. Gonzalez-Pujana, A. Cuevas, A. Izeta, K.L. Spiller, M. Igartua, E. Santos-Vizcaino, R.M. Hernandez, Human Hair Follicle-Derived Mesenchymal Stromal Cells from the Lower Dermal Sheath as a Competitive Alternative for Immunomodulation, Biomedicines. 10 (2022).

[16] U.K. Sinha, L.A. Gallagher, Effects of Steel Scalpel, Ultrasonic Scalpel, CO2 Laser, and Monopolar and Bipolar Electrosurgery on Wound Healing in Guinea Pig Oral Mucosa, The Laryngoscope. 113 (2003) 228-236.

[17] I. Garcia-Orue, G. Gainza, F.B. Gutierrez, J.J. Aguirre, C. Evora, J.L. Pedraz, R.M. Hernandez, A. Delgado, M. Igartua, Novel nanofibrous dressings containing rhEGF and Aloe vera for wound healing applications, Int. J. Pharm. 523 (2017) 556-566.

[18] Z. Shao, T. Yin, J. Jiang, Y. He, T. Xiang, S. Zhou, Wound microenvironment self-adaptive hydrogel with efficient angiogenesis for promoting diabetic wound healing, Bioactive Materials. 20 (2023) 561-573.

[19] Q.L. Loh, C. Choong, Three-Dimensional Scaffolds for Tissue Engineering Applications: Role of Porosity and Pore Size, Tissue Engineering Part B: Reviews. 19 (2013) 485-502.

[20] G.D. Mogoşanu, A.M. Grumezescu, Natural and synthetic polymers for wounds and burns dressing, Int. J. Pharm. 463 (2014) 127-136.

[21] K. Hiasa, M. Ishibashi, K. Ohtani, S. Inoue, Q. Zhao, S. Kitamoto, M. Sata, T. Ichiki, A. Takeshita, K. Egashira, Gene Transfer of Stromal Cell–Derived Factor-1α Enhances Ischemic Vasculogenesis and Angiogenesis via Vascular Endothelial Growth Factor/Endothelial Nitric Oxide Synthase–Related Pathway, Circulation. 109 (2004) 2454-2461.

[22] K. Yano, L.F. Brown, M. Detmar, Control of hair growth and follicle size by VEGF-mediated angiogenesis, J. Clin. Invest. 107 (2001) 409-417.

[23] B. Wang, X.M. Liu, Z.N. Liu, Y. Wang, X. Han, A.B. Lian, Y. Mu, M.H. Jin, J.Y. Liu, Human hair follicle-derived mesenchymal stem cells: Isolation, expansion, and differentiation, World J. Stem Cells. 12 (2020) 462-470.

[24] K. Ou, Y. Kuo, C. Wu, B. Huang, F. Pai, H. Chou, T. Saito, T. Ueno, Y. Cho, M. Huang, The Potential of a Hair Follicle Mesenchymal Stem Cell-Conditioned Medium for Wound Healing and Hair Follicle Regeneration, Applied Sciences. 10 (2020).

[25] W.J. King, P.H. Krebsbach, Growth factor delivery: How surface interactions modulate release in vitro and in vivo, Adv. Drug Deliv. Rev. 64 (2012) 1239-1256.

[26] I.B. Wall, R. Moseley, D.M. Baird, D. Kipling, P. Giles, I. Laffafian, P.E. Price, D.W. Thomas, P. Stephens, Fibroblast Dysfunction Is a Key Factor in the Non-Healing of Chronic Venous Leg Ulcers, J. Invest. Dermatol. 128 (2008) 2526-2540.

[27] M. Zou, Y. Teng, J. Wu, S. Liu, X. Tang, Y. Jia, Z. Chen, K. Zhang, Z. Sun, X. Li, J. Ye, R. Xu, F. Yuan, Fibroblasts: Heterogeneous Cells With Potential in Regenerative Therapy for Scarless Wound Healing, Frontiers in Cell and Developmental Biology. 9 (2021).

[28] M. Piipponen, D. Li, N.X. Landén, The Immune Functions of Keratinocytes in Skin Wound Healing, International Journal of Molecular Sciences. 21 (2020).

[29] T. Schreier, E. Degen, W. Baschong, Fibroblast migration and proliferation during in vitro wound healing, Res. Exp. Med. 193 (1993) 195-205.

[30] F. Mirshahi, J. Pourtau, H. Li, M. Muraine, V. Trochon, E. Legrand, J. Vannier, J. Soria, M. Vasse, C. Soria, SDF-1 activity on microvascular endothelial cells: consequences on angiogenesis in in vitro and in vivo models, Thromb. Res. 99 (2000) 587-594.

[31] C. Dunnill, T. Patton, J. Brennan, J. Barrett, M. Dryden, J. Cooke, D. Leaper, N.T. Georgopoulos, Reactive oxygen species (ROS) and wound healing: the functional role of ROS and emerging ROS-modulating technologies for augmentation of the healing process, Int Wound J. 14 (2017) 89-96.

[32] Y. Wang, R. Branicky, A. Noe, S. Hekimi, Superoxide dismutases: Dual roles in controlling ROS damage and regulating ROS signaling, J. Cell Biol. 217 (2018) 1915-1928.

[33] K. Las Heras, F. Royo, C. Garcia-Vallicrosa, M. Igartua, E. Santos-Vizcaino, J.M. Falcon-Perez, R.M. Hernandez, Extracellular vesicles from hair follicle-derived mesenchymal stromal cells: isolation, characterization and therapeutic potential for chronic wound healing, Stem Cell. Res. Ther. 13 (2022) 147-0.

[34] C. Bouffi, C. Bony, G. Courties, C. Jorgensen, D. Noel, IL-6-dependent PGE2 secretion by mesenchymal stem cells inhibits local inflammation in experimental arthritis, PLoS One. 5 (2010) e14247.

[35] D. Nawrocka, K. Kornicka, J. Szydlarska, K. Marycz, Basic Fibroblast Growth Factor Inhibits Apoptosis and Promotes Proliferation of Adipose-Derived Mesenchymal Stromal Cells Isolated from Patients with Type 2 Diabetes by Reducing Cellular Oxidative Stress, Oxid Med. Cell. Longev. 2017 (2017) 3027109.

[36] C. Hu, L. Zhao, C. Peng, L. Li, Regulation of the mitochondrial reactive oxygen species: Strategies to control mesenchymal stem cell fates ex vivo and in vivo, J. Cell. Mol. Med. 22 (2018) 5196-5207.

[37] R. Nunan, K.G. Harding, P. Martin, Clinical challenges of chronic wounds: searching for an optimal animal model to recapitulate their complexity, Dis Model Mech. 7 (2014) 1205-1213.

[38] P.A. Shiekh, A. Singh, A. Kumar, Exosome laden oxygen releasing antioxidant and antibacterial cryogel wound dressing OxOBand alleviate diabetic and infectious wound healing, Biomaterials. 249 (2020) 120020.

[39] K. Hu, S. Babapoor-Farrokhran, M. Rodrigues, M. Deshpande, B. Puchner, F. Kashiwabuchi, S.J. Hassan, L. Asnaghi, J.T. Handa, S. Merbs, C.G. Eberhart, G.L. Semenza, S. Montaner, A. Sodhi, Hypoxia-inducible factor 1 upregulation of both VEGF and ANGPTL4 is required to promote the angiogenic phenotype in uveal melanoma, Oncotarget; Vol 7, No 7. (2016).

[40] D.J. Ceradini, A.R. Kulkarni, M.J. Callaghan, O.M. Tepper, N. Bastidas, M.E. Kleinman, J.M. Capla, R.D. Galiano, J.P. Levine, G.C. Gurtner, Progenitor cell trafficking is regulated by hypoxic gradients through HIF-1 induction of SDF-1, Nat. Med. 10 (2004) 858-864.

[41] R. Geesala, N. Bar, N.R. Dhoke, P. Basak, A. Das, Porous polymer scaffold for on-site delivery of stem cells--Protects from oxidative stress and potentiates wound tissue repair, Biomaterials. 77 (2016) 1-13.

[42] A. Shafiee, A.S. Cavalcanti, N.T. Saidy, D. Schneidereit, O. Friedrich, A. Ravichandran, E.M. De-Juan-Pardo, D.W. Hutmacher, Convergence of 3D printed biomimetic wound dressings and adult stem cell therapy, Biomaterials. 268 (2021) 120558.

Las Heras et al. Stem Cell Research & Therapy (2022) 13:147
https://doi.org/10.1186/s13287-022-02824-0

Stem Cell Research & Therapy

RESEARCH Open Access

Extracellular vesicles from hair follicle-derived mesenchymal stromal cells: isolation, characterization and therapeutic potential for chronic wound healing

Kevin Las Heras[1,2], Félix Royo[3,4], Clara Garcia-Vallicrosa[3], Manoli Igartua[1,2,5], Edorta Santos-Vizcaino[1,2,5], Juan M Falcon-Perez[*,3,4,6] and Rosa Maria Hernandez[*,1,2,5].

[1]NanoBioCel Group, Laboratory of Pharmaceutics, School of Pharmacy (UPV/EHU), 01006 Vitoria-Gasteiz, Spain.
[2]Bioaraba, NanoBioCel Research Group, Vitoria-Gasteiz, Spain.
[3]Center for Cooperative Research in Biosciences (CIC bioGUNE), Basque Research and Technology Alliance (BRTA), Exosomes Laboratory, 48160 Derio, Spain
[4]Centro de Investigación Biomédica en Red de Enfermedades Hepáticas y Digestivas (CIBERehd), 28029 Madrid, Spain
[5]Biomedical Research Networking Centre in Bioengineering, Biomaterials and Nanomedicine (CIBER-BBN), 28029 Madrid, Spain.
[6]IKERBASQUE, Basque Foundation for Science, 48013 Bilbao, Spain
* Rosa Maria Hernandez and Juan M. Falcon-Perez equally share credit for senior authorship.
*E-mail addresses rosa.hernandez@ehu.eus and jfalcon@cicbiogune.es

Published in: *Stem Cell Research & Therapy*, 2022

Impact Factor 2020: *8.088* (Q1)

DOI: https://doi.org/10.1186/s13287-022-02824-0

Cat: BioMed Central

Abstract

Background: Mesenchymal stromal cells (MSCs) and their extracellular vesicles (MSC-EVs) have demonstrated to elicit immunomodulatory and pro-regenerative properties that are beneficial for the treatment of chronic wounds. Thanks to different mediators, MSC-EVs have shown to play an important role in the proliferation, migration and cell survival of different skin cell populations. However, there is still a big bid to achieve the most effective, suitable and available source of MSC-EVs.

Methods: We isolated, characterized and compared medium-large EVs (m-lEVs) and small EVs (sEVs) obtained from hair follicle-derived MSCs (HF-MSCs) against the gold standard in regenerative medicine, EVs isolated from adipose tissue-derived MSCs (AT-MSCs).

Results: We demonstrated that HF-EVs, as well as AT-EVs, expressed typical MSC-EVs markers (CD9, CD44, CD63, CD81 and CD105) among other different functional markers. We showed that both cell types were able to increase human dermal fibroblasts (HDFs) proliferation and migration. Moreover, both MSC-EVs were able to increase angiogenesis in human umbilical vein endothelial cells (HUVECs) and protect HDFs exposed to a hyperglycemic environment from oxidative stress and cytotoxicity.

Conclusions: Taken together, HF-EVs demonstrated to exhibit comparable potential to that of AT-EVs as promising candidates in the treatment of chronic wounds.

Background

Hair follicles (HFs) are skin appendages originated by the interactions of ectodermal-mesodermal cells in the early embryogenesis. HFs present a complex structure with a rich mixture of cell populations. It has been described that HFs contain different pools of stem cells — melanocyte, epithelial and mesenchymal stromal cells (MSCs) — that regulate hair growth, maintaining skin homeostasis and self-renewing processes continuously [1-3]. In the past decade, there has been an increasing interest in these hair follicle derived MSCs (HF-MSCs) due to their numerous advantages over other sources of MSCs — abundant availability of HFs that do not undergo functional and molecular changes in the human body and an easy collection not affected by gender or age — [2, 4, 5]. Furthermore, their role in skin homeostasis, hair growth and their pro-regenerative capacity are making these cells become one of the most suitable candidates for cell-based wound healing therapies [6-10]. Indeed, it has been observed that the direct administration of HF-MSCs can accelerate wound healing both in vitro and in vivo in diabetic mice models [11].

However, despite its demonstrated efficacy and safety, the use of cell therapy for chronic wound management have found important constraints through the harsh regulatory pathways and elevated production costs that impede its widespread use [7, 8, 12]. As a result, numerous researchers have studied the paracrine signaling of MSCs, which has been described as the main responsible for the therapeutic potential of these cells [13-15]. Among the bioactive cues that drive regenerative effects, extracellular vesicles (EVs) have gained special attention. In the form of membrane-surrounded units, EVs shuttle the messaging cargos of RNAs, DNAs and proteins to mediate intercellular communications [16]. Similarly to MSC-based therapies, MSCs-derived EVs (MSC-EVs) have demonstrated to elicit a wide variety of therapeutic effects in tissue repair and wound regeneration — immunomodulatory, proliferative, anti-apoptotic, pro-angiogenic effects etc. — [17-19]. Furthermore, EVs are more easily handled, characterized and stored than MSCs. In this regard, EVs-based therapies can be better standardized than cell-based therapies. Moreover, these therapies can be

commercialized under a softer regulation pathway than cell-based therapies, being considered “biological medicines” [20].

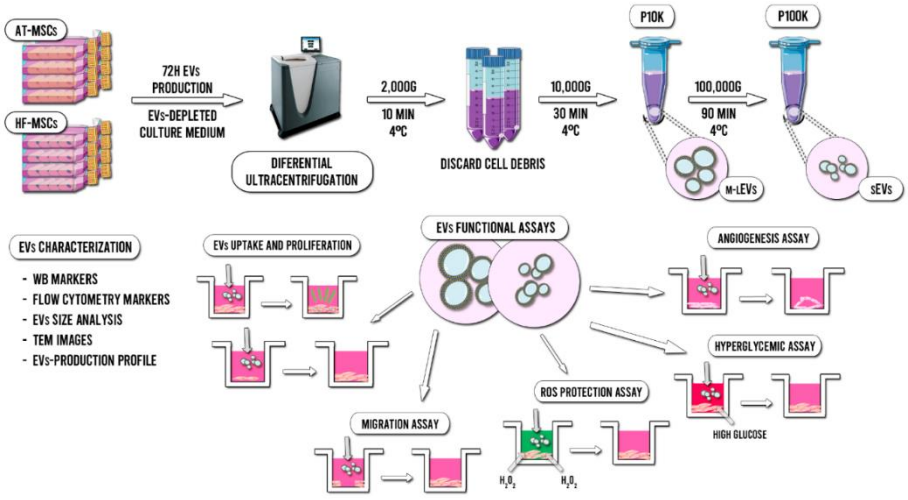

Fig. 1. Scheme of the isolation method, characterization and functional assays of HF-EVs and AT-EVs.

In this study, we report a complete characterization and functional comparison of EVs isolated from HF-MSCs (HF-EVs) against the gold standard in regenerative medicine, EVs derived from adipose tissue MSCs (AT-EVs) (Fig. 1). We have analyzed the MSC-EVs production profile, size, morphology and marker expression. Furthermore, we have compared the cell uptake and tested their potential in human dermal fibroblasts (HDFs) — one of the most important cell types involved in the wound healing process — and in human umbilical vein endothelial cells (HUVECs) to study the vascular behaviour of wounds. Following the MISEV 2018 guidelines [21], we have analyzed not only of the small EVs (sEVs) released by these cells, but also the medium-large EVs (m-lEVs) that are sometimes discarded, despite their demonstrated potential for regenerative medicine applications.

Materials and methods

EVs Isolation and Characterization

Cell Culture Conditions

HF-MSCs were isolated and characterized from HFs as previously described [22] and further cultured in Dulbecco's modified Eagle's medium (DMEM 49166-029, Gibco) supplemented with 10% of fetal bovine serum (FBS, Gibco) and 1% (v/v) penicillin/streptomycin (P/S, Gibco). AT-MSCs (ATCC® PCS-500-011TM) were also cultured under the same conditions. Adult Human Dermal Fibroblasts (HDFs, ATCC® PCS-201-012™) were cultured in fibroblasts basal medium (ATCC PCS-201-030TM) adding the fibroblasts growth kit-low serum (ATCC® PCS-201-041™) and 1% (v/v) penicillin/streptomycin (P/S, Gibco). Incubating conditions were 37 ^{o}C in a 5% CO2 atmosphere. Human umbilical vein endothelial cells (HUVECs, Lonza® C2517A) were cultured in the EGMTM-2 Endothelial Cell Growth Medium-2 BulletKitTM (Lonza® CC-3162) with 1% (v/v) penicillin/streptomycin (P/S, Gibco). For EVs production, DMEM medium was used with 10% of EV-depleted FBS — by overnight ultracentrifugation 100,000 × g (Beckman Coulter, Optima L-100XP) —. HF-MSCs and AT-MSCs were used at passages from 5 to 9 for EVs isolation. HDFs were used at passages 3 to 7. HUVECs were used at passages 3 to 7.

EVs isolation

All relevant data regarding the production, isolation and experimental section have been submitted to the EV-TRACK knowledgebase (EV-TRACK ID: EV210337) [23]. EVs were isolated and purified from the supernatant of HF-MSCs and AT-MSCs. At 70-80% of confluency, cells were washed thrice with PBS and the culture medium was replaced with EVs-depleted DMEM. After 72 h of production, the culture medium was collected and new medium was added. After three collections, cells were trypsinized, counted and further re-cultured. The collected medium was first centrifuged at 2,000 × g for 10 min at 4 ^{o}C to discard cell debris and then, freeze at -80 ^{o}C until the isolation and purification was given. All further centrifugation processes were performed at 4 ^{o}C. In brief, thawed culture supernatants were differentially centrifuged at 10,000 × g for 30 min to obtain m-lEVs — pellet 10K (P10K) — and the resulting supernatants at 100,000 × g for 90 min — pellet 100K (P100K) — to obtain sEVs. To reduce contaminating proteins, all pellets (P10K and P100K) were re-suspended in ice-cold PBS and

ultracentrifuged again. Finally, both pellets were immediately re-suspended in 120 μL of ice-cold PBS and freeze at -80 °C until use.

Nanoparticle tracking analysis

Particle concentration and size distribution within EV preparations was analyzed using the nanoparticle-tracking analysis (NTA), by measuring the rate of Brownian motion in a NanoSight LM10 system (Malvern Panalytical, Malvern, UK). The system was equipped with a fast video-capture and particle-tracking software. NTA post-acquisition settings were the same for all measurements. Each video was analyzed to give the mean, mode, and median vesicle size, as well as an estimate of the concentration. For measurement, original EVs suspension were diluted 1:100 with PBS and a volume of 500 μL were loaded on the camera, and 3 consecutive video recording of 40 seconds each were taken for every sample quantified.

Western blotting

PBS-resuspended EVs or cell lysates were mixed with 4×NuPAGE LDS Sample Buffer (Thermo Fisher Scientific, Waltham, MA, USA). The samples were incubated for 5 min at 37 °C, 65 °C, and 95 °C, and separated on 4–12% precast gels (from Thermo Fisher Scientific, Waltham, MA, USA), at a concentration of 5 μg/lane (Bradford determination). The proteins were transferred into PVDF membranes with the iBLOT2 system (Thermo Fisher Scientific, Waltham, MA, USA). Antibodies employed were: mouse monoclonal antibody against CD9 #209302 (R&D), Grp78 #40 (BD, East Rutherford, NJ, USA), CD13 #3D8 (Santa Cruz Biotechnology, Dallas, Tx, USA), EEA1 #14 (BD, East Rutherford, NJ, USA), CD63 #H5C6 (DSHB, Iowa City, IA, USA), LAMP1 #H4A3 (DSHB, Iowa City, IA, USA), alpha tubulin 1 #DM1A (Santa Cruz Biotechnology, Dallas, Tx, USA), CD81 #JS81 (BD, East Rutherford, NJ, USA), rabbit antibody against COX IV #4850 (Cell Signaling Technologies, Danvers, Ma, USA). All the primary antibodies were diluted 1:1000. Horseradish peroxidase (HRP)-conjugated secondary antibodies anti-mouse, rabbit and goat, were purchased from Jackson ImmunoResearch Lab, (West grove, PA, USA) to ensure minimal cross-reactivity across species.

Bead-based multiplex flow cytometry assay

All isolated EVs were subjected to a surface-marker characterization by using a flow cytometry bead-based multiplex analysis (MACSPlex Exosome Kit, human, Miltenyi Biotec. 130-108-813). Samples were processed according to manufacturer's protocol. Briefly, 2 μg of EVs were mixed with 120 μL of manufacturer's buffer and then, 15 μL of the MACSPlex Exosome Capture Beads were added. Then, 15 μL of the detection antibody cocktail — 5 μL of each MACSPlex exosome detection reagent CD9, CD63, CD81 — were added. After that, samples were incubated 1 h at room temperature, protected from the light, on rotation — 450 rpm —. Next, 500 μL of MACSPlex buffer were added and samples were centrifuged at 3000 × g for 5 min. Subsequently, 500 μL of supernatant were discarded and another 500 μL of buffer were added. Samples were incubated for 15 min at room temperature on rotation, protected from the light and then centrifuged 5 min at 3000 × g. Finally, 500 μL of supernatants were discarded and approximately 150 μL of samples were re-suspended and used for the analysis. The flow cytometry analysis was performed using the MACSQuant® Analyzer 10 (Miltenyi Biotec) and results were processed with the MACSQuant Analyzer 10 software (Miltenyi Biotec). The 39 single bead populations were gated to determine the APC signal intensity on each bead population and the median fluorescence intensity (MFI) for each capture bead was measured. For each population, background was corrected by subtracting the respective MFI values from non-EVs controls that were treated exactly like the EVs-samples. Furthermore, values of the corresponding isotype control were also subtracted. Only positive markers are shown in the graphics.

Cryo-Electron Microscopy (cryo-EM)

EVs (3-5 μL) were spotted on glow-discharged lacey grids and cryo-fixed by plunge freezing at -180 ^{o}C in liquid ethane with a Vibrobot (FEI, The Netherlands). Grids were observed with a JEM-2200FS/CR TEM (JEOL, Japan), operating at 200 kV. Image measurements were performed with Image J software and between 80-120 single EVs were measured on each group for size and protein-decoration analysis.

CD63 immunostaining

Cells were grown onto 12 mm glass coverslips and fixed with 4% formaldehyde, and permeabilized with 0.1% saponin and 0.1% BSA in PBS. Incubation with primary and secondary antibodies were performed in a humid camera for 1 h each. Following two-10 min washes in PBS, cells were mounting with Fluoromount-G™ Mounting Medium with 2-(4-amidinophenyl)-1 h-indole-6-carboxamidine (DAPI) (Thermo Fisher Scientific, Waltham, MA, USA) for nuclei staining. Imaging of the slides were taken in a Leica SP8 confocal microscope.

EVs uptake and proliferation by HDFs

EVs staining

In order to stain EVs, Vybrant™ DiO Cell-Labeling Solution (Invitrogen, Cat. V22886, Thermo Fisher Scientific, Waltham, MA, USA) was used. Briefly, cultured HF-MSCs and AT-MSCs were washed with PBS and 50 μL of dye in 10 mL of culture medium were added. Cells were incubated for 30 mins and after that, washed again thrice with PBS. Finally, EVs-depleted medium was added and a 72 h labeled-EVs production was obtained as previously described. As negative control, the same exact process was performed in flask without cells, to determine the possible carry-over of fluorescence by the culture medium.

EVs uptake by HDFs and Flow cytometry

To perform capture experiments, 500,000 HDFs per well were seeded in 6 well plates and 12 mm slides, and incubated overnight with MSC-EVs stained as described above diluted in 2 mL of medium. Slides were fixed and directly observed in a Leica SP8 confocal microscopy, while HDFs in wells were washed twice with PBS and detached from the plate using TrypLE Select (1X) (Gibco, 12604013) and directly observed in a Cytoflex flow cytometer (Beckman Coulter Inc, Chicago, Il, USA), and data analysis was performed using the CytExpert v2.4 software (Beckman Coulter Inc, Chicago, Il, USA).

Proliferation assay

HDFs were seeded in 96 well plates — 5000 cells/well — in 100 μL of complete medium. After 8 h of incubation, cells were washed with PBS and then cultured overnight with serum-free medium. After that, cells were washed with PBS and EVs

were administered — 1.5x1011 EVs/mL of P10K and 2x1011 and 4x1011 EVs/mL of P100K — in 100 μL of 1:5 complete medium in serum-free medium and incubated for 24 h. Complete medium was used as positive control. After that, cells were washed with PBS and 100 μL of CCK8 (Merck, Cat: 96992) 1:10 diluted in culture medium were added. After 4 h of incubation, absorbance was read with a plate reader (Infinite® 200 PRO series, TecanTrading AG, Männedorf, Switzerland) at 450 nm, using 650 nm as the reference wavelength.

Scratch Assay

To evaluate whether EVs can promote migration of HDFs a scratch assay was performed. HDFs were seeded — 70 μL at a density of 5x105 cells/mL — in each side of the 2 well IBIDI culture inserts® in 24-well plates (IBIDI, Cat. 80209) and subsequently were incubated for 8 h. Secondly, the culture medium was aspired and serum-free medium was added in order to minimize the cell proliferation. After an overnight incubation, culture inserts were extracted and the scratch was performed. Then, HDFs were washed with PBS, EVs were administered — 2.5x109 EVs/mL of P10K and 1x1010 EVs/mL of P100K — in 300 μL of serum-free medium and cells were incubated for 48 h. At pre-defined time-points — 0 h, 6 h, 12 h, 24 h, 36 h and 48 h — images of the closing area were taken by an optical microscope (Nikon, Japan). The percentage of migration in the area between wound edges was calculated by ImageJ software (National Institutes of Health, MA, USA).

Tube formation assay

To perform the tube formation assay 15 μL of Matrigel® matrix (Corning®, Cat. 356231) were added into the μ-Plate angiogenesis 96 well plates (IBIDI, Cat. 89646) and let polymerize for 30 min at 37 °C. HUVECs were seeded at a density of 4,5 x105 cells/mL in 30 μL of complete medium, 15 μL of PBS and 25 μL of EVs — 2x1011 EVs/mL of P10K and 3,5x1011 EVs/mL of P100K — in the matrigel bed. Medium with non-EVs control batches processed equally to the EVs batches was used as control. Complete medium was used as positive control. Following an incubation of 24 h, each well was photographed by an optical microscope (Nikon, Japan). After that, cells where stained with calcein AM (Invitrogen, “LIVE/DEAD™ Viability/Cytotoxicity Kit, for mammalian cells” Cat. L3224) and each well was

photographed by a Nikon epi-fluorescence microscope equipped with a DSD2 confocal modulus (Nikon, Japan). The observed tubes were analyzed by using the ImageJ software.

Cell survival under hyperglycaemia assay

The effect of EVs on cell survival under a hyperglycaemic environment was studied in HDFs. Briefly, 10,000 cells were cultured in 96 well plates for 24 h. After that, HDFs were pre-treated with EVs —1x1011 EVs/mL of P10K and 3x1011 EVs/mL of P100K — for 6 h, rinsed with PBS and exposed to hyperglycaemic conditions of 150 mM glucose in HDFs serum-free culture medium. Cells pre-treated with non-EVs control batches processed equally to the EVs batches were used as control. Cells pre-treated with complete medium were used as a positive control. Results were normalized against cells grown under non-hyperglycaemic conditions. The metabolic activity was observed at 24 h, 48 h and 72 h by CCK8 assay as described earlier. Cell viability at 72 h was also observed with calcein AM/Ethidium homodimer (Invitrogen, "LIVE/DEAD™ Viability/Cytotoxicity Kit, for mammalian cells" Cat. L3224) and each well was photographed by a Nikon epi-fluorescence microscope equipped with a DSD2 confocal modulus (Nikon, Japan).

Reactive oxygen species (ROS) protection assay

Cell viability of HDFs under a ROS environment was studied in the protection assay. In brief, HDFs —1x105 cells/well — were seeded in a 96-well plate and allowed to adhere. After 24 h, cells were washed with PBS and the EVs pre-treatment — 1x1011 EVs/mL of P10K and 3x1011 EVs/mL of P100K — was added for 2 h and 6 h respectively. After that, cells were washed and then incubated for 30 min under a ROS environment — 100 μL of serum free medium with 15 mM of H2O2 —. Then, cells were washed with PBS and incubated overnight in serum free medium to minimize the proliferation of the surviving cells. Finally, cells were washed with PBS and 100 μL of CCK8, 1:10 diluted in serum free culture medium, were added. After 4 h of incubation, the absorbance was read at 450 nm, using 650 nm as the reference wavelength. An alternative co-culture ROS assay was performed as follows. HDFs — 1x105 cells/well — were seeded in a 96-well plate and allowed to adhere. After 24 h, cells were washed with PBS and then EVs were

added in 100 μL of serum free medium with 625 μM of H2O2 for 4 h. After that, cells were washed with PBS and 100 μL of CCK8, 1:10 diluted in serum free culture medium, were added. After 4 h of incubation, absorbance was read. For all assays, medium with non-EVs control batches processed equally to the EVs batches was used as control and complete medium was used as positive control.

Statistical Analysis

Results are expressed as the mean ± standard deviation. When normally distributed, results were analyzed through Student's two-tailed t-test, to compare between two independent groups, or through a one-way ANOVA test for multiple comparisons. Based on the Levene test for the homogeneity of variances, Bonferroni or Tamhane post-hoc analyses were applied. In contrast, Mann-Whitney's non-parametric analysis was applied for non-normally distributed data. All the statistical computations were performed using SPSS 25.0 (SPSS®, Inc., Chicago, IL, USA).

Results

EVs Isolation and Characterization

As represented in Fig. 2A, Cryo-EM images showed that the majority of the obtained material was round-shaped and bi-membrane-bounded vesicular units. The diverse heterogeneity of the different populations of EVs can be appreciated by the distinct electron dense cargos and protein decorated / non-decorated membranes presented. For both cell types, NTA measurements showed sizes ranging from 100 nm to nearly 400 nm for the P100K EVs, and from 100 nm to 800 nm for the P10K (Fig. 2B).

We also analyzed and compared the morphology, size and protein decoration of the isolated EVs by using the cryo-EM images. We studied approximately 400 single EVs and the majority of the observed units had the aforementioned round shape morphology for both cell types. Notably, we also found a small population of EVs with irregular morphologies (Fig. S1) — multilayered vesicles, long tubular, etc. —. The size distribution of EVs from cryo-EM images revealed populations of smaller size — < 50nm — than by NTA, obtaining a higher proportion of sEVs for

both cell types (Fig. 2C). Moreover, when we analyzed the presence or absence of membrane protein decoration, we found that the majority of EVs were non-decorated for both cell types (Fig. 2C and 2D). The decoration percentages of m-lEVs were 9,38% and 7,82% for AT-EVs and HF-EVs respectively, whereas in the case of sEVs the percentages were 16,20% and 14,28% for AT-EVs and HF-EVs respectively. However, we did not observe differences in the diameter of decorated vs non-decorated EVs between each EVs population (Fig. S2).

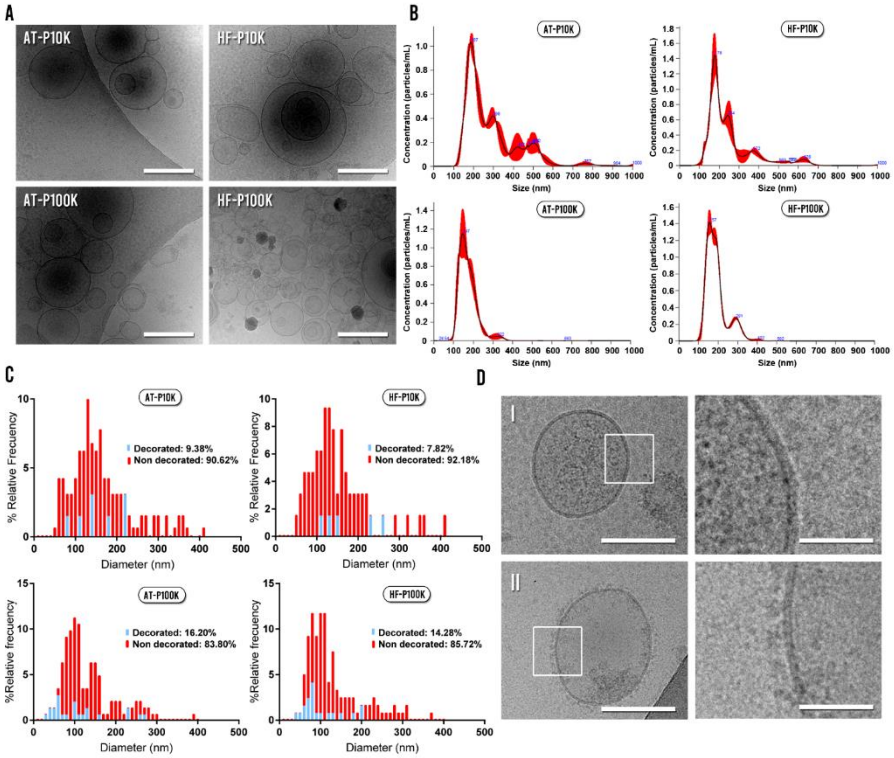

Fig. 2. EVs size, morphology and protein decoration analysis. (A) Cryo-EM images of EVs. Scale bars are 200 nm. (B) NTA size-profile of the isolated fractions. (C) Size profile and protein decoration analysis of the different fractions calculated by measuring Cryo-EM images. (D) Images of a non-decorated EV (I) and decorated EV (II) with their respective zoomed insets (right). Scale bars are 100 nm (left-sided images) and 20 nm (right-sided images).

When developing a EVs-based therapy it is crucial to achieve an adequate reproducibility in the batch-to-batch production. For such aim, we analyzed the

mean and the mode size of the isolated EVs for the different obtained batches — every EVs isolation for each cell passage —. We did not find significant differences in any of the parameters for the different MSC-EVs (Fig. 3A and 3B). Furthermore, we obtained low relative standard deviations in the isolated batches for both cell types and pellets (Fig. 3A and 3B). As expected, we observed that the mean and mode sizes of EVs were lower for the P100K EVs than for the P10K EVs for both cell types. The overall deviations of the mean and mode size were also lower for the P100K compared to the P10K (Fig. 3A and 3B). In contrast, the efficiency of the obtained batches in terms of number of isolated EVs per final cell count showed significant differences between both cell types (Fig. 3C). Our results demonstrate that HF-MSCs produce less EVs than AT-MSCs for both P10K and P100K. Moreover, all cell viabilities at the end of every batch were adequate — between 95 to 98% for both cell types —.

Marker analysis by western blotting (Fig. 3D) depicted the expression of CD13, CD81 and LAMP1 in P10K and P100K pellets derived from both cell types. In contrast, only AT-EVs showed bands for the rest of EV markers, with CD63 in both P10K and P100K, and CD9 in P100K. In the particular case of CD63, we observed different patterns; HF-MSCs retained this tetraspanin inside, while AT-MSCs showed it on m-lEVs and sEVs. We should mention that both MSC sources contain intracellular CD63 as exhibited by immunofluorescence images (Fig. S3). We have also analyzed the presence of non-vesicular markers, including COXIV — a mitochondrial — and GRP78 — endoplasmic reticulum — proteins, which appeared mostly in the P10K. Finally, TUB1, Hsp70, and EEA1 were only detected in the cells, and not in the vesicular fractions.

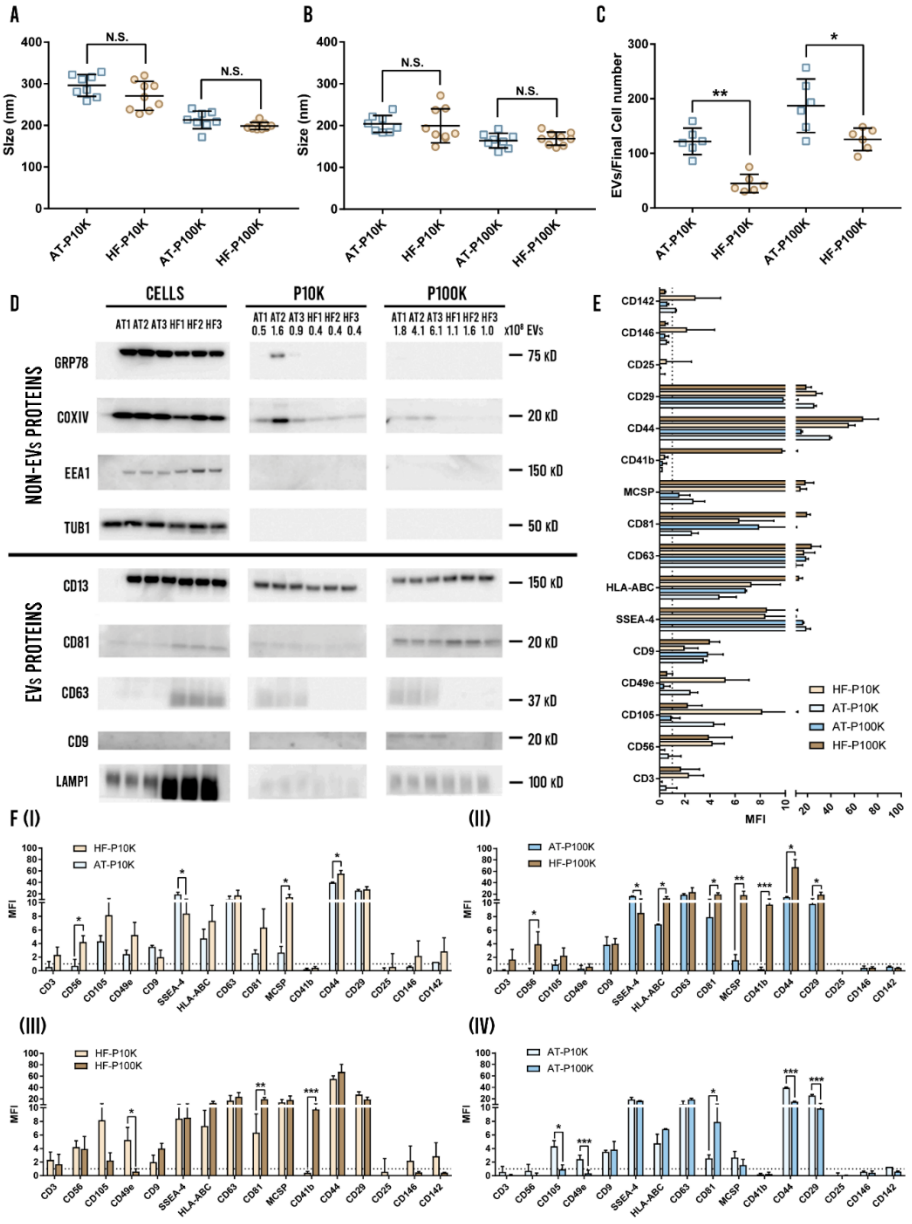

Fig. 3. EVs batch-to batch analysis, western blotting and flow cytometry surface marker analysis. (A) Mean size of each EVs fraction for the different batches (n=8). (B) Mode size of each EVs fraction for the different batches (n=8). (C) Number of EVs compared to final cell count (n=6). N.S. non-significant, * $p<0.05$, ** $p<0.005$ between groups. (D) Western blotting analysis of EVs and non-

EVs markers of three different batches for each cell type. (E) Multiplex bead-based flow cytometry assay for detection of EV surface markers (n=3). (F) Comparison of EVs surface marker expression from (E): AT-P10K vs HF-P10K (I), AT-P100K vs HF-P100K (II), HF-P10K vs HF-P100K (III), and AT-P10K vs AT-P100K (IV). * $p<0.05$, ** $p<0.005$ and *** $p<0.001$ between groups.

EVs were also evaluated by flow cytometry for the expression of 37 surface markers. We analyzed three different batches and found populations positive for CD3, CD9, CD25, CD29, CD41b, CD44, CD49e, CD56, CD63, CD81, CD105, CD142, CD146, MCSP, HLA-ABC/MHC-I and SSEA-4 (**Fig. 3E**). However, only CD9, CD29, CD44, CD63, CD81, CD105, MCSP, HLA-ABC and SSEA-4 were positive for all pellets and cell types. Nevertheless, we found some significant differences between both cell types and pellets. As observed, HF-P10K expressed CD56 — not in AT-P10K — and more CD44 and MCSP than AT-P10K; in contrast, AT-P10K expressed more SSEA-4 (**Fig. 3F-I**). Regarding the P100K, we observed the same differences concerning the expression of CD44, CD56 — not expressed in AT-P100K —, MCSP and SSEA-4 as in the P10K. Additionally, we achieved a higher expression of CD29, CD41b — not expressed in AT-P100K —, CD81 and HLA-ABC in the HF-P100K EVs (**Fig. 3F-II**). We also compared the P10K EVs and P100K EVs of the same cell type. As shown in Fig. 3F-III we found that P10K HF-EVs expressed more CD49b but lower CD81 and CD41b. On the other hand, P10K AT-EVs expressed more CD105, CD49e, CD44 and CD29 but lower CD81 than P100K AT-EVs (**Fig. 3F-IV**).

EVs uptake and proliferation by Human Dermal Fibroblasts

Uptake assay

After incubating HDF cells with EVs coming from fluorescence-labelled AT- and HF-MSCs, we observed a comparable uptake of EVs coming from both types of MSCs (**Fig. 4**). Although there is a higher percentage of positive events corresponding to AT-EVs preparations (**Fig. 4A-I,II**), the correction by number of EVs in the preparation, together with the variability of obtained data, make those changes non-significant (**Fig. 4A-III**). However, there were almost 10 times more capture events when the cells are incubated with P10K preparations, corresponding to m-lEVs, than 100K preparations (sEVs) (**Fig. 4A-III and Fig. S4**). This difference can be observed directly by immunofluorescence (**Fig. 4B**). A very

low carry-over of fluorescence was observed in medium that was not conditioned by HDFs (Fig. 4A, C).

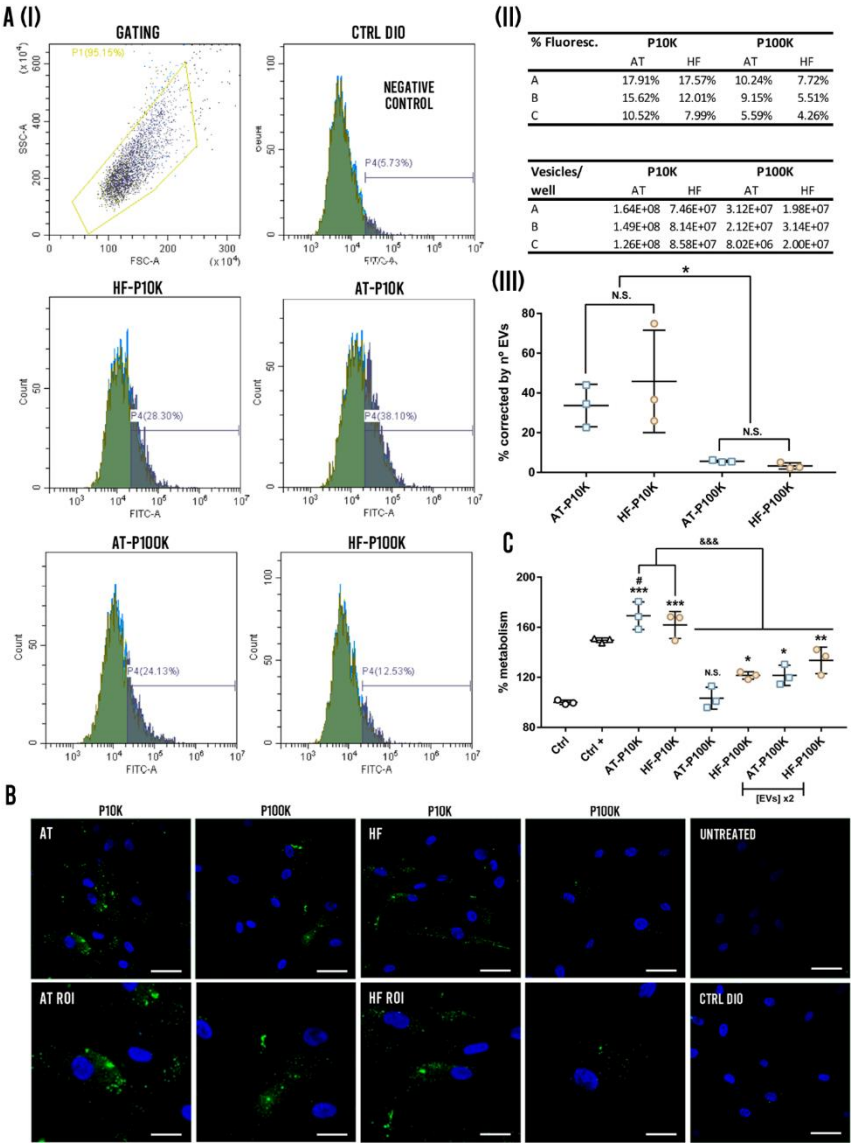

% Fluoresc.	P10K		P100K	
	AT	HF	AT	HF
A	17.91%	17.57%	10.24%	7.72%
B	15.62%	12.01%	9.15%	5.51%
C	10.52%	7.99%	5.59%	4.26%

Vesicles/ well	P10K		P100K	
	AT	HF	AT	HF
A	1.64E+08	7.46E+07	3.12E+07	1.98E+07
B	1.49E+08	8.14E+07	2.12E+07	3.14E+07
C	1.26E+08	8.58E+07	8.02E+06	2.00E+07

Fig. 4. EVs uptake by HDFs and proliferation assay. (A) EVs flow cytometry uptake: (I) Gating of the cell populations and percentage of positive events for the background control (Ctrl DIO), and the EV preparations of 10K and 100K for HF and AT cells. (II) The upper table shows the percentage of fluorescent cells after adding different preparations of EVs. Bottom table shows the number of

vesicles per well added for each preparation. (III) The graphs present the percentage of positive events according to the flow cytometry study corrected by the number of EVs for each type of EVs. * $p<0.05$, N.S. Non-significance. (B) Representative fluorescence micrographs of the capture of EVs and region of interest (ROI) for each preparation. The Fig. at the bottom show HDFs treated with the negative control corresponding to the carry-over of fluorescence of cell culture media never conditioned with HDFs, and untreated HDFs. (C) HDFs proliferation assay by CCK8 (n=3). N.S. Non-significant, * $p<0.05$, ** $p<0.005$, *** $p<0.001$ against the control group, # $p<0.05$ against the positive control group, &&& $p<0.001$ between groups.

Proliferation assay

It has been largely described that EVs promote the proliferation of different skin cell types such as HDFs among others [14]. When a chronic wound is given, the proliferative profile of the resident HDFs is impaired due to the impossibility to respond to the different cytokines and growth factors [24, 25]. In this regard, here, we compared the proliferative effect of the isolated MSC-EVs on HDFs. As shown in Fig. 4E, there is an important difference between the outcomes of P10K EVs as compared to the P100K EVs. P10K EVs showed an increase of approximately 60-70% of proliferation, as compared to the control, and AT-EVs, in addition, showed significant differences as compared to the positive control — complete medium — . In contrast, P100K EVs demonstrated a lower effect, which was dose-dependent. We did not notice significant differences between both cell types.

Scratch assay

In the scratch assay, we studied the pro-migratory effect of the MSC-EVs on HDFs. It is well-known that in chronic wound scenarios, there is also an impaired migration of these cells due to the harsh inflammatory environment and the impaired cell-to-cell communication [7, 24, 25]. In that sense, it is crucial to help these cells to increase their motility to favor the formation of granulation tissue ensuring an adequate closure of the wound. In this regard, we starved cells during the entire assay to minimize cell proliferation (Fig. 5A). Upon EVs treatment, we observed a faster wound closure of HDFs as compared to the control cells — treated with non-EVs control batches processed equally to the EVs batches — (Fig. 5B,C). A complete wound closure was achieved in all EVs-treated groups within 48 h, whereas the wound was still open in the control group (Fig. 5B). We did not

observe significant differences between any of the EVs groups however, AT-P10K and HF-P10K obtained earlier significant differences — vs control group — as compared to their respective P100K EVs. We also measured the migration rate of the HDFs. As observed in the Fig. 5D only at the time-point of 8 h we achieved an increased migration rate in all groups as compared to the control group. Surprisingly, we did not obtain significant differences among all groups in the rest of the time-points. These results depicted that the main effect of EVs on the migration of HDFs was given between 4-8 h of treatment and maintained during the rest of the time-points.

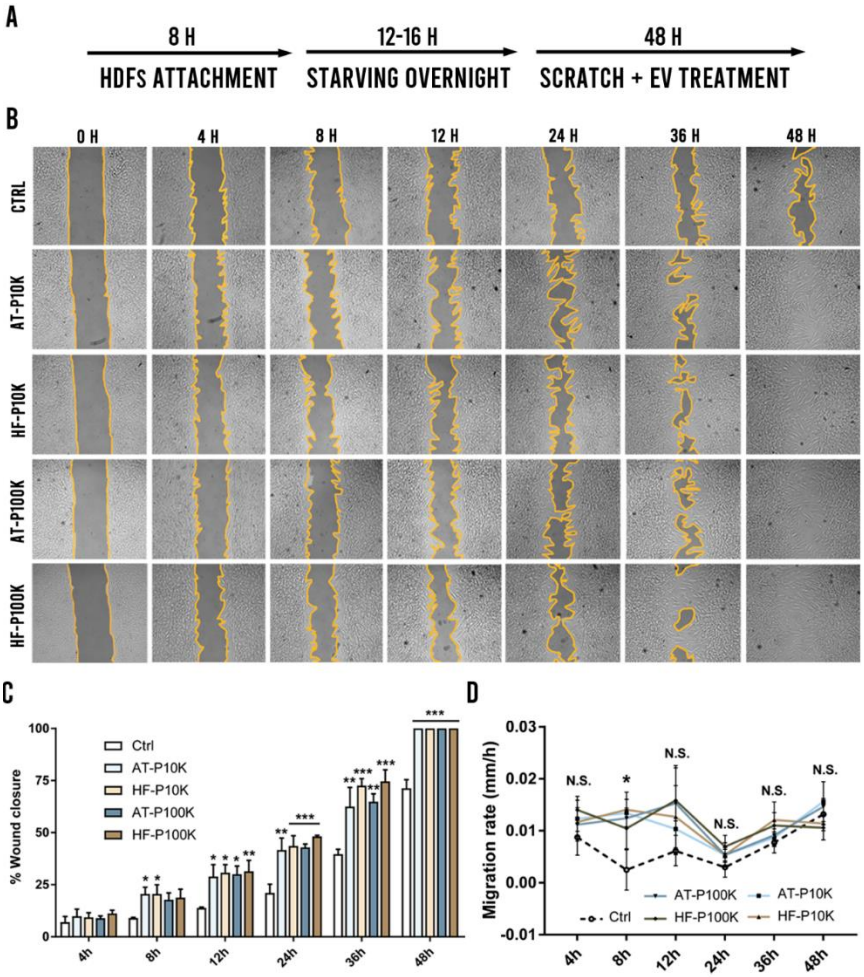

Fig. 5. Scratch assay. (A) Experimental setup. (B) Images of the treated and control groups at different time-points of the scratch assay (n=3). (C) Percentages of wound closure at the different time-points. * $p<0.05$, ** $p<0.005$, *** $p<0.001$ against the control group. (D) Migration rate of HDFs at different time-points. * $p<0.05$ of all groups against the control group. N.S. Non-significant.

Tube formation assay

The biological process of angiogenesis involves the proliferation, migration and tube formation of endothelial cells. The formation of new vessels can determine the outcome of chronic wound healing because the newly formed vessels allow the oxygenation and nutrient supply to the wound site [7, 26]. To analyze the effect of

the studied MSC-EVs on migration and tube formation of endothelial cells, EVs were incubated with HUVECs on a Matrigel® niche. As shown in Fig. 6A, the groups treated with EVs remarkably enhanced the number of formed tubes as compared to the control group — HUVECs treated with non-EVs control batches processed equally to the EVs batches —. We did not obtain significant differences between the EVs-treated groups and the positive control group — complete medium —. Neither were differences found within the groups treated with EVs — neither P10K nor P100K —.

Furthermore, we studied the tube diameter length and the number of branching points — union points of formed tubes — (Fig. 6B and 6C). We did not observe differences in the tube diameter length between the different cell types, pellets and controls but, in accordance with the number of formed tubes, the treated groups obtained a higher number of branching points in comparison with the control group (Fig. 6D). Moreover, AT-P10K, HF-P10K and HF-P100K obtained a higher number of branching points as compared to the positive control.

Reactive oxygen species (ROS) protection assay

Having achieved biological effects on HDFs proliferation and migration, we then studied the protective effects of EVs against ROS, which are commonly present in chronic wound scenarios [27]. As can be seen in the Fig. 6E, we did not obtain significant differences in the EVs-treated groups as compared to the control group in any of the performed assays. We observed that a 2 h and 6 h pre-treatment of HDFs with complete medium — positive control — did not showed differences in the ROS apoptotic protection as compared to the control group (Fig. 6E-I and 6E-II). However, in a 4 h of co-culture with EVs and H2O2, only the positive control achieved better outcomes as compared to the rest of the groups. This may be expected because of the presence of ascorbic acid in the medium supplementation (Fig. 6E-III).

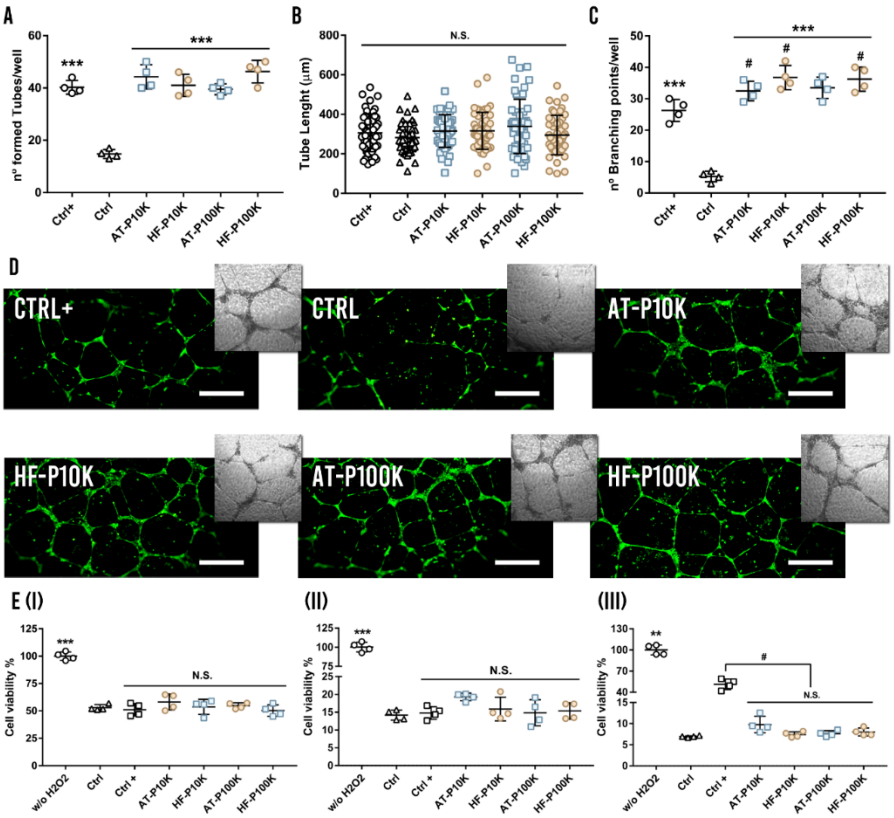

Fig. 6. Angiogenesis and antioxidant assays. (A) Number of formed tubes per well (n=4). (B) Diameter length of the formed tubes. (C) Number of branching points per well. *** $p<0.001$ against the control group, # $p<0.05$ against the positive control group, N.S. non-significance. (D) Calcein-stained fluorescence and brightfield images of the formed vessels. Scale bars are 500 μm. (E) Cell survival under a H2O2-mediated ROS environment (I) after a 2 h pre-treatment with EVs (n=4), (II) after a 6 h pre-treatment with EVs (n=4) and (III) under a 4 h co-treatment of cells with EVs and H2O2 (n=4). ** $p<0.005$, *** $p<0.001$, n.s. non significance against control group, # $p<0.05$ between groups.

Cell survival under hyperglycaemia assay

Diabetic ulcers — a kind of chronic wounds — are characterized by a persistent inflammatory status with insufficient oxygen and nutrient accessibility caused by elevated glucose levels. As a result, a hypoxic environment with an elevated oxidative stress is formed, leading fibroblasts, as well as other skin cell types, to

die [28, 29]. To study the cell survival of HDFs under a hyperglycemic environment we pre-treated HDFs with EVs for 6 h before exposing them to hyperglycemia. As observed in Fig. 7A, at 24 h we only obtained differences against the control group — HDFs treated with non-EVs control batches processed equally to the EVs batches — in the HF-P10K and positive control groups. However, after 48 h of hyperglycemic exposure, we achieved significant differences against the control in all the EVs-treated groups. Furthermore, AT-P10K and HF-P10K obtained higher outcomes as compared to the positive control group — complete medium —. We also observed that the EVs-treated groups did not obtain significant differences against the non-hyperglycemic group at this time point. Finally, at 72 h of hyperglycemia, we achieved significantly higher cell survival in the EVs-treated groups as compared to the control and positive control groups (Fig. 7B).

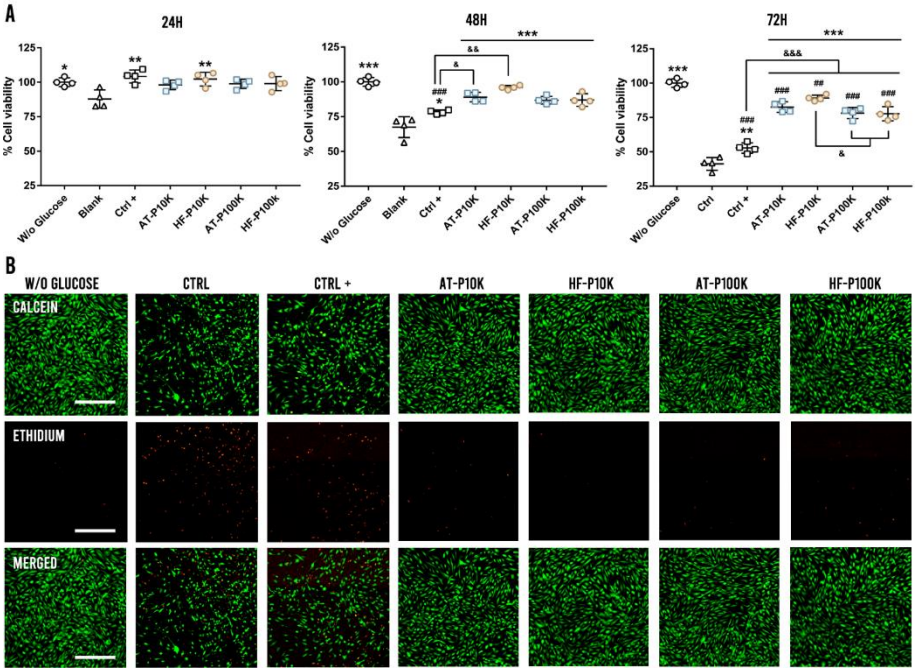

Fig. 7. Cell survival under hyperglycemia assay. (A) Percentage of cell viability under hyperglycemia at 24 h, 48 h and 72 h (n=4). * $p<0.05$, ** $p<0.005$, *** $p<0.001$ against the control group, ## $p<0.005$, ### $p<0.001$ against W/o glucose group, & $p<0.05$, && $p<0.005$, &&& $p<0.001$

between groups. (B) Calcein/ethidium stained images of the survival cells at 72 h of hyperglycemia. Scale bars are 500 μm.

Discussion

While MSC-EVs have gained the attention of scientific community in the field of tissue engineering and regenerative medicine, there is still a race for the development of the most suitable and effective MSC-EVs therapy. AT-EVs have largely demonstrated their potential in chronic wound healing scenarios [28, 30-36]. However, to the best of our knowledge, to date there is no work characterizing and analyzing the therapeutic potential of HF-EVs in this field, or in any other. For such aim, we first analyzed the size and morphology of the isolated EVs. Both AT-EVs and HF-EVs had round-shaped bi-membrane morphologies and the size ranges varied between 50-700 nm for P10K EVs and between 30-400 nm for P100K EVs by using NTA and Cryo-EM images. These size results are consistent with those reported in the literature using UC as the isolation method for MSC-EVs [37-40].

There is a vast number of works analyzing MSC-EVs by electron microscopy [41-44]. However, a few works have visualized MSC-EVs by using cryo-EM and none of them has quantified the percentage of their protein decoration [33, 45-47]. This technique allows reducing sample damaging and the appearance of artefacts caused by fixation, dehydratation or the addition of heavy metals [48]. Our results depicted that, by using UC as the isolation method, only a small percentage of MSC-EVs presented proteins decorating their membrane — approximately 8% on P10K EVs and 15% on P100K EVs —. Further studies should be carried out to analyze if the percentage of protein decoration on MSC-EVs would be modified by using different isolation/purification methods. However, a seminal work by Rizzo et al. described that, by using UC as the isolation method, the 90% of the isolated EVs — obtained from C. Neoformans — presented protein decorated membranes [49]. Moreover, another work by Noble et al. mentioned that m-lEVs had more protein-membrane decoration than sEVs in the MCF10A cell line by using cryo-EM images [50]. However, they did not quantify the percentage of membrane-decorated EVs. These results may suggest that the protein decoration of EVs could be more influenced by the EV-source rather than the biogenesis or isolation

method used. In addition, it has also been described the spontaneous formation of a "protein corona" around the surface of nanoparticles, viruses and EVs as a protein aggregation on membranes [51-53]. Thus, a more thorough analysis should be made to identify if these molecules are spontaneously formed or native components of EVs, and whether they influence the biological activity of these EVs. For example, some authors have argued that the presence of these protein coronas on different nanoparticles have a major influence on their bioavailability and biodistribution [52, 53].

To ensure the reproducibility and quality of EV-based treatments, the establishment of a reliable and standardized isolation method for EVs is crucial. For such purpose, we studied the batch-to-batch reproducibility of the isolated EVs. Despite mean and mode size results had adequate reproducibility between batches for both pellets and cell types, results depicted that the number of EVs regarding the final cell count had greater variations. These results may suggest that AT-MSCs produce naturally larger quantities of EVs than HF-MSCs in the studied conditions. The characterization of the EVs protein markers by western blotting showed the presence of CD13 — a marker of stemness associated to regeneration properties — in both cell lines [54], as well as the presence of CD81 in all the preparations. The results for CD63 presented a different trafficking of this molecule, since AT-MSCs released more protein in EVs, while HF-MSCs cells kept most of the protein intracellularly. This retention, together with the absence of CD9 in HF-EVs, the slightly increase of CD81 in the sEVs population secreted by HF-MSCs, and the retention of LAMP1 in HF-MSCs, suggest that both cell lines had a different balance of endosomal/ectosomal mechanism of EVs biogenesis [55]. Nevertheless, further studies inhibiting those routes would be necessary to clarify their relative importance. We also observed the presence of COXIV, a protein associated to mitochondria. The presence of mitochondrial proteins in some populations of EVs has been described in melanoma preparations [56], among other cell types, giving rise to the recently coined term "mitovesicles" [57].

The surface marker analysis of EVs by flow cytometry depicted significant differences in the expression profile of different proteins between both cell types and pellets. Using this technique, we demonstrated the presence of the

transmembrane proteins CD9, CD63, and CD81 in all EVs. Interestingly, the results observed for those markers differ from western blot analysis. The reasons behind may lie in the technical differences between both approaches; bead capture only measures exposed epitopes, while western blotting shows the contribution for all the protein content of the preparation. Western blot quantification has also information regarding the size of the protein. Fig. S5 shows the presence of bands detected by the antibody with higher strength in HF-EVs, below 37 kDa, which certainly can compensate the differences observed in the western blot between 37 and 50 kDa.

Another highly expressed marker in all of our EVs was SSEA-4, an embryonic stem cell marker popularly known as a "stemness" marker. It has been described the presence of this molecule in EVs from bone marrow MSCs (BM-MSCs), AT-MSCs [58, 59] as well as in other MSCs [60, 61]. Based on our findings, we observed the expression of SSEA-4 in sEVs and m-lEVs derived from both HF-MSCs and AT-MSCs. Furthermore, we also noticed the expression of CD105, a characteristic MSCs marker [62]. Specifically, we observed more expression in P10K EVs than in P100K EVs, for both cell types. In terms of functionality, AT-EVs and HF-EVs expressed several adhesion molecules such as CD29, CD44 and CD49e — mostly in P10K EVs —, which facilitate their homing to inflamed and injured tissues such as chronic wounds [63]. Another interesting marker found slightly represented in both P10K EVs — but not in P100K — was CD146 or melanoma cell adhesion molecule (MCAM), a molecule involved in permeability, monocyte transmigration and angiogenesis that is present in many tumors and endothelial cells [64, 65]. Another melanoma-associated marker found in all EVs — but especially found in HF-EVs — was MCSP. This molecule is a highly expressed marker in benign and malign melanomas and melanoma-derived EVs [66, 67]. However, the expression of MCSP in healthy tissues has also been described [66]. Ghali et al. demonstrated that HF-MSCs, among other hair follicle surrounding cells, express MCSP [68]. Thus, our results depicted that the EVs shuttled by HF-MSCs also express MCSP. Tissue factor (TF), also known as CD142 is recognized as one of the most important players in the coagulation process [69, 70]. Furthermore, it has been described that this marker also plays a role in wound re-epithelialization and necrosis [70]. The fact that principally P10K HF-EVs

expressed this marker may suggests a more important role for HF-EVs than AT-EVs in the earliest phases of the wound healing process. Another receptor surprisingly found only in HF-P100K was CD41b or integrin αIIβ. This marker is a well-known collagen-binding integrin found in MSCs, as well as in many other cell types such as platelets. [71-73]. Finally, the expression of CD56 was exclusively found in HF-EVs. The presence of CD56 has been commonly found in NK cells and EVs — with immunomodulatory properties [74, 75] — and in neural lineage cells [76]. However, It has been also described the presence of CD56 in HFs and this has been related to the maintenance of the hair follicle immune privilege [76-78]. Thus, the role of CD56 in HF-EVs should be investigated to clarify whether the presence of this molecule in HF-EVs may be related to immunomodulatory properties.

When we analyzed the HDFs uptake of EVs, we found no differences in the P10K and P100K uptake between both cell types. On the other hand, we found that these cells were able to better internalize m-lEVs than sEVs. Indeed, we observed an almost 10-fold fluorescence increase in HDFs after they captured m-lEVs as compared to sEVs. Although different aspects can influence this result, such as the number of membrane bound fluorochrome per vesicle in both m-lEV and sEVs, it is noteworthy that P10K EVs were able to induce a higher increase in cell proliferation than P100Ks in both cell types. More studies should be made in this regard to clarify whether these effects are related to a higher internalization or to intrinsic properties of the different EV populations. Furthermore, an additional analysis should be carried out in order the test the internalization efficacy of HDFs in the presence of other cell types such as phagocytes, keratinocytes etc. Regardless of that, our results confirmed that both m-lEVs and sEVs were able to increase proliferation of fibroblasts, as previously described in MSCs [35, 79]. Interestingly, we found that P10Ks were able to increase the proliferation of HDFs up to 25-40% more than P100Ks. It has been previously described the proliferative effect of m-lEVs on AT-MSCs [35], however, we have not found any work comparing the proliferative potency of sEVs vs m-lEVs in AT-MSCs neither in HF-MSCs. Promoting the migration of fibroblasts has also been an important requirement for every developing therapy intended for chronic wounds [7]. Besides the proliferative effects of MSC-EVs on different cell types, it has been also

described that MSC-EVs can also promote the migration of fibroblasts, among other cell types [80]. In this work, we demonstrated that HF-EVs and AT-EVs alike were able to promote the migration of HDFs. Furthermore, we found that the effect observed on HDFs migration was achieved between 4-8 h — regardless of cell and pellet type — 8 h and was maintained until the end of the assay.

Numerous studies have demonstrated that the oxidative stress increases tissue inflammation resulting in a stagnation of the wound healing process [81, 82]. In addition, a dysfunction of the vasculature, along with limited neovascularization and angiogenic processes, creates hypoxic conditions in chronic wounds [7, 83]. Some works have demonstrated that EVs derived from different cell populations can protect diverse cell types against ROS-induced apoptosis [84, 85]. In this regard, different MSC-EVs obtained from bone marrow or umbilical cord have demonstrated ROS-protective effects on cardiac stem cells and HaCaT cells [86, 87]. In contrast, only few researchers have described protective effects against ROS-induced apoptosis by means of AT-EVs on cardiomyocytes [88], NIH3T3 fibroblasts [28] and HDFs [89]. Here, we did not achieve such protective effects in any of the studied conditions with any of our pellet or cell types. In keeping with these results, Matsuoka et al. only observed a 10% of viability increase in the EVs-treated groups when compared to the control group. However, they did not employ a EVs-depleted medium in the assay. Based on all these findings, a more thorough analysis is warranted to clarify the role of MSC-EVs on the viability of HDFs under H2O2 oxidative stress.

It has been largely described the angiogenic potential of different MSC-EVs such as those produced by BM-MSCs, umbilical cord MSCs (UC-MSCs) or AT-MSCs, among others. Such effect has been attributed to the transfer of pro-angiogenic proteins — VEGF, PDGF, EGF, FGF etc. — and mi-RNAs including miR-31or miR-125 among others [90-92]. In this work, we found pro-angiogenic properties not only in AT-EVs but also in HF-EVs with both assayed pellets. Once again, we did not observe differences among groups in the size or morphology of the formed vessels. The need for increased blood flow and oxygenation reaches a high importance in diabetic chronic ulcers. The hyperglycemic microenvironment associated with diabetes challenges cell survival in diabetic wounds, causing

oxidative stress and delaying the healing. For example, it has been described that hyperglycemia destabilizes HIF-1α and impairs its function at a concentration of 30 mM [28]. Our results depicted that with only a 6 h of pre-treatment, all EVs were able to protect and increase cell survival of HDFs under a cytotoxic hyperglycemic environment after 24 h of treatment and at least until 72 h of assay. Interestingly, our results were even better than those obtained by the positive control group — complete medium —. Here, we found that both pellets from AT-MSCs and HF-MSCs were able to reduce oxidative stress and increase HDFs metabolism and viability under a hyperglycemic condition.

Conclusions

In conclusion, in this work, we describe for the first time to our knowledge, a complete characterization and functional comparison of m-lEVs and sEVs obtained from HF-MSCs against those obtained from AT-MSCs. Here, we made an in vitro screening of different MSC-EVs populations in different bio-relevant assays in order to analyze the efficacy of the formulations. We demonstrated the presence of the classical EV-markers among many others involved in biological processes not only in sEVs but also in m-lEVs. In this regard, HF-EVs showed a better "pro-regenerative" marker profile than AT-EVs for both m-lEVs and sEVs. We also analyzed the batch-to-batch production, the morphology and the protein decoration of these EVs depicting some differences between both cell types and pellets. Furthermore, we demonstrated that HF-EVs, equal than AT-EVs, were able to induce migration and proliferation in HDFs, as well as angiogenesis in HUVECs. However, we found that m-lEVs obtained better outcomes increasing HDFs proliferation. We did not observe protective effects against H2O2-induced oxidative stress in HDFs, but did prove that HF-EVs could protect HDFs from cell death and oxidative stress under hyperglycemic conditions to the same extent as AT-EVs. Altogether, we here postulate a promising source of EVs — not only sEVs but also m-lEVs — obtained from HF-MSCs with a great potential for chronic wound treatments and regenerative medicine therapies in general.

List of abbreviations

MSCs: Mesenchymal stromal cells; EVs: Extracellular vesicles; HFs: Hair follicles; AT: Adipose tissue; HDFs: Human dermal Fibroblasts; HUVECs: Human umbilical vein endothelial cells; NTA: Nanoparticle tracking analysis; WB: Western blot; Cryo-EM: Cryo electron microscopy; DAPI: 2-(4-amidinophenyl)-1 h-indole-6-carboxamidine; CCK8: Cell counting kit 8; ROS: Reactive oxygen species.

Declarations

ETHICS APPROVAL AND CONSENT TO PARTICIPATE

Hair follicles were obtained from occipital scalps of routine hair transplant procedures with the application of FUE technique (Clínica Dermatológica Ercilla, Spain). All patients signed an informed consent under an approved protocol (M10_2019_053, M30_2019_054) by the research ethics committee of the Basque Country.

CONSENT FOR PUBLICATION

Not applicable

DATA AVAILABILITY STATEMENT

Raw data is available from the corresponding author upon reasonable request.

COMPETING INTERESTS

The authors declare that no competing interest exists.

FUNDING

This research was funded by the Basque Government (Consolidated Groups, IT907-16 and PRE_2018_1_0412).

AUTHOR CONTRIBUTIONS

RMH, JMFP, ESV, KLEH and FR contributed to methodology and conceptualization; KLH, FR and CGV contributed to investigation; KLH and FR contributed to data analysis and curation; KLH and FR contributed to writing—

original draft; ESV, RMH, MI, FR and JMFP contributed to correction and edition of the manuscript; and RMH, MI and JMFP contributed to funding acquisition.

ACKNOWLEDGMENTS

Authors also acknowledge the electron microscopy platform of CIC bioGUNE and ICTS “NANBIOSIS” (Drug Formulation Unit, U10) for their contribution.

Supplementary information

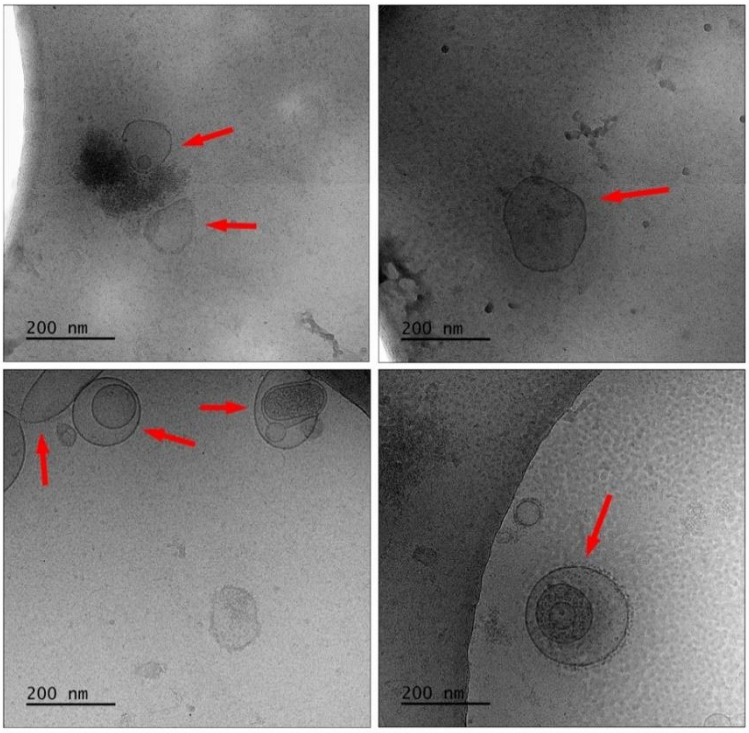

Fig. S1. Cryo-EM images of the diverse heterogeneity of EVs populations.

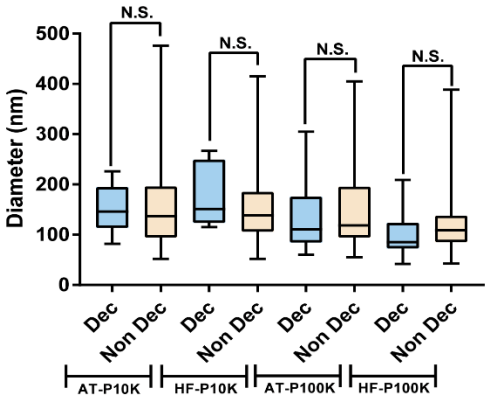

Fig. S2. Comparison in decoration of EVs vs EVs diameter.

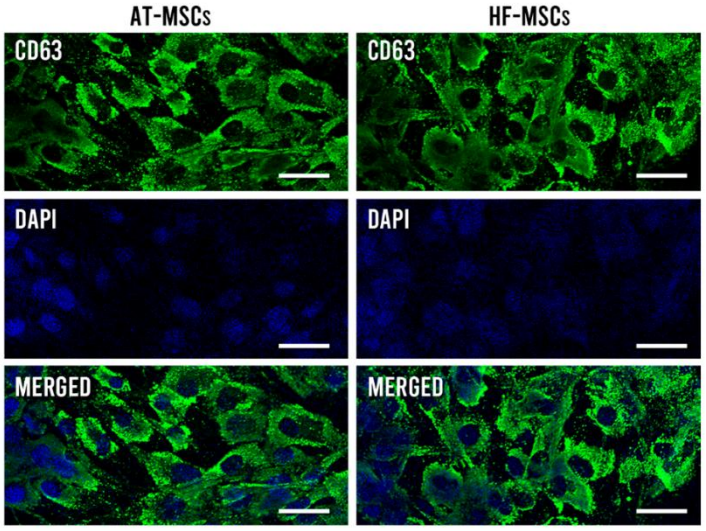

Fig. S3. CD63/DAPI staining of AT-MSCs and HF-MSCs. Scale bars are 40 μm.

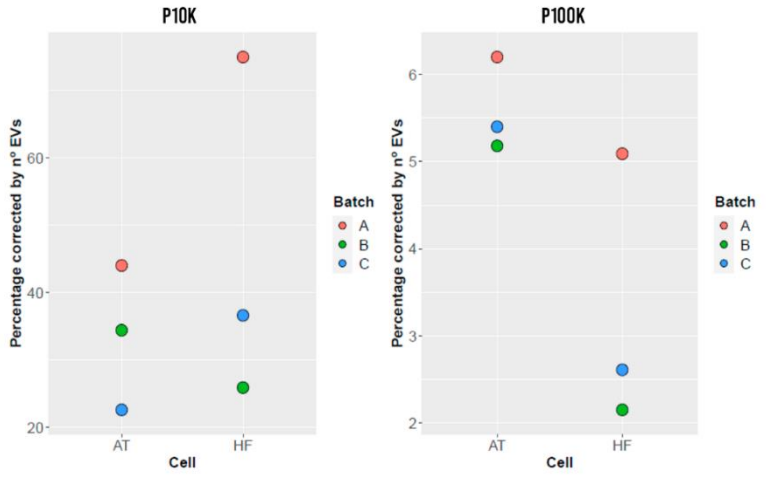

Fig. S4. Percentage of positive events according to the flow cytometry study corrected by the number of EVs for each type of EVs and for the different batch preparations.

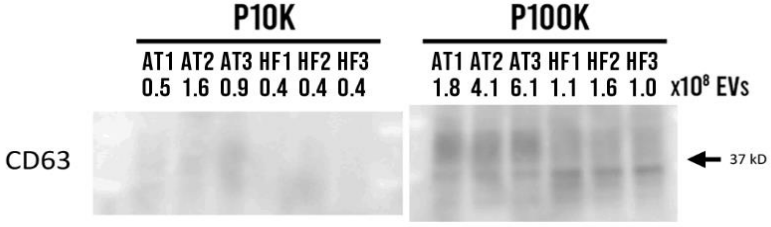

Fig. S5. CD63 Western Blot extended membrane

References

[1] P.A. Martino, N. Heitman, M. Rendl, The dermal sheath: An emerging component of the hair follicle stem cell niche, Exp. Dermatol. 30 (2021) 512-521.

[2] B. Wang, X.M. Liu, Z.N. Liu, Y. Wang, X. Han, A.B. Lian, Y. Mu, M.H. Jin, J.Y. Liu, Human hair follicle-derived mesenchymal stem cells: Isolation, expansion, and differentiation, World J. Stem Cells. 12 (2020) 462-470.

[3] P. Gentile, S. Garcovich, Advances in Regenerative Stem Cell Therapy in Androgenic Alopecia and Hair Loss: Wnt pathway, Growth-Factor, and Mesenchymal Stem Cell Signaling

Impact Analysis on Cell Growth and Hair Follicle Development, Cells. 8 (2019) 10.3390/cells8050466.

[4] D. Zhou, H. Cheng, J. Liu, L. Zhang, Establishment of human hair follicle mesenchymal stem cells with overexpressed human hepatocyte growth factor, Iran. J. Basic Med. Sci. 20 (2017) 662-675.

[5] Y. Wang, J. Liu, X. Tan, G. Li, Y. Gao, X. Liu, L. Zhang, Y. Li, Induced pluripotent stem cells from human hair follicle mesenchymal stem cells, Stem Cell. Rev. Rep. 9 (2013) 451-460.

[6] K.A.U. Gonzales, E. Fuchs, Skin and Its Regenerative Powers: An Alliance between Stem Cells and Their Niche, Dev. Cell. 43 (2017) 387-401.

[7] K. Las Heras, M. Igartua, E. Santos-Vizcaino, R.M. Hernandez, Chronic wounds: Current status, available strategies and emerging therapeutic solutions, J. Control. Release. 328 (2020) 532-550.

[8] Y. Han, X. Li, Y. Zhang, Y. Han, F. Chang, J. Ding, Mesenchymal Stem Cells for Regenerative Medicine, Cells. 8 (2019) 10.3390/cells8080886.

[9] P. Gentile, S. Garcovich, Systematic Review of Platelet-Rich Plasma Use in Androgenetic Alopecia Compared with Minoxidil((R)), Finasteride((R)), and Adult Stem Cell-Based Therapy, Int. J. Mol. Sci. 21 (2020) 10.3390/ijms21082702.

[10] P. Gentile, M.G. Scioli, A. Bielli, B. De Angelis, C. De Sio, D. De Fazio, G. Ceccarelli, A. Trivisonno, A. Orlandi, V. Cervelli, S. Garcovich, Platelet-Rich Plasma and Micrografts Enriched with Autologous Human Follicle Mesenchymal Stem Cells Improve Hair Re-Growth in Androgenetic Alopecia. Biomolecular Pathway Analysis and Clinical Evaluation, Biomedicines. 7 (2019) 10.3390/biomedicines7020027.

[11] D. Ma, J.E. Kua, W.K. Lim, S.T. Lee, A.W. Chua, In vitro characterization of human hair follicle dermal sheath mesenchymal stromal cells and their potential in enhancing diabetic wound healing, Cytotherapy. 17 (2015) 1036-1051.

[12] K.L. Heras, M. Igartua, E. Santos-Vizcaino, R.M. Hernandez, Cell-based dressings: A journey through chronic wound management, Biomaterials Advances. (2022) 212738.

[13] P.R. Baraniak, T.C. McDevitt, Stem cell paracrine actions and tissue regeneration, Regen. Med. 5 (2010) 121-143.

[14] A. Nagelkerke, M. Ojansivu, L. van der Koog, T.E. Whittaker, E.M. Cunnane, A.M. Silva, N. Dekker, M.M. Stevens, Extracellular vesicles for tissue repair and regeneration: evidence, challenges and opportunities, Adv. Drug Deliv. Rev. (2021).

[15] E. Munoz-Perez, A. Gonzalez-Pujana, M. Igartua, E. Santos-Vizcaino, R.M. Hernandez, Mesenchymal Stromal Cell Secretome for the Treatment of Immune-Mediated Inflammatory Diseases: Latest Trends in Isolation, Content Optimization and Delivery Avenues, Pharmaceutics. 13 (2021) 10.3390/pharmaceutics13111802.

[16] R. Kalluri, V.S. LeBleu, The biology, function, and biomedical applications of exosomes, Science. 367 (2020) 10.1126/science.aau6977.

[17] O.P.B. Wiklander, M.A. Brennan, J. Lotvall, X.O. Breakefield, S. El Andaloussi, Advances in therapeutic applications of extracellular vesicles, Sci. Transl. Med. 11 (2019) 10.1126/scitranslmed.aav8521.

[18] J. Cabral, A.E. Ryan, M.D. Griffin, T. Ritter, Extracellular vesicles as modulators of wound healing, Adv. Drug Deliv. Rev. 129 (2018) 394-406.

[19] D. Tsiapalis, L. O'Driscoll, Mesenchymal Stem Cell Derived Extracellular Vesicles for Tissue Engineering and Regenerative Medicine Applications, Cells. 9 (2020) 10.3390/cells9040991.

[20] A. K A Silva, M. Morille, M. Piffoux, S. Arumugam, P. Mauduit, J. Larghero, A. Bianchi, K. Aubertin, O. Blanc-Brude, D. Noel, E. Velot, C. Ravel, C. Elie-Caille, A. Sebbagh, C. Boulanger, C. Wilhelm, G. Rahmi, I. Raymond-Letron, K. Cherukula, T. Montier, C. Martinaud, J.M. Bach, O. Favre-Bulle, J. Spadavecchia, C. Jorgensen, P. Menasche, C. Aussel, J. Chopineau, M. Mosser, M. Ullah, N. Sailliet, N. Luciani, N. Mathieu, P.E. Rautou, S. Brouard, W. Boireau, S. Jauliac, M. Dedier, J.H. Trouvin, F. Gazeau, M. Trouillas, J. Peltzer, A. Monsel, S. Banzet, Development of extracellular vesicle-based medicinal products: a position paper of the group "Extracellular Vesicle translatiOn to clinicaL perspectiVEs - EVOLVE France", Adv. Drug Deliv. Rev. (2021) 114001.

[21] C. Thery, K.W. Witwer, E. Aikawa, M.J. Alcaraz, J.D. Anderson, R. Andriantsitohaina, A. Antoniou, T. Arab, F. Archer, G.K. Atkin-Smith, D.C. Ayre, J.M. Bach, D. Bachurski, H. Baharvand, L. Balaj, S. Baldacchino, N.N. Bauer, A.A. Baxter, M. Bebawy, C. Beckham, A. Bedina Zavec, A. Benmoussa, A.C. Berardi, P. Bergese, E. Bielska, C. Blenkiron, S. Bobis-Wozowicz, E. Boilard, W. Boireau, A. Bongiovanni, F.E. Borras, S. Bosch, C.M. Boulanger, X. Breakefield, A.M. Breglio, M.A. Brennan, D.R. Brigstock, A. Brisson, M.L. Broekman, J.F. Bromberg, P. Bryl-Gorecka, S. Buch, A.H. Buck, D. Burger, S. Busatto, D. Buschmann, B.

Bussolati, E.I. Buzas, J.B. Byrd, G. Camussi, D.R. Carter, S. Caruso, L.W. Chamley, Y.T. Chang, C. Chen, S. Chen, L. Cheng, A.R. Chin, A. Clayton, S.P. Clerici, A. Cocks, E. Cocucci, R.J. Coffey, A. Cordeiro-da-Silva, Y. Couch, F.A. Coumans, B. Coyle, R. Crescitelli, M.F. Criado, C. D'Souza-Schorey, S. Das, A. Datta Chaudhuri, P. de Candia, E.F. De Santana, O. De Wever, H.A. Del Portillo, T. Demaret, S. Deville, A. Devitt, B. Dhondt, D. Di Vizio, L.C. Dieterich, V. Dolo, A.P. Dominguez Rubio, M. Dominici, M.R. Dourado, T.A. Driedonks, F.V. Duarte, H.M. Duncan, R.M. Eichenberger, K. Ekstrom, S. El Andaloussi, C. Elie-Caille, U. Erdbrugger, J.M. Falcon-Perez, F. Fatima, J.E. Fish, M. Flores-Bellver, A. Forsonits, A. Frelet-Barrand, F. Fricke, G. Fuhrmann, S. Gabrielsson, A. Gamez-Valero, C. Gardiner, K. Gartner, R. Gaudin, Y.S. Gho, B. Giebel, C. Gilbert, M. Gimona, I. Giusti, D.C. Goberdhan, A. Gorgens, S.M. Gorski, D.W. Greening, J.C. Gross, A. Gualerzi, G.N. Gupta, D. Gustafson, A. Handberg, R.A. Haraszti, P. Harrison, H. Hegyesi, A. Hendrix, A.F. Hill, F.H. Hochberg, K.F. Hoffmann, B. Holder, H. Holthofer, B. Hosseinkhani, G. Hu, Y. Huang, V. Huber, S. Hunt, A.G. Ibrahim, T. Ikezu, J.M. Inal, M. Isin, A. Ivanova, H.K. Jackson, S. Jacobsen, S.M. Jay, M. Jayachandran, G. Jenster, L. Jiang, S.M. Johnson, J.C. Jones, A. Jong, T. Jovanovic-Talisman, S. Jung, R. Kalluri, S.I. Kano, S. Kaur, Y. Kawamura, E.T. Keller, D. Khamari, E. Khomyakova, A. Khvorova, P. Kierulf, K.P. Kim, T. Kislinger, M. Klingeborn, D.J. Klinke, M. Kornek, M.M. Kosanovic, A.F. Kovacs, E.M. Kramer-Albers, S. Krasemann, M. Krause, I.V. Kurochkin, G.D. Kusuma, S. Kuypers, S. Laitinen, S.M. Langevin, L.R. Languino, J. Lannigan, C. Lasser, L.C. Laurent, G. Lavieu, E. Lazaro-Ibanez, S. Le Lay, M.S. Lee, Y.X.F. Lee, D.S. Lemos, M. Lenassi, A. Leszczynska, I.T. Li, K. Liao, S.F. Libregts, E. Ligeti, R. Lim, S.K. Lim, A. Line, K. Linnemannstons, A. Llorente, C.A. Lombard, M.J. Lorenowicz, A.M. Lorincz, J. Lotvall, J. Lovett, M.C. Lowry, X. Loyer, Q. Lu, B. Lukomska, T.R. Lunavat, S.L. Maas, H. Malhi, A. Marcilla, J. Mariani, J. Mariscal, E.S. Martens-Uzunova, L. Martin-Jaular, M.C. Martinez, V.R. Martins, M. Mathieu, S. Mathivanan, M. Maugeri, L.K. McGinnis, M.J. McVey, D.G. Meckes, K.L. Meehan, I. Mertens, V.R. Minciacchi, A. Moller, M. Moller Jorgensen, A. Morales-Kastresana, J. Morhayim, F. Mullier, M. Muraca, L. Musante, V. Mussack, D.C. Muth, K.H. Myburgh, T. Najrana, M. Nawaz, I. Nazarenko, P. Nejsum, C. Neri, T. Neri, R. Nieuwland, L. Nimrichter, J.P. Nolan, E.N. Nolte-'t Hoen, N. Noren Hooten, L. O'Driscoll, T. O'Grady, A. O'Loghlen, T. Ochiya, M. Olivier, A. Ortiz, L.A. Ortiz, X. Osteikoetxea, O. Ostergaard, M. Ostrowski, J. Park, D.M. Pegtel, H. Peinado, F. Perut, M.W. Pfaffl, D.G. Phinney, B.C. Pieters, R.C. Pink, D.S. Pisetsky, E. Pogge von Strandmann, I. Polakovicova, I.K. Poon, B.H. Powell, I. Prada, L. Pulliam, P. Quesenberry, A. Radeghieri, R.L. Raffai, S. Raimondo, J. Rak, M.I. Ramirez, G. Raposo, M.S. Rayyan, N. Regev-Rudzki, F.L. Ricklefs, P.D. Robbins, D.D. Roberts, S.C. Rodrigues, E. Rohde, S. Rome, K.M. Rouschop, A. Rughetti, A.E. Russell, P. Saa, S. Sahoo, E. Salas-Huenuleo, C. Sanchez, J.A. Saugstad, M.J. Saul, R.M. Schiffelers, R. Schneider, T.H. Schoyen, A. Scott, E. Shahaj, S. Sharma, O. Shatnyeva, F. Shekari, G.V.

Shelke, A.K. Shetty, K. Shiba, P.R. Siljander, A.M. Silva, A. Skowronek, O.L. Snyder, R.P. Soares, B.W. Sodar, C. Soekmadji, J. Sotillo, P.D. Stahl, W. Stoorvogel, S.L. Stott, E.F. Strasser, S. Swift, H. Tahara, M. Tewari, K. Timms, S. Tiwari, R. Tixeira, M. Tkach, W.S. Toh, R. Tomasini, A.C. Torrecilhas, J.P. Tosar, V. Toxavidis, L. Urbanelli, P. Vader, B.W. van Balkom, van der Grein, S G, J. Van Deun, M.J. van Herwijnen, K. Van Keuren-Jensen, G. van Niel, M.E. van Royen, A.J. van Wijnen, M.H. Vasconcelos, I.J. Vechetti, T.D. Veit, L.J. Vella, E. Velot, F.J. Verweij, B. Vestad, J.L. Vinas, T. Visnovitz, K.V. Vukman, J. Wahlgren, D.C. Watson, M.H. Wauben, A. Weaver, J.P. Webber, V. Weber, A.M. Wehman, D.J. Weiss, J.A. Welsh, S. Wendt, A.M. Wheelock, Z. Wiener, L. Witte, J. Wolfram, A. Xagorari, P. Xander, J. Xu, X. Yan, M. Yanez-Mo, H. Yin, Y. Yuana, V. Zappulli, J. Zarubova, V. Zekas, J.Y. Zhang, Z. Zhao, L. Zheng, A.R. Zheutlin, A.M. Zickler, P. Zimmermann, A.M. Zivkovic, D. Zocco, E.K. Zuba-Surma, Minimal information for studies of extracellular vesicles 2018 (MISEV2018): a position statement of the International Society for Extracellular Vesicles and update of the MISEV2014 guidelines, J. Extracell Vesicles. 7 (2018) 1535750.

[22] B. Hernaez-Estrada, A. Gonzalez-Pujana, A. Cuevas, A. Izeta, K.L. Spiller, M. Igartua, E. Santos-Vizcaino, R.M. Hernandez, Human Hair Follicle-Derived Mesenchymal Stromal Cells from the Lower Dermal Sheath as a Competitive Alternative for Immunomodulation, Biomedicines. 10 (2022).

[23] EV-TRACK Consortium, J. Van Deun, P. Mestdagh, P. Agostinis, O. Akay, S. Anand, J. Anckaert, Z.A. Martinez, T. Baetens, E. Beghein, L. Bertier, G. Berx, J. Boere, S. Boukouris, M. Bremer, D. Buschmann, J.B. Byrd, C. Casert, L. Cheng, A. Cmoch, D. Daveloose, E. De Smedt, S. Demirsoy, V. Depoorter, B. Dhondt, T.A. Driedonks, A. Dudek, A. Elsharawy, I. Floris, A.D. Foers, K. Gartner, A.D. Garg, E. Geeurickx, J. Gettemans, F. Ghazavi, B. Giebel, T.G. Kormelink, G. Hancock, H. Helsmoortel, A.F. Hill, V. Hyenne, H. Kalra, D. Kim, J. Kowal, S. Kraemer, P. Leidinger, C. Leonelli, Y. Liang, L. Lippens, S. Liu, A. Lo Cicero, S. Martin, S. Mathivanan, P. Mathiyalagan, T. Matusek, G. Milani, M. Monguio-Tortajada, L.M. Mus, D.C. Muth, A. Nemeth, E.N. Nolte-'t Hoen, L. O'Driscoll, R. Palmulli, M.W. Pfaffl, B. Primdal-Bengtson, E. Romano, Q. Rousseau, S. Sahoo, N. Sampaio, M. Samuel, B. Scicluna, B. Soen, A. Steels, J.V. Swinnen, M. Takatalo, S. Thaminy, C. Thery, J. Tulkens, I. Van Audenhove, S. van der Grein, A. Van Goethem, M.J. van Herwijnen, G. Van Niel, N. Van Roy, A.R. Van Vliet, N. Vandamme, S. Vanhauwaert, G. Vergauwen, F. Verweij, A. Wallaert, M. Wauben, K.W. Witwer, M.I. Zonneveld, O. De Wever, J. Vandesompele, A. Hendrix, EV-TRACK: transparent reporting and centralizing knowledge in extracellular vesicle research, Nat. Methods. 14 (2017) 228-232.

[24] I.B. Wall, R. Moseley, D.M. Baird, D. Kipling, P. Giles, I. Laffafian, P.E. Price, D.W. Thomas, P. Stephens, Fibroblast dysfunction is a key factor in the non-healing of chronic venous leg ulcers, J. Invest. Dermatol. 128 (2008) 2526-2540.

[25] M.L. Zou, Y.Y. Teng, J.J. Wu, S.Y. Liu, X.Y. Tang, Y. Jia, Z.H. Chen, K.W. Zhang, Z.L. Sun, X. Li, J.X. Ye, R.S. Xu, F.L. Yuan, Fibroblasts: Heterogeneous Cells With Potential in Regenerative Therapy for Scarless Wound Healing, Front. Cell. Dev. Biol. 9 (2021) 713605.

[26] P. Martin, Wound healing--aiming for perfect skin regeneration, Science. 276 (1997) 75-81.

[27] C. Dunnill, T. Patton, J. Brennan, J. Barrett, M. Dryden, J. Cooke, D. Leaper, N.T. Georgopoulos, Reactive oxygen species (ROS) and wound healing: the functional role of ROS and emerging ROS-modulating technologies for augmentation of the healing process, Int. Wound. J. 14 (2017) 89-96.

[28] P.A. Shiekh, A. Singh, A. Kumar, Exosome laden oxygen releasing antioxidant and antibacterial cryogel wound dressing OxOBand alleviate diabetic and infectious wound healing, Biomaterials. 249 (2020) 120020.

[29] R. Nunan, K.G. Harding, P. Martin, Clinical challenges of chronic wounds: searching for an optimal animal model to recapitulate their complexity, Dis. Model. Mech. 7 (2014) 1205-1213.

[30] S. Shafei, M. Khanmohammadi, R. Heidari, H. Ghanbari, V. Taghdiri Nooshabadi, S. Farzamfar, M. Akbariqomi, N.S. Sanikhani, M. Absalan, G. Tavoosidana, Exosome loaded alginate hydrogel promotes tissue regeneration in full-thickness skin wounds: An in vivo study, J. Biomed. Mater. Res. A. 108 (2020) 545-556.

[31] C. Wang, M. Wang, T. Xu, X. Zhang, C. Lin, W. Gao, H. Xu, B. Lei, C. Mao, Engineering Bioactive Self-Healing Antibacterial Exosomes Hydrogel for Promoting Chronic Diabetic Wound Healing and Complete Skin Regeneration, Theranostics. 9 (2019) 65-76.

[32] Y. An, S. Lin, X. Tan, S. Zhu, F. Nie, Y. Zhen, L. Gu, C. Zhang, B. Wang, W. Wei, D. Li, J. Wu, Exosomes from adipose-derived stem cells and application to skin wound healing, Cell Prolif. 54 (2021) e12993.

[33] J.S. Choi, W.L. Cho, Y.J. Choi, J.D. Kim, H.A. Park, S.Y. Kim, J.H. Park, D.G. Jo, Y.W. Cho, Functional recovery in photo-damaged human dermal fibroblasts by human adipose-derived stem cell extracellular vesicles, J. Extracell Vesicles. 8 (2019) 1565885.

[34] M. Pomatto, C. Gai, F. Negro, M. Cedrino, C. Grange, E. Ceccotti, G. Togliatto, F. Collino, M. Tapparo, F. Figliolini, T. Lopatina, M.F. Brizzi, G. Camussi, Differential Therapeutic Effect of Extracellular Vesicles Derived by Bone Marrow and Adipose Mesenchymal Stem Cells on Wound Healing of Diabetic Ulcers and Correlation to Their Cargoes, Int. J. Mol. Sci. 22 (2021) 10.3390/ijms22083851.

[35] S. Ren, J. Chen, D. Duscher, Y. Liu, G. Guo, Y. Kang, H. Xiong, P. Zhan, Y. Wang, C. Wang, H.G. Machens, Z. Chen, Microvesicles from human adipose stem cells promote wound healing by optimizing cellular functions via AKT and ERK signaling pathways, Stem Cell. Res. Ther. 10 (2019) 47-x.

[36] P. Gentile, S. Garcovich, Concise Review: Adipose-Derived Stem Cells (ASCs) and Adipocyte-Secreted Exosomal microRNA (A-SE-miR) Modulate Cancer Growth and proMote Wound Repair, J. Clin. Med. 8 (2019) 10.3390/jcm8060855.

[37] J.H. Lee, D.H. Ha, H.K. Go, J. Youn, H.K. Kim, R.C. Jin, R.B. Miller, D.H. Kim, B.S. Cho, Y.W. Yi, Reproducible Large-Scale Isolation of Exosomes from Adipose Tissue-Derived Mesenchymal Stem/Stromal Cells and Their Application in Acute Kidney Injury, Int. J. Mol. Sci. 21 (2020) 10.3390/ijms21134774.

[38] M. Franquesa, M.J. Hoogduijn, E. Ripoll, F. Luk, M. Salih, M.G. Betjes, J. Torras, C.C. Baan, J.M. Grinyo, A.M. Merino, Update on controls for isolation and quantification methodology of extracellular vesicles derived from adipose tissue mesenchymal stem cells, Front. Immunol. 5 (2014) 525.

[39] J. Fafian-Labora, M. Morente-Lopez, M.J. Sanchez-Dopico, O.J. Arntz, van de Loo, F A J, J. De Toro, M.C. Arufe, Influence of mesenchymal stem cell-derived extracellular vesicles in vitro and their role in ageing, Stem Cell. Res. Ther. 11 (2020) 13-0.

[40] M.Y. Konoshenko, E.A. Lekchnov, A.V. Vlassov, P.P. Laktionov, Isolation of Extracellular Vesicles: General Methodologies and Latest Trends, Biomed. Res. Int. 2018 (2018) 8545347.

[41] M. Nakazaki, T. Morita, K.L. Lankford, P.W. Askenase, J.D. Kocsis, Small extracellular vesicles released by infused mesenchymal stromal cells target M2 macrophages and promote TGF-beta upregulation, microvascular stabilization and functional recovery in a rodent model of severe spinal cord injury, J. Extracell Vesicles. 10 (2021) e12137.

[42] L.J. Born, K.H. Chang, P. Shoureshi, F. Lay, S. Bengali, A.T.W. Hsu, S.N. Abadchi, J.W. Harmon, S.M. Jay, HOTAIR-Loaded Mesenchymal Stem/Stromal Cell Extracellular Vesicles Enhance Angiogenesis and Wound Healing, Adv. Healthc. Mater. (2021) e2002070.

[43] S.C. Tao, S.C. Guo, M. Li, Q.F. Ke, Y.P. Guo, C.Q. Zhang, Chitosan Wound Dressings Incorporating Exosomes Derived from MicroRNA-126-Overexpressing Synovium Mesenchymal Stem Cells Provide Sustained Release of Exosomes and Heal Full-Thickness Skin Defects in a Diabetic Rat Model, Stem Cells Transl. Med. 6 (2017) 736-747.

[44] D. Ti, H. Hao, C. Tong, J. Liu, L. Dong, J. Zheng, Y. Zhao, H. Liu, X. Fu, W. Han, LPS-preconditioned mesenchymal stromal cells modify macrophage polarization for resolution of chronic inflammation via exosome-shuttled let-7b, J. Transl. Med. 13 (2015) 308-6.

[45] E. Priglinger, J. Strasser, B. Buchroithner, F. Weber, S. Wolbank, D. Auer, E. Grasmann, C. Arzt, D. Sivun, J. Grillari, J. Jacak, J. Preiner, M. Gimona, Label-free characterization of an extracellular vesicle-based therapeutic, J. Extracell Vesicles. 10 (2021) e12156.

[46] K.S. Lee, J. Lee, H.K. Kim, S.H. Yeom, C.H. Woo, Y.J. Jung, Y.E. Yun, S.Y. Park, J. Han, E. Kim, J.H. Sul, J.M. Jung, J.H. Park, J.S. Choi, Y.W. Cho, D.G. Jo, Extracellular vesicles from adipose tissue-derived stem cells alleviate osteoporosis through osteoprotegerin and miR-21-5p, J. Extracell Vesicles. 10 (2021) e12152.

[47] M. Monguio-Tortajada, S. Roura, C. Galvez-Monton, J.M. Pujal, G. Aran, L. Sanjurjo, M. Franquesa, M.R. Sarrias, A. Bayes-Genis, F.E. Borras, Nanosized UCMSC-derived extracellular vesicles but not conditioned medium exclusively inhibit the inflammatory response of stimulated T cells: implications for nanomedicine, Theranostics. 7 (2017) 270-284.

[48] I. Orlov, A.G. Myasnikov, L. Andronov, S.K. Natchiar, H. Khatter, B. Beinsteiner, J.F. Menetret, I. Hazemann, K. Mohideen, K. Tazibt, R. Tabaroni, H. Kratzat, N. Djabeur, T. Bruxelles, F. Raivoniaina, L.D. Pompeo, M. Torchy, I. Billas, A. Urzhumtsev, B.P. Klaholz, The integrative role of cryo electron microscopy in molecular and cellular structural biology, Biol. Cell. 109 (2017) 81-93.

[49] J. Rizzo, S.S.W. Wong, A.D. Gazi, F. Moyrand, T. Chaze, P.H. Commere, S. Novault, M. Matondo, G. Pehau-Arnaudet, F.C.G. Reis, M. Vos, L.R. Alves, R.C. May, L. Nimrichter, M.L. Rodrigues, V. Aimanianda, G. Janbon, Cryptococcus extracellular vesicles properties and their use as vaccine platforms, J. Extracell Vesicles. 10 (2021) e12129.

[50] J.M. Noble, L.M. Roberts, N. Vidavsky, A.E. Chiou, C. Fischbach, M.J. Paszek, L.A. Estroff, L.F. Kourkoutis, Direct comparison of optical and electron microscopy methods for structural characterization of extracellular vesicles, J. Struct. Biol. 210 (2020) 107474.

[51] E.A. Toth, L. Turiak, T. Visnovitz, C. Cserep, A. Mazlo, B.W. Sodar, A.I. Forsonits, G. Petovari, A. Sebestyen, Z. Komlosi, L. Drahos, A. Kittel, G. Nagy, A. Bacsi, A. Denes, Y.S. Gho, K.E. Szabo-Taylor, E.I. Buzas, Formation of a protein corona on the surface of extracellular vesicles in blood plasma, J. Extracell Vesicles. 10 (2021) e12140.

[52] K. Ezzat, M. Pernemalm, S. Palsson, T.C. Roberts, P. Jarver, A. Dondalska, B. Bestas, M.J. Sobkowiak, B. Levanen, M. Skold, E.A. Thompson, O. Saher, O.K. Kari, T. Lajunen, E. Sverremark Ekstrom, C. Nilsson, Y. Ishchenko, T. Malm, M.J.A. Wood, U.F. Power, S. Masich, A. Linden, J.K. Sandberg, J. Lehtio, A.L. Spetz, S. El Andaloussi, The viral protein corona directs viral pathogenesis and amyloid aggregation, Nat. Commun. 10 (2019) 2331-2.

[53] W. Xiao, H. Gao, The impact of protein corona on the behavior and targeting capability of nanoparticle-based delivery system, Int. J. Pharm. 552 (2018) 328-339.

[54] M.J. Lin, S. Li, L.J. Yang, D.Y. Ye, L.Q. Xu, X. Zhang, P.N. Sun, C.J. Wei, Plasma membrane vesicles of human umbilical cord mesenchymal stem cells ameliorate acetaminophen-induced damage in HepG2 cells: a novel stem cell therapy, Stem Cell. Res. Ther. 11 (2020) 225-z.

[55] M. Mathieu, N. Nevo, M. Jouve, J.I. Valenzuela, M. Maurin, F.J. Verweij, R. Palmulli, D. Lankar, F. Dingli, D. Loew, E. Rubinstein, G. Boncompain, F. Perez, C. Thery, Specificities of exosome versus small ectosome secretion revealed by live intracellular tracking of CD63 and CD9, Nat. Commun. 12 (2021) 4389-2.

[56] S.C. Jang, R. Crescitelli, A. Cvjetkovic, V. Belgrano, R. Olofsson Bagge, K. Sundfeldt, T. Ochiya, R. Kalluri, J. Lotvall, Mitochondrial protein enriched extracellular vesicles discovered in human melanoma tissues can be detected in patient plasma, J. Extracell Vesicles. 8 (2019) 1635420.

[57] P. D'Acunzo, R. Perez-Gonzalez, Y. Kim, T. Hargash, C. Miller, M.J. Alldred, H. Erdjument-Bromage, S.C. Penikalapati, M. Pawlik, M. Saito, M. Saito, S.D. Ginsberg, T.A. Neubert, C.N. Goulbourne, E. Levy, Mitovesicles are a novel population of extracellular vesicles of mitochondrial origin altered in Down syndrome, Sci. Adv. 7 (2021) 10.1126/sciadv.abe5085. Print 2021 Feb.

[58] C. Cavallo, G. Merli, R.M. Borzi, N. Zini, S. D'Adamo, M. Guescini, B. Grigolo, A. Di Martino, S. Santi, G. Filardo, Small Extracellular Vesicles from adipose derived stromal cells significantly attenuate in vitro the NF-kappaB dependent inflammatory/catabolic environment of osteoarthritis, Sci. Rep. 11 (2021) 1053-7.

[59] E. Gonzalez-Cubero, M.L. Gonzalez-Fernandez, L. Gutierrez-Velasco, E. Navarro-Ramirez, V. Villar-Suarez, Isolation and characterization of exosomes from adipose tissue-derived mesenchymal stem cells, J. Anat. 238 (2021) 1203-1217.

[60] A. Adamo, J. Brandi, S. Caligola, P. Delfino, R. Bazzoni, R. Carusone, D. Cecconi, R. Giugno, M. Manfredi, E. Robotti, E. Marengo, G. Bassi, P. Takam Kamga, G. Dal Collo, A. Gatti, A. Mercuri, M. Arigoni, M. Olivero, R.A. Calogero, M. Krampera, Extracellular Vesicles Mediate Mesenchymal Stromal Cell-Dependent Regulation of B Cell PI3K-AKT Signaling Pathway and Actin Cytoskeleton, Front. Immunol. 10 (2019) 446.

[61] F.J. Lv, R.S. Tuan, K.M. Cheung, V.Y. Leung, Concise review: the surface markers and identity of human mesenchymal stem cells, Stem Cells. 32 (2014) 1408-1419.

[62] G. Qiu, G. Zheng, M. Ge, J. Wang, R. Huang, Q. Shu, J. Xu, Functional proteins of mesenchymal stem cell-derived extracellular vesicles, Stem Cell. Res. Ther. 10 (2019) 359-6.

[63] C.R. Harrell, M.G. Jankovic, C. Fellabaum, A. Volarevic, V. Djonov, A. Arsenijevic, V. Volarevic, Molecular Mechanisms Responsible for Anti-inflammatory and Immunosuppressive Effects of Mesenchymal Stem Cell-Derived Factors, Adv. Exp. Med. Biol. 1084 (2019) 187-206.

[64] K. Harhouri, A. Kebir, B. Guillet, A. Foucault-Bertaud, S. Voytenko, M.D. Piercecchi-Marti, C. Berenguer, E. Lamy, F. Vely, P. Pisano, L. Ouafik, F. Sabatier, J. Sampol, N. Bardin, F. Dignat-George, M. Blot-Chabaud, Soluble CD146 displays angiogenic properties and promotes neovascularization in experimental hind-limb ischemia, Blood. 115 (2010) 3843-3851.

[65] Z. Wang, Q. Xu, N. Zhang, X. Du, G. Xu, X. Yan, CD146, from a melanoma cell adhesion molecule to a signaling receptor, Signal. Transduct Target Ther. 5 (2020) 148.

[66] M. de Bruyn, A.A. Rybczynska, Y. Wei, M. Schwenkert, G.H. Fey, R.A. Dierckx, A. van Waarde, W. Helfrich, E. Bremer, Melanoma-associated Chondroitin Sulfate Proteoglycan (MCSP)-targeted delivery of soluble TRAIL potently inhibits melanoma outgrowth in vitro and in vivo, Mol. Cancer. 9 (2010) 301-301.

[67] J. Wang, A. Wuethrich, A.A. Sina, R.E. Lane, L.L. Lin, Y. Wang, J. Cebon, A. Behren, M. Trau, Tracking extracellular vesicle phenotypic changes enables treatment monitoring in melanoma, Sci. Adv. 6 (2020) eaax3223.

[68] L. Ghali, S.T. Wong, N. Tidman, A. Quinn, M.P. Philpott, I.M. Leigh, Epidermal and hair follicle progenitor cells express melanoma-associated chondroitin sulfate proteoglycan core protein, J. Invest. Dermatol. 122 (2004) 433-442.

[69] M. Hoffman, The Tissue Factor Pathway and Wound Healing, Semin. Thromb. Hemost. 44 (2018) 142-150.

[70] A. Inbal, A. Lubetsky, T. Krapp, D. Castel, A. Shaish, G. Dickneitte, L. Modis, L. Muszbek, A. Inbal, Impaired wound healing in factor XIII deficient mice, Thromb. Haemost. 94 (2005) 432-437.

[71] A. Brahmer, E. Neuberger, L. Esch-Heisser, N. Haller, M.M. Jorgensen, R. Baek, W. Mobius, P. Simon, E.M. Kramer-Albers, Platelets, endothelial cells and leukocytes contribute to the exercise-triggered release of extracellular vesicles into the circulation, J. Extracell Vesicles. 8 (2019) 1615820.

[72] S.M. Jung, M. Moroi, Platelets interact with soluble and insoluble collagens through characteristically different reactions, J. Biol. Chem. 273 (1998) 14827-14837.

[73] C. Popov, T. Radic, F. Haasters, W.C. Prall, A. Aszodi, D. Gullberg, M. Schieker, D. Docheva, Integrins alpha2beta1 and alpha11beta1 regulate the survival of mesenchymal stem cells on collagen I, Cell. Death Dis. 2 (2011) e186.

[74] S.M. Poznanski, A.A. Ashkar, Shining light on the significance of NK cell CD56 brightness, Cell. Mol. Immunol. 15 (2018) 1071-1073.

[75] B. Bielekova, M. Catalfamo, S. Reichert-Scrivner, A. Packer, M. Cerna, T.A. Waldmann, H. McFarland, P.A. Henkart, R. Martin, Regulatory CD56(bright) natural killer cells mediate immunomodulatory effects of IL-2Ralpha-targeted therapy (daclizumab) in multiple sclerosis, Proc. Natl. Acad. Sci. U. S. A. 103 (2006) 5941-5946.

[76] H.H. Van Acker, A. Capsomidis, E.L. Smits, V.F. Van Tendeloo, CD56 in the Immune System: More Than a Marker for Cytotoxicity? Front. Immunol. 8 (2017) 892.

[77] R.C. Beljaards, G. Kirtschig, Expression of neural cell adhesion molecule (CD56) in basal and squamous cell carcinoma, Dermatol. Surg. 34 (2008) 1577-1579.

[78] T. Ito, N. Ito, M. Saatoff, H. Hashizume, H. Fukamizu, B.J. Nickoloff, M. Takigawa, R. Paus, Maintenance of hair follicle immune privilege is linked to prevention of NK cell attack, J. Invest. Dermatol. 128 (2008) 1196-1206.

[79] A. Shabbir, A. Cox, L. Rodriguez-Menocal, M. Salgado, E. Van Badiavas, Mesenchymal Stem Cell Exosomes Induce Proliferation and Migration of Normal and Chronic Wound Fibroblasts, and Enhance Angiogenesis In Vitro, Stem Cells Dev. 24 (2015) 1635-1647.

[80] E. Manchon, N. Hirt, J.D. Bouaziz, N. Jabrane-Ferrat, R. Al-Daccak, Stem Cells-Derived Extracellular Vesicles: Potential Therapeutics for Wound Healing in Chronic Inflammatory Skin Diseases, Int. J. Mol. Sci. 22 (2021) 10.3390/ijms22063130.

[81] M. Schafer, S. Werner, Oxidative stress in normal and impaired wound repair, Pharmacol. Res. 58 (2008) 165-171.

[82] T.J. James, M.A. Hughes, G.W. Cherry, R.P. Taylor, Evidence of oxidative stress in chronic venous ulcers, Wound Repair Regen. 11 (2003) 172-176.

[83] C.K. Sen, Wound healing essentials: let there be oxygen, Wound Repair Regen. 17 (2009) 1-18.

[84] G. Bodega, M. Alique, L. Puebla, J. Carracedo, R.M. Ramirez, Microvesicles: ROS scavengers and ROS producers, J. Extracell Vesicles. 8 (2019) 1626654.

[85] J. Xiao, Y. Pan, X.H. Li, X.Y. Yang, Y.L. Feng, H.H. Tan, L. Jiang, J. Feng, X.Y. Yu, Cardiac progenitor cell-derived exosomes prevent cardiomyocytes apoptosis through exosomal miR-21 by targeting PDCD4, Cell. Death Dis. 7 (2016) e2277.

[86] B. Shi, Y. Wang, R. Zhao, X. Long, W. Deng, Z. Wang, Bone marrow mesenchymal stem cell-derived exosomal miR-21 protects C-kit+ cardiac stem cells from oxidative injury through the PTEN/PI3K/Akt axis, PLoS One. 13 (2018) e0191616.

[87] G. Zhao, F. Liu, Z. Liu, K. Zuo, B. Wang, Y. Zhang, X. Han, A. Lian, Y. Wang, M. Liu, F. Zou, P. Li, X. Liu, M. Jin, J.Y. Liu, MSC-derived exosomes attenuate cell death through suppressing AIF nucleus translocation and enhance cutaneous wound healing, Stem Cell. Res. Ther. 11 (2020) 174-8.

[88] Z. Liu, Y. Xu, Y. Wan, J. Gao, Y. Chu, J. Li, Exosomes from adipose-derived mesenchymal stem cells prevent cardiomyocyte apoptosis induced by oxidative stress, Cell. Death Discov. 5 (2019) 79-5. eCollection 2019.

[89] T. Matsuoka, K. Takanashi, K. Dan, K. Yamamoto, K. Tomobe, T. Shinozuka, Effects of mesenchymal stem cell-derived exosomes on oxidative stress responses in skin cells, Mol. Biol. Rep. (2021).

[90] D. Todorova, S. Simoncini, R. Lacroix, F. Sabatier, F. Dignat-George, Extracellular Vesicles in Angiogenesis, Circ. Res. 120 (2017) 1658-1673.

[91] C. Merino-Gonzalez, F.A. Zuniga, C. Escudero, V. Ormazabal, C. Reyes, E. Nova-Lamperti, C. Salomon, C. Aguayo, Mesenchymal Stem Cell-Derived Extracellular Vesicles Promote Angiogenesis: Potencial Clinical Application, Front. Physiol. 7 (2016) 24.

[92] X. Bian, K. Ma, C. Zhang, X. Fu, Therapeutic angiogenesis using stem cell-derived extracellular vesicles: an emerging approach for treatment of ischemic diseases, Stem Cell. Res. Ther. 10 (2019) 158-z

Journal of Controlled Release 328 (2020) 532–550

Contents lists available at ScienceDirect

Journal of Controlled Release

journal homepage: www.elsevier.com/locate/jconrel

Review article

Chronic wounds: Current status, available strategies and emerging therapeutic solutions

K. Las Heras [a,c], M. Igartua [a,b,c], E. Santos-Vizcaino [a,b,c,*] and R. M. Hernandez [a,b,c,*].

[a] NanoBioCel Group, Laboratory of Pharmaceutics, School of Pharmacy, University of the Basque Country (UPV/EHU), Paseo de la Universidad 7, 01006 Vitoria-Gasteiz, Spain

[b] Biomedical Research Networking Centre in Bioengineering, Biomaterials and Nanomedicine (CIBER-BBN), 01006 Vitoria-Gasteiz, Spain

[c] Bioaraba, NanoBiocel research group, Vitoria-Gasteiz, Spain.

* Co-corresponding authors at: Laboratory of Pharmaceutics, University of the Basque Country, School of Pharmacy, Vitoria-Gasteiz, 01006, Spain.

Email addresses: Rosa Maria Hernandez: rosa.hernandez@ehu.eus / Edorta Santos-Vizcaino: edorta.santos@ehu.eus

.....

Published in: *Journal of Controlled Release*, 2020

Impact Factor 2020: ***9.776*** (Q1, D1)

DOI: https://doi.org/10.1016/j.jconrel.2020.09.039

Cat: Elsevier

Contents

Abbreviations: Adipose tissue-derived mesenchymal stem cells (ATMSCs), bioengineered living skin equivalents (BeLSEs), biopolymeric porous scaffolds (BPS), bone marrow derived stem cells (BMSCs), calcium peroxide (CPO), carboxymethyl cellulose (CMC), clustered regularly interspaced short palindromic repeats-associated protein 9 (CRISPR/Cas9), computer-aided-design (CAD), connective tissue growth factor (CTGF), dendritic epithelial T cells (DETCs), DLP-based printing-dynamic optical projection stereolithography (DOPsL), electrical stimulation (ES), endothelial progenitor cells (EPC), epidermal growth factor (EGF), exosomes (Exos), extracellular matrix (ECM), extracellular vesicles (EVs), fetal context (FC), fibroblast growth factors (FGFs), full-thickness skin graft (FTSG), granulocyte-macrophage colony-stimulating factor (GMCSF), graphene oxide (GO), growth factors (GFs), hair follicle mesenchymal stem cells (HFMSCs), hepatocyte growth factor (HGF), human leukocyte antigen (HLA), human umbilical cord blood mononuclear cells (hUCB-MNCs), hyperbaric oxygen therapy (HBOT), indoleamine 2,3-dioxygenase (IDO), insulin-like growth factor 1 (IGF-1), interferon gamma (IFN-γ), keratinocyte growth factors (KGFs), layer-by-layer (LBL), matrix metalloproteinases (MMPs), mesenchymal stem cells (MSCs), N-acetyl cysteine (NAC), nanostructure lipid carriers (NLCs), negative pressure wound therapy (NPWT), neutrophil activating peptide-2 (NAP-2), nitric oxide (NO), platelet-derived growth factor (PDGF), platelet factor-4 (PF-4), platelet rich plasma (PRP), polycaprolactone (PCL), polyethylene glycol (PEG), polyethylene oxide (PEO), polyvinyl acid (PVA), polyvinyl pirrolidone (PVP), propylene glycol (PG), reactive oxygen species (ROS), solid lipid nanoparticles (SLNs), split-thickness skin graft (STSG), stem cells (SCs), stromal-cell-derived factor-1 (SDF-1), tissue inhibitor of metalloproteinases 1 (TIMP1), transforming growth factor (TGF), tumor necrosis factor (TNF), vascular endothelial growth factor (VEGF).

Abstract

In the past decades, adequate and well-planned management of chronic wounds has reached an elevated importance to improve human´s quality of life and extend life expectancy. The need for more complex and biomimetic strategies has fueled the exploration of numerous emerging technologies. However, the development of new therapies requires an extensive knowledge of the wound healing process and the key players involved in it. In that sense, this review seeks to bring researchers an updated description of the wound healing process, combining the traditionally-told phase progression with the presence and function of diverse stem cells and other involved mediators. Furthermore, the present work discusses a wide variety of strategies for accelerating wound healing; from systemic or local dressing-free therapies, to cell-free dressings including films, biopolymeric porous scaffolds, electrospun nanofiber meshes and hydrogels. Finally, emerging therapy solutions derived from the development of 3D bioprinting and CRISPR/Cas9 technology or the application of extracellular vesicles in healing chronic wounds are also discussed.

1. Introduction

In healthy individuals, wound closure is a highly accurate and well-orchestrated process. Nevertheless, shortcomings in this process lead to approximately 40 million chronic wound patients worldwide, reaching epidemic proportions, causing a huge economic impact on health-care systems and, ultimately, on country´s economy [1-3]. In fact, it has been described that chronic wounds can impact quality of life as profoundly as heart and renal diseases. Furthermore, mortality for some patients with chronic wounds nowadays rivals that of cancer patients. Aging, obesity, diabetes, sensory neuropathies, autoimmune diseases or cardiovascular disorders constitute some of the reasons that cause the aforementioned pathology [4,5]. According to the latest report of the "Global Wound Care Market" (2016), the sector achieved a value of approximately $18 billion. Furthermore, this amount is projected to reach approximately $26 billion worldwide by the end of 2023 [6]. Thus, it is not surprising that, over the last decades, an adequate and well-planned management of chronic wounds has become important due to both the improvement of humans' life quality and the increase of life expectancy.

One of the first medical manuscripts — written on a stone tablet — talking about wound management, dates back to 2200 B.C. This tablet describes the ''three healing gestures'': washing the wounds, making the plasters (nowadays wound dressings), and covering the wound. There is also evidence that beer, vinegar, wine, milk, animal grease, leaves, trees´ resin or honey have been used by the Chinese, Sumerians or Egyptians for treatment of wounds. Boiled water, wine or honey were possibly the most widely used components for wound covering ointments by that time [7,8]. The wound covering therapy gained high importance in the middle and modern ages. Ambroise Paré (1510-1590) exemplifies the predicament in that field by that time; "I dressed the wound; GOD healed it" [8]. But it was not until the 19th century when the antiseptic technique appeared as a major breakthrough for acute and chronic wound healing. As early as the 20th century, the advent of modern wound healing management arrived, and with it, the appearance of the first "tissue engineering" steps [9]. Great advances in biomaterials field and deeper knowledge about wound healing process have given rise a wide number of novel therapies and strategies. Thus, the paradigm in the

treatment of chronic wounds has changed during the last years. Nowadays, more than 5,000 wound care products are already marketed, most of them being dressings with different properties.

In this review article, we briefly discuss the physiology of the normal wound healing, the causes and pathology of an inadequate healing, and the currently available cell-free strategies for chronic wound management. Furthermore, we describe the latest advances with the appearance of 3D bioprinting, the CRISPR/Cas9 technology and the application of extracellular vesicles (EVs).

2. Wound healing process: normal vs insufficient healing

In order to find an effective therapeutic strategy, it is essential to understand the anatomy of the skin and the healing process, both physiological and pathological. Indeed, the scarring process, which is initiated just after tissue damage occurs, involves a step-by-step, precise and well-orchestrated cascade that is related to the appearance of several cell types in the wound environment at different moments.

2.1 Normal cutaneous wound healing

In healthy people, wound healing comprises 4 stages: hemostasis, inflammation, proliferation and remodeling phase (Fig. 1) [10].

Hemostasis occurs immediately after an injury to rapidly recover the barrier function. It starts triggering a hydrogen peroxide gradient, essential for the immune cell recruitment [10]. This is accompanied by a vasoconstriction process, a platelet aggregation and finally, the formation of a blood clot that covers the wound, decreasing blood loss and acting as a “scaffold-like” structure for the migration of immune cells and residential skin cells [11]. In addition, platelets within the blood clot release a variety of platelet-specific proteins such as platelet factor 4 (PF-4); thrombin and fibrinogen; adhesion molecules; pro- and anti-angiogenic factors such as vascular endothelial growth factor (VEGF) and endostatin respectively; growth factors such as epidermal growth factor (EGF), platelet-derived growth factor (PDGF) and transforming growth factor (TGF-β); and cytokines/chemokines like neutrophil activating peptide-2 (NAP-2) and platelet-derived stromal-cell-

derived factor-1 (SDF-1α) [12-14]. The secreted molecules induce the migration and activation of macrophages, neutrophils, fibroblasts, smooth muscle cells, endothelial cells and circulating bone marrow derived stem cells (BMSCs) to the wound niche [15].

The inflammatory phase initiates within few hours after injury and is fueled by bacterial byproducts, secreted cytokines/chemokines and platelet-derived mediators. After an increase in vascular permeability, neutrophils firstly and monocytes/macrophages later, infiltrate the wound site killing bacteria and removing debris and damaged matrix proteins [16]. Neutrophils release proteases such as matrix metalloproteinases (MMPs), antimicrobial peptides, reactive oxygen species (ROS) and growth factors such as TGF-β [17]. Monocytes arrive afterwards (within 24 hours) and transform predominantly into M1 macrophages (pro-inflammatory) with the aim of amplifying the inflammation process. This is mediated by nitric oxide (NO), ROS, IL-1, IL-6, IL-8, tumor necrosis factor alpha (TNF-α) and MMPs [18]. Lymphocytes are the final inflammatory cells attracted to the wound niche. γδ+ T cells produce mediators such us insulin growth factor 1 (IGF-1), fibroblast growth factors (FGFs) or keratinocytes growth factors (KGFs), involved in the survival and growth of immune cells, fibroblasts and keratinocytes. αβ+ T cells (CD4+, CD8+ and Treg), also present in the inflammatory stage, have an important role acting against pathogenic microorganisms [1,12,19].

In the later stage of the inflammatory phase, M2 macrophages (anti-inflammatory/pro-wound healing) derived from monocytes or switched from M1 macrophages, release VEGF, PDGF, IGF-1, FGFs, TGF-β1 and IL-10, which induce cell migration, proliferation and matrix formation. They also produce tissue inhibitor of metalloproteinases 1 (TIMP1) in order to counteract MMPs [20]. The switching to the M2 profile, leads to the release of different mediators that enable angiogenesis and tissue granulation, thereby assisting in the transition to the proliferation stage.

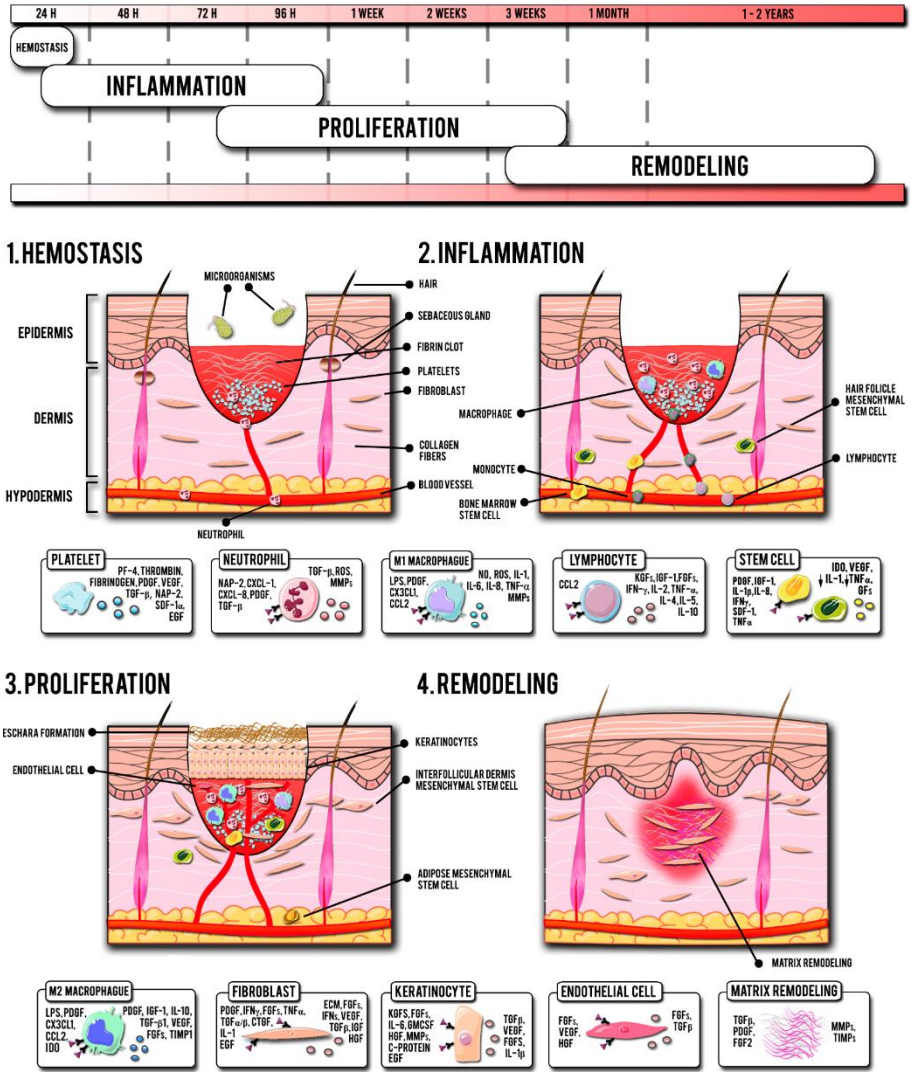

Fig. 1. Normal wound healing steps: Hemostasis, inflammation, proliferation and remodeling. In cell boxes: the left-handed cytokines, GFs, etc. stimulate cells and the right-handed ones are secreted by these cells.

Within the present phase, BMSCs are attracted towards areas of tissue injury in order to regulate the inflammatory phase and give way to the proliferation phase. BMSCs show chemotaxis mediated by inflammatory cytokines and growth factors, including PDGF, IGF-1, IL-1β, IL-8, interferon gamma (IFN-γ), SDF-1 and TNF-α

[21]. Hair follicle-derived mesenchymal stem cells (HFMSCs) are also attracted to the wound site within the first three days from the different neighbor stem cell niches [22]. Once they are present at sites of injury, mesenchymal stem cells (MSCs) present immunosuppressive effects upregulating the secretion of Indoleamine 2,3-dioxygenase (IDO), downregulating the production of proinflammatory cytokines such as IL-1 and TNFα and decreasing the number of inflammatory cells [23,24]. MSCs also modify the response of T cells, as well as the proliferation and migration of B and NK cells. Furthermore, MSCs affect the behavior of monocytes, granulocytes and dendritic cells, while also induce macrophages to switch from M1 to M2 phenotype [21]. Finally, MSCs are able to produce and remodel extracellular matrix (ECM), increase angiogenesis and differentiate into diverse cell types (keratinocytes, endothelial cells etc.) [25].

With the resolution of inflammation and the progressive phenotype transition of monocytes and macrophages into anti-inflammatory cell types (M2 macrophages) — thanks to the immunomodulatory mediators mainly secreted by MSCs — proliferation phase begins. The main focus of this period is the development of granulation tissue, which aids at restoring the vascular network while covering the denuded wound surface [26]. In the present stage, fibroblasts, regulated by cytokines and growth factors such as PDGF, FGFs, EGF, TNFα, TGFα/β, connective tissue growth factor (CTGF) and IL-1, deposit large amounts of ECM to close tissue gaps, releasing at the same time more cytokines such as FGFs, IFNs, TGFβ, VEGF, IGFs and hepatocyte growth factor (HGF) [10,14,27,28]. Re-epithelialization process requires the presence (migration and proliferation) of keratinocytes, which are mainly stimulated by different cytokines and growth factors including EGF, KGFs, FGFs, IL-6, granulocyte-macrophage colony-stimulating factor (GMCSF) and enzymes such MMPs or activated protein C [29,30]. Keratinocytes, in response, mainly release growth factors such as TGFβ, VEGF, FGFs and IL-1β. They migrate and proliferate to achieve wound coverage, followed by stratification and differentiation to eventually rebuild the skin epidermal barrier [10]. In the current phase, the neovascularization process reaches its highest point throught both vasculogenesis — de novo formation of blood vessels by mesoderm derived endothelial progenitor cells (EPC) — and angiogenesis —

proliferation and migration of endothelial cells from pre-existing vessels — [31]. Finally the cellular network formed gives way to the formation of an immature granulation tissue, with large amount of fibroblasts, M2 macrophages and poorly organized collagen bundles entwined with capillaries [32]. On the other hand, BMSCs and adipose tissue-derived mesenchymal stem cells (ATMSCs) are also implicated in the formation of granulation tissue and the re-epithelialization [33]. For example, BMSCs have demonstrated capacity to differentiate into keratinocytes, dermal fibroblasts, endothelial cells and pericytes [33,34]. Furthermore, the strong secretome released by the different MSCs (BMSCs, ATMSCs, and HFMSCs) has been reported to influence the activation, migration and proliferation of different cell types in the present proliferation phase [21].

Remodeling, the final phase of the healing process, extends for a year or longer and it is characterized by a progressive decrease in cellularity and vasculature [16]. The resolution of the granulation tissue and scar formation is driven by various MMPs and their inhibitors. Fibroblasts, the main cellular player in the present phase, act increasing the amount of type I collagen and other ECM components, while the MMPs act breaking down disorganized collagen that previously served as a template, manly of type III [10,35,36]. Any disturbance in the balance presented by MMPs and their inhibitors triggers the development of keloids and hypertrophic scars (excessive ECM accumulation); or the formation, on the other hand, of chronic wounds (excessive ECM degradation).

2.2 Insufficient healing (Chronic wounds)

When tissue repair is ineffective, it can lead to ulcerative skin damage such as venous leg ulcers, arterial ulcers, diabetic foot ulcers and pressure ulcers [1]. Although extensively debated, the duration of a wound to be considered as “chronic” is generally taken to be more than three months [37]. As mentioned before, different disorders (e.g. diabetes, aging, cardiovascular diseases etc.) constitute some of the reasons for the appearance of a chronic wound. Below we focus on the interruption of normal healing process due to an insufficient healing.

Chronic wounds are characterized by a persistent inflammation, impaired angiogenesis, difficult re-epithelialization, dysregulated levels of cytokines/growth

factors and/or increased protease activity [38]. For example, some mediators such as IL-1, IL-6, TNFα and MMPs are constantly upregulated, whereas the expression of TIMPs appears downregulated [28]. At a cellular level, there are many disturbances that occur in chronic wounds. Neutrophils exhibit phenotypic changes, a decreased infiltration and transendothelial cell migration, and a longer stay in the wound. Furthermore, chronic wounds show reduced M2 macrophage profile induction and lower antibacterial activity [39,40]. Disturbances in macrophage function are also presented in chronic wounds and can lead to aberrant repair. Macrophages show an uncontrolled inflammatory mediator and growth factor production, together with an imbalance in the M1/M2 profile ratio (M1 pro-inflammatory predominance). Furthermore, a failed communication is given between macrophages and other important players including endothelial cells, epithelial cells, fibroblasts, and stem or tissue progenitor cells [41].

Some studies argue that keratinocytes presented in chronic wounds are hyperproliferative, exhibit an impaired migratory potential and they lack expression of differentiation markers [32,42-44]. Due to those abnormalities they are unable to migrate and help in the closure process. In contrast, some other works claim that, in presence of chronic wound fluid, there is a reduced keratinocyte proliferation in addition to the reduced migratory activity [45-47]. Despite this discordance, the hyperproliferative keratinocyte status appears to be the most accepted approach lately.

Finally, fibroblasts are unable to respond to inflammatory mediators and growth factors, resulting in a decreased proliferative capacity [48,49]. These molecular and cellular abnormalities impede the deposition of ECM and the formation of granulation tissue, leading to the formation of chronic wounds. With these precedents, a bast number of different therapies have been developed from the past centuries, to nowadays.

3. Therapies

In the present section, we detail methods for the delivery or application of therapeutic agents, from the traditional wound care management to the new

perspectives and insights of wound healing. In Fig. 2 we illustrate some of the principal chronic wound therapies.

3.1 Dressing free therapies

3.1.1 Systemic administration

It is widely known that in many skin disorders, such as severe burns or chronic wounds, high doses of systemically administered drugs such as antibiotics are required to achieve local therapeutic effects. Systemic antibiotics have been used to improve symptom management and reduce further deterioration and infections [50]. However, the use of systemic antibiotics have demonstrated that can barely penetrate into wound biofilms, being, the use of an antisepsis method, a better approach to treat or prevent bacteria in wounds [51].

Another investigated systemic approach is the administration of antibodies and peptides. Some recent studies have demonstrated the beneficial use of systemic infliximab (anti TNF-α) in the treatment of recalcitrant ulcerating necrobiosis lipoidica [52,53]. Another peptidic successful approach was described using a systemic administration of the neuropeptide α-melanocyte-stimulating hormone. The treatment led to a more regenerative healing process with less scar formation and a better collagen fiber organization [54]. Exenatide hormone also showed beneficial effects on systemic, tissue metabolic, inflammatory and healing markers; promoting positive responses even in fibroblast functions [55]. Finally, the systemic use of amino acids or derivatives, such as proline or N-acetyl cysteine, have demonstrated also positive effects on wound healing, even being more effective than its local administration [56,57].

Despite these results, overall systemic administration is limited by the difficulties with tissue targeting and the off target adverse effects. Therefore, in wound applications, direct delivery of bioactive compounds to the specific site is preferred in most cases, being increasingly accepted as the most adequate delivery strategy for chronic wounds.

3.1.2 Local therapies

As a result of the large exposed surface of the chronic wounds and the adverse effects derived from a systemic administration, the local management of the different therapies is the most common treatment for cutaneous wound healing.

Physical treatments

Debridement — elimination of dead tissues and foreign material from the wound bed — is a traditional and central aspect of wound management. A regular maintenance debridement (surgical, biosurgical — using larvae — mechanical, autolytic, chemical or enzymatic) has demonstrated to stimulate the wound healing process [10,58]. Another long-stablished approach for local wound management is the compression therapy, the mainstay of venous leg ulcers treatment. It involves the application of external and gradual pressure with special bandages or "ready to use" layered compression bandage systems. This therapy helps to reverse the pathological variations of the venous system (e.g. "venous hypertension") that are a cause of ulceration [59-61]. Negative pressure wound therapy (NPWT) is another traditional therapy introduced in the decade of the nineties, consisting in the removal of wound exudates by vacuum device [62]. NPWT, which is generally not used alone, has demonstrated to reduce edema and bacterial burden, increase local perfusion, promote angiogenesis and enhance granulation tissue formation [62,63]. The success of NPWT has been proved by different studies [64,65]. However, some works have claimed that results remain still unclear and a greater number of robust studies are needed to support its wide spread use [66,67].

Another wound healing physical therapy, electrical stimulation (ES), uses current pulses of electromagnetic energy applied to treat chronic wounds. Used as an adjuvant therapy, ES have demonstrated enhanced wound healing rate faster than standard wound care in the clinic. These effects have been attributed to an increased fibroblasts stimulation in addition to an enhanced collagen, α-smooth muscle, TGF-β and VEGF production [68-70]. Hyperbaric oxygen therapy (HBOT) has also demonstrated satisfactory outcomes in the treatment of chronic wounds. The efficacy of this therapy may involve increased neovascularization, reduction in the presence of proinflammatory enzymes and an increased production of collagen and growth factors [71,72]. However, a 2015 Cochrane review about HBOT concluded that this therapy significantly improved wound healing in the first days

but not at long term and that more trials are needed to properly evaluate HBOT in people with chronic wounds [73].

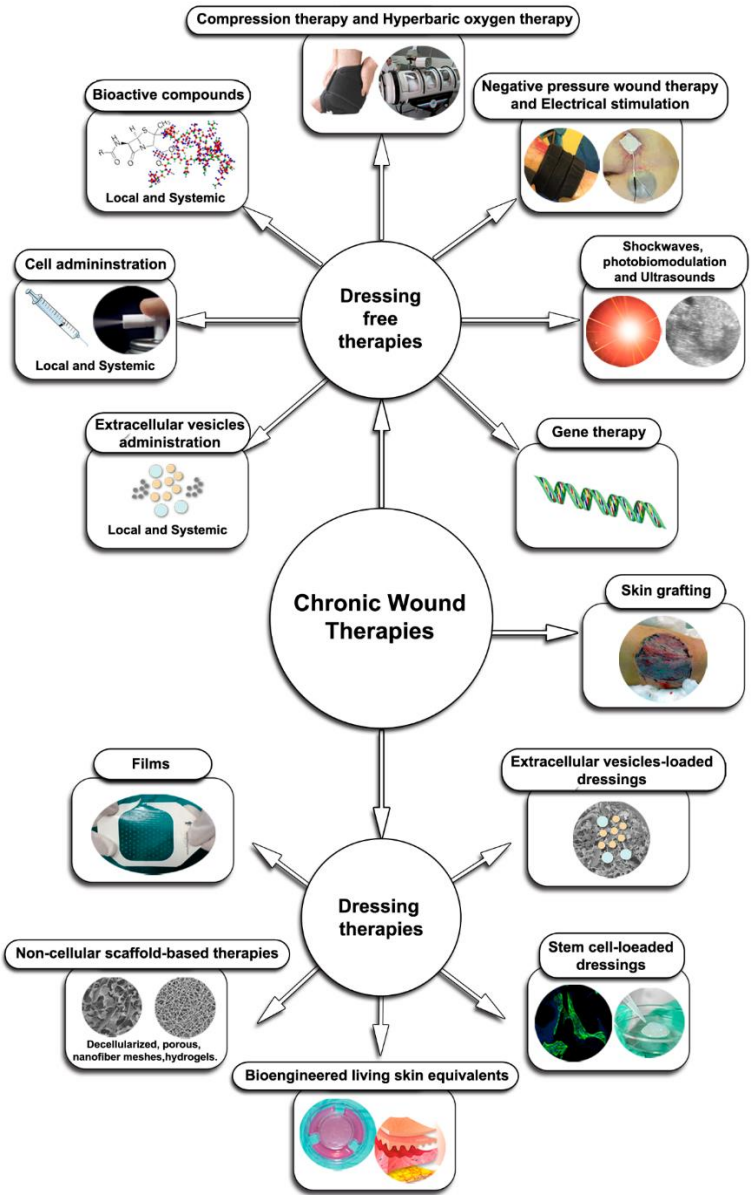

Fig. 2. Chronic wound therapies. Some images have been reproduced from Wikimedia Commons [81].

Shockwaves, photobiomodulation and ultrasounds have also been subject of research for local chronic wound management. Although shockwaves may aid the healing of venous leg ulcers through the promotion of angiogenesis and reduction of inflammation, a recent Cochrane review found no randomized controlled trials assessing the effectiveness of shockwaves in the healing of venous leg ulcers [74]. Photobiomodulation — treatment with light from LEDs, lasers and other light sources, in the wavelength range from visual to infrared — has become a mainstream wound repair modality. Different works have highlighted that photobiomodulation increased blood perfusion, reduced neutrophil infiltration, enhanced fibroblast proliferation, wound epithelialization and wound closure [75]. However, a recent systematic review suggested that there is still a lack of consensus on treatment parameters such as dose, wavelength, and therapeutic outcomes in the reviewed studies [76]. Finally, both high frequency and low frequency ultrasounds have been explored for wound healing purposes. Both strategies have shown great results in pressure or diabetic ulcers treatment, but there is conflict regarding the effectiveness of low-frequency over high-frequency ultrasounds. Furthermore, there are currently no standardized treatment protocols for ultrasound treatments [77-80].

Pharmacological treatments

Drugs as antiseptics or antimicrobials have been extensively used topically in wound care. It is widely known that chronic wounds are usually colonized or even infected by bacteria. In that sense, systemically used antibiotics rarely penetrate into wound biofilms, but when used topically they can be effective. For example, antiseptics such as iodine, chlorhexidine, ethacridine, or silver; and antibiotics such as gentamicin, tetracycline, chloramphenicol, vancomycin, framycetin, and mupiricin have been largely administered, demonstrating clear benefits [82-84]. Furthermore, a vast lists of natural compounds known to have antibacterial, angiogenic, and regenerative effects have also been used in wound healing management, including rosemary oil, curcumin, berberine, Aloe Vera or thyme extract honey, among others [83,85].

Growth factors (GFs) are biologically active peptides which regulate cell growth, differenciation, communication and migration throughout all wound healing stages.

Topically administered — in form of gels, creams, intralesional injections etc. —, GFs continue to be studied as a treatment for chronic wounds. It has been demonstrated that these mediators exert notable effects in skin healing without any obvious secondary effects. EGF, PDGF, bFGF, GMCSF and TGF-β are different GFs used topically in wound healing applications [32,83,85]. However, PDGF-BB formulated in a gel is the only GF approved by FDA (1997) and EMA (2003), with the name of Regranex® (Johnson & Johnson), for wound healing applications. Moreover, in Japan, bFGF formulated in a spray, with the name of Fiblast® (Kaken Pharmaceutical), is in clinical use for pressure ulcers since 2001 [85]. Besides, autologous platelet rich plasma (PRP), which is a rich source of multiple GFs, have demonstrated great results in healing rates in numerous studies with different formulations [32,86]. However, given the short half-life of GFs, mainly because of the enzymatic degradation in the wound bed, their sustained release becomes crucial to succeed in the wound tissue repair [83].

Encapsulation into micro- or nanocarriers allows sustained and localized delivery of therapeutics. These carriers are usually produced in form of core-shell structures with the therapeutic cargo in the core cavity [83,87,88]. Thus, some studies have reported the use of liposomes as a protective and sustained drug delivery carriers for chronic wounds. For example, Xu et al. prepared a liposome with silk fibroin hydrogel core encapsulating bFGF that was able to accelerate wound healing in mice, particularly by inducing angiogenesis [89]. In that sense, new generation of liposomes, known as transfersomes, have been studied in the field of wound healing. Transfersomes are lipid vesicles that offer a versatile delivery concept for improving the stability and to be used with a wide variety of active compounds. They possess an ultra-flexible vesicle membrane and thus, are highly deformable, been able to penetrate through pores in the stratum corneum less than one-tenth of their own diameter [90]. Thus, Choi et al. conjugated protamine to the N-termini of different GFs — EGF, PDGF-A and IGF-1 — and subsequently complexed them with hyaluronic acid (HA) forming the transfersomes. This system significantly accelerated wound closure rate in diabetic mice [91]. Another transfersome-based therapy loading baicalin — a molecule known for its antioxidant, anti-inflammatory and anticarcinogenic activity — showed that a daily application of transfersomes, in a mice model, achieved

complete skin restoration inhibiting inflammatory markers such as edema, IL-1β and TNF-α [92]. Both works administered the developed transfersomes in an aqueous vehicle in a non-occlusive way in order to facilitate the skin-penetration thanks to a transepidermal osmotic gradient.

Additionally, many studies have highlighted the use of polymeric, inorganic and lipid nanoparticles in wound related scenarios. Numerous antibiotics or antimicrobial peptides (e.g. Amphotericin B, norfloxacin, LL37 etc.) have been formulated in polymeric nanoparticles enhancing wound healing in mice and showing great activity against different microorganisms in vitro [93-96]. Metallic and semi conductive inorganic nanoparticles (e.g. cooper, iron oxide, zinc oxide, silver and titanium dioxide), alone or with graphene oxide (GO), are usually used in wound healing due to their antimicrobial activity and elevated penetration through skin cells membrane [88,97]. Finally, both solid lipid nanoparticles (SLNs) and nanostructured lipid carriers (NLCs) have been used as carriers for wound healing, protecting GFs and other encapsulated molecules from the enzymatic degradation and allowing a sustained drug delivery [98-101]. In this regard, the administration of rhEGF-loaded SLNs and NLCs has been proved to be effective in compromised-healing db/db mice [102]. Furthermore, these rhEGF-NLCs have also been tested in a more relevant wound healing model, the porcine full-thickness excisional wound model. Results demonstrated that rhEGF-NLCs topically administered increased wound closure and percentage of healed wounds compared with empty NLCs or intralesional injections of rhEGF. Moreover, rhEGF-NLCs improved collagen deposition, microvasculature formation and fibroblast proliferation and migration [103].

Another different and recent strategy to enhance the presence of growth factors and cytokines is the administration of genes encoding these mediators. For that purpose, the genetic material is transferred through viral or non-viral vectors formulated in intralesional injections [32]. In addition, the application of gene silencing strategies by means of miRNAs and siRNAs is increasing and becoming extremely influential in the treatments of wounds [104]. Different researchers have studied, miR-99, -126, -132, 155, -184, -198, -203, -205 and miR-210 finding that they are able to regulate proliferation, differentiation and migration of different skin

cells (keratinocytes and endothelial cells) [32,105]. Furthermore, some studies have investigated siRNAs as a selective inhibitor of fibrotic tissue growth factors, MMPs, proinflammatory cytokines, p53 etc. to achieve a faster and fully functional healing of chronic wounds [105-108].

3.2 Skin grafting

Skin grafting is the chosen procedure for reconstructing skin defects in different anatomical localizations and is considered the gold-standard for the care of thermal injuries. This therapeutic strategy provides an adequate coverage of the wound, protecting against infections, as well as initiating and accelerating the wound healing process [109]. When a graft contains the epidermis and a part of the dermis it is called split-thickness skin graft (STSG). In contrast, when a graft comprises the epidermis and the whole dermis, it is called full-thickness skin graft (FTSG). STSGs can be used for large injury coverage, being able to survive in grafted zones with less vasculature. However, STSGs suffer from graft contracture during the process of healing. In contrast, FTSGs require a better vasculature in the grafted zone, but experience less contract during healing and are, in that sense, preferred for exposed areas of the body (e.g. face or neck) [10]. Finally, there also exist epidermal skin grafts that only comprises epidermis layer of the skin. In this approach, keratinocytes are the main cell type involved in the therapeutic effect, secreting growth factors, mediators and stimulating the endogenous wound healing process [110].

Skin grafts can come from the same patient (autograft), from another dead or alive patient (allograft) and from other animals (xenografts). Autologous grafts have demonstrated promising results in clinical trials for diabetic foot ulcers. However, autologous grafting is painful in addition to the limited and available donor sites [109,111]. On the other hand, skin allografts from cadaveric or living donors are widely used nowadays, but are limited by availability and cost. On the contrary, xenografts (mainly form porcine skin) solve the availability problem, the higher cost and the limited dressing size of allografts, but they usually present host immunogenic response in less than a week [109,112,113]. However, recent studies have shown that genetically-engineered pig skin xenografts now survive as long as

an allograft and, importantly, if there is a rejection of a skin xenograft is not detrimental to a subsequent allograft or different therapeutic approach [114].

3.3 Dressing therapies

Cellular and molecular complexity of wound healing process requires a controlled spatiotemporal delivery of biologicals. Skin grafting has been described and used as wound healing promoter since the year 600 B.C. and has evolved rapidly giving rise to more advanced strategies since the XIX century (Fig. 3) [115]. In the current century, a wide number of dressing therapies have been developed to provide moisture-retentive properties, protect the wound bed from physical and mechanical stress, provide a provisional matrix for cell migration, ECM deposition and neovascularization — which pave the way for new tissue formation —, and release drugs and bioactive molecules. Many sources are currently being used to develop these biomaterial-based systems; from biological ones including fibrin, fibronectin, gelatin, collagen, alginate, chitosan, hyaluronan, starch, lactose etc., to synthetic compounds such as polyglycolic acid (PGA), polylactic acid (PLA), polyacrylic acid (PAA), polyvinyl acid (PVA) etc. [116]. Dressing therapies may be divided into films, non-cellular scaffold-based therapies, bioengineered living skin equivalents (BeLSEs) — mono/bi-layered cellular therapy mimicking the skin structure — and stem cell-loaded scaffolds. In the present work we will discuss about the different advances in non-cellular dressing therapies.

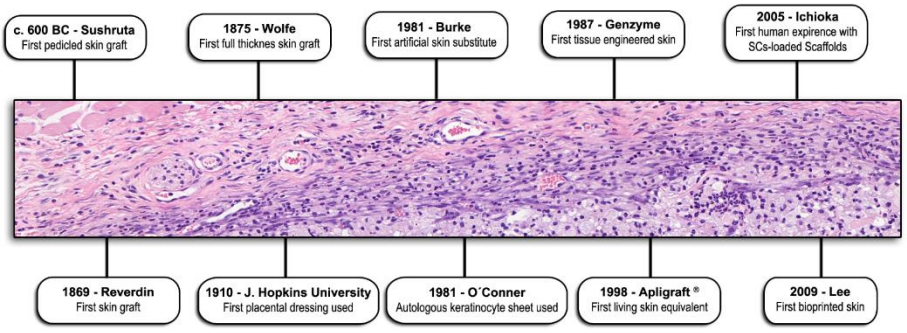

Fig. 3. Timeline of wound covering therapies used in medicine. SCs: Stem cells [115,117-121].

3.3.1 Films

Films are thin, elastic, usually transparent and adhesive sheets of one or a combination of different biopolymers. Films are normally gas and water vapor permeable, but impermeable to fluid and bacteria, thereby protecting wounds against water loss and external microorganisms. The principal advantages of these dressings include (but are not limited to) the possibility to visualize the wound progression, the drug loading potential, and the flexibility to use them as a primary or secondary dressing. However, they lack good swelling properties, which may lead to excess exudate accumulation [122].

Polyurethane, silicon, collagen, chitosan, alginate and hyaluronic acid are some of the most commonly used polymers for the development of these formulations. The use of films for wound healing applications can be traced back to the beginning of the 20th century and nowadays there are plenty of options commercialized. For example, there are monolayered films marketed such as BioclusiveTM (Johnson & Johnson), Tegaderm® Films (3MTM) and Transeal® (DeRoyal) which are composed of polyurethane; or SimpurityTM transparent films composed of silicon (SafenSimpleTM), among others. In addition, there are bilayered choices also available, usually composed of a silicon layer combined with a polysaccharide, protein or synthetic polymer layer. The bilayered structure allows the integration of the inner layer in the wound bed, while the external layer — usually the silicon made one — provides wound protection and avoids the water vapor loss. Biobrane® (S&N) — silicon/nylon with collagen —, Hyalomatrix® (Medline) — silicon with hyaluronic acid — and Integra® (Integra LifeSciences Corp.) — silicon with collagen/glycosaminoglycan — are three bilayered marketed options [32,122].

Besides all the commercialized products, other films with a wide variety of polymers are currently under investigation. Due to its antimicrobial properties, biocompatibility, biodegradability and its excellent mechanical properties, chitosan has gained popularity in the wound healing field and film development in the past decades [123,124]. Lupeol-loaded chitosan/gelatin films (prepared by casting) showed antioxidant and antimicrobial properties and an adequate biocompatibility

when cultured with NIH/3T3 fibroblast [100]. Garcia-Orue et al. also developed a chitosan/gelatin film with a bioinspired bilayered structure. The external layer was composed of lactose-mediated crosslinking of gelatin, providing mechanical support and hydrolytic resistance and protection to the developed device. In contrast, the inner layer was composed of gelatin crosslinked with citric acid and chitosan. This inner layer composition resulted in a porous matrix with great swelling capacity [125]. More recent studies have investigated the effects of chitosan films. Briefly, they all have shown antimicrobial action and remarkable wound healing properties when tested in-vivo [126-129]. Other polysaccharides have also been used for film development. Films formed from carboxymethyl cellulose and polyethylene glycol (PEG) also showed absence of toxicity in NIH 3T3 fibroblast cell and demonstrated a better healing profile than untreated groups in both normal and diabetic Wistar albino rats [130].

Proteins including fibroin, collagen, gelatin or soy have also served for the progression in field of films. Srivastava et al. and Rivadeneira et al. developed fibroin-dextran and soy-protein-agar films respectively, demonstrating complete absence of toxicity in L929 fibroblast cells. In addition, both films showed a controlled-released profile and antimicrobial effect when being loaded with antibiotics [131,132]. Finally, films made of solely collagen or gelatin and loaded with different antioxidant/anti-inflammatory and antimicrobial compounds (Astaxanthin or Clinoptilolite-Ag) have been recently studied. Briefly, both films showed antibacterial properties with a complete absence of toxicity in-vivo and a controlled drug release profile [133,134].

3.3.2 Non-cellular scaffold-based therapies

Scaffolds, usually referred to as 3D biomaterial-based frameworks, are matrices or constructs that provide protection, moisture retention and their own therapeutic effects depending on its composition and/or cargo [116]. There are many processes to develop biopolymeric scaffolds; from traditional casting, hydrogel formation, extracellular matrix decellularization and electrospinning, to new 3D bioprinting techniques. Here we divided non-cellular scaffold-based therapies into:

Decellularized matrices, biopolymeric porous scaffolds (BPS), nanofiber meshes and hydrogels

Decellularized matrices

Decellularized matrices are defined as animal/human derived ECMs in which all cells have been removed during the manufacturing process or are not present from the outset. The polymers most commonly obtained are from natural origin (collagen, hyaluronic acid etc.) due its inherent biocompatibility, bioactivity and ECM resemblance [135].

Because of its principal role in ECM, collagens are the main constituents of decellularized matrices. The function of collagen in wound healing and tissue repair is vital for maintaining the structural and biological integrity of the ECM. In addition, collagen is a dynamic and flexible protein that experiences continuous re-modeling to refine cellular behavior and tissue function [136]. Thus, its elevated use in dressings for chronic wounds is well documented and justified by a vast number of publications in the literature [137,138]. Collagen-based decellularized matrices are derived from a wide variety of anatomical locations, including human cadavers, human placental tissue, porcine small intestine submucosa, etc. Currently, there are three commercialized decellularized matrices mainly composed of collagen. Oasis® (Healthpoint) is a naturally derived decellularized ECM from the porcine small intestine submucosa (>90% collagen type I). This matrix is also embedded with proteoglycans, glycosaminoglycans, fibronectin and various growth factors that increase its biological bioactivity and damp the inhibitory effects of MMPs [139,140]. Graftjacket® (Wright medical technology) is a decellularized donated human tissue that retains collagen, elastin, proteoglycans and the internal matrix of the dermis. The Graftjacket® matrix provides a scaffold for host cell repopulation, revascularization and, ultimately, conversion to host tissue. In addition, it is coupled with excellent tensile and suture retention strength [141]. Finally, Dermacell® (LifeNet Health) is a human allograft decellularized with MATRACELL® technology, using anionic detergents to remove nucleic acids. This technology yields a strong, decellularized matrix that facilitates cell proliferation, migration and vascularization. The use of MATRACELL® technology also allows Dermacell® to minimize the possibility of an immune response [142]. Furthermore,

these products, in contrast to decellularized ECM xenografts, are classified as human cell, tissues and cellular and tissue-based products by the FDA, obtaining lower legal restrictions for its approval and application [32,135].

Placental membranes have also been used for over 100 years. This is mainly because of their collagen and growth factor-rich ECM and their safety derived from the absence of expression of the human leukocyte antigens (HLA-A, HLA-B, HAL-DR), which prevents them from immunological rejection [104,143]. The major asset of this therapy is the elevated amount of growth factors, MMPs, TIMPs, immunosuppressive factors and antimicrobial peptides that promote critical cell responses, reducing the risk of rejection and promoting wound healing events [144,145]. There are more than 25 commercialized available decellularized placental membrane products (Grafix®, NEOX®, etc.) and multiple clinical trials currently evaluating the efficacy of the newer ones [146,147].

Biopolymeric porous scaffolds

BPS offer several advantages over acellular naturally derived matrices and cell-based therapies, including cost efficacy, longer shelf life and limited risk of rejection. BPS need to meet several requirements to be used as a wound dressing (**Fig. 4**). For example, they must be easily manufacturable, biodegradable and biocompatible, while their structure must present adequate mechanical properties, interconnected porosity and high swelling capacity [148]. In other words, an optimal and effective BPS must recapitulate structural and functional aspects of the human ECM.

For that purpose, several polymers have been used; from proteins, polysaccharides, proteoglycans or glycolipids, to pure synthetic polymers [149]. Many BPS have been commercialized and successfully used in clinic in the past years: polysaccharide-based scaffolds such as Talymed® (Marine Polymer Technologies Inc.) and Hyalomatrix® (Anika Therapeutics); collagen-based scaffolds such as Pelnac® (Eurosurgical Ltd.) and Terudermis® (Olympus Terumo Biomaterilas Corp.); and pure synthetic scaffolds such as Suprathel® (Surgicorp), a lactide trimethylene carbonate with capronolactone matrix [150-157].

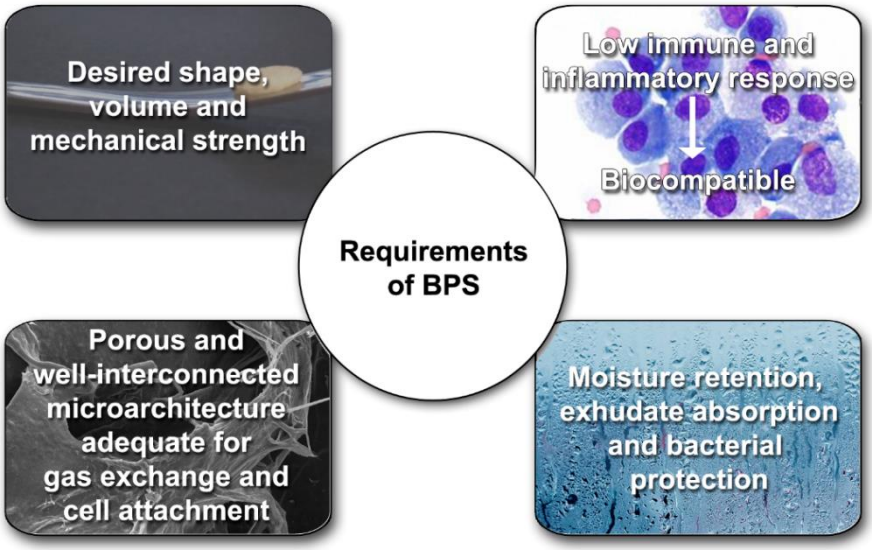

Fig. 4. Requirements of ideal BPS

In the recent years, many BPS have been developed with the aim of improving their mechanical and functional properties, and thereby increase healing rates. In addition, new BPS are intended to house different cell populations within their microarchitecture. For such aim, diverse polymers able to form well-organized structures (e.g. alginate, chitosan, PEG, polycaprolactone, etc.) have been largely combined with ECM molecules (e.g. collagen, fibrin, hyaluronic acid, etc.), in order to increase the stability and biocompatibility of the developed devices (Fig. 5 I) [136,158]. In that sense, several works about protein-based BPS have been published. Li et al. achieved a controlled release profile of N-acetyl cysteine (NAC) — an antioxidant molecule — with GO-collagen BPS. In addition, the developed devices, demonstrated complete healing rate in 14 days with faster collagen deposition, better epithelialization and increased vascularization against the control — non-NAC-loaded group and non-GO group — in a rat wound model [159]. Same NAC-release dressing concept has also recently been studied by other researchers for wound healing applications (Fig. 5) [160,161]. Another brilliant strategy based on collagen BPS has been recently developed by Roussakis and co-workers. The studied BPS incorporated a phosphorescent oxygen sensor to monitor the physiological oxygen levels — in diabetic mice —

using in vivo phosphorescence imaging, compatible with commercially available imaging instruments. The oxygen sensing BPS allowed a non-invasive measurement of oxygenation in vivo, providing a new capability for BPS to serve as biocompatible and biodegradable theranostic devices to promote and assess tissue oxygenation during wound healing [162].

Despite the fact that collagen is the most exploited protein for BPS development and that many more investigations have been recently published following the same idea [163-167], other proteins such as fibrin, fibrinogen, laminin, soy protein, gelatin etc. have also been investigated for chronic wound healing applications [32]. Our group combined a vegetal protein (soy protein) with β-chitin — both compounds obtained from waste by-products from the food industry — resulting in highly-porous sponge-like BPS. Results demonstrated that the sponge-like BPS possessed excellent biocompatibility both in vitro and in vivo with a huge swelling (1300% swelling) and cell loading capacity (up to 700,000 cells in 18,85 mm3 diameter BPS) [168]. In addition, gelatin-based BPS loaded with Silver nanoparticles (antiseptic) and curcumin (antioxidant, anti-inflammatory) have been proposed for wound healing therapies. The obtained results in this work showed the expected antioxidant and antibacterial effects, with an absence of toxicity in vitro (L929 fibroblast cells) [169].

On the other hand, BPS mainly composed of polysaccharides such as hyaluronic acid or chitosan, both actively involved in different wound healing stages, also produced an accelerated healing process with optimal aesthetic and functional results [170,171]. Finally, pure non-biological BPS have also been subject of research with remarkable results. Shiekh et al. developed calcium peroxide (CPO)/polyurethane BPS with sustained oxygen delivery properties [172]. In the line of oxygen releasing biomaterials also, in another study, researchers developed a biphasic calcium phosphate/PCL BPS coated with different ratios of the oxygen releasing agent CPO [173]. Both studies demonstrated a maintaining in oxygen supply, cell viability and proliferation under hypoxic conditions. Those abovementioned strategies show that both natural and synthetic polymers can complement each other to develop constructs with a wide variety of properties and suitability for wound healing applications.

Nanofiber meshes

Nanofiber meshes are scaffold-like constructs produced generally by applying an electric field, between a spinneret and a collector, into polymeric solutions through a high voltage supply. In the past years numerous studies have highlighted the potential of these dressings for: drug loading and controlled release [174-177], protein and genetic material delivery [178-182] and as a cell carrier systems [183-185] (Fig. 5 II). The value of this technique resides in its tunability. For example, the release rate of drugs or molecules may be modified by adjusting the fiber diameter, the pore size or the porosity. This flexibility in the fabrication process also gives to this technique the advantage of producing nanofibrous scaffolds with morphological, architectural and topographical features similar to those of the natural ECM of the skin [183,186].

Different molecule-loaded mesh fabrication techniques have been developed in the past years. The 3D expansion of 2D nanofiber mesh has led Zhang et al. to the development of chitosan-dressings with improved capacity for promoting blood coagulation, showing accelerate wound healing and reducing scar formation in a mouse model with full-thickness skin defects [187]. By means of layer-by-layer (LBL) assembly technique it is possible to preserve the bioactivity of cytokines and growth factors, allowing a tunable release rate of these compounds by just varying the number of layers [188,189]. Tu et al. developed a construct consisting of electrospun nanofibers of silk fibroin coated with amphoteric carboxymethyl chitosan by means of electrostatic LBL self-assembly. This nanofiber mesh showed stronger antibacterial activity as the number of amphoteric layers increased [190].

Another different technique, coaxial electrospinning, is an innovative extension of electrospinning that enables the formation of core-shell structures with the use of two concentrically aligned capillaries. This robust technique has allowed the encapsulation of water-soluble bioactive agents, proteins, DNA, cell, bacteria, viruses and even cell organelles [192,193]. PVA, PCL, polyethylene oxide (PEO), polyvinyl pyrrolidone (PVP), cellulose acetate are the most commonly used polymers for this technique [194]. Numerous coaxial electrospinning-based nanofiber meshes — loaded with drugs/proteins — have showed promising results in wound healing applications [195-197]. A recent work followed by Zahedi et al.

used this technique to develop a chitosan, PCL and keratin nanofiber mesh loaded with Aloe Vera extract. The ECM-mimicking mesh showed a complete absence of toxicity in vitro and suitability for a subsequent cell adhesion [198]. Finally, Shitole et al. investigated PVP/PCL nanofibrous construct modified with poly-l-lysine. An absence of toxicity and antimicrobial properties against both Gram-positive (S. aureus) and Gram-negative (E. coli) bacteria were observed. Furthermore, the lysine modified matrices demonstrated lower pro-inflammatory cytokine expression (TNF-α and IL-1β) in Mouse RAW 264.7 macrophage cells when comparing to non-modified PVP/PCL meshes [199].

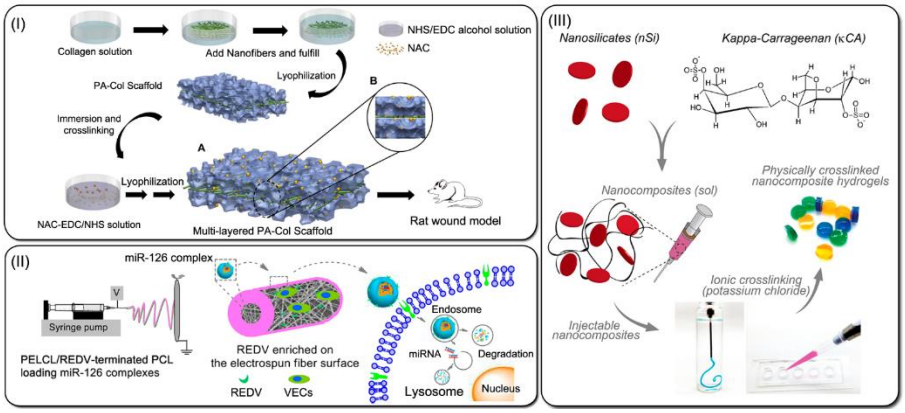

Fig. 5. I. Schematic illustration showing the fabrication procedure for multi-layered NAC-PA-Collagen BPS. Reproduced from [160]. II. Schematic illustration for preparation of a dual-functional nanofiber meshes target-delivery of miR-126 complexes to vascular endothelial cells. Reproduced with permission from [182]. III. Synthesis of κCA-nanosilicate hydrogels. Schematic representation of the fabrication of injectable nanocomposite hydrogels by combining kappa carrageenan (κCA) and nanosilicates (nSi) crosslinked in KCl solution. Reproduced with permission from [191]. NAC: N-acetyl-cysteine, PA: Polyamide, Col: Collagen, PCL: Polycaprolactone.

Hydrogels

Hydrogels are interconnected and hydrophilic polymeric chains forming flexible 3D networks that contain elevated proportions of water. Hydrogels have been investigated and used for wound healing applications since late eighties [200]. Due to its elevated water content, hydrogels are ideal in dry wounds, where they have the ability to rehydrate the niche and maintain the moist environment.

Importantly, the high-water content also produces a cooling effect that helps to relief the wound pain. In contrast, being used in wounds with high exudates can produce a fluid accumulation that can lead to skin maceration and subsequent bacterial proliferation [122,200]. Hydrogels lack good mechanical strength but, unlike BPS or films, they have the ability to mold to the shape of the skin defect once injected. The most commonly used polymers for hydrogels range from natural (hyaluronan, fibronectin, chitosan, gelatin or alginate) to synthetic polymers (polymethacrylates, PVP, etc.) [32,201]. Examples of commercialized hydrogels are: Aquaflo® (Covidien), composed of PEG and propylene glycol (PG); Intrasite Gel® (Smith and Nephew), made of carboxymethyl cellulose (CMC), sodium CMC (Na CMC) and PG; Granugel® (Convatec) composed of pectin, CMC and PG; and Purilon Gel® (Coloplast) mainly composed of Na CMC [200].

In the present century different preclinical and clinical studies with hydrogels as biological vehicles for the treatment of chronic wounds have yielded successful results. Different growth factor-enriched hydrogels have been used in rats and humans with promising results [202-204]. However, more complex and biomimetic hydrogels have been subject of investigations. In that sense, Zhang et al. developed a wearable biomimetic thin-hydrogel composed of HA, vitamin E, dopamine, and β-cyclodextrin that mimics the fetal context (FC) and fetal ECM. This thin-hydrogel recreates the FC of sterility, hypoxia, persistent moisture, seamless adhesion to the skin and optimum stress–stretch resistance. When tested in BALB/c mice the hydrogels induced fibroblast migration, suppressed the overexpression of TGF-β1, and mediating the collagen synthesis, distribution, and reestablishment. As a result, these thin-hydrogels accelerated wound healing and gained a normal dermal collagen architecture [205]. A brilliant work by Blacklow et al. developed mechanically active alginate-chitosan hydrogels that combine high stretchability, tissue adhesion, toughness, and antimicrobial properties. The aim of the developed devices was mimicking the embryonic wound contraction adhering strongly to the skin and actively contracting wounds as a response to the skin temperature. The in vitro and in vivo studies — on full-thickness excision wound healing model — demonstrated their efficacy in supporting and accelerating skin wound healing [206]. Another approach investigated hydrogels entrapping EGF-loaded nanoparticles, which significantly enhanced the wound

closure by promoting the formation of granulation tissue, angiogenesis and collagen deposition in rats [207]. Similarly, the use of liposome/GF-loaded hydrogel has reported an accelerated wound closure with increased vascular vessel formation in mice [89].

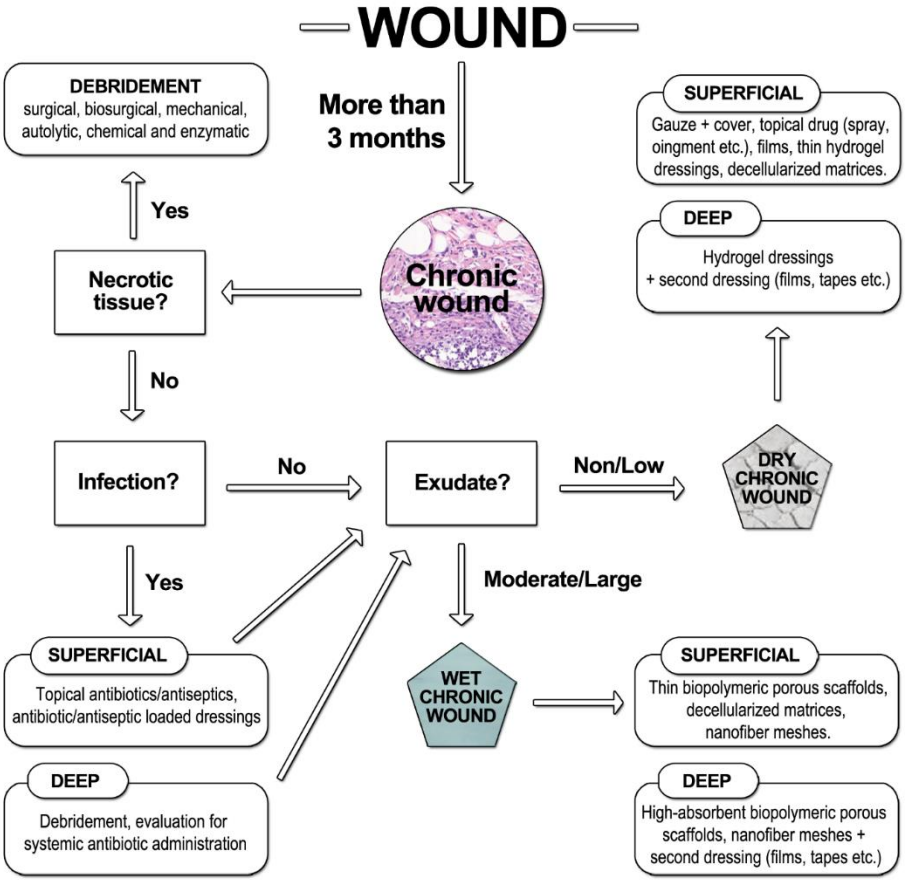

Fig. 6. Wound assessment and dressing selection criteria.

Recent works have shown different strategies for hydrogel-loaded systems — as molecule nanocarriers — such as nanodiamonds, protamine complexes, gold/silver nanoparticles etc. (Fig. 5 III) [191,208-211]. Finally, the use of hydrogels as DNA transporters is also under investigation. Hyaluronan-based hydrogels containing DNA-plasmids that codify for VEGF resulted in pro-angiogenic effects improving diabetic mice wound healing [212]. Another recent work by Wang et al.

using a hyaluronan/dextran in situ forming hydrogel also laden with VEGF DNA-plasmid accelerated a splinted excisional burn wound by inhibiting inflammation response and promoting microvascularization in rats [213].

With the myriad of dressing strategies available, we have sought to simplify the decision process by highlighting the key elements of wound assessment and how to match these to different wounds (Fig. 6).

4. Emerging therapy solutions

4.1 3D bioprinted dressings

3D bioprinting is a fast-emerging additive manufacturing technology which uses data computer-aided-design (CAD) to deposit combinations of cells, bioactive compounds and biomaterials (bioinks) and thus form 3D matrices with high spatial resolution and repeatability [214]. Bioprinting generally comprises four basic steps: firstly, studying the tissue for an appropriate bioink selection and matrix design; secondly, transferring all the information to the designing computer program; thirdly, tuning up the bioink; and finally, creating the designed 3D bioprinted dressing. Nowadays there are four kinds of bioprinting technologies: inkjet-based bioprinting, extrusion-based bioprinting, laser-assisted printing and dynamic optical projection stereolithography (DOPsL) [214-217]. Particular characteristics of each technique are well-descried by Zhu et al. [218]. Similar to hydrogels and BPS, 3D bioprinted dressings use a range of natural (cellulose, alginate, hyaluronic acid, collagen, chitin, fibrinogen, etc.) and synthetic (PCL, PLGA etc.) polymers [115,219]. Compared to the other dressing production techniques, 3D bioprinting is more personalized and precise, has a better flexibility in the manufacturing process and offers a faster and reproducible construction (shortening the patient waiting time) with also the possibility of an in situ administration. Fig. 7 details the main advantages and drawbacks of 3D bioprinting technology.

In a recent study, Intini et al. developed 3D bioprinted chitosan-based scaffold that demonstrated an improved diabetic wound healing when compared to both untreated mice and mice treated with a commercial product (CMC with calcium alginate covered by a semi-permeable layer of polyurethane) [222]. Another work

by Xu and coworkers highlighted the great properties of nanocellulose as a component for bioinks in terms of mechanical properties and biocompatibility. Furthermore, when formulated with gelatin methacrylate, obtained scaffolds demonstrated improved fibroblast proliferation [223].

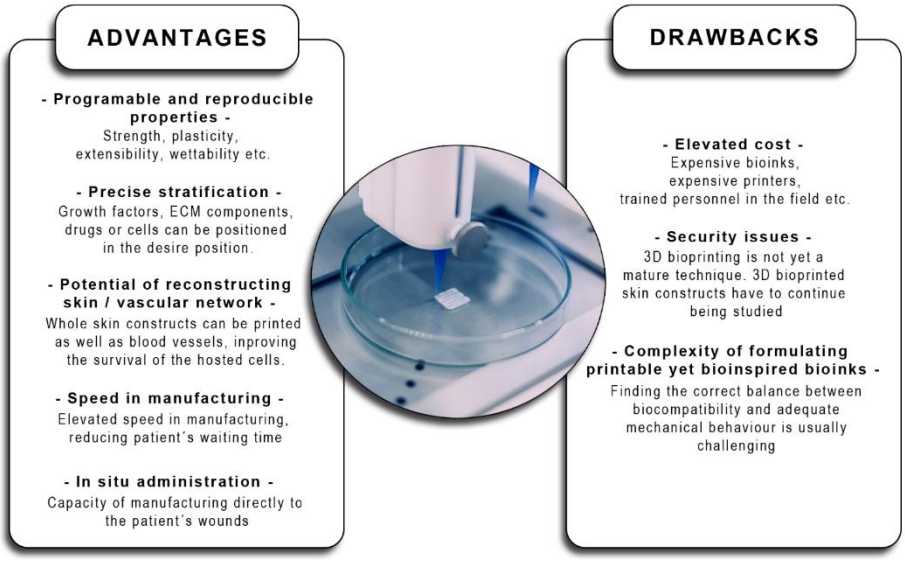

Fig. 7. Advantages and drawbacks of 3D bioprinting [219-221]. Image reproduced from Wikimedia Commons [81].

Numerous dressings have shown a controlled release of drugs but, for the first time, Long et al. developed a 3D bioprinted hydrogel (chitosan-pectin) showing a controlled release of lidocaine hydrochloride fitting the Korsmeyer-Peppas model [224]. The real-time monitoring of wound healing has always been a challenge for dressings. A recent work developed a naturally-originated silk-sericin-based transparent hydrogel that was prepared and evaluated for the visualization of wound care. The hydrogel demonstrated steerable physical properties and adequate biocompatibility through 3D bioprinting, thus allowing the wound monitoring [225]. Supplying oxygen to the wound bed or the deepest areas within the cell constructs — to support cell metabolism, proliferation etc. — still remains a major challenge in tissue engineering. Thus, numerous researchers have tried to find a solution by including oxygen releasing materials in their 3D bioprinted dressing designs. For example, Touri et al. developed a 3D bioprinted calcium

phosphate scaffold with calcium peroxide as an oxygen releasing agent in a PCL matrix and Lu et al. developed an alginate printed hydrogel with also calcium phosphate as an oxygen releasing agent. Both dressings demonstrated that 3D bioprinted oxygen-releasing devices alleviated hypoxia, maintaining oxygen availability, and even ensuring proliferation of seeded cells, whilst also reducing hypoxia-induced apoptosis [226,227].

4.2 CRISPR revolution

The clustered regularly interspaced short palindromic repeats-associated protein 9 (CRISPR/Cas9) system has provided a genome editing technology that can accurately target different genomic sites to repair or disrupt a specific gene [228]. The Cas9 and the other Cas systems have been widely applied for the identification of therapeutic targets, generation of animal models, identification of gene functions and, thereby, development of gene therapies. Furthermore this system has been used to alleviate disease symptoms of different pathologies [229]. CRISPR/Cas9 technology is potentially utilizable for chronic wound healing approaches since it has the potential to leverage and mobilize a wide variety of molecular mediators for healing, without inducing immune response [230]. Thus, by using this technology it has been possible to access genetic targets to manipulate the wound microenvironment in a more precise way and with extremely lower off-target modifications than the other gene-editing techniques. For example, recent works achieved the genetic ex-vivo reprograming of BM-MSCs to overexpress PDGF-B and promote healing [231]. Other authors reported the correction of some genes in fibroblasts of patients suffering dystrophic epidermolysis bulbosa, a pathology causing slow-healing wounds on the skin [232]. Nevertheless, the future of this technology is likely to reside in ex-vivo reprograming of cells to be injected or loaded in dressings — overexpressing GFs or pro-healing cytokines—, rather than in reprograming the cells of the wound bed through local CRISPR/Cas9 administration.

4.3 Extracellular Vesicles as a cell-free wound healing approach

EVs are advanced and compacted systems of cell-to-cell communication, by which the different cell types can exchange information in the form of nucleic acid

species, proteins or lipids. EVs were first discovered in 1983 [233,234] and in 1989 they were given the name of “exosomes” [235]. Nowadays the term “exosomes” (Exos) is referred to small EVs that are released from the interior of any cell, via the multivesicular endosomal pathway. Exos are one of the different EVs released from cells, together with microvesicles (or ectosomes) and apoptotic bodies. Exos, microvesicles and apoptotic bodies differ from each other on the cargo content (proteins, RNA, etc.) and size: 30-150 nm for Exos, 100-1000 nm for microvesicles and 50-5000 nm for apoptotic bodies [236]. When developing EV therapeutics for wound healing applications, it is mandatory to consider the cellular source. EVs from inflammatory cells obviously mediate different biological functions than those released from MSCs. Thus, the use of EVs in wound healing applications is mainly focused on the MSCs-EVs, because of their demonstrated immunomodulatory function and regenerative capacity [237].

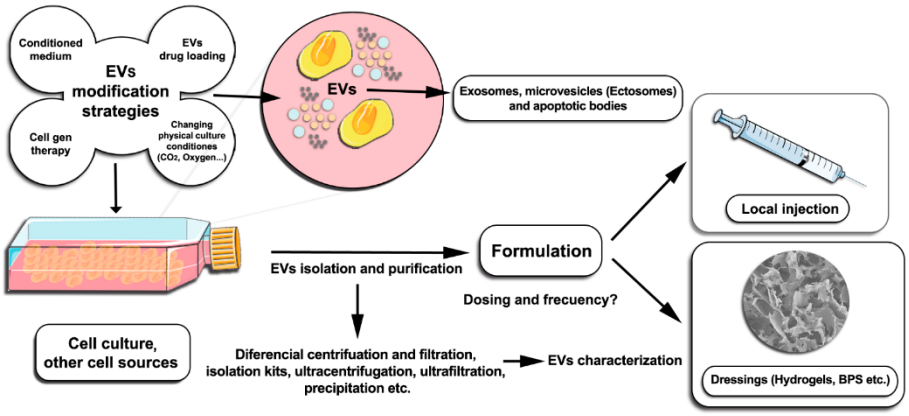

Fig. 8. EVs formulation and administration

An important aspect is the way the EVs are administered, because it influences their biodistribution. Therefore, this needs to be considered when developing a wound healing therapeutic approach [238]. In Fig. 8 we summarized the different described methods for EVs-formulation and administration in wounds. Recent works have highlighted the therapeutic potential of EVs for cutaneous wound healing in different animal models, which are well summarized by Cabral et al. [236]. The vast majority of therapeutic approaches with EVs are formulated in injections: topical, subcutaneous, intramuscular or intravenous. However, EVs

administration in injection can affect their function due to a rapid clearance rate [239]. Recently, novel wound dressings comprising different combinations of EVs and biomaterials have been raised (Table 1).

Only a few in vivo EVs-loaded approaches have been tested with promising results. Fang et al. developed a hydrogel (HydroMatrix®) coated with human umbilical cord MSCs-Exos. The study highlighted a reduction in scar formation and myofibroblast accumulation in comparison with control group [240]. A chitosan-based hydrogel incorporating micro-RNA-126-overexpressing SMSCs-Exos demonstrated an accelerated re-epithelialization with a remarkable increased angiogenesis in comparison with control group and Exos-free dressing [241]. Another in vivo approach using a chitosan/silk GMSCs-Exos-loaded hydrogel demonstrated great swelling and moisture retention properties with enhanced re-epithelialization, collagen deposition and microvessel and nerve density in comparison with control and Exos-free hydrogel groups [242]. A double-approach dressing therapy was described by Xu et al. They developed another chitosan/silk hydrogel and loaded it with Exos from PRP and an anti-inflammatory polysaccharide obtained from C. zedoaria (ZWP). The combined therapy demonstrated enhanced wound closure when compared against the control group and the groups consisting of hydrogel with only one component (Exos or ZWP) [244].

A multifocal approach using a self-healing hydrogel (methyl cellulose and chitosan) loaded with ATMSCs exosomes was also recently described. The Exos-loaded system enhanced wound closure rates, angiogenesis, re-epithelialization and collagen deposition in comparison with the control and Exos-free system. In addition, the developed system showed antimicrobial properties [245]. Light-triggerable hydrogels have also been studied with Exos cargo in wound healing. Henriques-Antunes and co-workers showed that the HA hydrogel loaded with hUCB-MNCs (human umbilical cord blood mononuclear cells) increased closure kinetics of wounds treated with single/multiple doses of Exos, showing values comparable to those obtained with Regranex®. This pro-healing activity was related to an increase in neovascularization, enhanced re-epithelialization and an alteration in the expression of 7 miRNAs at different times during wound healing.

Furthermore, they demonstrated that the multiple administration protocol produced more beneficial effects than the single dose administration of the same total concentration of Exos [246].

Two more recent Exos-loaded hydrogels were developed (alginate and methyl cellulose/chitosan) with promising results in full thickness cutaneous wound model. The cellulose/chitosan hydrogel developed by Wang et al. demonstrated excellent biocompatibility and self-healing properties. Furthermore, when the exosome-loaded — from placental MSCs — hydrogels where tested in db/db mice they showed an increased angiogenesis and a reduced cell apoptosis. The healed area in the Exos-loaded hydrogel group was filled with neo-tissues and even hair follicles and glands were detected at day 15 [247]. Finally, the alginate hydrogels developed by Shafei et al. where loaded with Exos from ATMSCs. Briefly, the physical and biochemical properties proved that the fabricated system was biodegradable and biocompatible. In addition, the Exos-loaded hydrogel improved wound closure, collagen synthesis, and neo-vessel formation in the wound area [248].

These recent findings have demonstrated that EVs derived from different cell types can promote wound healing when they are both carried in dressings or locally injected. However, apart from sharing the fact that EVs — in the vast majority of studies — were isolated from culture conditioned medium, there are many aspects that vary greatly, such as differences in the cellular origin, the isolation procedure and/or the quantification method. All this probably resulted in disparate proportions of different EVs populations and different levels of lipids and protein contaminants [236,250]. Furthermore, the differences in dosage units contribute to this lack of standardization. Taking these and other specific issues relevant to clinical translation into consideration, it is clear that there is a need for more pre-clinical studies with the aim of shedding light onto the precise mechanisms that govern the effects mediated by such still barely known, ill-defined and heterogenous EVs.

Table 1: EVs-loaded dressings for wound healing applications. SMSCs (synovium mesenchymal stem cells), GMSCs (gingival mesenchymal stem cells). UCB-MNCs (umbilical cord blood mononuclear cells). Placental mesenchymal stem cells (PMSCs).

Scaffold	*Cell type EVs source*	*Treatment*	*Model*	*Results*	*Ref.*
HydroMatrix®	**Umbilical cord-MSCs**	Hydrogel coated hUC_MSCs-Exos	Diabetic rat full thickness cutaneous wound	Reduction in scar formation and myofibroblasts accumulation	**Fang, 2016** [124]
Chitosan BPS	**SMSCs**	Chitosan hydrogel incorporating SMSCs-Exos	Diabetic rat full thickness cutaneous wound	Accelerated re-epithelialization, enhanced angiogenesis and promotion of collagen maturity.	**Tao, 2017** [125]
Chitosan/silk fibroin hydrogel	**GMSCs**	Chitosan/silk hydrogel loaded with GMSCs-Exos	Diabetic rat skin defect	Enhanced re-epithelialization and collagen deposition. More microvessel and nerve density compared to control and Exos-free hydrogel	**Shi, 2017** [126]
PVA hydrogel	**hMSCs**	PVA hydrogel loaded with hMSCs EVs	*In vitro*	EVs used as prodrug carriers (curcumin) demonstrated long term anti-inflammatory potential.	**Fuhrmann, 2018** [127]
Chitosan/silk fibroin hydrogel	**PRP**	Chitosan/silk fibroin hydrogel loaded with PRP-Exos and a polysaccharide isolated from *C. zedoaria* (ZWP)	Diabetic rat full thickness cutaneous wound	Exos/ZWP-loaded hydrogels showed enhanced wound closure vs control and vs Exos-hydrogel / ZWP-hydrogel.	**Xu, 2018** [128]
Poly-L-lysine/pluronic F127/ oxidative HA hydrogel	**ATMSCs**	ATMSCs-Exos loaded in a Poly-L-lysine/pluronic F127/ oxidative HA self-healing hydrogel	Diabetic rat full thickness cutaneous wounds	Exos-loaded hydrogel enhanced wound closure rate, angiogenesis, re-epithelialization and collagen deposition vs control and Exos-free hydrogel.	**Wang, 2019** [129]
Hyaluronic acid (HA) light disassembly hydrogel	**hUCB-MNCs**	Hyaluronic acid (HA) hydrogel loaded with hUCB-MNCs in a photocleavable linker	Diabetic rat full thickness cutaneous wounds	The Exos-loaded hydrogel demonstrated a robust enhancement in wound closure vs control, single dose Exos and PDGF-BB commercialized therapy.	**Henriques-Antunes, 2019** [130]
Methyl-cellulose/chitosan hydrogel	**PMSCs**	Methyl-cellulose/chitosan hydrogel loaded with PMSCs-Exos	Diabetic rat full thickness cutaneous wound	Accelerated wound closure with enhanced angiogenesis and inhibited apoptosis in Exos-loaded hydrogel vs control/hydrogel Exos-free/Hydrogel-free Exos	**Wang, 2019** [131]
Alginate hydrogel	**ATMSCs**	Alginate hydrogel loaded with ATMSCs-Exos	Full-thickness excisional wound model	The Exos-loaded system improved wound closure, collagen synthesis and vessel formation in wound area.	**Shafei, 2020** [132]
OxOBand scaffolds (polyurethane)	**ATMSCs**	Polyurethane oxygen releasing scaffolds loaded with ATMSCs-Exos	Diabetic rat full thickness cutaneous wounds	This approach prevented infection and ulceration. Furthermore, improved wound healing with increased collagen deposition, and re-epithelialization.	**Shiekh, 2020** [133]

5. Concluding remarks and future perspectives

The elevated complexity of the wound healing process requires a precise and spatio-temporally adequate treatment in order to success with the therapy. There is a large number of factors involved and, in some of them, the temporal sequence in the healing process is not yet elucidated. One first step would be identifying and restoring particular abnormalities, utilizing personalized medicine in order to achieve a successful therapy.

As a response to a demanding therapy that better mimics the ECM, cell-loaded dressings became the main attraction in wound dressings´ field. The first cell-loaded dressing commercialized— a BeLSE — was in 1998 under the name of Apligraf® (Organogenesis, INC). However, nowadays, its medical application in real patients is not common because of its cost-efficacy and rejection issues [251]. Furthermore, Apligraf® and Dermagraft® (Organogenesis, INC) — another BeLSE approved by the FDA in 2001 — have shown lower rates in wound healing with higher costs in different prospective, comparative trials carried out together with decellularized matrices such as Epifix® or Oasis® [252,253]. In addition, one of the latest BeLSEs that appeared in the market, Theraskin® (Soluble systems, LLC) demonstrated no differences in healing rates against Apligraf® in a multicenter, prospective, randomized study for chronic wound healing applications [254].

With this lack of success in BeLSEs clinical application, stem cells became the main players in the chronic wound research. Investigations with stem cell-loaded dressings have been described since the beginning of the 21st century; however, with 5 clinical trials completed and at least another 3 in progress, there is no available products already marketed. The safety problems related to stem cell treatments (risk of tumor growth and metastasis) [255] and the harder commercialization pathway, compared to non-cellular based products, are promoting novel therapies based on different cell-free therapeutic strategies. With the appearance of 3D bioprinting technology or the increasing knowledge in the intercellular functions of EVs, a precise, multi-focal and multi-target cell-free dressing strategy may be achieved. Furthermore, adding up different combinations

of bioactive compounds, therapies may act in more than one phase of the wound healing process, thus helping to recapitulate the native tissue environment.

Considerations regarding the clinical translation of the latest advances and technologies should comprise the optimization of the cost-effectiveness, together with the accomplishment of the strict regulatory pathways. Indeed, the major challenge consists in moving from laboratory approaches to clinically acceptable practices operating under safety, reproducibility and high effective requirements.

Acknowledgments

Authors acknowledge the financial support from the Spanish Ministry of Economy and Competitiveness through the "RETOS" Program (NANGROW project, RTC-2017-6696-1) and from the Basque Government (Grupos Consolidados, IT907-16). K. Las Heras thanks the Basque Government (Department of Education, Universities and Research) for the PhD grant (PRE_2018_1_0412).

Declarations or conflicts of interest

None.

References

[1] S.A. Eming, P. Martin, M. Tomic-Canic, Wound repair and regeneration: Mechanisms, signaling, and translation, Science translational medicine. 6 (2014) 265sr6.

[2] M. Olsson, K. Jarbrink, U. Divakar, R. Bajpai, Z. Upton, A. Schmidtchen, J. Car, The humanistic and economic burden of chronic wounds: A systematic review, Wound Repair Regen. 27 (2019) 114-125.

[3] R. Zhao, H. Liang, E. Clarke, C. Jackson, M. Xue, Inflammation in Chronic Wounds, International journal of molecular sciences. 17 (2016) 2085.

[4] J.G. Powers, C. Higham, K. Broussard, T.J. Phillips, Wound healing and treating wounds: Chronic wound care and management, J. Am. Acad. Dermatol. 74 (2016) 607-6.

[5] Q. Cheng, M. Gibb, N. Graves, K. Finlayson, R.E. Pacella, Cost-effectiveness analysis of guideline-based optimal care for venous leg ulcers in Australia, BMC Health Serv. Res. 18 (2018) 421-3.

[6] C.D. Weller, V. Team, G. Sussman, First-Line Interactive Wound Dressing Update: A Comprehensive Review of the Evidence, Front. Pharmacol. 11 (2020) 155.

[7] R.D. Forrest, Early history of wound treatment, J. R. Soc. Med. 75 (1982) 198-205.

[8] I.K. Cohen, Lessons from the history of wound healing, Clin. Dermatol. 25 (2007) 3-8.

[9] J.B. Shah, The history of wound care, J. Am. Col. Certif Wound. Spec. 3 (2011) 65-66.

[10] B.K. Sun, Z. Siprashvili, P.A. Khavari, Advances in skin grafting and treatment of cutaneous wounds, Science. 346 (2014) 941-945.

[11] R.G. Reish, E. Eriksson, Scars: a review of emerging and currently available therapies, Plast. Reconstr. Surg. 122 (2008) 1068-1078.

[12] M. Rodrigues, N. Kosaric, C.A. Bonham, G.C. Gurtner, Wound Healing: A Cellular Perspective, Physiol. Rev. 99 (2019) 665-706.

[13] E.M. Golebiewska, A.W. Poole, Platelet secretion: From haemostasis to wound healing and beyond, Blood Rev. 29 (2015) 153-162.

[14] J. Hardwicke, D. Schmaljohann, D. Boyce, D. Thomas, Epidermal growth factor therapy and wound healing--past, present and future perspectives, Surgeon. 6 (2008) 172-177.

[15] R.M. Thushara, M. Hemshekhar, Basappa, K. Kemparaju, K.S. Rangappa, K.S. Girish, Biologicals, platelet apoptosis and human diseases: An outlook, Crit. Rev. Oncol. Hematol. 93 (2015) 149-158.

[16] G.C. Gurtner, S. Werner, Y. Barrandon, M.T. Longaker, Wound repair and regeneration, Nature. 453 (2008) 314-321.

[17] T.A. Wilgus, S. Roy, J.C. McDaniel, Neutrophils and Wound Repair: Positive Actions and Negative Reactions, Adv. Wound. Care. (New Rochelle). 2 (2013) 379-388.

[18] L.M. Morton, T.J. Phillips, Wound healing and treating wounds: Differential diagnosis and evaluation of chronic wounds, J. Am. Acad. Dermatol. 74 (2016) 589-6.

[19] W.L. Havran, J.M. Jameson, Epidermal T cells and wound healing, J. Immunol. 184 (2010) 5423-5428.

[20] P. Krzyszczyk, R. Schloss, A. Palmer, F. Berthiaume, The Role of Macrophages in Acute and Chronic Wound Healing and Interventions to Promote Pro-wound Healing Phenotypes, Front. Physiol. 9 (2018) 419.

[21] M.S. Hu, M.R. Borrelli, H.P. Lorenz, M.T. Longaker, D.C. Wan, Mesenchymal Stromal Cells and Cutaneous Wound Healing: A Comprehensive Review of the Background, Role, and Therapeutic Potential, Stem Cells Int. 2018 (2018) 6901983.

[22] K.A.U. Gonzales, E. Fuchs, Skin and Its Regenerative Powers: An Alliance between Stem Cells and Their Niche, Dev. Cell. 43 (2017) 387-401.

[23] L. Liu, Y. Yu, Y. Hou, J. Chai, H. Duan, W. Chu, H. Zhang, Q. Hu, J. Du, Human umbilical cord mesenchymal stem cells transplantation promotes cutaneous wound healing of severe burned rats, PLoS One. 9 (2014) e88348.

[24] A.W. Yeung, A.C. Terentis, N.J. King, S.R. Thomas, Role of indoleamine 2,3-dioxygenase in health and disease, Clin. Sci. (Lond). 129 (2015) 601-672.

[25] S.I. Motegi, O. Ishikawa, Mesenchymal stem cells: The roles and functions in cutaneous wound healing and tumor growth, J. Dermatol. Sci. 86 (2017) 83-89.

[26] I. Aukhil, Biology of wound healing, Periodontol. 2000. 22 (2000) 44-50.

[27] P.A. Efron, L.L. Moldawer, Cytokines and wound healing: the role of cytokine and anticytokine therapy in the repair response, J. Burn Care Rehabil. 25 (2004) 149-160.

[28] S. Barrientos, O. Stojadinovic, M.S. Golinko, H. Brem, M. Tomic-Canic, Growth factors and cytokines in wound healing, Wound Repair Regen. 16 (2008) 585-601.

[29] I. Pastar, O. Stojadinovic, N.C. Yin, H. Ramirez, A.G. Nusbaum, A. Sawaya, S.B. Patel, L. Khalid, R.R. Isseroff, M. Tomic-Canic, Epithelialization in Wound Healing: A Comprehensive Review, Adv. Wound. Care. (New Rochelle). 3 (2014) 445-464.

[30] A. Ridiandries, J.T.M. Tan, C.A. Bursill, The Role of Chemokines in Wound Healing, Int. J. Mol. Sci. 19 (2018) 10.3390/ijms19103217.

[31] F. Moccia, S. Negri, M. Shekha, P. Faris, G. Guerra, Endothelial Ca(2+) Signaling, Angiogenesis and Vasculogenesis: just What It Takes to Make a Blood Vessel, Int. J. Mol. Sci. 20 (2019) 10.3390/ijms20163962.

[32] M. Xue, R. Zhao, H. Lin, C. Jackson, Delivery systems of current biologicals for the treatment of chronic cutaneous wounds and severe burns, Adv. Drug Deliv. Rev. 129 (2018) 219-241.

[33] M. Sasaki, R. Abe, Y. Fujita, S. Ando, D. Inokuma, H. Shimizu, Mesenchymal stem cells are recruited into wounded skin and contribute to wound repair by transdifferentiation into multiple skin cell type, J. Immunol. 180 (2008) 2581-2587.

[34] K.C. Rustad, V.W. Wong, M. Sorkin, J.P. Glotzbach, M.R. Major, J. Rajadas, M.T. Longaker, G.C. Gurtner, Enhancement of mesenchymal stem cell angiogenic capacity and stemness by a biomimetic hydrogel scaffold, Biomaterials. 33 (2012) 80-90.

[35] J.M. Reinke, H. Sorg, Wound repair and regeneration, Eur. Surg. Res. 49 (2012) 35-43.

[36] M. Xue, C.J. Jackson, Extracellular Matrix Reorganization During Wound Healing and Its Impact on Abnormal Scarring, Adv. Wound. Care. (New Rochelle). 4 (2015) 119-136.

[37] A. Stojadinovic, J.W. Carlson, G.S. Schultz, T.A. Davis, E.A. Elster, Topical advances in wound care, Gynecol. Oncol. 111 (2008) 70.

[38] P. Martin, R. Nunan, Cellular and molecular mechanisms of repair in acute and chronic wound healing, Br. J. Dermatol. 173 (2015) 370-378.

[39] O. Soehnlein, S. Steffens, A. Hidalgo, C. Weber, Neutrophils as protagonists and targets in chronic inflammation, Nat. Rev. Immunol. 17 (2017) 248-261.

[40] E. Kolaczkowska, P. Kubes, Neutrophil recruitment and function in health and inflammation, Nat. Rev. Immunol. 13 (2013) 159-175.

[41] T.A. Wynn, K.M. Vannella, Macrophages in Tissue Repair, Regeneration, and Fibrosis, Immunity. 44 (2016) 450-462.

[42] M.L. Usui, J.N. Mansbridge, W.G. Carter, M. Fujita, J.E. Olerud, Keratinocyte migration, proliferation, and differentiation in chronic ulcers from patients with diabetes and normal wounds, J. Histochem. Cytochem. 56 (2008) 687-696.

[43] T.N. Demidova-Rice, M.R. Hamblin, I.M. Herman, Acute and impaired wound healing: pathophysiology and current methods for drug delivery, part 2: role of growth factors in normal and pathological wound healing: therapeutic potential and methods of delivery, Adv. Skin Wound Care. 25 (2012) 349-370.

[44] O. Stojadinovic, I. Pastar, S. Vukelic, M.G. Mahoney, D. Brennan, A. Krzyzanowska, M. Golinko, H. Brem, M. Tomic-Canic, Deregulation of keratinocyte differentiation and activation: a hallmark of venous ulcers, J. Cell. Mol. Med. 12 (2008) 2675-2690.

[45] G.S. Schultz, R.G. Sibbald, V. Falanga, E.A. Ayello, C. Dowsett, K. Harding, M. Romanelli, M.C. Stacey, L. Teot, W. Vanscheidt, Wound bed preparation: a systematic approach to wound management, Wound Repair Regen. 11 Suppl 1 (2003) 1.

[46] B. Bucalo, W.H. Eaglstein, V. Falanga, Inhibition of cell proliferation by chronic wound fluid, Wound Repair Regen. 1 (1993) 181-186.

[47] O.C. Thamm, P. Koenen, N. Bader, A. Schneider, S. Wutzler, E.A. Neugebauer, T.A. Spanholtz, Acute and chronic wound fluids influence keratinocyte function differently, Int. Wound. J. 12 (2015) 143-149.

[48] J. Cha, T. Kwak, J. Butmarc, T.A. Kim, T. Yufit, P. Carson, S.J. Kim, V. Falanga, Fibroblasts from non-healing human chronic wounds show decreased expression of beta ig-h3, a TGF-beta inducible protein, J. Dermatol. Sci. 50 (2008) 15-23.

[49] S. Patel, A. Maheshwari, A. Chandra, Biomarkers for wound healing and their evaluation, J. Wound Care. 25 (2016) 46-55.

[50] D.A. Ramasubbu, V. Smith, F. Hayden, P. Cronin, Systemic antibiotics for treating malignant wounds, Cochrane Database Syst. Rev. 8 (2017) CD011609.

[51] G. Daeschlein, Antimicrobial and antiseptic strategies in wound management, Int. Wound. J. 10 Suppl 1 (2013) 9-14.

[52] D. Basoulis, K. Fragiadaki, N. Tentolouris, P.P. Sfikakis, A. Kokkinos, Anti-TNFalpha treatment for recalcitrant ulcerative necrobiosis lipoidica diabeticorum: A case report and review of the literature, Metabolism. 65 (2016) 569-573.

[53] J.A. Fehlman, N.M. Burkemper, T.A. Missall, Ulcerative necrobiosis lipoidica in the setting of anti-tumor necrosis factor-alpha and hydroxychloroquine treatment for rheumatoid arthritis, JAAD Case Rep. 3 (2017) 127-130.

[54] K.S. de Souza, T.A. Cantaruti, G.M. Azevedo, D.A. Galdino, C.M. Rodrigues, R.A. Costa, N.M. Vaz, C.R. Carvalho, Improved cutaneous wound healing after intraperitoneal injection of alpha-melanocyte-stimulating hormone, Exp. Dermatol. 24 (2015) 198-203.

[55] M. Wolak, T. Staszewska, M. Juszczak, M. Galdyszynska, E. Bojanowska, Anti-inflammatory and pro-healing impacts of exendin-4 treatment in Zucker diabetic rats: Effects on skin wound fibroblasts, Eur. J. Pharmacol. 842 (2019) 262-269.

[56] H. Ozkaya, T. Omma, Y.M. Bag, K. Uzunoglu, M. Isildak, M.E. Duymus, K. Kismet, M. Senes, V. Fidanci, P. Celepli, S. Hucumenoglu, Y. Aral, Topical and Systemic Effects of N-acetyl Cysteine on Wound Healing in a Diabetic Rat Model, Wounds. 31 (2019) 91-96.

[57] H. Aydin, C. Tatar, O.A. Savas, T. Karsidag, B. Ozer, N. Dursun, A. Bekem, A. Unal, I.S. Tuzun, The Effects of Local and Systemic Administration of Proline on Wound Healing in Rats, J. Invest. Surg. (2018) 1-7.

[58] V. Falanga, H. Brem, W.J. Ennis, R. Wolcott, L.J. Gould, E.A. Ayello, Maintenance debridement in the treatment of difficult-to-heal chronic wounds. Recommendations of an expert panel, Ostomy Wound. Manage. Suppl (2008) 2-5.

[59] E.A. Nelson, S.E. Bell-Syer, Compression for preventing recurrence of venous ulcers, Cochrane Database Syst. Rev. (9):CD002303. doi (2014) CD002303.

[60] V. Team, P.G. Chandler, C.D. Weller, Adjuvant therapies in venous leg ulcer management: A scoping review, Wound Repair Regen. 27 (2019) 562-590.

[61] P. Moscicka, M.T. Szewczyk, J. Cwajda-Bialasik, A. Jawien, The role of compression therapy in the treatment of venous leg ulcers, Adv. Clin. Exp. Med. 28 (2019) 847-852.

[62] S. Lalezari, C.J. Lee, A.A. Borovikova, D.A. Banyard, K.Z. Paydar, G.A. Wirth, A.D. Widgerow, Deconstructing negative pressure wound therapy, Int. Wound. J. 14 (2017) 649-657.

[63] G.E. Glass, G.F. Murphy, A. Esmaeili, L.M. Lai, J. Nanchahal, Systematic review of molecular mechanism of action of negative-pressure wound therapy, Br. J. Surg. 101 (2014) 1627-1636.

[64] U. Sadat, G. Chang, A. Noorani, S.R. Walsh, P.D. Hayes, K. Varty, Efficacy of TNP on lower limb wounds: a meta-analysis, J. Wound Care. 17 (2008) 45-48.

[65] M. Wynn, S. Freeman, The efficacy of negative pressure wound therapy for diabetic foot ulcers: A systematised review, J. Tissue Viability. 28 (2019) 152-160.

[66] J. Webster, P. Scuffham, M. Stankiewicz, W.P. Chaboyer, Negative pressure wound therapy for skin grafts and surgical wounds healing by primary intention, Cochrane Database Syst. Rev. (10):CD009261. doi (2014) CD009261.

[67] E.L. Anghel, P.J. Kim, Negative-Pressure Wound Therapy: A Comprehensive Review of the Evidence, Plast. Reconstr. Surg. 138 (2016) 129S-37S.

[68] L.C. Kloth, Electrical Stimulation Technologies for Wound Healing, Adv. Wound. Care. (New Rochelle). 3 (2014) 81-90.

[69] W.J. Ennis, C. Lee, K. Gellada, T.F. Corbiere, T.J. Koh, Advanced Technologies to Improve Wound Healing: Electrical Stimulation, Vibration Therapy, and Ultrasound-What Is the Evidence? Plast. Reconstr. Surg. 138 (2016) 94S-104S.

[70] C. Khouri, S. Kotzki, M. Roustit, S. Blaise, F. Gueyffier, J.L. Cracowski, Hierarchical evaluation of electrical stimulation protocols for chronic wound healing: An effect size meta-analysis, Wound Repair Regen. 25 (2017) 883-891.

[71] S.R. Thom, Oxidative stress is fundamental to hyperbaric oxygen therapy, J. Appl. Physiol. (1985). 106 (2009) 988-995.

[72] G. Han, R. Ceilley, Chronic Wound Healing: A Review of Current Management and Treatments, Adv. Ther. 34 (2017) 599-610.

[73] P. Kranke, M.H. Bennett, M. Martyn-St James, A. Schnabel, S.E. Debus, S. Weibel, Hyperbaric oxygen therapy for chronic wounds, Cochrane Database Syst. Rev. (6):CD004123. doi (2015) CD004123.

[74] B. Cooper, P. Bachoo, Extracorporeal shock wave therapy for the healing and management of venous leg ulcers, Cochrane Database Syst. Rev. 6 (2018) CD011842.

[75] D.P. Kuffler, Photobiomodulation in promoting wound healing: a review, Regen. Med. 11 (2016) 107-122.

[76] R.C. Mosca, A.A. Ong, O. Albasha, K. Bass, P. Arany, Photobiomodulation Therapy for Wound Care: A Potent, Noninvasive, Photoceutical Approach, Adv. Skin Wound Care. 32 (2019) 157-167.

[77] A. Polak, A. Franek, E. Blaszczak, A. Nawrat-Szoltysik, J. Taradaj, L. Wiercigroch, P. Dolibog, M. Stania, G. Juras, A prospective, randomized, controlled, clinical study to evaluate the efficacy of high-frequency ultrasound in the treatment of Stage II and Stage III pressure ulcers in geriatric patients, Ostomy Wound. Manage. 60 (2014) 16-28.

[78] S.J. Kavros, R. Coronado, Diagnostic and Therapeutic Ultrasound on Venous and Arterial Ulcers: A Focused Review, Adv. Skin Wound Care. 31 (2018) 55-65.

[79] A. Rastogi, A. Bhansali, S. Ramachandran, Efficacy and Safety of Low-Frequency, Noncontact Airborne Ultrasound Therapy (Glybetac) For Neuropathic Diabetic Foot Ulcers: A Randomized, Double-Blind, Sham-Control Study, Int. J. Low Extrem Wounds. 18 (2019) 81-88.

[80] O. Ngo, E. Niemann, V. Gunasekaran, P. Sankar, M. Putterman, A. Lafontant, S. Nadkarni, R.A. DiMaria-Ghalili, M. Neidrauer, L. Zubkov, M. Weingarten, D.J. Margolis, P.A. Lewin, Development of Low Frequency (20-100 kHz) Clinically Viable Ultrasound Applicator for Chronic Wound Treatment, IEEE Trans. Ultrason. Ferroelectr. Freq. Control. 66 (2019) 572-580.

[81] Wikimedia Commons. Web page: commons.wikimedia.org, (accessed April 13, 2020)

[82] S. O'Meara, D. Al-Kurdi, Y. Ologun, L.G. Ovington, M. Martyn-St James, R. Richardson, Antibiotics and antiseptics for venous leg ulcers, Cochrane Database Syst. Rev. (1):CD003557. doi (2014) CD003557.

[83] S. Nour, N. Baheiraei, R. Imani, M. Khodaei, A. Alizadeh, N. Rabiee, S.M. Moazzeni, A review of accelerated wound healing approaches: biomaterial- assisted tissue remodeling, J. Mater. Sci. Mater. Med. 30 (2019) 120-6.

[84] G. Norman, J.C. Dumville, Z.E. Moore, J. Tanner, J. Christie, S. Goto, Antibiotics and antiseptics for pressure ulcers, Cochrane Database Syst. Rev. 4 (2016) CD011586.

[85] M. Otero-Vinas, V. Falanga, Mesenchymal Stem Cells in Chronic Wounds: The Spectrum from Basic to Advanced Therapy, Adv. Wound. Care. (New Rochelle). 5 (2016) 149-163.

[86] M.J. Hesseler, N. Shyam, Platelet-rich plasma and its utility in medical dermatology: A systematic review, J. Am. Acad. Dermatol. 81 (2019) 834-846.

[87] G. Gainza, J.J. Aguirre, J.L. Pedraz, R.M. Hernandez, M. Igartua, rhEGF-loaded PLGA-Alginate microspheres enhance the healing of full-thickness excisional wounds in diabetised Wistar rats, Eur. J. Pharm. Sci. 50 (2013) 243-252.

[88] P.S. Korrapati, K. Karthikeyan, A. Satish, V.R. Krishnaswamy, J.R. Venugopal, S. Ramakrishna, Corrigendum to "Recent advancements in nanotechnological strategies in selection, design and delivery of biomolecules for skin regeneration" [Mater. Sci. Eng. C, 67 (2016) 747-765, Mater. Sci. Eng. C. Mater. Biol. Appl. 68 (2016) 996.

[89] H.L. Xu, P.P. Chen, D.L. ZhuGe, Q.Y. Zhu, B.H. Jin, B.X. Shen, J. Xiao, Y.Z. Zhao, Liposomes with Silk Fibroin Hydrogel Core to Stabilize bFGF and Promote the Wound Healing of Mice with Deep Second-Degree Scald, Adv. Healthc. Mater. 6 (2017) 10.1002/adhm.201700344. Epub 2017 Jun 29.

[90] H.A. Benson, Transfersomes for transdermal drug delivery, Expert Opin. Drug Deliv. 3 (2006) 727-737.

[91] J.U. Choi, S.W. Lee, R. Pangeni, Y. Byun, I.S. Yoon, J.W. Park, Preparation and in vivo evaluation of cationic elastic liposomes comprising highly skin-permeable growth factors combined with hyaluronic acid for enhanced diabetic wound-healing therapy, Acta Biomater. 57 (2017) 197-215.

[92] M. Manconi, M.L. Manca, C. Caddeo, D. Valenti, C. Cencetti, O. Diez-Sales, A. Nacher, S. Mir-Palomo, M.C. Terencio, D. Demurtas, J.C. Gomez-Fernandez, F.J. Aranda, A.M. Fadda, P. Matricardi, Nanodesign of new self-assembling core-shell gellan-transfersomes loading baicalin and in vivo evaluation of repair response in skin, Nanomedicine. 14 (2018) 569-579.

[93] K.K. Chereddy, C.H. Her, M. Comune, C. Moia, A. Lopes, P.E. Porporato, J. Vanacker, M.C. Lam, L. Steinstraesser, P. Sonveaux, H. Zhu, L.S. Ferreira, G. Vandermeulen, V. Preat, PLGA nanoparticles loaded with host defense peptide LL37 promote wound healing, J. Control. Release. 194 (2014) 138-147.

[94] D.A. Sanchez, D. Schairer, C. Tuckman-Vernon, J. Chouake, A. Kutner, J. Makdisi, J.M. Friedman, J.D. Nosanchuk, A.J. Friedman, Amphotericin B releasing nanoparticle topical treatment of Candida spp. in the setting of a burn wound, Nanomedicine. 10 (2014) 269-277.

[95] V. Dave, K. Kushwaha, R.B. Yadav, U. Agrawal, Hybrid nanoparticles for the topical delivery of norfloxacin for the effective treatment of bacterial infection produced after burn, J. Microencapsul. 34 (2017) 351-365.

[96] I. Garcia-Orue, G. Gainza, C. Girbau, R. Alonso, J.J. Aguirre, J.L. Pedraz, M. Igartua, R.M. Hernandez, LL37 loaded nanostructured lipid carriers (NLC): A new strategy for the topical treatment of chronic wounds, Eur. J. Pharm. Biopharm. 108 (2016) 310-316.

[97] V.K.H. Bui, D. Park, Y.C. Lee, Chitosan Combined with ZnO, TiO(2) and Ag Nanoparticles for Antimicrobial Wound Healing Applications: A Mini Review of the Research Trends, Polymers (Basel). 9 (2017) 10.3390/polym9010021.

[98] G. Gainza, M. Pastor, J.J. Aguirre, S. Villullas, J.L. Pedraz, R.M. Hernandez, M. Igartua, A novel strategy for the treatment of chronic wounds based on the topical administration of rhEGF-loaded lipid nanoparticles: In vitro bioactivity and in vivo effectiveness in healing-impaired db/db mice, J. Control. Release. 185 (2014) 51-61.

[99] M. Fumakia, E.A. Ho, Nanoparticles Encapsulated with LL37 and Serpin A1 Promotes Wound Healing and Synergistically Enhances Antibacterial Activity, Mol. Pharm. 13 (2016) 2318-2331.

[100] K.K. Patel, D.B. Surekha, M. Tripathi, M.M. Anjum, M.S. Muthu, R. Tilak, A.K. Agrawal, S. Singh, Antibiofilm Potential of Silver Sulfadiazine-Loaded Nanoparticle Formulations: A Study on the Effect of DNase-I on Microbial Biofilm and Wound Healing Activity, Mol. Pharm. 16 (2019) 3916-3925.

[101] G.G. Eskiler, G. Cecener, G. Dikmen, U. Egeli, B. Tunca, Talazoparib Loaded Solid Lipid Nanoparticles: Preparation, Characterization and Evaluation of the Therapeutic Efficacy In vitro, Curr. Drug Deliv. 16 (2019) 511-529.

[102] G. Gainza, W.S. Chu, R.H. Guy, J.L. Pedraz, R.M. Hernandez, B. Delgado-Charro, M. Igartua, Development and in vitro evaluation of lipid nanoparticle-based dressings for topical treatment of chronic wounds, Int. J. Pharm. 490 (2015) 404-411.

[103] G. Gainza, D.C. Bonafonte, B. Moreno, J.J. Aguirre, F.B. Gutierrez, S. Villullas, J.L. Pedraz, M. Igartua, R.M. Hernandez, The topical administration of rhEGF-loaded nanostructured lipid carriers (rhEGF-NLC) improves healing in a porcine full-thickness excisional wound model, J. Control. Release. 197 (2015) 41-47.

[104] D. Chouhan, N. Dey, N. Bhardwaj, B.B. Mandal, Emerging and innovative approaches for wound healing and skin regeneration: Current status and advances, Biomaterials. 216 (2019) 119267.

[105] P. Rousselle, F. Braye, G. Dayan, Re-epithelialization of adult skin wounds: Cellular mechanisms and therapeutic strategies, Adv. Drug Deliv. Rev. 146 (2019) 344-365.

[106] J.R. Martin, C.E. Nelson, M.K. Gupta, F. Yu, S.M. Sarett, K.M. Hocking, A.C. Pollins, L.B. Nanney, J.M. Davidson, S.A. Guelcher, C.L. Duvall, Local Delivery of PHD2 siRNA from ROS-Degradable Scaffolds to Promote Diabetic Wound Healing, Adv. Healthc. Mater. 5 (2016) 2751-2757.

[107] N. Li, H.C. Luo, M. Ren, L.M. Zhang, W. Wang, C.L. Pan, L.Q. Yang, G.J. Lao, J.J. Deng, K.J. Mai, K. Sun, C. Yang, L. Yan, Efficiency and Safety of beta-CD-(D3)7 as siRNA

Carrier for Decreasing Matrix Metalloproteinase-9 Expression and Improving Wound Healing in Diabetic Rats, ACS Appl. Mater. Interfaces. 9 (2017) 17417-17426.

[108] P.S. Rabbani, A. Zhou, Z.M. Borab, J.A. Frezzo, N. Srivastava, H.T. More, W.J. Rifkin, J.A. David, S.J. Berens, R. Chen, S. Hameedi, M.H. Junejo, C. Kim, R.A. Sartor, C.F. Liu, P.B. Saadeh, J.K. Montclare, D.J. Ceradini, Novel lipoproteoplex delivers Keap1 siRNA based gene therapy to accelerate diabetic wound healing, Biomaterials. 132 (2017) 1-15.

[109] M.P. Rowan, L.C. Cancio, E.A. Elster, D.M. Burmeister, L.F. Rose, S. Natesan, R.K. Chan, R.J. Christy, K.K. Chung, Burn wound healing and treatment: review and advancements, Crit. Care. 19 (2015) 243-2.

[110] M. Kanapathy, N. Hachach-Haram, N. Bystrzonowski, J.T. Connelly, E.A. O'Toole, D.L. Becker, A. Mosahebi, T. Richards, Epidermal grafting for wound healing: a review on the harvesting systems, the ultrastructure of the graft and the mechanism of wound healing, Int. Wound. J. 14 (2017) 16-23.

[111] T.B. Santema, P.P. Poyck, D.T. Ubbink, Skin grafting and tissue replacement for treating foot ulcers in people with diabetes, Cochrane Database Syst. Rev. 2 (2016) CD011255.

[112] K. Vig, A. Chaudhari, S. Tripathi, S. Dixit, R. Sahu, S. Pillai, V.A. Dennis, S.R. Singh, Advances in Skin Regeneration Using Tissue Engineering, Int. J. Mol. Sci. 18 (2017) 10.3390/ijms18040789.

[113] A.A. Leto Barone, M. Mastroianni, E.A. Farkash, C. Mallard, A. Albritton, R. Torabi, D.A. Leonard, J.M. Kurtz, D.H. Sachs, C.L. Cetrulo, Genetically modified porcine split-thickness skin grafts as an alternative to allograft for provision of temporary wound coverage: preliminary characterization, Burns. 41 (2015) 565-574.

[114] T. Yamamoto, H. Iwase, T.W. King, H. Hara, D.K.C. Cooper, Skin xenotransplantation: Historical review and clinical potential, Burns. 44 (2018) 1738-1749.

[115] S.P. Tarassoli, Z.M. Jessop, A. Al-Sabah, N. Gao, S. Whitaker, S. Doak, I.S. Whitaker, Skin tissue engineering using 3D bioprinting: An evolving research field, J. Plast. Reconstr. Aesthet. Surg. 71 (2018) 615-623.

[116] A. Rahmani Del Bakhshayesh, N. Annabi, R. Khalilov, A. Akbarzadeh, M. Samiei, E. Alizadeh, M. Alizadeh-Ghodsi, S. Davaran, A. Montaseri, Recent advances on biomedical applications of scaffolds in wound healing and dermal tissue engineering, Artif. Cells Nanomed Biotechnol. 46 (2018) 691-705.

[117] W. Lee, J.C. Debasitis, V.K. Lee, J.H. Lee, K. Fischer, K. Edminster, J.K. Park, S.S. Yoo, Multi-layered culture of human skin fibroblasts and keratinocytes through three-dimensional freeform fabrication, Biomaterials. 30 (2009) 1587-1595.

[118] J.T. Egana, F.A. Fierro, S. Kruger, M. Bornhauser, R. Huss, S. Lavandero, H.G. Machens, Use of human mesenchymal cells to improve vascularization in a mouse model for scaffold-based dermal regeneration, Tissue Eng. Part A. 15 (2009) 1191-1200.

[119] D.F. MacFarlane, Current techniques in skin grafting, Adv. Dermatol. 22 (2006) 125-138.

[120] D. Wainwright, M. Madden, A. Luterman, J. Hunt, W. Monafo, D. Heimbach, R. Kagan, K. Sittig, A. Dimick, D. Herndon, Clinical evaluation of an acellular allograft dermal matrix in full-thickness burns, J. Burn Care Rehabil. 17 (1996) 124-136.

[121] F.B. Stillaert, C. Di Bartolo, J.A. Hunt, N.P. Rhodes, E. Tognana, S. Monstrey, P.N. Blondeel, Human clinical experience with adipose precursor cells seeded on hyaluronic acid-based spongy scaffolds, Biomaterials. 29 (2008) 3953-3959.

[122] K.C. Broussard, J.G. Powers, Wound dressings: selecting the most appropriate type, Am. J. Clin. Dermatol. 14 (2013) 449-459.

[123] S.M. Ahsan, M. Thomas, K.K. Reddy, S.G. Sooraparaju, A. Asthana, I. Bhatnagar, Chitosan as biomaterial in drug delivery and tissue engineering, Int. J. Biol. Macromol. 110 (2018) 97-109.

[124] M. Andonegi, K.L. Heras, E. Santos-Vizcaino, M. Igartua, R.M. Hernandez, K. de la Caba, P. Guerrero, Structure-properties relationship of chitosan/collagen films with potential for biomedical applications, Carbohydr. Polym. 237 (2020) 116159.

[125] I. Garcia-Orue, E. Santos-Vizcaino, A. Etxabide, J. Uranga, A. Bayat, P. Guerrero, M. Igartua, K. de la Caba, R.M. Hernandez, Development of Bioinspired Gelatin and Gelatin/Chitosan Bilayer Hydrofilms for Wound Healing, Pharmaceutics. 11 (2019) 10.3390/pharmaceutics11070314.

[126] N. Devi, J. Dutta, Preparation and characterization of chitosan-bentonite nanocomposite films for wound healing application, Int. J. Biol. Macromol. 104 (2017) 1897-1904.

[127] A. Shah, M. Ali Buabeid, E.A. Arafa, I. Hussain, L. Li, G. Murtaza, The wound healing and antibacterial potential of triple-component nanocomposite (chitosan-silver-sericin) films loaded with moxifloxacin, Int. J. Pharm. 564 (2019) 22-38.

[128] M. Kumorek, I.M. Minisy, T. Krunclova, M. Vorsilakova, K. Venclikova, E.M. Chanova, O. Janouskova, D. Kubies, pH-responsive and antibacterial properties of self-assembled multilayer films based on chitosan and tannic acid, Mater. Sci. Eng. C. Mater. Biol. Appl. 109 (2020) 110493.

[129] M. Choi, N. Hasan, J. Cao, J. Lee, S.P. Hlaing, J.W. Yoo, Chitosan-based nitric oxide-releasing dressing for anti-biofilm and in vivo healing activities in MRSA biofilm-infected wounds, Int. J. Biol. Macromol. 142 (2020) 680-692.

[130] P. Basu, U. Narendrakumar, R. Arunachalam, S. Devi, I. Manjubala, Characterization and Evaluation of Carboxymethyl Cellulose-Based Films for Healing of Full-Thickness Wounds in Normal and Diabetic Rats, ACS Omega. 3 (2018) 12622-12632.

[131] C.M. Srivastava, R. Purwar, A. Gupta, D. Sharma, Dextrose modified flexible tasar and muga fibroin films for wound healing applications, Mater. Sci. Eng. C. Mater. Biol. Appl. 75 (2017) 104-114.

[132] J. Rivadeneira, M.C. Audisio, A. Gorustovich, Films based on soy protein-agar blends for wound dressing: Effect of different biopolymer proportions on the drug release rate and the physical and antibacterial properties of the films, J. Biomater. Appl. 32 (2018) 1231-1238.

[133] A. Veeruraj, L. Liu, J. Zheng, J. Wu, M. Arumugam, Evaluation of astaxanthin incorporated collagen film developed from the outer skin waste of squid Doryteuthis singhalensis for wound healing and tissue regenerative applications, Mater. Sci. Eng. C. Mater. Biol. Appl. 95 (2019) 29-42.

[134] P. Hubner, N. Donati, L.K.M. Quines, I.C. Tessaro, N.R. Marcilio, Gelatin-based films containing clinoptilolite-Ag for application as wound dressing, Mater. Sci. Eng. C. Mater. Biol. Appl. 107 (2020) 110215.

[135] D.A. Taylor, L.C. Sampaio, Z. Ferdous, A.S. Gobin, L.J. Taite, Decellularized matrices in regenerative medicine, Acta Biomater. 74 (2018) 74-89.

[136] S. Chattopadhyay, R.T. Raines, Review collagen-based biomaterials for wound healing, Biopolymers. 101 (2014) 821-833.

[137] A.J. Singer, R.A. Clark, Cutaneous wound healing, N. Engl. J. Med. 341 (1999) 738-746.

[138] J. Heino, The collagen receptor integrins have distinct ligand recognition and signaling functions, Matrix Biol. 19 (2000) 319-323.

[139] L. Shi, S. Ramsay, R. Ermis, D. Carson, In vitro and in vivo studies on matrix metalloproteinases interacting with small intestine submucosa wound matrix, Int. Wound. J. 9 (2012) 44-53.

[140] L. Shi, V. Ronfard, Biochemical and biomechanical characterization of porcine small intestinal submucosa (SIS): a mini review, Int. J. Burns Trauma. 3 (2013) 173-179.

[141] N.J. Turner, S.F. Badylak, The Use of Biologic Scaffolds in the Treatment of Chronic Nonhealing Wounds, Adv. Wound. Care. (New Rochelle). 4 (2015) 490-500.

[142] M.A. Moore, B. Samsell, G. Wallis, S. Triplett, S. Chen, A.L. Jones, X. Qin, Decellularization of human dermis using non-denaturing anionic detergent and endonuclease: a review, Cell. Tissue Bank. 16 (2015) 249-259.

[143] A.R. Silini, A. Cargnoni, M. Magatti, S. Pianta, O. Parolini, The Long Path of Human Placenta, and Its Derivatives, in Regenerative Medicine, Front. Bioeng. Biotechnol. 3 (2015) 162.

[144] M.J. Lopez-Valladares, M. Teresa Rodriguez-Ares, R. Tourino, F. Gude, M. Teresa Silva, J. Couceiro, Donor age and gestational age influence on growth factor levels in human amniotic membrane, Acta Ophthalmol. 88 (2010) 211.

[145] L.E. Dickinson, S. Gerecht, Engineered Biopolymeric Scaffolds for Chronic Wound Healing, Front. Physiol. 7 (2016) 341.

[146] M.C. Moore, A. Van De Walle, J. Chang, C. Juran, P.S. McFetridge, Human Perinatal-Derived Biomaterials, Adv. Healthc. Mater. 6 (2017) 10.1002/adhm.201700345. Epub 2017 Aug 7.

[147] A. Pourmoussa, D.J. Gardner, M.B. Johnson, A.K. Wong, An update and review of cell-based wound dressings and their integration into clinical practice, Ann. Transl. Med. 4 (2016) 457.

[148] R.S. Kirsner, A.C. Vivas, Lower-extremity ulcers: diagnosis and management, Br. J. Dermatol. 173 (2015) 379-390.

[149] G.D. Mogosanu, A.M. Grumezescu, Natural and synthetic polymers for wounds and burns dressing, Int. J. Pharm. 463 (2014) 127-136.

[150] S.S. Scherer, G. Pietramaggiori, J. Matthews, S. Perry, A. Assmann, A. Carothers, M. Demcheva, R.C. Muise-Helmericks, A. Seth, J.N. Vournakis, R.C. Valeri, T.H. Fischer, H.B. Hechtman, D.P. Orgill, Poly-N-acetyl glucosamine nanofibers: a new bioactive material

to enhance diabetic wound healing by cell migration and angiogenesis, Ann. Surg. 250 (2009) 322-330.

[151] C.S. Hankin, J. Knispel, M. Lopes, A. Bronstone, E. Maus, Clinical and cost efficacy of advanced wound care matrices for venous ulcers, J. Manag. Care. Pharm. 18 (2012) 375-384.

[152] E.A. Maus, Successful treatment of two refractory venous stasis ulcers treated with a novel poly-N-acetyl glucosamine-derived membrane, BMJ Case Rep. 2012 (2012) 10.1136/bcr.03.2012.6091.

[153] R. Simman, W. Mari, S. Younes, M. Wilson, Use of Hyaluronic Acid-Based Biological Bilaminar Matrix in Wound Bed Preparation: A Case Series, Eplasty. 18 (2018) e17.

[154] G. Nicoletti, M.M. Tresoldi, A. Malovini, M. Visaggio, A. Faga, S. Scevola, Versatile use of dermal substitutes: A retrospective survey of 127 consecutive cases, Indian. J. Plast. Surg. 51 (2018) 46-53.

[155] I.S. Whitaker, S. Prowse, T.S. Potokar, A critical evaluation of the use of Biobrane as a biologic skin substitute: a versatile tool for the plastic and reconstructive surgeon, Ann. Plast. Surg. 60 (2008) 333-337.

[156] T. Liu, C. Qiu, C. Ben, H. Li, S. Zhu, One-step approach for full-thickness skin defect reconstruction in rats using minced split-thickness skin grafts with Pelnac overlay, Burns Trauma. 7 (2019) 19-0. eCollection 2019.

[157] H. Schwarze, M. Kuntscher, C. Uhlig, H. Hierlemann, L. Prantl, C. Ottomann, B. Hartmann, Suprathel, a new skin substitute, in the management of partial-thickness burn wounds: results of a clinical study, Ann. Plast. Surg. 60 (2008) 181-185.

[158] A. Gomes, C. Teixeira, R. Ferraz, C. Prudencio, P. Gomes, Wound-Healing Peptides for Treatment of Chronic Diabetic Foot Ulcers and Other Infected Skin Injuries, Molecules. 22 (2017) 10.3390/molecules22101743.

[159] J. Li, C. Zhou, C. Luo, B. Qian, S. Liu, Y. Zeng, J. Hou, B. Deng, Y. Sun, J. Yang, Q. Yuan, A. Zhong, J. Wang, J. Sun, Z. Wang, N-acetyl cysteine-loaded graphene oxide-collagen hybrid membrane for scarless wound healing, Theranostics. 9 (2019) 5839-5853.

[160] J. Hou, L. Chen, M. Zhou, J. Li, J. Liu, H. Fang, Y. Zeng, J. Sun, Z. Wang, Multi-Layered Polyamide/Collagen Scaffolds with Topical Sustained Release of N-Acetylcysteine for Promoting Wound Healing, Int. J. Nanomedicine. 15 (2020) 1349-1361.

[161] J. Hou, L. Chen, Z. Liu, J. Li, J. Yang, A. Zhong, M. Zhou, Y. Sun, L. Guo, Y. Yang, J. Sun, Z. Wang, Sustained release of N-acetylcysteine by sandwich structured polycaprolactone/collagen scaffolds for wound healing, J. Biomed. Mater. Res. A. 107 (2019) 1414-1424.

[162] E. Roussakis, R.V. Ortines, B.L. Pinsker, C.T. Mooers, C.L. Evans, L.S. Miller, X. Calderon-Colon, Theranostic biocomposite scaffold membrane, Biomaterials. 212 (2019) 17-27.

[163] H. Lee, H.M. Woo, B.J. Kang, Impact of collagen-alginate composition from microbead morphological properties to microencapsulated canine adipose tissue-derived mesenchymal stem cell activities, J. Biomater. Sci. Polym. Ed. 29 (2018) 1042-1052.

[164] L. Gil-Cifuentes, R.A. Jimenez, M.R. Fontanilla, Evaluation of collagen type I scaffolds including gelatin-collagen microparticles and Aloe vera in a model of full-thickness skin wound, Drug Deliv. Transl. Res. 9 (2019) 25-36.

[165] J. Natarajan, B.K.R. Sanapalli, M. Bano, S.K. Singh, M. Gulati, Karri, V V S R, Nanostructured Lipid Carriers of Pioglitazone Loaded Collagen/Chitosan Composite Scaffold for Diabetic Wound Healing, Adv. Wound. Care. (New Rochelle). 8 (2019) 499-513.

[166] J. Chu, P. Shi, W. Yan, J. Fu, Z. Yang, C. He, X. Deng, H. Liu, PEGylated graphene oxide-mediated quercetin-modified collagen hybrid scaffold for enhancement of MSCs differentiation potential and diabetic wound healing, Nanoscale. 10 (2018) 9547-9560.

[167] do Amaral, R J F C, N.M.A. Zayed, E.I. Pascu, B. Cavanagh, C. Hobbs, F. Santarella, C.R. Simpson, C.M. Murphy, R. Sridharan, A. Gonzalez-Vazquez, B. O'Sullivan, F.J. O'Brien, C.J. Kearney, Functionalising Collagen-Based Scaffolds With Platelet-Rich Plasma for Enhanced Skin Wound Healing Potential, Front. Bioeng. Biotechnol. 7 (2019) 371.

[168] K. Las Heras, E. Santos-Vizcaino, T. Garrido, F. Borja Gutierrez, J.J. Aguirre, K. de la Caba, P. Guerrero, M. Igartua, R.M. Hernandez, Soy protein and chitin sponge-like scaffolds: from natural by-products to cell delivery systems for biomedical applications, Green Chem. (2020).

[169] L. Loan Khanh, N. Thanh Truc, N. Tan Dat, N. Thi Phuong Nghi, V. van Toi, N. Thi Thu Hoai, T. Ngoc Quyen, T. Thi Thanh Loan, N. Thi Hiep, Gelatin-stabilized composites of silver nanoparticles and curcumin: characterization, antibacterial and antioxidant study, Sci. Technol. Adv. Mater. 20 (2019) 276-290.

[170] B. De Angelis, D'Autilio, M F L M, F. Orlandi, G. Pepe, S. Garcovich, M.G. Scioli, A. Orlandi, V. Cervelli, P. Gentile, Wound Healing: In Vitro and In Vivo Evaluation of a Bio-Functionalized Scaffold Based on Hyaluronic Acid and Platelet-Rich Plasma in Chronic Ulcers, J. Clin. Med. 8 (2019) 10.3390/jcm8091486.

[171] B. Vigani, S. Rossi, G. Sandri, M.C. Bonferoni, C.M. Caramella, F. Ferrari, Hyaluronic acid and chitosan-based nanosystems: a new dressing generation for wound care, Expert Opin. Drug Deliv. 16 (2019) 715-740.

[172] P.A. Shiekh, A. Singh, A. Kumar, Oxygen-Releasing Antioxidant Cryogel Scaffolds with Sustained Oxygen Delivery for Tissue Engineering Applications, ACS Appl. Mater. Interfaces. 10 (2018) 18458-18469.

[173] M. Touri, F. Moztarzadeh, N.A.A. Osman, M.M. Dehghan, M. Mozafari, 3D-printed biphasic calcium phosphate scaffolds coated with an oxygen generating system for enhancing engineered tissue survival, Mater. Sci. Eng. C. Mater. Biol. Appl. 84 (2018) 236-242.

[174] Y.J. Son, W.J. Kim, H.S. Yoo, Therapeutic applications of electrospun nanofibers for drug delivery systems, Arch. Pharm. Res. 37 (2014) 69-78.

[175] Q. Zhang, Y. Li, Z.Y.W. Lin, K.K.Y. Wong, M. Lin, L. Yildirimer, X. Zhao, Electrospun polymeric micro/nanofibrous scaffolds for long-term drug release and their biomedical applications, Drug Discov. Today. 22 (2017) 1351-1366.

[176] R.S. Bhattarai, R.D. Bachu, S.H.S. Boddu, S. Bhaduri, Biomedical Applications of Electrospun Nanofibers: Drug and Nanoparticle Delivery, Pharmaceutics. 11 (2018) 10.3390/pharmaceutics11010005.

[177] I. Garcia-Orue, G. Gainza, P. Garcia-Garcia, F.B. Gutierrez, J.J. Aguirre, R.M. Hernandez, A. Delgado, M. Igartua, Composite nanofibrous membranes of PLGA/Aloe vera containing lipid nanoparticles for wound dressing applications, Int. J. Pharm. 556 (2019) 320-329.

[178] S. Lee, G. Jin, J.H. Jang, Electrospun nanofibers as versatile interfaces for efficient gene delivery, J. Biol. Eng. 8 (2014) 30-30. eCollection 2014.

[179] E.R. Lorden, H.M. Levinson, K.W. Leong, Integration of drug, protein, and gene delivery systems with regenerative medicine, Drug Deliv. Transl. Res. 5 (2015) 168-186.

[180] S. Babitha, L. Rachita, K. Karthikeyan, E. Shoba, I. Janani, B. Poornima, K. Purna Sai, Electrospun protein nanofibers in healthcare: A review, Int. J. Pharm. 523 (2017) 52-90.

[181] H. Frizzell, T.J. Ohlsen, K.A. Woodrow, Protein-loaded emulsion electrospun fibers optimized for bioactivity retention and pH-controlled release for peroral delivery of biologic therapeutics, Int. J. Pharm. 533 (2017) 99-110.

[182] F. Zhou, M. Wen, P. Zhou, Y. Zhao, X. Jia, Y. Fan, X. Yuan, Electrospun membranes of PELCL/PCL-REDV loading with miRNA-126 for enhancement of vascular endothelial cell adhesion and proliferation, Mater. Sci. Eng. C. Mater. Biol. Appl. 85 (2018) 37-46.

[183] K.M. Kennedy, A. Bhaw-Luximon, D. Jhurry, Cell-matrix mechanical interaction in electrospun polymeric scaffolds for tissue engineering: Implications for scaffold design and performance, Acta Biomater. 50 (2017) 41-55.

[184] Z.I. Foraida, T. Kamaldinov, D.A. Nelson, M. Larsen, J. Castracane, Elastin-PLGA hybrid electrospun nanofiber scaffolds for salivary epithelial cell self-organization and polarization, Acta Biomater. 62 (2017) 116-127.

[185] S. Lee, S. Yun, K.I. Park, J.H. Jang, Sliding Fibers: Slidable, Injectable, and Gel-like Electrospun Nanofibers as Versatile Cell Carriers, ACS Nano. 10 (2016) 3282-3294.

[186] N. Mayet, Y.E. Choonara, P. Kumar, L.K. Tomar, C. Tyagi, L.C. Du Toit, V. Pillay, A comprehensive review of advanced biopolymeric wound healing systems, J. Pharm. Sci. 103 (2014) 2211-2230.

[187] K. Zhang, X. Bai, Z. Yuan, X. Cao, X. Jiao, Y. Li, Y. Qin, Y. Wen, X. Zhang, Layered nanofiber sponge with an improved capacity for promoting blood coagulation and wound healing, Biomaterials. 204 (2019) 70-79.

[188] I. Sebe, P. Szabo, B. Kallai-Szabo, R. Zelko, Incorporating small molecules or biologics into nanofibers for optimized drug release: A review, Int. J. Pharm. 494 (2015) 516-530.

[189] G. Cheng, C. Yin, H. Tu, S. Jiang, Q. Wang, X. Zhou, X. Xing, C. Xie, X. Shi, Y. Du, H. Deng, Z. Li, Controlled Co-delivery of Growth Factors through Layer-by-Layer Assembly of Core-Shell Nanofibers for Improving Bone Regeneration, ACS Nano. 13 (2019) 6372-6382.

[190] H. Tu, G. Wu, Y. Yi, M. Huang, R. Liu, X. Shi, H. Deng, Layer-by-layer immobilization of amphoteric carboxymethyl chitosan onto biocompatible silk fibroin nanofibrous mats, Carbohydr. Polym. 210 (2019) 9-16.

[191] G. Lokhande, J.K. Carrow, T. Thakur, J.R. Xavier, M. Parani, K.J. Bayless, A.K. Gaharwar, Nanoengineered injectable hydrogels for wound healing application, Acta Biomater. 70 (2018) 35-47.

[192] H. Jiang, L. Wang, K. Zhu, Coaxial electrospinning for encapsulation and controlled release of fragile water-soluble bioactive agents, J. Control. Release. 193 (2014) 296-303.

[193] J. Yoon, H.S. Yang, B.S. Lee, W.R. Yu, Recent Progress in Coaxial Electrospinning: New Parameters, Various Structures, and Wide Applications, Adv Mater. 30 (2018) e1704765.

[194] B. Pant, M. Park, S.J. Park, Drug Delivery Applications of Core-Sheath Nanofibers Prepared by Coaxial Electrospinning: A Review, Pharmaceutics. 11 (2019) 10.3390/pharmaceutics11070305.

[195] J.S. Choi, S.H. Choi, H.S. Yoo, Coaxial electrospun nanofibers for treatment of diabetic ulcers with binary release of multiple growth factors, J. Mater. Chem. 21 (2011) 5258-5267.

[196] E. Shoba, R. Lakra, M. Syamala Kiran, P.S. Korrapati, Fabrication of core-shell nanofibers for controlled delivery of bromelain and salvianolic acid B for skin regeneration in wound therapeutics, Biomed. Mater. 12 (2017) 035005-605X/aa6684.

[197] S. Tort, F. Acarturk, A. Besikci, Evaluation of three-layered doxycycline-collagen loaded nanofiber wound dressing, Int. J. Pharm. 529 (2017) 642-653.

[198] E. Zahedi, A. Esmaeili, N. Eslahi, M.A. Shokrgozar, A. Simchi, Fabrication and Characterization of Core-Shell Electrospun Fibrous Mats Containing Medicinal Herbs for Wound Healing and Skin Tissue Engineering, Mar. Drugs. 17 (2019) 10.3390/md17010027.

[199] A.A. Shitole, P. Raut, P. Giram, P. Rade, A. Khandwekar, B. Garnaik, N. Sharma, Poly (vinylpyrrolidone)iodine engineered poly (epsilon-caprolactone) nanofibers as potential wound dressing materials, Mater. Sci. Eng. C. Mater. Biol. Appl. 110 (2020) 110731.

[200] E. Caló, V.V. Khutoryanskiy, Biomedical applications of hydrogels: A review of patents and commercial products, European Polymer Journal. 65 (2015) 252-267.

[201] J.S. Boateng, K.H. Matthews, H.N. Stevens, G.M. Eccleston, Wound healing dressings and drug delivery systems: a review, J. Pharm. Sci. 97 (2008) 2892-2923.

[202] D.B. Hom, J.C. Manivel, Promoting healing with recombinant human platelet-derived growth factor--BB in a previously irradiated problem wound, Laryngoscope. 113 (2003) 1566-1571.

[203] S. Beckert, S. Haack, H. Hierlemann, F. Farrahi, P. Mayer, A. Konigsrainer, S. Coerper, Stimulation of steroid-suppressed cutaneous healing by repeated topical

application of IGF-I: different mechanisms of action based upon the mode of IGF-I delivery, J. Surg. Res. 139 (2007) 217-221.

[204] M. Qiu, D. Chen, C. Shen, J. Shen, H. Zhao, Y. He, Platelet-Rich Plasma-Loaded Poly(d,l-lactide)-Poly(ethylene glycol)-Poly(d,l-lactide) Hydrogel Dressing Promotes Full-Thickness Skin Wound Healing in a Rodent Model, Int. J. Mol. Sci. 17 (2016) 10.3390/ijms17071001.

[205] D. Zhang, G. Cai, S. Mukherjee, Y. Sun, C. Wang, B. Mai, K. Liu, C. Yang, Y. Chen, Elastic, Persistently Moisture-Retentive, and Wearable Biomimetic Film Inspired by Fetal Scarless Repair for Promoting Skin Wound Healing, ACS Appl. Mater. Interfaces. 12 (2020) 5542-5556.

[206] S.O. Blacklow, J. Li, B.R. Freedman, M. Zeidi, C. Chen, D.J. Mooney, Bioinspired mechanically active adhesive dressings to accelerate wound closure, Sci. Adv. 5 (2019) eaaw3963.

[207] X. Li, X. Ye, J. Qi, R. Fan, X. Gao, Y. Wu, L. Zhou, A. Tong, G. Guo, EGF and curcumin co-encapsulated nanoparticle/hydrogel system as potent skin regeneration agent, Int. J. Nanomedicine. 11 (2016) 3993-4009.

[208] S. Pacelli, F. Acosta, A.R. Chakravarti, S.G. Samanta, J. Whitlow, S. Modaresi, R.P.H. Ahmed, J. Rajasingh, A. Paul, Nanodiamond-based injectable hydrogel for sustained growth factor release: Preparation, characterization and in vitro analysis, Acta Biomater. 58 (2017) 479-491.

[209] J.P. Jee, R. Pangeni, S.K. Jha, Y. Byun, J.W. Park, Preparation and in vivo evaluation of a topical hydrogel system incorporating highly skin-permeable growth factors, quercetin, and oxygen carriers for enhanced diabetic wound-healing therapy, Int. J. Nanomedicine. 14 (2019) 5449-5475.

[210] S. Kumar, R.K. Majhi, A. Singh, M. Mishra, A. Tiwari, S. Chawla, P. Guha, B. Satpati, H. Mohapatra, L. Goswami, C. Goswami, Carbohydrate-Coated Gold-Silver Nanoparticles for Efficient Elimination of Multidrug Resistant Bacteria and in Vivo Wound Healing, ACS Appl. Mater. Interfaces. 11 (2019) 42998-43017.

[211] D.J. Page, C.E. Clarkin, R. Mani, N.A. Khan, J.I. Dawson, N.D. Evans, Injectable nanoclay gels for angiogenesis, Acta Biomater. 100 (2019) 378-387.

[212] T. Tokatlian, C. Cam, T. Segura, Porous hyaluronic acid hydrogels for localized nonviral DNA delivery in a diabetic wound healing model, Adv. Healthc. Mater. 4 (2015) 1084-1091.

[213] P. Wang, S. Huang, Z. Hu, W. Yang, Y. Lan, J. Zhu, A. Hancharou, R. Guo, B. Tang, In situ formed anti-inflammatory hydrogel loading plasmid DNA encoding VEGF for burn wound healing, Acta Biomater. 100 (2019) 191-201.

[214] S.V. Murphy, A. Atala, 3D bioprinting of tissues and organs, Nat. Biotechnol. 32 (2014) 773-785.

[215] C. Mandrycky, Z. Wang, K. Kim, D.H. Kim, 3D bioprinting for engineering complex tissues, Biotechnol. Adv. 34 (2016) 422-434.

[216] L. Koch, A. Deiwick, S. Schlie, S. Michael, M. Gruene, V. Coger, D. Zychlinski, A. Schambach, K. Reimers, P.M. Vogt, B. Chichkov, Skin tissue generation by laser cell printing, Biotechnol. Bioeng. 109 (2012) 1855-1863.

[217] A.P. Zhang, X. Qu, P. Soman, K.C. Hribar, J.W. Lee, S. Chen, S. He, Rapid fabrication of complex 3D extracellular microenvironments by dynamic optical projection stereolithography, Adv Mater. 24 (2012) 4266-4270.

[218] W. Zhu, X. Ma, M. Gou, D. Mei, K. Zhang, S. Chen, 3D printing of functional biomaterials for tissue engineering, Curr. Opin. Biotechnol. 40 (2016) 103-112.

[219] P. He, J. Zhao, J. Zhang, B. Li, Z. Gou, M. Gou, X. Li, Bioprinting of skin constructs for wound healing, Burns Trauma. 6 (2018) 5-x. eCollection 2018.

[220] Y. Huang, X.F. Zhang, G. Gao, T. Yonezawa, X. Cui, 3D bioprinting and the current applications in tissue engineering, Biotechnol. J. 12 (2017) 10.1002/biot.201600734. Epub 2017 Jul 4.

[221] C.F. Marques, G.S. Diogo, S. Pina, J.M. Oliveira, T.H. Silva, R.L. Reis, Collagen-based bioinks for hard tissue engineering applications: a comprehensive review, J. Mater. Sci. Mater. Med. 30 (2019) 32-x.

[222] C. Intini, L. Elviri, J. Cabral, S. Mros, C. Bergonzi, A. Bianchera, L. Flammini, P. Govoni, E. Barocelli, R. Bettini, M. McConnell, 3D-printed chitosan-based scaffolds: An in vitro study of human skin cell growth and an in-vivo wound healing evaluation in experimental diabetes in rats, Carbohydr. Polym. 199 (2018) 593-602.

[223] W. Xu, B.Z. Molino, F. Cheng, P.J. Molino, Z. Yue, D. Su, X. Wang, S. Willför, C. Xu, G.G. Wallace, On Low-Concentration Inks Formulated by Nanocellulose Assisted with Gelatin Methacrylate (GelMA) for 3D Printing toward Wound Healing Application, ACS Appl. Mater. Interfaces. 11 (2019) 8838-8848.

[224] J. Long, A.E. Etxeberria, A.V. Nand, C.R. Bunt, S. Ray, A. Seyfoddin, A 3D printed chitosan-pectin hydrogel wound dressing for lidocaine hydrochloride delivery, Mater. Sci. Eng. C. Mater. Biol. Appl. 104 (2019) 109873.

[225] C.S. Chen, F. Zeng, X. Xiao, Z. Wang, X.L. Li, R.W. Tan, W.Q. Liu, Y.S. Zhang, Z.D. She, S.J. Li, Three-Dimensionally Printed Silk-Sericin-Based Hydrogel Scaffold: A Promising Visualized Dressing Material for Real-Time Monitoring of Wounds, ACS Appl. Mater. Interfaces. 10 (2018) 33879-33890.

[226] M. Touri, F. Moztarzadeh, N.A.A. Osman, M.M. Dehghan, M. Mozafari, 3D-printed biphasic calcium phosphate scaffolds coated with an oxygen generating system for enhancing engineered tissue survival, Mater. Sci. Eng. C. Mater. Biol. Appl. 84 (2018) 236-242.

[227] Z. Lu, X. Jiang, M. Chen, L. Feng, Y.J. Kang, An oxygen-releasing device to improve the survival of mesenchymal stem cells in tissue engineering, Biofabrication. 11 (2019) 045012-5090/ab332a.

[228] A.V. Anzalone, P.B. Randolph, J.R. Davis, A.A. Sousa, L.W. Koblan, J.M. Levy, P.J. Chen, C. Wilson, G.A. Newby, A. Raguram, D.R. Liu, Search-and-replace genome editing without double-strand breaks or donor DNA, Nature. 576 (2019) 149-157.

[229] W.H. Wu, Y.T. Tsai, S. Justus, G.Y. Cho, J.D. Sengillo, Y. Xu, T. Cabral, C.S. Lin, A.G. Bassuk, V.B. Mahajan, S.H. Tsang, CRISPR Repair Reveals Causative Mutation in a Preclinical Model of Retinitis Pigmentosa: A Brief Methodology, Methods Mol. Biol. 1715 (2018) 191-205.

[230] J.W. Sessions, D.G. Armstrong, S. Hope, B.D. Jensen, A review of genetic engineering biotechnologies for enhanced chronic wound healing, Exp. Dermatol. 26 (2017) 179-185.

[231] N. Kosaric, W. Srifa, G.C. Gurtner, M.H. Porteus, Abstract 100: Human Mesenchymal Stromal Cells Engineered to Overexpress PDGF-B Using CRISPR/Cas9/rAAV6-based Tools Improve Wound Healing, Plastic and Reconstructive Surgery Global Open. 5 (2017) 74.

[232] S. Takashima, S. Shinkuma, Y. Fujita, T. Nomura, H. Ujiie, K. Natsuga, H. Iwata, H. Nakamura, A. Vorobyev, R. Abe, H. Shimizu, Efficient Gene Reframing Therapy for Recessive Dystrophic Epidermolysis Bullosa with CRISPR/Cas9, J. Invest. Dermatol. 139 (2019) 1711-1721.e4.

[233] B.T. Pan, R.M. Johnstone, Fate of the transferrin receptor during maturation of sheep reticulocytes in vitro: selective externalization of the receptor, Cell. 33 (1983) 967-978.

[234] C. Harding, J. Heuser, P. Stahl, Receptor-mediated endocytosis of transferrin and recycling of the transferrin receptor in rat reticulocytes, J. Cell Biol. 97 (1983) 329-339.

[235] R.M. Johnstone, A. Bianchini, K. Teng, Reticulocyte maturation and exosome release: transferrin receptor containing exosomes shows multiple plasma membrane functions, Blood. 74 (1989) 1844-1851.

[236] J. Cabral, A.E. Ryan, M.D. Griffin, T. Ritter, Extracellular vesicles as modulators of wound healing, Adv. Drug Deliv. Rev. 129 (2018) 394-406.

[237] O.P.B. Wiklander, M.A. Brennan, J. Lotvall, X.O. Breakefield, S. El Andaloussi, Advances in therapeutic applications of extracellular vesicles, Sci. Transl. Med. 11 (2019) 10.1126/scitranslmed.aav8521.

[238] O.P. Wiklander, J.Z. Nordin, A. O'Loughlin, Y. Gustafsson, G. Corso, I. Mager, P. Vader, Y. Lee, H. Sork, Y. Seow, N. Heldring, L. Alvarez-Erviti, C.I. Smith, K. Le Blanc, P. Macchiarini, P. Jungebluth, M.J. Wood, S.E. Andaloussi, Extracellular vesicle in vivo biodistribution is determined by cell source, route of administration and targeting, J. Extracell Vesicles. 4 (2015) 26316.

[239] X. Liu, Y. Yang, Y. Li, X. Niu, B. Zhao, Y. Wang, C. Bao, Z. Xie, Q. Lin, L. Zhu, Integration of stem cell-derived exosomes with in situ hydrogel glue as a promising tissue patch for articular cartilage regeneration, Nanoscale. 9 (2017) 4430-4438.

[240] S. Fang, C. Xu, Y. Zhang, C. Xue, C. Yang, H. Bi, X. Qian, M. Wu, K. Ji, Y. Zhao, Y. Wang, H. Liu, X. Xing, Umbilical Cord-Derived Mesenchymal Stem Cell-Derived Exosomal MicroRNAs Suppress Myofibroblast Differentiation by Inhibiting the Transforming Growth Factor-beta/SMAD2 Pathway During Wound Healing, Stem Cells Transl. Med. 5 (2016) 1425-1439.

[241] S.C. Tao, S.C. Guo, M. Li, Q.F. Ke, Y.P. Guo, C.Q. Zhang, Chitosan Wound Dressings Incorporating Exosomes Derived from MicroRNA-126-Overexpressing Synovium

Mesenchymal Stem Cells Provide Sustained Release of Exosomes and Heal Full-Thickness Skin Defects in a Diabetic Rat Model, Stem Cells Transl. Med. 6 (2017) 736-747.

[242] Q. Shi, Z. Qian, D. Liu, J. Sun, X. Wang, H. Liu, J. Xu, X. Guo, GMSC-Derived Exosomes Combined with a Chitosan/Silk Hydrogel Sponge Accelerates Wound Healing in a Diabetic Rat Skin Defect Model, Front. Physiol. 8 (2017) 904.

[243] G. Fuhrmann, R. Chandrawati, P.A. Parmar, T.J. Keane, S.A. Maynard, S. Bertazzo, M.M. Stevens, Engineering Extracellular Vesicles with the Tools of Enzyme Prodrug Therapy, Adv Mater. 30 (2018) e1706616.

[244] N. Xu, L. Wang, J. Guan, C. Tang, N. He, W. Zhang, S. Fu, Wound healing effects of a Curcuma zedoaria polysaccharide with platelet-rich plasma exosomes assembled on chitosan/silk hydrogel sponge in a diabetic rat model, Int. J. Biol. Macromol. 117 (2018) 102-107.

[245] C. Wang, M. Wang, T. Xu, X. Zhang, C. Lin, W. Gao, H. Xu, B. Lei, C. Mao, Engineering Bioactive Self-Healing Antibacterial Exosomes Hydrogel for Promoting Chronic Diabetic Wound Healing and Complete Skin Regeneration, Theranostics. 9 (2019) 65-76.

[246] H. Henriques-Antunes, R.M.S. Cardoso, A. Zonari, J. Correia, E.C. Leal, A. Jiménez-Balsa, M.M. Lino, A. Barradas, I. Kostic, C. Gomes, J.M. Karp, E. Carvalho, L. Ferreira, The Kinetics of Small Extracellular Vesicle Delivery Impacts Skin Tissue Regeneration, ACS Nano. 13 (2019) 8694-8707.

[247] C. Wang, C. Liang, R. Wang, X. Yao, P. Guo, W. Yuan, Y. Liu, Y. Song, Z. Li, X. Xie, The fabrication of a highly efficient self-healing hydrogel from natural biopolymers loaded with exosomes for the synergistic promotion of severe wound healing, Biomater. Sci. 8 (2019) 313-324.

[248] S. Shafei, M. Khanmohammadi, R. Heidari, H. Ghanbari, V. Taghdiri Nooshabadi, S. Farzamfar, M. Akbariqomi, N.S. Sanikhani, M. Absalan, G. Tavoosidana, Exosome loaded alginate hydrogel promotes tissue regeneration in full-thickness skin wounds: An in vivo study, J. Biomed. Mater. Res. A. 108 (2020) 545-556.

[249] P.A. Shiekh, A. Singh, A. Kumar, Exosome laden oxygen releasing antioxidant and antibacterial cryogel wound dressing OxOBand alleviate diabetic and infectious wound healing, Biomaterials. 249 (2020) 120020.

[250] A. Golchin, S. Hosseinzadeh, A. Ardeshirylajimi, The exosomes released from different cell types and their effects in wound healing, J. Cell. Biochem. 119 (2018) 5043-5052.

[251] P. Kemp, History of regenerative medicine: looking backwards to move forwards, Regen. Med. 1 (2006) 653-669.

[252] C.M. Zelen, T.E. Serena, L. Gould, L. Le, M.J. Carter, J. Keller, W.W. Li, Treatment of chronic diabetic lower extremity ulcers with advanced therapies: a prospective, randomised, controlled, multi-centre comparative study examining clinical efficacy and cost, Int. Wound. J. 13 (2016) 272-282.

[253] M.J. Carter, C. Waycaster, K. Schaum, A.M. Gilligan, Cost-effectiveness of three adjunct cellular/tissue-derived products used in the management of chronic venous leg ulcers, Value Health. 17 (2014) 801-813.

[254] M.A. Towler, E.W. Rush, M.K. Richardson, C.L. Williams, Randomized, Prospective, Blinded-Enrollment, Head-To-Head Venous Leg Ulcer Healing Trial Comparing Living, Bioengineered Skin Graft Substitute (Apligraf) with Living, Cryopreserved, Human Skin Allograft (TheraSkin), Clin. Podiatr. Med. Surg. 35 (2018) 357-365.

[255] V. Volarevic, B.S. Markovic, M. Gazdic, A. Volarevic, N. Jovicic, N. Arsenijevic, L. Armstrong, V. Djonov, M. Lako, M. Stojkovic, Ethical and Safety Issues of Stem Cell-Based Therapy, Int. J. Med. Sci. 15 (2018) 36-45.

135 (2022) 212738

Contents lists available at ScienceDirect

Biomaterials Advances

journal homepage: www.journals.elsevier.com/materials-science-and-engineering-c

Review

Cell-based dressings: A journey through chronic wound management

K. Las Heras [a,c], M. Igartua [a,b,c], E. Santos-Vizcaino [a,b,c,*] and R. M. Hernandez [a,b,c,*].

[a] NanoBioCel Group, Laboratory of Pharmaceutics, School of Pharmacy, University of the Basque Country (UPV/EHU), Paseo de la Universidad 7, 01006 Vitoria-Gasteiz, Spain

[b] Biomedical Research Networking Centre in Bioengineering, Biomaterials and Nanomedicine (CIBER-BBN), 01006 Vitoria-Gasteiz, Spain

[c] Bioaraba, NanoBiocel research group, Vitoria-Gasteiz, Spain.

* Co-corresponding authors at: Laboratory of Pharmaceutics, University of the Basque Country, School of Pharmacy, Vitoria-Gasteiz, 01006, Spain.

Email addresses: Rosa Maria Hernandez: rosa.hernandez@ehu.eus / Edorta Santos-Vizcaino: edorta.santos@ehu.eus

.....

Published in: *Biomaterials Advances*, 2022

Impact Factor 2021: ***8.457*** (Q1)

DOI: https://doi.org/10.1016/j.bioadv.2022.212738

Cat: Elsevier

Abstract

The field of regenerative medicine has undergone a paradigm shift in recent decades thanks to the emergence of novel therapies based on the use of living organisms. The development of cell-based strategies has become a trend for the treatment of different conditions and pathologies. In this sense, the need for more adequate, biomimetic and well-planned treatments for chronic wounds has found different and innovative strategies, based on the combination of cells with dressings, which seek to revolutionize the wound healing management. Therefore, the objective of this review is to analyze the current state and the latest advances in the research of cell-based dressings for chronic wounds, ranging from traditional and "second generation" bioengineered living skin equivalents to mesenchymal stem cell dressings; the latter include biopolymeric porous scaffolds, electrospun nanofiber meshes, hydrogels and 3D printed bio-printed dressings. Finally, this review updates the completed and ongoing clinical trials in this field and encourages researchers to rethink these new approaches, manufacturing processes and mechanisms of action, as well as their administration strategies and timings.

The Path of Cell-based Dressings for Chronic Wound Healing

During the past 30 years, there has been a paradigm shift in the field of regenerative medicine, mainly due to the use of living organisms. Acting as secretome-delivery agents, cells have become a therapy trend in a wide variety of tissue-related pathologies [1]. Concretely, in chronic wounds (Box 1) the use of cells — adult and/or mesenchymal stromal cells (MSCs) — included in dressings is growing rapidly and reinventing itself. Cell-based dressings emerged due to the need for more complex and biomimetic therapies that provide moisture retentive, protective, structural or pharmacological properties. The key-point of these bio-systems is the capability to simultaneously carry and/or deliver cells like fibroblasts, keratinocytes, macrophages or MSCs and biological molecules such as cytokines, extracellular matrix (ECM) components and growth factors [2,3]. Thus, these cell-based strategies aim to reduce the continuous inflammatory state, normalize the impaired inter-cellular communication and promote the regeneration of chronic wounds.

Skin grafting was the first cell-containing wound covering strategy, first used in modern medicine in 1869. A century later, in the 1970´s, the problem of the finite donor skin graft supply resulted in the research and development of the first cell-based engineered dressings: bioengineered living skin equivalents (BeLSEs) [4]. It was not until 1998 when the Food and Drug Administration (FDA) approved the first BeLSE, Apligraf® (Organogenesis, Inc.). However, issues with dressing-rejections and inferior effectiveness in clinical trials against decellularized dressings have impeded its widespread used in clinic [5-7]. In parallel, MSC-based dressing research was also rapidly growing due to the encouraging results obtained by these cells in several pathologies such as diabetes mellitus; graft vs host disease or Crohn´s disease [8]. The first human experience with MSC-based dressings (MSC-Ds) was in the 2000´s [9]. Since then, this strategy has become one of the major research trends in chronic wound healing.

In the present review, we will discuss the status, latest trends and emerging therapy solutions in cell-based dressing research for chronic wounds, mainly focusing on the recent advances of MSC-Ds therapies. Furthermore, we have

added a necessary and intuitive schematic classification of MSC-Ds development including 3D bioprinted dressings, as they are not emerging but well-established therapies in research nowadays. Finally, we have critically analyzed these therapies since the growing number of related works had not led to a great progress in the field, overrating, in this sense, their true potential.

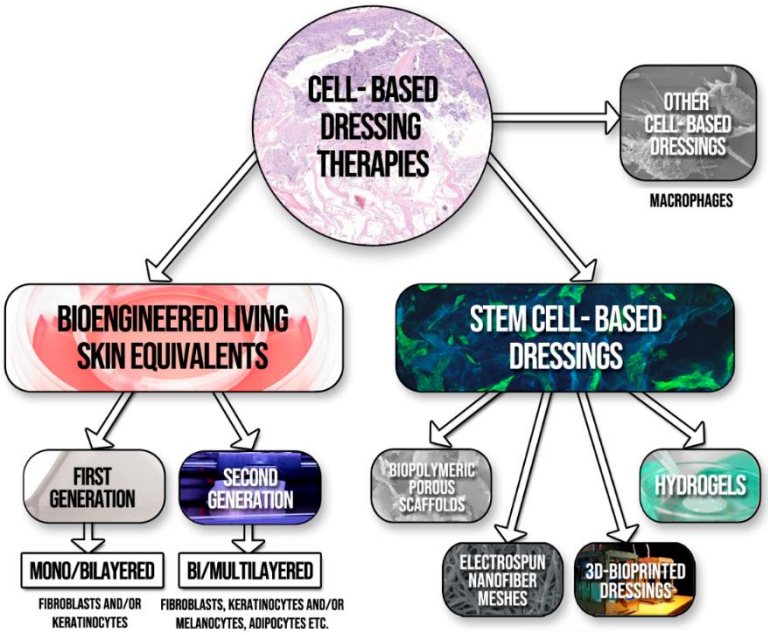

Fig. 1. Cell-based dressing therapies. Some images have been reproduced from Wikimedia commons [10].

Cell-based dressing strategies

There is strong supporting evidence that cell-based dressings are able to create an adequate regenerative environment, promoting tissue remodeling and acting as an inductive template for wound healing [11]. In Fig. 1, we have schematized the different cell-based dressing therapies. Throughout the review, we will discuss the role of BeLSEs and MSC-Ds. Readers interested in other types of cell-based dressings are referred to [2].

The first steps: Bioengineered living skin equivalents

Marketed products and efficacy issues

As described by Metcalfe et al. an ideal BeLSE should be a durable bilayered construct, morphologically and biochemically similar to the native skin and readily available for easy use and long-term storage [12]. In this regard, this therapy comprises natural or synthetic dressings combined with allogenic cells (essentially fibroblasts or/and keratinocytes). The principal role of these BeLSEs is to achieve an integration within the host tissue — to replace the damaged tissue — acting as a template for the healing process. BeLSEs can be classified depending on the number of layers — mono-, bi- or three-layered — and the anatomical structure — epidermal, dermal or mixture — [13,14]. Despite BeLSEs investigations dating back to more than 40 years ago, currently there are few commercialized BeLSEs for chronic wound healing: Dermagraft® (Organogenesis, Inc.) — as a dermal BeLSE —; Apligraf® (Organogenesis, Inc.), Theraskin® (Soluble systems LLC), OrCel® (Forticell Bioscience, Inc.) and StrataGraft® (Mallinckrodt Pharmaceuticals) — as dermo/epidermal BeLSEs —; and Laserskin® (Fidia Advanced Polymeric) and MySkin® (Celltran LTD) — as epidermal BeLSEs — [15,16].

Despite the fact that Apligraf® and Dermagraft® have demonstrated higher rates of wound closure than conventional therapies [13], they have also shown worse outcomes, with higher costs, compared to natural acellular matrices Epifix® or Oasis® in different prospective, comparative studies [5,7]. Furthermore, there is only one study in where different BeLSEs are directly compared. In this paper, a point-by-point comparative evaluation is conducted between Theraskin® and Apligraf®, demonstrating a significant decrease in cost (42.2%) in the Theraskin® cohort compared to the Apligraf® cohort. However, there was not statistical significant differences in healing rates in either 12 or 20 weeks results [6].

Demanding new approaches: complex structures and the "second generation" of BeLSEs

Due to the reduced BeLSEs clinical implementation caused by their poor improvement in the chronic wound management, novel BeLSEs have been investigated in the past decade [2]. In this regard, some researchers have explored the development of more complex constructs for deep chronic wounds. Different studies created three-layered

BeLSEs by adding to dermo-epidermal structures a third layer that “mimicks” the hypodermis. A couple of approaches developed by Huang et al. and Lin et al. explored dermo-epidermal structures — made by electrospun chitosan and polycaprolactone respectively — adding a third layer imitating the basement membrane [17,18]. However, none of these approaches developed a faithful hypodermis with cellular components — mainly composed of adipocytes — that provides nutrients to the upper layers. Finally, Kober et al. developed a three-layered fibrin-based BeLSEs with a hypodermis layer seeded with adipocytes and AT-MSCs. They demonstrated that the artificial hypodermis had a comparable amount of lipid accumulation and glycerol release than native skin. Furthermore, they achieved a normal proliferation of AT-MSCs and fibroblasts and the differenciation of the AT-MSCs into adipocytes upon 4 weeks of culture. Finally, the keratinocytes-composed layer formed a functional epithelial-like barrier [19].

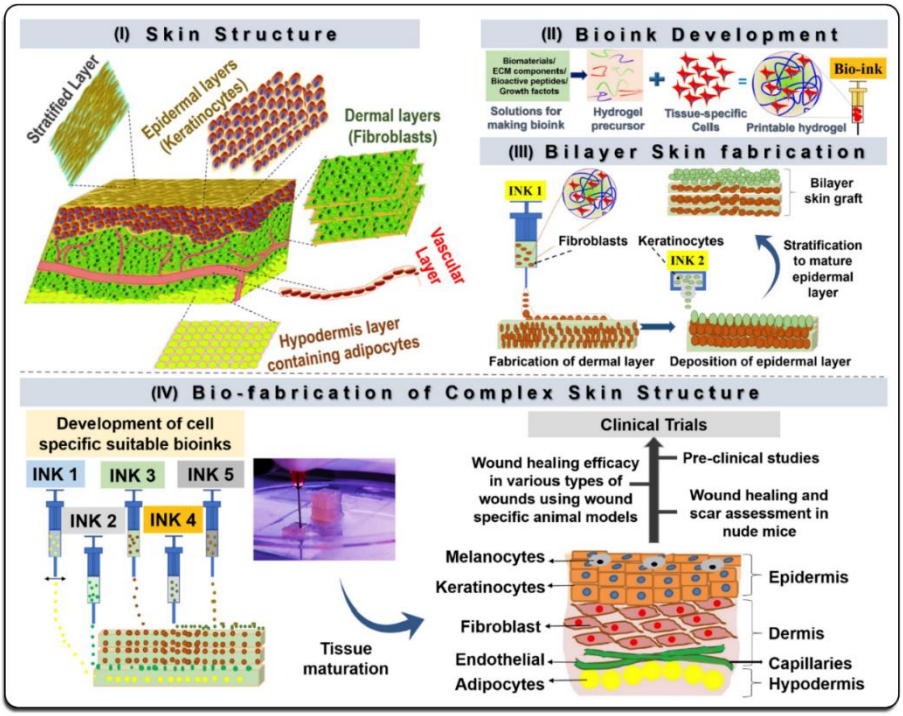

Fig. 2. Schematic representation of developmental stages of 3D bioprinting technique for designing a complex skin architecture in future. (I) Determining the layered structure of skin for designing a computer aided design (CAD) program, (II) Development of a suitable bioink for skin bioprinting, (III)

Designing a simple bilayer skin construct using two types of bioinks for fabricating dermal and epidermal structures and (IV) Designing a complex skin structure containing adipocytes, blood capillaries, dermal, epidermal cells and its assessment strategies. The diagram depicts the flow of advancement done in the field of skin tissue engineering using 3D bioprinting technology and its future scope. Reproduced with permission from [20].

Despite great advancements in this approach, one of the main problems of the traditional development of BeLSEs is that cells usually need long expansion-times after being seeded into the BeLSEs. Furthermore, these dressings usually lack reproducibility of cell seeding and distribution. In this sense, in the recent years, the "second generation" of more sophisticated and precise BeLSEs has been developed. This development is being led by one of the most exciting and recent tools for dressings´ fabrication, the 3D bioprinting. This technique enables a faster, cheaper and more easily reproduced method to develop BeLSEs [21,22]. Furthermore, the 3D bioprinting technique opens up the possibility of constructing dressings, by printing cells, soluble factors and polymers in a desired pattern with the help of extremely precise Cartesian robots [23]. Fig. 2 illustrates the process for developing the "second generation" of 3D bioprinted BeLSEs.

Due to the rapid advancement of this technique, the search for effective polymers to develop more bioactive bioinks has resulted in a myriad of polymeric options. In this regard, the presence of collagen in all connective tissue — together with its biodegradability, biocompatibility and easy availability — make this compound a good starting point for the formulation of bioinks in the development of 3D bioprinted BeLSEs. Indeed, Lee et al. used a collagen-based bioink for the development of the first 3D bioprinted BeLSE back in 2009. They were able to print a multilayered composite with two cell-loaded layers of keratinocytes and fibroblasts respectively. Furthermore, they reported an adequate viability of these cells and their capacity to proliferate in culture [24]. Since then, many other researchers have also worked on collagen-based BeLSEs with encouraging results that have helped in the establishment and advancement of that composition of bioink [25-33]. One of these works, reported the development of a bi-layered BeLSE by mixing microextrusion bioprinting for the dermal layer and inkjet bioprinting for the epidermal layer. This latest technique allowed them to achieve a perfectly distributed epidermal layer composed of neonatal human epidermal keratinocytes similar to the human skin [33]. Another brilliant work by Min et al. investigated the use of extrusion bioprinting to develop a bilayered BeLSE also

incorporating melanocytes in the epidermal layer. They reported the formation of different naevus-like structures in the epidermal layer and the proliferation and interaction of the melanocytes with the keratinocytes upon 4 days of culture [31].

However, some other compounds instead of collagen have recently achieved attention. The use of gelatin methacryloyl and platelet lysate together with human dermal fibroblasts (HDFs) has allowed Daikuara et al. to develop a promising dermal BeLSE. This device achieved a sustained release of growth factors — platelet derived growth factor (PDGF), vascular endothelial growth factor (VEGF), epidermal growth factor (EGF), fibroblasts growth factor (FGF) and transforming growth factor β1 (TGF-β1) — and, more importantly, an increased synthesis and deposition of ECM molecules such as collagens I/III, fibronectin and elastin in vitro [34]. Another approach by Cubo et al. used a fibrin-based bioink combined with human plasma to develop a bilayered dermo-epidermal BeLSE — using HDFs and human keratinocytes obtained from skin biopsies —. Briefly, the developed construct was very similar to the human skin, demonstrating wound healing properties and neovascularization in an immunodeficient rodent model in vivo and allowing the researchers to produce BeLSEs in amounts and times appropriate for a clinical and commercial use [35].

With the passing of time, more diverse and sophisticated 3D printed BeLSEs have been developed. It is known that patients who suffer from chronic wounds respond more positively when rapid treatments are available, resulting in earlier protection and closure of wounds. In line with this thinking, a recent research investigated a BeLSE constructed by a skin bioprinting device that provides rapid on-site management of extensive wounds. The developed BeLSE was composed of a first layer of fibrinogen/collagen with fibroblasts printed directly onto the wound, followed by an equal amount of printed thrombin in order to form a fibrin gel. The second layer was printed on the top of the fibroblast layer and was composed of fibrinogen/collagen with keratinocytes and thrombin as crosslinker. When tested in a full-thickness wound skin model on pigs, these BeLSEs demonstrated an extensive collagen deposition arranged in organized fibers and a wide mature vascular formation [36].

However, despite the fast advance and the complexity of the new BeLSEs developed, there is still a remaining challenge. These cell-based dressings usually fail in engraftment efficiency because they lack dermal vascular networks that are essential for the

integration within the host tissue. Consequently, a recent work by Baltazar et al. described the fabrication of an implantable vascularized BeLSE. The dressing was composed of a collagen-based first layer with fibroblasts, human endothelial cells derived from cord blood, human endothelial colony forming cells and human placental pericytes. Moreover, a second layer was then added composed of the collagen-bioink with keratinocytes. Results in vitro described the formation of vascular constructs and the maturation of keratinocytes. When implanted on the dorsum of immunodeficient mice, union of the vascular constructs of the dressing with the microvessels of the wound niche occurred and the dressing become perfused within 4 weeks after implantation [37]. Finally, following all the aforementioned approaches, Kim et al. developed a complex construct by using a combination of two 3D bioprinting techniques [38] — extrusion and inkjet-based — to develop a three-layered vascularized BeLSE. The developed system was composed of polycaprolactone/gelatin bioink — with human keratinocytes for the epidermal layer and human fibroblasts for the dermal layer — and the hypodermic layer was composed of an adipose-fibrinogen bioink. Vessels were printed using human umbilical vein endothelial cells (HUVECs) in a thrombin/gelatin-based bioink. The developed BeLSE, along with their bioprinting strategy, allowed Kim et al. to reduce costs in terms of manufacturing time — 50 times — and culture medium used — 10 times — compared with the conventional transwell manufacturing system. However, this device has not been tested in functional in vitro assays yet [39].

Recent works have also follow the vascularized BeLSEs strategy with well stablished, reproducible and standardized protocols [40]. In this regard, it clearly appears that to overcome the oxygen limitations of chronic wounds and to ensure an optimal integration within the host tissue, 3D printed vascularized BeLSEs are bridging the gap in the search for more effective, personalized and innovative cell-based therapies.

The revolution of mesenchymal stromal cell-laden dressings

Due to encouraging results in different inflammatory pathologies and the reduced clinical implementation of the commercialized BeLSEs, MSC-Ds were developed as a promising alternative for chronic wound healing applications. The unique immunomodulatory and pro-regenerative properties of MSCs (Box 2) make them an invaluable cell type for the repair of chronic tissue injuries [36-42]. MSC-Ds, like other cell-based dressings, not only provide moisture retention, external protection and a

structure for delivery of cell mediators etc., but they can also act as a niche for the preservation of the stemness or, if desired, for the differenciation of these cells. Rather than integrating within the host tissue, the action of MSC-Ds rely on the orchestration of the wound closure throught the paracrine secretion of therapeutic mediators such as cytokines, growth factors and extracellular vesicles (EVs). There are many studies highlighting that MSC-Ds therapies accelerate wound healing comparing to direct MSCs administration techniques on both animal models and humans [41,42]. In that sense, below, we have reviewed different MSC-Ds and classified them into biopolymeric porous scaffolds (BPSs), electrospun nanofiber meshes (ENMs), hydrogels and 3D bioprinted dressings. Furthermore, we have carried out an update of the different, ongoing or completed, clinical trials with MSC-Ds for chronic wound healing applications.

Biopolymeric porous scaffolds

BPSs are easily manufacturable and biocompatible constructs that possess adequate mechanical and physicochemical properties, as well as an interconnected porosity and high swelling capacity [43]. The use of BPSs has grown rapidly in the past decades, mainly due to the ease of manufacturing — generally by casting — being one of the most studied MSC-Ds nowadays. From proteins, polysaccharides, proteoglycans or glycolipids to pure synthetic polymers; a wide variety of polymers have been utilized to develop these biomaterial-based systems, which are well described by Mogosanu et al. and Rahmani Del Bakhshayesh et al. [44,45]. However, ECM protein-based BPSs or its derivatives — usually combined with other molecules to improve mechanical properties — are the current BPSs research trend.

Interestingly, a composite BPS — consisting of gelatin with chitosan and hyaluronic acid (HA), and developed by Weinstein-Oppenheimer and colleagues — showed an elevated in vitro biocompatibility when was MSC-laden. These MSC-Ds were further tested in rabbits, demonstrating their biocompatibility, a degradability time between 1-2 weeks and an enhanced re-epithelization capacity. When finally proven in a human case, they showed a partial biodegradation within one week, early regeneration capacity and absence of rejection signs (Fig. 3 I) [46]. Another effective protein-approach developed by Kang et al. described the preparation of BPSs made of collagen combined with HA for the vehiculization of adipose tissue-MSCs (AT-MSCs) and human umbilical vein endothelial cells (HUVECs). With the purpose of investigating and evaluating their effects

in angiogenesis, these co-cultured MSC-Ds were combined with low-intensity pulsed ultrasound (LIPUS) — enhances and regulates VEGF expression and promotes messenger RNA (mRNA) expression of different collagens —. The results obtained in vivo showed that the AT-MSCs/HUVECs BPSs, combined with LIPUS, had a great angiogenesis-promoting capability, thus achieving a combined therapeutic efficacy (**Fig. 3 II**) [47].

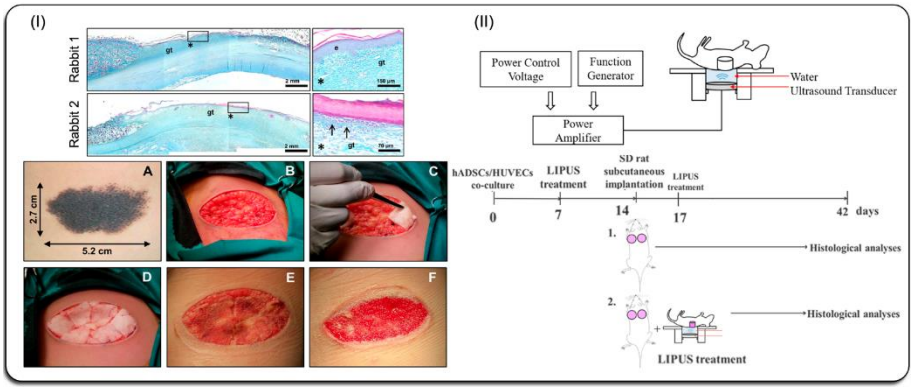

Fig. 3. Composite image of various BPSs design considerations and applications in wound healing. (I) Rabbits´ histology shows wound healing in the epidermis zone and a region of granulation tissue (gt). Human clinical case. The MSC-D was used to cover a nevus resection wound of 2.7 × 5.2 cm2 applied over a period of 4 weeks. A. Congenital melanocytic nevus. B. Skin wound after the surgery. C. Procedure used to dress the wound. D. Wound dressing covering the whole wound. E. Wound dressing after 7 days. F. Wound dressing after 4 weeks of surgery. Reproduced with permission from ref [46]. (II) Experimental designs and schedules of in vitro cell culture and in vivo implantation. Reproduced with permission from ref [47].

Despite the huge popularity and volume of work in MSC-laden collagen-based BPSs [48-50] — and other human protein-based BPSs in general [51,52] —, vegetal proteins are also being subject of research in the field. In that sense, our group developed a soy protein with β-chitin sponge-like BPS — both compounds reutilized from waste by-products of the food industry —. The developed device presented excellent biocompatibility, not only in vitro but also in vivo, showing an important swelling capacity — nearly 1300% — and an elevated AT-MSCs loading capacity of up to 4x104 cells/mm3 of BPS [53]. This approach demonstrated that valorized waste by-products could also be an excellent source of MSC-Ds.

Finally, pure synthetic BPSs have achieved encouraging results for MSC-based chronic wound therapies — the wide range of synthetic scaffolding combinations are described by Chaudhari et al. [54] —. Indeed, due to their excellent physicochemical and easy-handling properties polyethylene glycol (PEG), polyurethane and graphene are the focus of synthetic BPSs development. For example, Geesala et al developed pure PEG–polyurethane BPSs loaded with bone marrow-derived MSCs (BM-MSCs). The evaluated MSC-Ds were used in a murine wound model and results depicted significant increase in fibroblast proliferation, collagen deposition and antioxidant enzyme activities — catalase, etc. —. Furthermore, a decreased expression of pro-inflammatory cytokines — IL-1β, tumor necrosis factor alpha (TNF-α), IL-8, etc. — with an increased expression of anti-inflammatory cytokines — IL-10, IL-13 — was given [55]. Due to their aforementioned excellent physicochemical and inherent antibacterial properties, graphene-based BPSs are currently being investigated for innovative wound healing purposes [56,57]. These excellent properties have driven Li et al. and Chu et al. to develop graphene-based BPSs combined with BM-MSCs. Briefly, both strategies showed synergistic effects and promoted wound closure through angiogenesis and collagen deposition enhancement in rodent models [58,59].

Electrospun Nanofiber Meshes

Over the last decade, there has been a considerable progress in dressings´ design considerations due to introduction of electrospinning. ENMs have been proven to be suitable candidates for wound delivery of bioactive molecules — i.e. growth factors, antibiotics and other small molecules — [60,61]. ENMs have been designed to mimic the ECM, providing more favorable and precise conditions for cell attachment, proliferation and cell-drug interaction [11,62]. These factors have led to an increasing number of works in the field.

The most popular natural polymers used to create ENMs have been HA, gelatin, chitosan, alginate, collagen, silk fibroin etc. Among the synthetic polymers used, poly-lactic glycolic acid (PLGA), poly-ethylene glycol (PEG) and poly-caprolactone (PCL) have been the main players for the ENMs design and development [63]. In this regard, PCL — a hydrophobic and biocompatible aliphatic polyester — has been widely used to develop ENMs since the beginning to nowadays, due to its suitability for manufacturing and adequate biocompatibility. As a result, many works have been recently published with a

wide variety of cell-based ENM strategies. Su et al. developed a PCL-ENMs loaded with AT-MSCs that were able to produce significantly higher levels of anti-inflammatory and pro-angiogenic cytokines in vitro compared to AT-MSCs cultured on microplates. In a rat wound-healing model, these MSC-Ds accelerated wound closure, promoted macrophage recruitment and enhanced the M2 macrophage polarization — pro-regenerative profile — [64]. Another recent PCL-based approach by Chen et al. combined BM-MSCs with an ENM — with radically/vertically aligned fibers — able to completely recover their shape and maintain structural integrity after mechanical stress. These MSC-Ds were able to promote granulation tissue formation, angiogenesis, collagen deposition, and switch the macrophage response to a pro-regenerative profile [65].

Combined ENM-based therapies are also being investigated with the objective of targeting different healing stages with a unique avant-garde MSC-D. Following this path, Lotfi et al. developed an effective gelatin-based ENM strategy combining the effect of AT-MSCs co-cultured with keratinocytes. These MSC-Ds were tested on a rat wound model and the observed results demonstrated that the wound closure rate was significantly higher in the co-cultured ENM group compared to the other groups — unique culture and control —. The expression levels of VEGF, collagen type 1, and CD34 was also significantly higher in the co-cultured ENMs group compared to the ones observed in the other groups [66]. Another brilliant strategy developed by Phan-Nguyen and coworkers utilized PCL combined with gelatin to create an ENM able to spontaneously assemble within 3 days in cell culture plate. Briefly, they seeded AT-MSCs onto the PCL/gelatin ENMs and demonstrated in-vivo that the MSC-D was able to accelerate wound healing and increase the pan-keratin and collagen levels in a C57BL/6 mice model [67]. Although other recent published works investigate different polymers such as silk fibroin [68], the latest advances around this technology focus on the size-reduction of the electrospinning instrument, leading to the construction of handheld electrospinning systems [69-71]. However, none of these developed devices have been already proven with cell-based strategies.

Hydrogels

Hydrogels are insoluble, swellable and hydrophilic devices that contain an elevated water proportion and a structural microarchitecture that closely mimics the native ECM

structure. These formulations have been investigated in chronic wound scenarios since the late 80´s [72]. Due to their elevated water content, hydrogels are usually employed in dry wounds as they have the ability to maintain the moist environment, refresh the wound bed and even reduce the wound pain [11]. As well as BPSs, a wide range of matrix-forming polymers — chitin, chitosan, collagen, gelatin, etc. — have been used to develop therapies with MSC-laden hydrogels — readers should refer to [2,72,73] for further insight —.

Similar to the development of BPSs, the use of proteins and/or polysaccharides as MSCs-based hydrogel-forming molecules is still very popular. Different AT-MSC-laden hydrogels, mainly composed of gelatin, have been developed and recently tested in different in vivo rodent models (**Fig. 4 I**). These investigations reported that hydrogels were able to enhance the vascularization of wounds and reduced the healing time [74-76]. A polysaccharide-based strategy by Xu et al. investigated a composite chitosan-based hydrogel combined with glycerol phosphate sodium and cellulose nanocrystals for immobilization of human umbilical cord-MSCs. The MSC-Ds were tested in rats, and the paracrine effects of the undifferentiated MSCs combined with the dressings achieved significantly accelerated wound closure, tissue remodeling, microcirculation, re-epithelialization and even hair follicle regeneration. These MSC-Ds also promoted collagen deposition and decreased the secretion of some inflammatory factors — TNF-α and IL-1β — [77]. Bai et al. also proposed a chitosan-based BM-MSC-laden hydrogel — combined with HA and collagen — with self-healing properties. The BM-MSCs loaded into the hydrogel were able to increase the secretion TGF-β1, VEGF and b-FGF in the 3D hydrogel environment as compared to the 2D cultured cells. Finally, the developed MSC-Ds were able to promote wound healing in vivo with also the decrease in inflammatory cell infiltration and the increase in granulation tissue formation, collagen deposition and neovascularization [78]. Further recent evaluations of chitosan and chitin-based hydrogels have also shown adequate biocompatibility and suitability for MSCs immobilization, highlighting the great potential of this approach for chronic wound management [79-81] (**Fig. 4 II**).

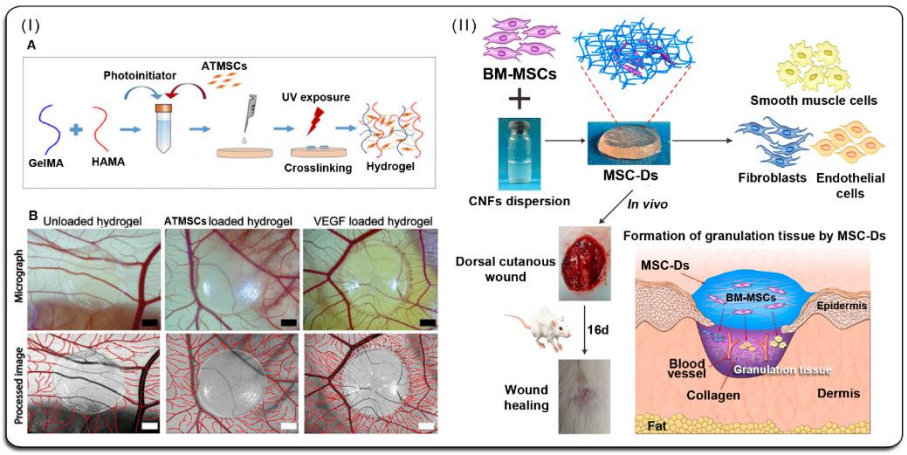

Fig. 4. Composite image of different hydrogel-based MSC-Ds design considerations and applications in wound healing. (I) A. Creating a bicomponent hydrogel; a solution of methacrylated gelatin and methacrylated HA was formed by rehydrating lyophilized powders of both in media alone (control hydrogel) or media containing cells (cell-containing hydrogel) then crosslinked by the addition of a photoinitiator and UV irradiation for 40s. B. Evaluation of the angiogenic properties of the hydrogel in the chick chorioallantoic membrane (CAM) assay. Micrographs (upper row) and semi-automatic processed images (lower row) of the hydrogel, hydrogel containing AT-MSCs and hydrogel containing VEGF (positive control), taken on Day 14 of embryonic development. Reproduced with permission from ref [74]. (II) A scheme of experimental design and illustration of differentiation process of BM-MSCs. A scheme of the differentiation process of BM-MSCs encapsulated in the chitin nanofibers (CNFs) hydrogel in vitro and in vivo, illustrating their differentiation induced by CNFs hydrogel and contribution to the formation of granulation tissue for better wound healing. Reproduced with permission from ref [79].

Over the past decade, the great potential of MSC-based hydrogels has met the wound healing efficacy of decellularized extracellular matrices (dECMs). Thanks to their low immunogenicity, adequate biocompatibility and the ability to maintain the specific functional structure of their original tissue source, some researchers have explored the development of dECM-based hydrogels [11]. In this regard, Chen and co-workers utilized human adipose tissue to develop a decellularized adipose tissue hydrogel combined with AT-MSCs to accelerate chronic wound healing. They achieved a hydrogel that was able to support AT-MSCs adhesion and proliferation, even increasing the delivery of AT-MSCs-secreted hepatocyte growth factor (HGF) compared to 2D cultured cells. This approach was finally tested in a full thickness skin wound model in diabetic mice, and

the results demonstrated greater closure in the AT-MSC hydrogel group with an enhanced neovascularization effect [82]. Another dECM-based hydrogel obtained from adipose tissue and developed by Pu et al. also achieved an increased wound closure in an in vivo rat model. Briefly, the developed dECM-based hydrogel maintained some proteins of the tissue source — Collagen I/IV, fibronectin and laminin — and, when combined with AT-MSCs, it was able to reduce the wound size with also an increased neovascularization [83].

Finally, latest trends in MSC-based hydrogel research are focusing not only on the composition and the type of MSC, but also on the immunomodulatory potential of these units and also the in situ administration of these formulations. Many researchers have claimed that in order to fully elicit the immunomodulatory effects of MSCs, they must be activated — also called the "licensing" process — with inflammatory mediators such as interferon-gamma (IFN-γ) [84-86]. Following these precedents, our group developed a bioinspired multifunctional collagen-alginate hydrogel that combined 3D biomimetic MSC culture and sustained inflammatory licensing. The inclusion of IFN-γ-laden heparin-coated microbeads allowed us a prolonged immunomodulatory licensing of MSCs, resulting in an enhanced suppression of T cell proliferation in vitro [87]. Other researchers are also following this approach, developing effective in situ injectable IFN-γ-functionalized hydrogels with different compositions — PEG and silk fibroin —. Briefly, these works also demonstrated promising immunomodulatory effects on T-cell proliferation and a great effectiveness in wound healing applications in vivo [88,89].

3D bioprinted dressings

3D bioprinting technology has undoubtedly revolutionized manifold fields of tissue engineering and regenerative medicine, as the strategy has improved dressings´ biomimetic aspect. As mentioned before, 3D bioprinted matrices can be constructed with a desired strength, porosity, interconnectivity and biodegradability to recreate the best ECM-like scenario for cell attachment and proliferation. In the 2010´s decade, integration of 3D bioprinting technologies with MSCs research popularly emerged. As a result, MSCs such as AT-MSC or BM-MSCs have been reported to work with different bioinks — collagen, fibrin etc. — in tissue regeneration [90].

Consequently, one of the most used 3D bioprinting techniques — laser assisted bioprinting (LaBP) technology — has allowed Skardal et al. the development of a 3D bioprinted dressing with MSCs to investigate wound healing properties. In an in vivo experiment BM-MSCs and amniotic-fluid MSCs seeded in a fibrin-collagen 3D bioprinted dressing showed an increased microvessel density and capillary diameter compared to wounds treated with the cell-free counterpart. Due to fluorescent tracking, these results were attributed to the cell-released secretome, rather than direct cell-to-cell interactions. Thanks to this technique, Skardal et al. achieved a more reproducible method to develop a co-cultured MSC-D as compared to the traditional seeding methods [91]. More recent works, also demonstrated the effectiveness of BM-MSCs alone in different LaBP 3D bioprinted dressings as promoters of angiogenesis, re-epithelialization and granulation tissue formation [92].

On the other hand, another trendy 3D bioprinting technique — the extrusion — has also been successfully investigated for the development of 3D bioprinted MSC-Ds. A research carried out by Rutz et al. developed 3D bioprinted MSC-Ds composed of gelatin combined with fibrinogen. The developed MSC-Ds showed an elevated matrix deposition that helped to form a skin-like tissue construct in vitro [93]. Furthermore, with the same technique, Kim and coworkers used a skin-derived decellularized ECM as “bioink” for the development of 3D bioprinted MSC-Ds laden with endothelial progenitor cells (EPCs) and AT-MSC. The developed “bioink” retained the major ECM components of skin in addition to favorable growth factors and cytokines. In vivo results revealed that the 3D bioprinted MSC-Ds accelerated wound closure, neovascularization and even re-epithelization. The use of the 3D printing technique allowed this group to place both cell types in a desire and precise pattern achieving a complex MSC-D with an elevated reproducibility [94]. In another approach, Li et al. developed extrusion-based mussel-inspired 3D bioprinted MSC-Ds loaded with AT-MSCs. Briefly, MSC-Ds produced more pro-angiogenic and immunomodulatory factors than 2D cultures in vitro and the conditioned medium collected from cultured MSC-Ds sped wound closure, enhanced vascularization, and promoted macrophage switching from M1 to M2 phenotype in the wound bed [95].

Finally, due to all the technical advancement during this last decade, research is now also focusing — as well as the electrospinning technique — on the development of handheld 3D skin bioprinters for in situ formulation of skin constructs [96,97]. Such

portable 3D bioprinters can revolutionize the wound care market, as patients will not have to wait for the in vitro expansion of cell-based dressings. Furthermore, it is likely that this technology, in a near future, could also be used for emergencies such as burn traumas and could be incorporated as part of the standard equipment in medical vehicles for an immediate point-of-care treatment.

An update on clinical trials of MSC–based dressings

The clinical implementation of all MSC-D therapies is extremely vital to validate proof of concept and preclinical observations in animal models. Clinical trials not only reveal the therapy outcomes, but also unfold information such as costs of treatment and safety/risks of patients involved in the study. Herein, we have tried to summarize all clinical trial reports on MSC-D therapies for chronic wound healing (Table 1). Although several instances of preclinical animal investigations have been published, there have only been a handful of clinical trials employing these strategies in humans.

Table 1. Summary of the clinical trial data using MSC-Ds for chronic wound healing (NIH Clinical trials and EudraCT consulted 10-12-2021)

Dressing	*MSC type*	*Treatment*	*Wound type*	*Phase / n*	*Results*	*Date*	*Ref.*
Terudermis® (BPS)	Autologous BM-MSCs	BM-MSCs seeded in Terudermis®.	Idiopathic lower leg ulcer	Case Report n=1	Good granulation tissue at 2 weeks	2005	[134]
Pelnac™ (BPS)	Autologous BM-MSCs	BM-MSCs seeded in Pelnac™.	Trauma / Venous ulcers / Burn / Decubitus ulcers	Phase I n=20	11 healed within 8 weeks; 2 burn patients mostly healed. 3 healed within 3 weeks; 2 healed after 2 applications. 2 died for unrelated pathology before end of clinical	2008	[135]
Surgicoll (BPS)	Autologous BM-MSCs	Group 1: BM-MSCs seeded in Surgicoll. Group 2: BM-MSCs suspension. Group 3: Suspension + GF and fibrin glue	Diabetic foot ulcers	Phase I n=8	3 complete healing of wound. 5 patients significantly decreased in wound size	2011	[136]
Hydrogel (unknown composition)	Allogenic AT-MSC	Application of allogenic AT-MSC in form of hydrogel	Diabetic foot ulcers	Phase I/II n=59	16/22 wound closure at week 8 in treatment group. 8/17 wound closure at week 8 in control group. 82% vs 53% in wound closure at week 12	2015	[137]

Alginate hydrogel	Allogenic placenta derived MSCs	Allogenic placenta-derived MSCs loaded alginate hydrogel	Diabetic foot ulcers	Case report n=1	Patient's foot ulcer was almost healed at week 3	2017	[138]
Collagen BPS	Allogenic BM-MSCs	Allogenic BM-MSCs (REDDSTAR ORBCEL-M) seeded in a collagen BPS	Diabetic foot ulcers	Phase Ib n=9	Ongoing	Started August 2016	2015-005580-16
Medical collagen BPS	Umbilical cord MSCs	Application of medical collagen scaffold with umbilical cord MSCs.	Skin defects	Phase I/II n=30	Not yet recruiting (unknown status)	Started February, 2016	NCT02672280
Hydrogel of [137]	Allogenic AT-MSC	Application of allogenic AT-MSC in form of hydrogel	Diabetic foot ulcers	Phase III n=164	Ongoing	Started December 2017	NCT03370874
Curcumin loaded nanoparticles into collagen-alginate BPS	Autologous AT-MSC	AT-MSC seeded in Curcumin loaded chitosan nanoparticles into collagen-alginate SCAFFOLD	Diabetic foot ulcers	Phase 1 n=40	Not yet recruiting (unknown status)	Started October 2017	NCT03259217

Collagen BPS	Allogenic BM-MSCs	Application of allogenic BM-MSCs-laden collagen SCAFFOLD	Diabetic foot ulcers	Phase I n=9	Terminated (stopped because of lack of recruitment)	Started April 2018	NCT03509870
Hydrogel (unknown composition)	Allogenic AT-MSC	Application of allogenic AT-MSC in form of hydrogel	Diabetic foot ulcers	Phase II n=44	Recruiting	Started November 2018	NCT03754465
Decellularized human skin matrix	Allogenic WJ-MSCs	WJ-MSCs seeded in a decellularized human skin matrix	Epidermolysis Bulbosa and other chronic wounds	Phase I/II n=100	Ongoing	Started September 2020	2018-003890-91
Fibrin matrix obtained from PRP	AT-MSCs	Application of AT-MSCs injected at the edges of the ulcer and seeded in a fibrin matrix obtained from PRP	Refractory chronic wounds	Phase I n=5	Ongoing	Started September 2020	2019-004637-16
Decellularized amniotic membrane BPS	WJ-MSCs and HDFs	WJ-MSCs and HDFs seeded on a decellularized amniotic membrane BPS	Chronic ulcers	Case series n=5	Total skin regeneration and re-epithelialization was achieve in all patients at nine days of treatment	2021	[139]

Concluding remarks and future scope

With the latest advances in cell-based dressings´ research and the poor clinical translation, more complex and precise strategies are being developed to address the multiple dysregulations that are responsible for undermining the proper functioning of skin. Recent breakthroughs in cell-based dressing design hold great potential to help improve patients´ quality of life and prevent further health complications.

The current chronic wound cell-based treatment "race" is extensive, innovative and multidisciplinary. Indeed, this marathon is now focusing on 3D bioprinting. Advances with this technique have offered precise cell patterning in predefined dressings´ locations, which has enabled a better recapitulation of the micro-architectural organization of native skin. Thanks to this advancement, the two different cell-based dressing strategies for wound healing — being secretome-delivery agents with bioactive structural constructs for cell hosting or, in contrast, cell-based matrices able to being integrated within the host tissue for accompanying chronic wounds all along the healing process — can be developed in a more precise and reproducible manner. Nonetheless, many works reported in the literature using 3D printing have taken advantage of the "hype" surrounding the technique to develop MSC-based dressings that do not present any advantage compared to the other approaches. In that sense, this field awaits the development of more active bioinks that will include the combination of various cell types — fibroblasts, keratinocytes, melanocytes, MSCs and even endothelial cells — to faithfully mimic the native skin microenvironment, also with the presence of hair follicles, microvessels or even sweat glands. In situ formed and self-healing hydrogels are also taking advantage on the race for the first approved treatments as they are effective as well as easily manufactured, handled and administered. Furthermore, the licensing of MSCs has opened the door to more effective therapies as their secretory profile can be modified to potentiate different effects. Another important therapy in the field, the ENMs, have retained their importance due to their simplicity, despite being a fairly old construction methodology. However, the large amount of parameters that affect the dressing construction hinders the reproducibility across different research groups. In contrast, the possibility to combine this technique with other ones, such as 3D bioprinting, may lead to more biomimetic and effective therapies. Furthermore, the direction of this technique, among others including 3D bioprinting or hydrogels, is also focusing on the

development of in situ administration devices. Evidence suggests that in the near future, clinicians will be able to use hand-held electrospinning devices or 3D bioprinters to apply cell-based dressings on chronic wounds — or even other major injuries such as severe burns — in hospitals or even in patient´s homes.

Another key-point for the final implementation of cell-based dressings in the clinic is the cost of production. Nowadays, cell-based therapies for chronic wounds are much more expensive than the standard wound care therapies. It is essential to achieve scalable, reproducible and effective manufacturing of cell-based dressings to reduce production costs. Furthermore, the administration periods of these therapies should be carefully analyzed. When cell-based dressings are utilized with the aim of being integrated within the host tissue, it could be important to maintain these dressings for longer periods than the standard therapies not to "break" the healing process. In this regard, the traditional care protocol of debridement and treatment of chronic wounds could be unfavorable, since removing these dressings and adding new ones would be inconsistent with their mechanism of action and will end increasing the cost of these therapies too. Research in this direction should be carried out to clarify whether these constructs should be administered following the traditional approach or, in contrast, should change the paradigm of the traditional chronic wound care.

The current development of a wide range of smart and innovative cell-based dressing strategies to tackle chronic wound healing is both motivational and stimulating in the pursuit of further progress. However, cost-benefit considerations and a more difficult commercialization pathway — compared to non-cellular dressings — are hindering their implementation in clinic. The regulatory affairs of these cell-based dressings are not only slowing-down their clinical use, but also causing the disinterest of many companies and institutions on the investment and development of such therapies. Nevertheless, we strongly believe that in this decade, more precise, effective, innovative, and even cheaper cell-based dressings could break into the standard market of chronic wound management.

Acknowledgments

Authors acknowledge the financial support from the Spanish Ministry of Economy and Competitiveness through the "RETOS" Program (NANGROW

project, RTC-2017-6696-1) and from the Basque Government (Grupos Consolidados, IT907-16). K. Las Heras thanks the Basque Government (Department of Education, Universities and Research) for the PhD grant (PRE_2018_1_0412).

Author Contributions

K. Las Heras outlined, conceptualized, wrote the draft manuscript and created all figures and tables. M. Igartua obtained funding and discussed and approved the final version of the manuscript. E. Santos-Vizcaino performed a critical literature research, revised and edited the draft manuscript and approved the final version. RM Hernandez obtained funding, supervised the development of the manuscript, contributed with comments and approved the final version of the manuscript.

Competing interests

The authors declare no competing interests.

Box 1: Chronic wounds (Insufficient healing)

When tissue repair is ineffective, due to various disorders — e.g. diabetes, aging, cardiovascular diseases, etc. —, it can lead to ulcerative skin damage such as venous leg ulcers, arterial ulcers, diabetic foot ulcers or pressure ulcers [11]. Chronic wounds are characterized by a persistent inflammation, hard re-epithelialization, impaired angiogenesis, dysregulated levels of cytokines/growth factors and/or increased protease activity. For example, some mediators such as IL-6, IL-1, matrix metalloproteinases (MMPs) or TNFα are constantly upregulated, whereas the expression of TIMPs appears downregulated [11,104]. On the other hand, at a cellular level, many disturbances occur in the wound niche (Fig. 1).

Figure 1. Cellular disturbances in chronic wounds. (GF) Growth factors.

Polimorphonuclear neutrophils exhibit a decreased infiltration and transendothelial cell migration, phenotypic changes — defects in the recruitment and chemotaxis capacity and an increased ROS production —, a lower antibacterial activity and a longer permanence in the wound. Furthermore, these cells have shown a reduced M2 macrophage profile induction and an increased IL-1β production induction by macrophages in chronic wounds [105,106]. Disturbances in macrophages are also usual in chronic wounds and can lead to anomalous repair. Macrophages exhibit a dysregulated inflammatory cytokine and growth factor production, all along with a M1 pro-inflammatory predominance in the M1/M2 profile ratio. Furthermore, there is an aberrant and altered communication — mainly due to the harsh environment with elevated protease activity — between macrophages and other cells including epithelial cells, endothelial cells, fibroblasts, and stem or tissue pro-genitor cells [107]. Despite there not being a consensus on the scientific community, the hyperproliferative keratinocyte status appears to be the most accepted approach lately in chronic

wounds. Furthermore, these cells exhibit an altered migratory potential, increased MMPs production and they lack expression of differentiation markers [2,11,108]. Finally, due to the aforementioned inflammatory environment, fibroblasts are unable to respond to growth factors and inflammatory cytokines, resulting in a decreased proliferative capacity and increased MMPs production [108-110]. These cellular and molecular abnormalities obstruct the deposition of ECM and the formation of the granulation tissue, resulting in the formation of chronic wounds.

Box 2: Effects of MSCs in Wound Healing

MSCs accelerate wound closure by modulating inflammation, increasing angiogenesis, promoting granulation tissue formation, regulating ECM remodeling and enhancing re-epithelialization (Fig. 2). Indeed, these effects are mediated by two mechanisms; cell-cell interactions and paracrine signaling, being the latter, the main player [111,112].

Immunomodulation

It has been described that MSCs regulate both innate and adaptive immunity through modulating several functions in different immune cells — T, B and natural killer lymphocytes, monocytes, macrophages and dendritic cells — such as activation, proliferation, maturation and cytolytic activities. These effects are mediated by cell-cell interactions — programmed Death-ligand 1 (PD-L1) and Fas Ligand (Fas-L) union to T cells —secreted mediators — indoleamine 2,3-dioxygenase (IDO), TGF-β1, IL-10, prostaglandin E2 (PGE-2), HGF, Galectins 1 and 9 (GAL-1 and GAL-9), nitric oxide (NO), interleukin-1 receptor antagonist (IL-1Ra) and finally, cargo content of the secreted EVs (miRNAs etc.). Furthermore, MSCs have demonstrated a reduction in the secretion of pro-inflammatory cytokines — such as IL-1 and TNF-α — and intercellular adhesion molecule 1 (ICAM1) by other cell types like macrophages or neutrophils [113,114].

Angiogenesis

The pro-angiogenic effects of MSCs are mainly attributed to the secretion of soluble factors including vascular endothelial growth factor (VEGF), angiogenin, angiopoietin, IL-8, monocyte chemoattractant protein-1 (MCP-1) or HGF and

extracellular vesicles (EVs) encapsulating pro-angiogenic mi-RNAs such as miR-30, miR424, miR-125 etc. and proteins [115-119]. Indeed, MSCs have demonstrated the capability to increase the density of microvessels and even, some studies have suggested that MSCs could participate in the vasculogenesis process through differentiation into vascular endothelial cells [118,119].

ECM remodeling

MSCs have demonstrated an enhanced wound healing and ECM remodeling through increased fibroblasts and keratinocytes migration, fibroblasts proliferation and even collagen and elastin secretion from these cells. Furthermore, MSCs are able to inhibit matrix metalloproteinase-1 (MMP-1) — released by keratinocytes — helping, in that vein, to maintain the cytokine and growth factor communication and the balance of ECM remodeling during the final steps of wound healing [108,114,118].

Macroscopic changes

The skin regeneration potential of MSCs at a macroscopic level comes from their demonstrated capacity to increase epidermis thickness and dermal ridges. Additionally, MSCs also promote the formation of hair follicles, sweat glands, and other normal skin appendages [118].

Figure 1. MSCs effects and mediators. EVs effects are represented with yellowish circles. Vascular endothelial growth factor (VEGF), monocyte chemoattractant protein-1 (MCP-1), hepatocyte growth factor (HGF), indoleamine 2,3-diox-ygenase (IDO), transforming growth factor beta-1 (TGF-β1), prostaglandin E-2 (PGE-2), nitric oxide (NO), interleukin-1 receptor antagonist (IL-1Ra), tumor necrosis factor alpha (TNF-α), programmed death-ligand 1 (PD-L1), FAS ligand (FAS-L), matrix metalloproteinase 1 (MMP-1). Some images have been reproduced from Wikimedia commons [10].

References

[1] A.A. Abdeen, K. Saha, Manufacturing Cell Therapies Using Engineered Biomaterials, Trends Biotechnol. 35 (2017) 971-982.

[2] M. Xue, R. Zhao, H. Lin, C. Jackson, Delivery systems of current biologicals for the treatment of chronic cutaneous wounds and severe burns, Adv. Drug Deliv. Rev. 129 (2018) 219-241.

[3] K. Vig, A. Chaudhari, S. Tripathi, S. Dixit, R. Sahu, S. Pillai, V.A. Dennis, S.R. Singh, Advances in Skin Regeneration Using Tissue Engineering, Int. J. Mol. Sci. 18 (2017) 10.3390/ijms18040789.

[4] S.P. Tarassoli, Z.M. Jessop, A. Al-Sabah, N. Gao, S. Whitaker, S. Doak, I.S. Whitaker, Skin tissue engineering using 3D bioprinting: An evolving research field, J. Plast. Reconstr. Aesthet. Surg. 71 (2018) 615-623.

[5] C.M. Zelen, T.E. Serena, L. Gould, L. Le, M.J. Carter, J. Keller, W.W. Li, Treatment of chronic diabetic lower extremity ulcers with advanced therapies: a prospective, randomised, controlled, multi-centre comparative study examining clinical efficacy and cost, Int. Wound. J. 13 (2016) 272-282.

[6] M.A. Towler, E.W. Rush, M.K. Richardson, C.L. Williams, Randomized, Prospective, Blinded-Enrollment, Head-To-Head Venous Leg Ulcer Healing Trial Comparing Living, Bioengineered Skin Graft Substitute (Apligraf) with Living, Cryopreserved, Human Skin Allograft (TheraSkin), Clin. Podiatr. Med. Surg. 35 (2018) 357-365.

[7] M.J. Carter, C. Waycaster, K. Schaum, A.M. Gilligan, Cost-effectiveness of three adjunct cellular/tissue-derived products used in the management of chronic venous leg ulcers, Value Health. 17 (2014) 801-813.

[8] M. Otero-Vinas, V. Falanga, Mesenchymal Stem Cells in Chronic Wounds: The Spectrum from Basic to Advanced Therapy, Adv. Wound. Care. (New Rochelle). 5 (2016) 149-163.

[9] S. Ichioka, S. Kouraba, N. Sekiya, N. Ohura, T. Nakatsuka, Bone marrow-impregnated collagen matrix for wound healing: experimental evaluation in a microcirculatory model of angiogenesis, and clinical experience, Br. J. Plast. Surg. 58 (2005) 1124-1130.

[10] Wikimedia Commons

,.

[11] K. Las Heras, M. Igartua, E. Santos-Vizcaino, R.M. Hernandez, Chronic wounds: Current status, available strategies and emerging therapeutic solutions, J. Control. Release. 328 (2020) 532-550.

[12] A.D. Metcalfe, M.W. Ferguson, Tissue engineering of replacement skin: the crossroads of biomaterials, wound healing, embryonic development, stem cells and regeneration, J. R. Soc. Interface. 4 (2007) 413-437.

[13] L.E. Dickinson, S. Gerecht, Engineered Biopolymeric Scaffolds for Chronic Wound Healing, Front. Physiol. 7 (2016) 341.

[14] W. Oualla-Bachiri, A. Fernandez-Gonzalez, M.I. Quinones-Vico, S. Arias-Santiago, From Grafts to Human Bioengineered Vascularized Skin Substitutes, Int. J. Mol. Sci. 21 (2020) 10.3390/ijms21218197.

[15] C. Dai, S. Shih, A. Khachemoune, Skin substitutes for acute and chronic wound healing: an updated review, J. Dermatolog Treat. (2020) 1-10.

[16] D. Snyder, N. Sullivan, D. Margolis, K. Schoelles, No title, (2020).

[17] S. Haldar, A. Sharma, S. Gupta, S. Chauhan, P. Roy, D. Lahiri, Bioengineered smart trilayer skin tissue substitute for efficient deep wound healing, Mater. Sci. Eng. C. Mater. Biol. Appl. 105 (2019) 110140.

[18] H.Y. Lin, S.H. Chen, S.H. Chang, S.T. Huang, Tri-layered chitosan scaffold as a potential skin substitute, J. Biomater. Sci. Polym. Ed. 26 (2015) 855-867.

[19] J. Kober, A. Gugerell, M. Schmid, L.P. Kamolz, M. Keck, Generation of a Fibrin Based Three-Layered Skin Substitute, Biomed. Res. Int. 2015 (2015) 170427.

[20] D. Chouhan, N. Dey, N. Bhardwaj, B.B. Mandal, Emerging and innovative approaches for wound healing and skin regeneration: Current status and advances, Biomaterials. 216 (2019) 119267.

[21] A.V. Do, B. Khorsand, S.M. Geary, A.K. Salem, 3D Printing of Scaffolds for Tissue Regeneration Applications, Adv. Healthc. Mater. 4 (2015) 1742-1762.

[22] M.A. Mofazzal Jahromi, P. Sahandi Zangabad, S.M. Moosavi Basri, K. Sahandi Zangabad, A. Ghamarypour, A.R. Aref, M. Karimi, M.R. Hamblin, Nanomedicine and advanced technologies for burns: Preventing infection and facilitating wound healing, Adv. Drug Deliv. Rev. 123 (2018) 33-64.

[23] W.C. Yan, P. Davoodi, S. Vijayavenkataraman, Y. Tian, W.C. Ng, J.Y.H. Fuh, K.S. Robinson, C.H. Wang, 3D bioprinting of skin tissue: From pre-processing to final product evaluation, Adv. Drug Deliv. Rev. 132 (2018) 270-295.

[24] W. Lee, J.C. Debasitis, V.K. Lee, J.H. Lee, K. Fischer, K. Edminster, J.K. Park, S.S. Yoo, Multi-layered culture of human skin fibroblasts and keratinocytes through three-dimensional freeform fabrication, Biomaterials. 30 (2009) 1587-1595.

[25] V. Lee, G. Singh, J.P. Trasatti, C. Bjornsson, X. Xu, T.N. Tran, S.S. Yoo, G. Dai, P. Karande, Design and fabrication of human skin by three-dimensional bioprinting, Tissue Eng. Part C. Methods. 20 (2014) 473-484.

[26] L. Koch, A. Deiwick, S. Schlie, S. Michael, M. Gruene, V. Coger, D. Zychlinski, A. Schambach, K. Reimers, P.M. Vogt, B. Chichkov, Skin tissue generation by laser cell printing, Biotechnol. Bioeng. 109 (2012) 1855-1863.

[27] L. Koch, S. Kuhn, H. Sorg, M. Gruene, S. Schlie, R. Gaebel, B. Polchow, K. Reimers, S. Stoelting, N. Ma, P.M. Vogt, G. Steinhoff, B. Chichkov, Laser printing of skin cells and human stem cells, Tissue Eng. Part C. Methods. 16 (2010) 847-854.

[28] S. Michael, H. Sorg, C.T. Peck, L. Koch, A. Deiwick, B. Chichkov, P.M. Vogt, K. Reimers, Tissue engineered skin substitutes created by laser-assisted bioprinting form skin-like structures in the dorsal skin fold chamber in mice, PLoS One. 8 (2013) e57741.

[29] G. Kim, S. Ahn, H. Yoon, Y. Kim, W. Chun, A cryogenic direct-plotting system for fabrication of 3D collagen scaffolds for tissue engineering, J. Mater. Chem. 19 (2009) 8817-8823.

[30] W.L. Ng, J.T.Z. Qi, W.Y. Yeong, M.W. Naing, Proof-of-concept: 3D bioprinting of pigmented human skin constructs, Biofabrication. 10 (2018) 025005-5090/aa9e1e.

[31] D. Min, W. Lee, I.H. Bae, T.R. Lee, P. Croce, S.S. Yoo, Bioprinting of biomimetic skin containing melanocytes, Exp. Dermatol. 27 (2018) 453-459.

[32] N. Mori, Y. Morimoto, S. Takeuchi, Perfusable and stretchable 3D culture system for skin-equivalent, Biofabrication. 11 (2018) 011001-5090/aaed12.

[33] H. Lee, J.A. Park, S. Kim, Y. Jo, D. Kang, S. Jung, 3D microextrusion-inkjet hybrid printing of structured human skin equivalents, Bioprinting. 22 (2021) e00143.

[34] L.Y. Daikuara, Z. Yue, D. Skropeta, G.G. Wallace, In vitro characterisation of 3D printed platelet lysate-based bioink for potential application in skin tissue engineering, Acta Biomater. 123 (2021) 286-297.

[35] N. Cubo, M. Garcia, J.F. Del Canizo, D. Velasco, J.L. Jorcano, 3D bioprinting of functional human skin: production and in vivo analysis, Biofabrication. 9 (2016) 015006-5090/9/1/015006.

[36] M. Albanna, K.W. Binder, S.V. Murphy, J. Kim, S.A. Qasem, W. Zhao, J. Tan, I.B. El-Amin, D.D. Dice, J. Marco, J. Green, T. Xu, A. Skardal, J.H. Holmes, J.D. Jackson, A. Atala,

J.J. Yoo, In Situ Bioprinting of Autologous Skin Cells Accelerates Wound Healing of Extensive Excisional Full-Thickness Wounds, Sci. Rep. 9 (2019) 1856-w.

[37] T. Baltazar, J. Merola, C. Catarino, C.B. Xie, N.C. Kirkiles-Smith, V. Lee, S. Hotta, G. Dai, X. Xu, F.C. Ferreira, W.M. Saltzman, J.S. Pober, P. Karande, Three Dimensional Bioprinting of a Vascularized and Perfusable Skin Graft Using Human Keratinocytes, Fibroblasts, Pericytes, and Endothelial Cells, Tissue Eng. Part A. 26 (2020) 227-238.

[38] B.S. Kim, J.S. Lee, G. Gao, D.W. Cho, Direct 3D cell-printing of human skin with functional transwell system, Biofabrication. 9 (2017) 025034-5090/aa71c8.

[39] B.S. Kim, G. Gao, J.Y. Kim, D.W. Cho, 3D Cell Printing of Perfusable Vascularized Human Skin Equivalent Composed of Epidermis, Dermis, and Hypodermis for Better Structural Recapitulation of Native Skin, Adv. Healthc. Mater. 8 (2019) e1801019.

[40] M.M. Sanchez, J.T. Morgan, Generation of Self-assembled Vascularized Human Skin Equivalents, J. Vis. Exp. (168). doi (2021) 10.3791/62125.

[41] L. Xu, L. Ding, L. Wang, Y. Cao, H. Zhu, J. Lu, X. Li, T. Song, Y. Hu, J. Dai, Umbilical cord-derived mesenchymal stem cells on scaffolds facilitate collagen degradation via upregulation of MMP-9 in rat uterine scars, Stem Cell. Res. Ther. 8 (2017) 84-0.

[42] J. Guo, H. Hu, J. Gorecka, H. Bai, H. He, R. Assi, T. Isaji, T. Wang, O. Setia, L. Lopes, Y. Gu, A. Dardik, Adipose-derived mesenchymal stem cells accelerate diabetic wound healing in a similar fashion as bone marrow-derived cells, Am. J. Physiol. Cell. Physiol. 315 (2018) C885-C896.

[43] R.S. Kirsner, A.C. Vivas, Lower-extremity ulcers: diagnosis and management, Br. J. Dermatol. 173 (2015) 379-390.

[44] A. Rahmani Del Bakhshayesh, N. Annabi, R. Khalilov, A. Akbarzadeh, M. Samiei, E. Alizadeh, M. Alizadeh-Ghodsi, S. Davaran, A. Montaseri, Recent advances on biomedical applications of scaffolds in wound healing and dermal tissue engineering, Artif. Cells Nanomed Biotechnol. 46 (2018) 691-705.

[45] G.D. Mogosanu, A.M. Grumezescu, Natural and synthetic polymers for wounds and burns dressing, Int. J. Pharm. 463 (2014) 127-136.

[46] C.R. Weinstein-Oppenheimer, D.I. Brown, R. Coloma, P. Morales, M. Reyna-Jeldes, M.J. Diaz, E. Sanchez, C.A. Acevedo, Design of a hybrid biomaterial for tissue engineering: Biopolymer-scaffold integrated with an autologous hydrogel carrying mesenchymal stem-cells, Mater. Sci. Eng. C. Mater. Biol. Appl. 79 (2017) 821-830.

[47] P.L. Kang, H.H. Huang, T. Chen, K.C. Ju, S.M. Kuo, Angiogenesis-promoting effect of LIPUS on hADSCs and HUVECs cultured on collagen/hyaluronan scaffolds, Mater. Sci. Eng. C. Mater. Biol. Appl. 102 (2019) 22-33.

[48] I. Pena-Villalobos, I. Casanova-Maldonado, P. Lois, C. Prieto, C. Pizarro, J. Lattus, G. Osorio, V. Palma, Hyperbaric Oxygen Increases Stem Cell Proliferation, Angiogenesis and Wound-Healing Ability of WJ-MSCs in Diabetic Mice, Front. Physiol. 9 (2018) 995.

[49] S. Ding, Y. Xu, X. Yan, Y. Lin, Q. Tan, Effect of Collagen Scaffold With Bcl-2-Modified Adipose-Derived Stem Cells on Diabetic Mice Wound Healing, Int. J. Low Extrem Wounds. (2019) 1534734619880055.

[50] H.D. Zomer, T.D.S. Jeremias, B. Ratner, A.G. Trentin, Mesenchymal stromal cells from dermal and adipose tissues induce macrophage polarization to a pro-repair phenotype and improve skin wound healing, Cytotherapy. 22 (2020) 247-260.

[51] C.W. Lin, Y.K. Chen, K.C. Tang, K.C. Yang, N.C. Cheng, J. Yu, Keratin scaffolds with human adipose stem cells: Physical and biological effects toward wound healing, J. Tissue Eng. Regen. Med. 13 (2019) 1044-1058.

[52] D.S. Feldman, J.F. McCauley, Mesenchymal Stem Cells and Transforming Growth Factor-beta(3) (TGF-beta(3)) to Enhance the Regenerative Ability of an Albumin Scaffold in Full Thickness Wound Healing, J. Funct. Biomater. 9 (2018) 10.3390/jfb9040065.

[53] K. Las Heras, E. Santos-Vizcaino, T. Garrido, F. Borja Gutierrez, J.J. Aguirre, K. de la Caba, P. Guerrero, M. Igartua, R.M. Hernandez, Soy protein and chitin sponge-like scaffolds: from natural by-products to cell delivery systems for biomedical applications, Green Chem. (2020).

[54] A.A. Chaudhari, K. Vig, D.R. Baganizi, R. Sahu, S. Dixit, V. Dennis, S.R. Singh, S.R. Pillai, Future Prospects for Scaffolding Methods and Biomaterials in Skin Tissue Engineering: A Review, Int. J. Mol. Sci. 17 (2016) 10.3390/ijms17121974.

[55] R. Geesala, N. Bar, N.R. Dhoke, P. Basak, A. Das, Porous polymer scaffold for on-site delivery of stem cells--Protects from oxidative stress and potentiates wound tissue repair, Biomaterials. 77 (2016) 1-13.

[56] H.E. Karahan, C. Wiraja, C. Xu, J. Wei, Y. Wang, L. Wang, F. Liu, Y. Chen, Graphene Materials in Antimicrobial Nanomedicine: Current Status and Future Perspectives, Adv. Healthc. Mater. 7 (2018) e1701406.

[57] I. Lasocka, E. Jastrzebska, L. Szulc-Dabrowska, M. Skibniewski, I. Pasternak, M.H. Kalbacova, E.M. Skibniewska, The effects of graphene and mesenchymal stem cells in cutaneous wound healing and their putative action mechanism, Int. J. Nanomedicine. 14 (2019) 2281-2299.

[58] J. Chu, P. Shi, W. Yan, J. Fu, Z. Yang, C. He, X. Deng, H. Liu, PEGylated graphene oxide-mediated quercetin-modified collagen hybrid scaffold for enhancement of MSCs differentiation potential and diabetic wound healing, Nanoscale. 10 (2018) 9547-9560.

[59] Z. Li, H. Wang, B. Yang, Y. Sun, R. Huo, Three-dimensional graphene foams loaded with bone marrow derived mesenchymal stem cells promote skin wound healing with reduced scarring, Mater. Sci. Eng. C. Mater. Biol. Appl. 57 (2015) 181-188.

[60] M. Liu, X.P. Duan, Y.M. Li, D.P. Yang, Y.Z. Long, Electrospun nanofibers for wound healing, Mater. Sci. Eng. C. Mater. Biol. Appl. 76 (2017) 1413-1423.

[61] D. Chouhan, N. Dey, N. Bhardwaj, B.B. Mandal, Emerging and innovative approaches for wound healing and skin regeneration: Current status and advances, Biomaterials. 216 (2019) 119267.

[62] C. Wang, J. Wang, L. Zeng, Z. Qiao, X. Liu, H. Liu, J. Zhang, J. Ding, Fabrication of Electrospun Polymer Nanofibers with Diverse Morphologies, Molecules. 24 (2019) 10.3390/molecules24050834.

[63] I. Behere, G. Ingavle, In vitro and in vivo advancement of multifunctional electrospun nanofiber scaffolds in wound healing applications: Innovative nanofiber designs, stem cell approaches, and future perspectives, J. Biomed. Mater. Res. A. (2021).

[64] N. Su, P.L. Gao, K. Wang, J.Y. Wang, Y. Zhong, Y. Luo, Fibrous scaffolds potentiate the paracrine function of mesenchymal stem cells: A new dimension in cell-material interaction, Biomaterials. 141 (2017) 74-85.

[65] S. Chen, H. Wang, Y. Su, J.V. John, A. McCarthy, S.L. Wong, J. Xie, Mesenchymal stem cell-laden, personalized 3D scaffolds with controlled structure and fiber alignment promote diabetic wound healing, Acta Biomater. 108 (2020) 153-167.

[66] M. Lotfi, H. Naderi-Meshkin, E. Mahdipour, A. Mafinezhad, R. Bagherzadeh, H.R. Sadeghnia, H. Esmaily, M. Maleki, H. Hasssanzadeh, M. Ghayaour-Mobarhan, H.R. Bidkhori, A.R. Bahrami, Adipose tissue-derived mesenchymal stem cells and keratinocytes co-culture on gelatin/chitosan/beta-glycerol phosphate nanoscaffold in skin regeneration, Cell Biol. Int. (2019).

[67] O.V. Pham-Nguyen, J.U. Shin, H. Kim, H.S. Yoo, Self-assembled cell sheets composed of mesenchymal stem cells and gelatin nanofibers for the treatment of full-thickness wounds, Biomater. Sci. 8 (2020) 4535-4544.

[68] J.E. Millan-Rivero, C.M. Martinez, P.A. Romecin, S.D. Aznar-Cervantes, M. Carpes-Ruiz, J.L. Cenis, J.M. Moraleda, N.M. Atucha, D. Garcia-Bernal, Silk fibroin scaffolds seeded with Wharton's jelly mesenchymal stem cells enhance re-epithelialization and reduce formation of scar tissue after cutaneous wound healing, Stem Cell. Res. Ther. 10 (2019) 126-6.

[69] J. Haik, R. Kornhaber, B. Blal, M. Harats, The Feasibility of a Handheld Electrospinning Device for the Application of Nanofibrous Wound Dressings, Adv. Wound. Care. (New Rochelle). 6 (2017) 166-174.

[70] S. Xu, C. Qin, M. Yu, R. Dong, X. Yan, H. Zhao, W. Han, H. Zhang, Y. Long, A battery-operated portable handheld electrospinning apparatus, Nanoscale. 7 (2015) 12351-12355.

[71] R. Dong, Y. Jia, C. Qin, L. Zhan, X. Yan, L. Cui, Y. Zhou, X. Jiang, Y. Long, In situ deposition of a personalized nanofibrous dressing via a handy electrospinning device for skin wound care, Nanoscale. 8 (2016) 3482-3488.

[72] E. Caló, V.V. Khutoryanskiy, Biomedical applications of hydrogels: A review of patents and commercial products, European Polymer Journal. 65 (2015) 252-267.

[73] J.S. Chin, L. Madden, S.Y. Chew, D.L. Becker, Drug therapies and delivery mechanisms to treat perturbed skin wound healing, Adv. Drug Deliv. Rev. 149-150 (2019) 2-18.

[74] G. Eke, N. Mangir, N. Hasirci, S. MacNeil, V. Hasirci, Development of a UV crosslinked biodegradable hydrogel containing adipose derived stem cells to promote vascularization for skin wounds and tissue engineering, Biomaterials. 129 (2017) 188-198.

[75] L.C. Hsu, B.Y. Peng, M.S. Chen, B. Thalib, M. Ruslin, T.D.X. Tung, H.H. Chou, K.L. Ou, The potential of the stem cells composite hydrogel wound dressings for promoting wound healing and skin regeneration: In vitro and in vivo evaluation, J. Biomed. Mater. Res. B. Appl. Biomater. 107 (2019) 278-285.

[76] S. Tyeb, P.A. Shiekh, V. Verma, A. Kumar, Adipose-Derived Stem Cells (ADSCs) Loaded Gelatin-Sericin-Laminin Cryogels for Tissue Regeneration in Diabetic Wounds, Biomacromolecules. 21 (2020) 294-304.

[77] H. Xu, S. Huang, J. Wang, Y. Lan, L. Feng, M. Zhu, Y. Xiao, B. Cheng, W. Xue, R. Guo, Enhanced cutaneous wound healing by functional injectable thermo-sensitive chitosan-based hydrogel encapsulated human umbilical cord-mesenchymal stem cells, Int. J. Biol. Macromol. 137 (2019) 433-441.

[78] H. Bai, N. Kyu-Cheol, Z. Wang, Y. Cui, H. Liu, H. Liu, Y. Feng, Y. Zhao, Q. Lin, Z. Li, Regulation of inflammatory microenvironment using a self-healing hydrogel loaded with BM-MSCs for advanced wound healing in rat diabetic foot ulcers, J. Tissue Eng. 11 (2020) 2041731420947242.

[79] K. Shou, Y. Huang, B. Qi, X. Hu, Z. Ma, A. Lu, C. Jian, L. Zhang, A. Yu, Induction of mesenchymal stem cell differentiation in the absence of soluble inducer for cutaneous wound regeneration by a chitin nanofiber-based hydrogel, J. Tissue Eng. Regen. Med. 12 (2018) e867-e880.

[80] K. Ravishankar, M. Venkatesan, R.P. Desingh, A. Mahalingam, B. Sadhasivam, R. Subramaniyam, R. Dhamodharan, Biocompatible hydrogels of chitosan-alkali lignin for potential wound healing applications, Mater. Sci. Eng. C. Mater. Biol. Appl. 102 (2019) 447-457.

[81] J.L. Soriano-Ruiz, P. Galvez-Martin, E. Lopez-Ruiz, J. Suner-Carbo, A.C. Calpena-Campmany, J.A. Marchal, B. Clares-Naveros, Design and evaluation of mesenchymal stem cells seeded chitosan/glycosaminoglycans quaternary hydrogel scaffolds for wound healing applications, Int. J. Pharm. 570 (2019) 118632.

[82] Z. Chen, B. Zhang, J. Shu, H. Wang, Y. Han, Q. Zeng, Y. Chen, J. Xi, R. Tao, X. Pei, W. Yue, Y. Han, Human decellularized adipose matrix derived hydrogel assists mesenchymal stem cells delivery and accelerates chronic wound healing, J. Biomed. Mater. Res. A. (2020).

[83] W. Pu, J. Ren, Y. Chen, J. Shu, L. Cui, Y. Han, J. Xi, X. Pei, W. Yue, Y. Han, Injectable human decellularized adipose tissue hydrogel containing stem cells enhances wound healing in mouse, Colloids Surf. Physicochem. Eng. Aspects. 604 (2020) 125268.

[84] M.W. Lee, S. Ryu, D.S. Kim, K.W. Sung, H.H. Koo, K.H. Yoo, Strategies to improve the immunosuppressive properties of human mesenchymal stem cells, Stem Cell. Res. Ther. 6 (2015) 179-y.

[85] M. Krampera, L. Cosmi, R. Angeli, A. Pasini, F. Liotta, A. Andreini, V. Santarlasci, B. Mazzinghi, G. Pizzolo, F. Vinante, P. Romagnani, E. Maggi, S. Romagnani, F. Annunziato, Role for interferon-gamma in the immunomodulatory activity of human bone marrow mesenchymal stem cells, Stem Cells. 24 (2006) 386-398.

[86] C. Liang, E. Jiang, J. Yao, M. Wang, S. Chen, Z. Zhou, W. Zhai, Q. Ma, S. Feng, M. Han, Interferon-γ mediates the immunosuppression of bone marrow mesenchymal stem cells on T-lymphocytes in vitro, Hematology. 23 (2018) 44-49.

[87] A. Gonzalez-Pujana, K.H. Vining, D.K.Y. Zhang, E. Santos-Vizcaino, M. Igartua, R.M. Hernandez, D.J. Mooney, Multifunctional biomimetic hydrogel systems to boost the immunomodulatory potential of mesenchymal stromal cells, Biomaterials. 257 (2020) 120266.

[88] X. Zheng, Z. Ding, W. Cheng, Q. Lu, X. Kong, X. Zhou, G. Lu, D.L. Kaplan, Microskin-Inspired Injectable MSC-Laden Hydrogels for Scarless Wound Healing with Hair Follicles, Adv. Healthc. Mater. (2020) e2000041.

[89] J.R. Garcia, M. Quiros, W.M. Han, M.N. O'Leary, G.N. Cox, A. Nusrat, A.J. Garcia, IFN-gamma-tethered hydrogels enhance mesenchymal stem cell-based immunomodulation and promote tissue repair, Biomaterials. 220 (2019) 119403.

[90] P. He, J. Zhao, J. Zhang, B. Li, Z. Gou, M. Gou, X. Li, Bioprinting of skin constructs for wound healing, Burns Trauma. 6 (2018) 5-x. eCollection 2018.

[91] A. Skardal, D. Mack, E. Kapetanovic, A. Atala, J.D. Jackson, J. Yoo, S. Soker, Bioprinted amniotic fluid-derived stem cells accelerate healing of large skin wounds, Stem Cells Transl. Med. 1 (2012) 792-802.

[92] Z.M. Jessop, A. Al-Sabah, M.D. Gardiner, E. Combellack, K. Hawkins, I.S. Whitaker, 3D bioprinting for reconstructive surgery: Principles, applications and challenges, J. Plast. Reconstr. Aesthet. Surg. 70 (2017) 1155-1170.

[93] A.L. Rutz, K.E. Hyland, A.E. Jakus, W.R. Burghardt, R.N. Shah, A multimaterial bioink method for 3D printing tunable, cell-compatible hydrogels, Adv Mater. 27 (2015) 1607-1614.

[94] B.S. Kim, Y.W. Kwon, J.S. Kong, G.T. Park, G. Gao, W. Han, M.B. Kim, H. Lee, J.H. Kim, D.W. Cho, 3D cell printing of in vitro stabilized skin model and in vivo pre-vascularized skin patch using tissue-specific extracellular matrix bioink: A step towards advanced skin tissue engineering, Biomaterials. 168 (2018) 38-53.

[95] T. Li, H. Ma, H. Ma, Z. Ma, L. Qiang, Z. Yang, X. Yang, X. Zhou, K. Dai, J. Wang, Mussel-Inspired Nanostructures Potentiate the Immunomodulatory Properties and Angiogenesis of Mesenchymal Stem Cells, ACS Appl. Mater. Interfaces. 11 (2019) 17134-17146.

[96] N. Hakimi, R. Cheng, L. Leng, M. Sotoudehfar, P.Q. Ba, N. Bakhtyar, S. Amini-Nik, M.G. Jeschke, A. Gunther, Handheld skin printer: in situ formation of planar biomaterials and tissues, Lab. Chip. 18 (2018) 1440-1451.

[97] F. Agostinacchio, X. Mu, S. Dire, A. Motta, D.L. Kaplan, In Situ 3D Printing: Opportunities with Silk Inks, Trends Biotechnol. (2020).

[98] S. Ichioka, S. Kouraba, N. Sekiya, N. Ohura, T. Nakatsuka, Bone marrow-impregnated collagen matrix for wound healing: experimental evaluation in a microcirculatory model of angiogenesis, and clinical experience, Br. J. Plast. Surg. 58 (2005) 1124-1130.

[99] T. Yoshikawa, H. Mitsuno, I. Nonaka, Y. Sen, K. Kawanishi, Y. Inada, Y. Takakura, K. Okuchi, A. Nonomura, Wound therapy by marrow mesenchymal cell transplantation, Plast. Reconstr. Surg. 121 (2008) 860-877.

[100] H. Ravari, D. Hamidi-Almadari, M. Salimifar, S. Bonakdaran, M.R. Parizadeh, G. Koliakos, Treatment of non-healing wounds with autologous bone marrow cells, platelets, fibrin glue and collagen matrix, Cytotherapy. 13 (2011) 705-711.

[101] K.C. Moon, H.S. Suh, K.B. Kim, S.K. Han, K.W. Young, J.W. Lee, M.H. Kim, Potential of Allogeneic Adipose-Derived Stem Cell-Hydrogel Complex for Treating Diabetic Foot Ulcers, Diabetes. 68 (2019) 837-846.

[102] X. Zeng, Y. Tang, K. Hu, W. Jiao, L. Ying, L. Zhu, J. Liu, J. Xu, Three-week topical treatment with placenta-derived mesenchymal stem cells hydrogel in a patient with diabetic foot ulcer: A case report, Medicine (Baltimore). 96 (2017) e9212.

[103] S. Hashemi, A.A. Mohammadi, K. Moshirabadi, M. Zardosht, Effect of dermal fibroblasts and mesenchymal stem cells seeded on an amniotic membrane scaffold in skin regeneration: A case series, J Cosmet Dermatol. n/a (2021).

[104] P. Martin, R. Nunan, Cellular and molecular mechanisms of repair in acute and chronic wound healing, Br. J. Dermatol. 173 (2015) 370-378.

[105] O. Soehnlein, S. Steffens, A. Hidalgo, C. Weber, Neutrophils as protagonists and targets in chronic inflammation, Nat. Rev. Immunol. 17 (2017) 248-261.

[106] E. Kolaczkowska, P. Kubes, Neutrophil recruitment and function in health and inflammation, Nat. Rev. Immunol. 13 (2013) 159-175.

[107] T.A. Wynn, K.M. Vannella, Macrophages in Tissue Repair, Regeneration, and Fibrosis, Immunity. 44 (2016) 450-462.

[108] M.P. Caley, V.L. Martins, E.A. O'Toole, Metalloproteinases and Wound Healing, Adv. Wound. Care. (New Rochelle). 4 (2015) 225-234.

[109] J. Cha, T. Kwak, J. Butmarc, T.A. Kim, T. Yufit, P. Carson, S.J. Kim, V. Falanga, Fibroblasts from non-healing human chronic wounds show decreased expression of beta ig-h3, a TGF-beta inducible protein, J. Dermatol. Sci. 50 (2008) 15-23.

[110] S. Patel, A. Maheshwari, A. Chandra, Biomarkers for wound healing and their evaluation, J. Wound Care. 25 (2016) 46-55.

[111] M.J. Hoogduijn, E. Lombardo, Mesenchymal Stromal Cells Anno 2019: Dawn of the Therapeutic Era? Concise Review, Stem Cells Transl. Med. 8 (2019) 1126-1134.

[112] S. Maxson, E.A. Lopez, D. Yoo, A. Danilkovitch-Miagkova, M.A. Leroux, Concise review: role of mesenchymal stem cells in wound repair, Stem Cells Transl. Med. 1 (2012) 142-149.

[113] A. Gonzalez-Pujana, M. Igartua, E. Santos-Vizcaino, R.M. Hernandez, Mesenchymal stromal cell based therapies for the treatment of immune disorders: recent milestones and future challenges, Expert Opin. Drug Deliv. 17 (2020) 189-200.

[114] P. Hu, Q. Yang, Q. Wang, C. Shi, D. Wang, U. Armato, I.D. Pra, A. Chiarini, Mesenchymal stromal cells-exosomes: a promising cell-free therapeutic tool for wound healing and cutaneous regeneration, Burns Trauma. 7 (2019) 38-8. eCollection 2019.

[115] M. Gong, B. Yu, J. Wang, Y. Wang, M. Liu, C. Paul, R.W. Millard, D.S. Xiao, M. Ashraf, M. Xu, Mesenchymal stem cells release exosomes that transfer miRNAs to endothelial cells and promote angiogenesis, Oncotarget. 8 (2017) 45200-45212.

[116] X. Liang, L. Zhang, S. Wang, Q. Han, R.C. Zhao, Exosomes secreted by mesenchymal stem cells promote endothelial cell angiogenesis by transferring miR-125a, J. Cell. Sci. 129 (2016) 2182-2189.

[117] M. Komaki, Y. Numata, C. Morioka, I. Honda, M. Tooi, N. Yokoyama, H. Ayame, K. Iwasaki, A. Taki, N. Oshima, I. Morita, Exosomes of human placenta-derived mesenchymal stem cells stimulate angiogenesis, Stem Cell. Res. Ther. 8 (2017) 219-9.

[118] D.E. Lee, N. Ayoub, D.K. Agrawal, Mesenchymal stem cells and cutaneous wound healing: novel methods to increase cell delivery and therapeutic efficacy, Stem Cell. Res. Ther. 7 (2016) 37-6.

[119] H.K. Kim, S.G. Lee, S.W. Lee, B.J. Oh, J.H. Kim, J.A. Kim, G. Lee, J.D. Jang, Y.A. Joe, A Subset of Paracrine Factors as Efficient Biomarkers for Predicting Vascular Regenerative Efficacy of Mesenchymal Stromal/Stem Cells, Stem Cells. 37 (2019) 77-8

Chapter 4

Summary in Spanish

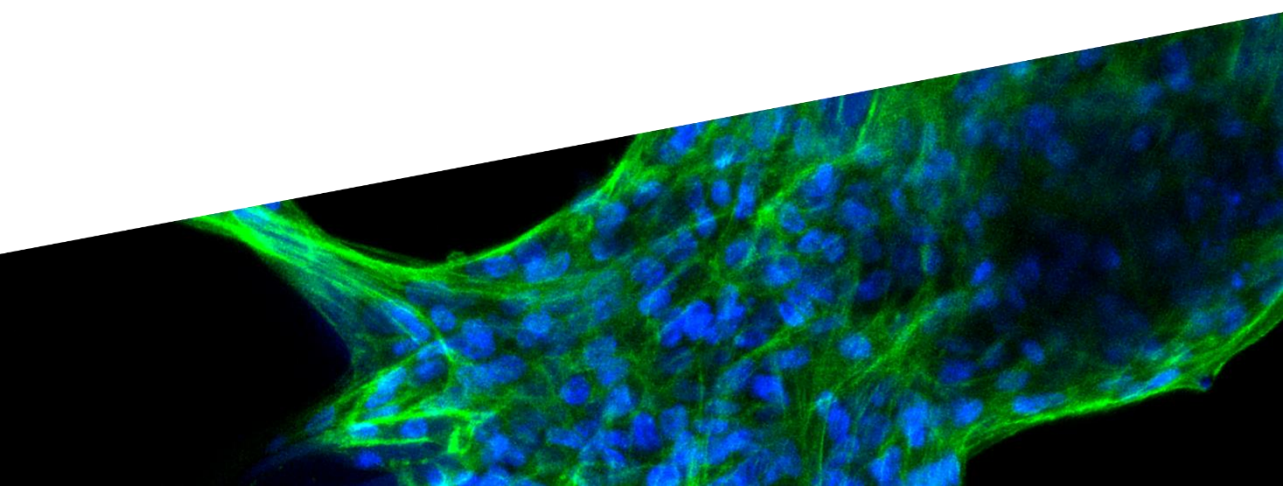

Las heridas son tan antiguas como lo es el ser humano. Desde nuestra infancia, cuando sufrimos numerosos rasguños y cortes, hasta nuestra vejez, cuando diferentes patologías, golpes, cirugías etc. pueden provocar graves lesiones tisulares, los humanos experimentamos de manera recurrente el ciclo de del daño y la reparación de tejidos. Generalmente, las heridas cicatrizan en pocos días o semanas en un proceso sin incidencias. Sin embargo, hay ocasiones en las que la cicatrización de heridas sufre problemas. Generalmente, las heridas se dividen en agudas y crónicas, con ciertos subtipos en cada grupo. Cuando se da la lesión tisular, todas las heridas son tratadas como agudas, independientemente de su origen o naturaleza. No obstante, cuando estas lesiones tardan más de tres meses en cicatrizar, son tratadas como heridas crónicas. Entre los estados fisiológicos y patológicos que pueden provocar un retraso o incidencia en la cicatrización; el envejecimiento, la diabetes, las infecciones, los problemas vasculares y el cáncer son las principales causas.

El proceso de cicatrización de heridas tras una lesión tisular implica una compleja interacción de; múltiples tipos de células (células inmunitarias, células de la piel, células estromales mesenquimales (MSCs), etc.), mediadores moleculares y la matriz extracelular circundante (ECM). Este proceso sigue una cascada celular y molecular perfectamente orquestada por múltiples mediadores. En individuos sanos, este proceso de cicatrización de heridas comprende cuatro etapas: hemostasia, inflamación, proliferación y remodelación. Sin embargo, cuando el proceso de cicatrización se estanca en alguna de ellas, es necesario actuar desde un abordaje farmacoterapéutico.

Este es el caso de algunas heridas agudas que pueden quedarse estancadas en la fase de hemostasia, normalmente como efectos secundarios a coagulopatías, problemas metabólicos, algunos cánceres o trastornos genéticos. El mecanismo circundante detrás de estas anomalías normalmente reside en una alteración de la agregación plaquetaria y/o la formación de coágulos que conduce a una pérdida continua de sangre sin un cierre adecuado de la herida. Por ejemplo, en patologías como la epistaxis severa — generalmente la epistaxis posterior —, estas heridas pueden aparecer con asidua periodicidad causando importantes problemas en la salud y calidad de vida de los pacientes. Hoy en día, el tratamiento estándar no quirúrgico de estas heridas hemorrágicas agudas consiste en el empleo de presión combinado con

biomateriales que cubren la herida y absorben la sangre (gasas, apósitos, etc.). Sin embargo, es necesario desarrollar nuevos tratamientos más bioactivos que puedan evitar la cauterización o la cirugía y que ayuden a reducir la pérdida de sangre y el tiempo de curación al mismo tiempo que ayuden a mejorar la calidad de vida de las personas que lo padecen — por ejemplo; reduciendo las molestias en los pacientes con epistaxis al extraer/introducir las gasas o los tapones nasales —.

Por otro lado, algunas lesiones tisulares pueden quedar estancadas en la segunda fase del proceso normal de cicatrización de heridas, la fase inflamatoria, dando lugar a heridas crónicas. Este tipo de heridas se caracterizan por permanecer en un estado inflamatorio constante mostrando una angiogénesis alterada y una intercomunicación celular desregulada debido a una elevada actividad proteolítica. Todas estas alteraciones celulares y moleculares impiden una correcta deposición de ECM y finalmente impiden una correcta formación de tejido de granulación. A pesar de que actualmente existe una amplia variedad de tratamientos disponibles en el mercado para este tipo de heridas, aún existe la necesidad de desarrollar terapias más precisas y efectivas que aborden los múltiples factores involucrados en el proceso de cicatrización de heridas. En este sentido, las estrategias basadas en biomateriales, en forma de apósitos, han sido las principales opciones para el tratamiento de este tipo de heridas desde siglos atrás. Sin embargo, estos biomateriales no solo deberían proporcionar adecuadas propiedades fisicoquímicas y de retención de humedad, sino que también deberían apoyar el proceso de cicatrización, modulando el comportamiento celular y molecular ajustando así el microambiente de la herida.

Ya sea en la primera fase (heridas hemorrágicas agudas) o en la segunda fase (heridas crónicas) allí donde se produzca el estancamiento de la cicatrización, el enfoque terapéutico basado en biomateriales es la primera elección. Sin embargo, en el caso de las heridas crónicas, el tratamiento requiere de un enfoque más complejo que eventualmente pueda actuar a diferentes niveles del proceso de cicatrización. En consecuencia, durante este siglo se han desarrollado nuevas terapias combinando células con biomateriales. En este sentido, estos biomateriales proporcionan una matriz con propiedades bioactivas que favorece la retención celular y que consecuentemente liberan mediadores que interactúan con el microambiente de la herida ayudando a conseguir una cicatrización más rápida y funcional.

Por ello en esta tesis doctoral se ha desarrollado un nuevo biomaterial hemostático cicatrizante, en forma de esponja o "scaffold", compuesto por proteina de la soja y β-quitina capaz de albergar células en su microarquitectura. Además, con el pensamiento actual de ser respetuoso con el medioambiente y buscar la reducción de residuos en todos los niveles de la producción, los materiales que forman el scaffold son obtenidos de deshechos de la industria alimentaria. Así, gracias a este pensamiento de "economía circular" podemos demostrar que subproductos de la industria pueden ser reutilizados para producir nuevos dispositivos terapéuticos.

En el primer estudio de esta tesis doctoral, conseguimos sintetizar el scaffold y posteriormente caracterizarlo. Gracias a los análisis de infrarrojos con transformada de Fourier y espectrometría de rayos X demostramos que la combinación de ambos compuestos, la proteina de la soja y la β-quitina, se da mediante interacciones físicas por enlaces de hidrógeno entre los grupos hidroxilo de la β-quitina y los grupos laterales polares (hidroxilo, carboxilo, amino) de los aminoácidos de la proteina de la soja. Posteriormente estudiamos su arquitectura confirmando que estos scaffolds presentaban una porosidad elevada y con una microestructura bien interconectada. Además, la capacidad de absorción del material fue elevada, llegando a absorber 13 veces su peso en fluido. Por otro lado, su perfil de degradación acuoso demostró que los scaffolds no sufren degradación hidrolítica. Sin embargo, en presencia de enzimas degradantes de matriz extracelular como la colagenasa, el scaffold se degradó en 2h. Finalmente decidimos comprobar la biocompatibilidad de los scaffolds en cultivos celulares y en modelos murinos. Así, demostramos que, mediante un previo proceso de limpieza o condicionamiento de los biomateriales mediante diálisis, presentaban una biocompatibilidad adecuada para su uso en cicatrización de heridas.

En el segundo estudio decidimos testar las propiedades hemostáticas de nuestros scaffolds para comprobar si podrían ser útiles en la cicatrización de heridas hemorrágicas agudas como la epistaxis. Para ello, incluimos en el estudio dos grupos de comparación, uno usando gasas médicas y otro usando Merocel, el "standard" global en el tratamiento de epistaxis. Primeramente, observamos en el perfil mecánico que los scaffolds presentaban una mayor capacidad de expansión que el de los otros dos biomaterials, lo cual resulta interesante de cara a ejercer mayor presión en la pared nasal para el tratamiento de la epistaxis. Posteriormente testamos las propiedades

hemostáticas de los tres biomateriales. Descubrimos que los scaffolds presentaban una mayor degradación en presencia de sangre. Esta propiedad es muy interesante para reducir las molestias a los pacientes cuando se les retira el tratamiento. Además, los resultados de adhesión de glóbulos rojos y plaquetas mostraron que los scaffolds eran capaces de retener una mayor cantidad de estas células adheridas en su microestructura lo que, gracias a un posterior ensayo de coagulación, demostró que estaba directamente relacionado con una mayor capacidad coagulante. Finalmente testamos estos materiales en un modelo en roedores de amputación de cola y los scaffolds demostraron reducir el tiempo de sangrado frente a los otros dos materiales.

En el tercer estudio decidimos combinar nuestros scaffolds con las MSCs, tanto las obtenidas de tejido adiposo como las extraídas de los folículos pilosos. Durante este experimento observamos que las MSCs se adherían y proliferaban dentro de los scaffolds manteniendo una alta viabilidad hasta los 7 días de experimento. Durante este periodo, además, las MSCs liberaron gran cantidad de citoquinas y factores de crecimiento favorables para el proceso de cicatrización de heridas como el VEGF, EGF, SDF-1α entre otros. Posteriormente demostramos que los scaffolds cargados con las MSCs eran capaces de promover la migración de fibroblastos y queratinocitos. Además, incrementaron la formación de vasos en células endoteliales. Por otro lado, el secretoma liberado por estos sistemas demostró que protegía a los fibroblastos de la muerte celular derivada de altas concentraciones de especies reactivas de oxígeno y glucosa. Curiosamente, no observamos diferencias significativas en los resultados de todos estos experimentos entre los dos tipos de MSCs. Finalmente testamos los scaffolds cargados con MSCs en un modelo murino con cicatrización dificultada. En este procedimiento observamos que los scaffolds con ambos tipos celulares redujeron el tiempo de cicatrización de las heridas frente a control y a los scaffolds sin células. Además, observamos que los scaffolds con MSCs redujeron la inflamación en la herida e incrementaron la re-epitelialización y la deposición de colágeno logrando un cierre más rápido y funcional.

Finalmente, para el cuarto estudio de esta tesis doctoral, analizamos los efectos cicatrizantes de las vesículas extracelulares (EVs) liberadas por las MSCs. Se ha descrito que, al igual que las MSCs, las EVs que estas liberan tienen efectos antiinflamatorios, inmunomoduladores y regenerativos. Para ello, en primer lugar, aislamos las EVs por

centrifugación diferencial generando dos poblaciones, las EVs grandes, aisladas a 10,000 x g (P10K) y las EVs pequeñas, aisladas a 100,000 x g (P100K). Después de obtener estas dos poblaciones, observamos que ambos tipos celulares presentaban los marcadores vesiculares estandarizados CD9, CD63 y CD81 además de una gran cantidad de otros marcadores involucrados en multitud de procesos biológicos. También pudimos analizar su tamaño y morfología a través de microscopía electrónica y técnicas de "nanotracking". Observamos que no había diferencias entre los distintos tipos celulares, pero si entre las distintas poblaciones de EVs, presentando más decoración proteica a modo de corona en las vesículas pequeñas. Finalmente testamos estas EVs en ensayos funcionales tales como el ensayo de migración de fibroblastos, angiogénesis o los ensayos de protección frente a especies reactivas de oxígeno e hiperglicemia. Pudimos comprobar que tanto los dos tipos celulares como las dos poblaciones vesiculares fueron capaces de incrementar la migración en fibroblastos y la formación de vasos en células endoteliales frente a control. Por otro lado, no pudimos observar efectos protectores frente a especies reactivas de oxígeno, sin embargo, si pudimos observar un efecto de protección en fibroblastos frente a la muerte celular por hiperglicemia.

Como conclusión de esta tesis doctoral, aquí se presenta el desarrollo y caracterización de un scaffold tipo esponja obtenido de productos de deshecho de la industria alimentaria con capacidad hemostática y de adhesión celular. La primera propiedad ha servido para demostrar que el scaffold presenta ventajas frente a los tratamientos de primera línea en clínica para heridas hemorrágicas agudas como la epistaxis. Gracias a la segunda propiedad, hemos podido desarrollar una terapia combinado el scaffold con MSCs mostrando resultados prometedores en cicatrización de heridas *in vitro* en *in viv*o. Finalmente, a modo de terapia libre de células hemos caracterizado las EVs secretadas por estas células y hemos demostrado que presentan también una gran eficacia en cicatrización de heridas *in vitro*.